The Effects of Specific Force on Self-Motion Perception in a Simulation Environment

Bruno Jorge Correia Grácio

The Effects of Specific Force on Self-Motion Perception in a Simulation Environment

Bruno Jorge Correia Grácio

Author email: `bj.gracio@gmail.com`

The Effects of Specific Force on Self-Motion Perception in a Simulation Environment

PROEFSCHRIFT

ter verkrijging van de graad van doctor
aan de Technische Universiteit Delft,
op gezag van de Rector Magnificus prof.ir. K.Ch.A.M. Luyben,
voorzitter van het College voor Promoties,
in het openbaar te verdedigen
op vrijdag 15 november 2013 om 12.30 uur

door

Bruno Jorge CORREIA GRÁCIO

Ingenieur Luchtvaart en Ruimtevaart
geboren te Rio de Mouro, Portugal.

Dit proefschrift is goedgekeurd door de promotoren:

Prof.dr.ir. M. Mulder
Prof.dr. J.E. Bos

Copromotor:

Dr.ir. M.M. van Paassen

"To Infinity and Beyond"
- Buzz Lightyear

Summary

The Effects of Specific Force on Self-Motion Perception in a Simulation Environment

Bruno Jorge Correia Grácio

Motion-base simulators allow humans to experience specific maneuvers in a safe and controlled environment, where visual and inertial cues are generated to create the illusion of controlling a real vehicle. Although the simulator visual motion cues can be similar in amplitude to the ones experienced in the real vehicle, the inertial cues of the real vehicle often require a linear or angular displacement significantly higher than what the motion-base simulator is capable of. Therefore, the vehicle inertial cues have to be transformed, via a Motion Cueing Algorithm (MCA), into simulator inertial cues that are within the simulator physical limits.

Classically, MCAs minimize the error between the vehicle motion cues and the ones generated by the simulator platform motion system. Although this method works relatively well for small vehicle motions, humans will detect the simulator limitations when these motions increase both in amplitude and duration, which could affect immersion in the simulation and training effectiveness. A possible solution for this problem could be to use the motion as perceived by humans rather than the actual physical vehicle motion. Here, one would minimize the error between the perceived vehicle and simulator motion cues.

Humans perceive self-motion by fusing information from different sensory modalities in the central nervous system (CNS). The accurate perception of self-motion is essential for locomotion and spatial orientation. However, when humans move in artificial environments (e.g., flying or driving) they might exper-

ience motion illusions. For example, when experiencing specific forces (i.e., the total reaction force acting on a body per unit of mass, in m/s^2) humans might perceive body translation, tilt, or both. Therefore, to design MCAs using self-motion perception knowledge, it is necessary to first understand how humans perceive motion in a simulation environment. This is particularly interesting for specific forces because of the tilt-translation ambiguity and because changes in specific forces can quickly drive the simulator close to its physical limits.

The main goal of this thesis is to investigate how specific forces affect human self-motion perception in a simulation environment. For that, the thesis is divided in two parts: the vestibular system part and the visual-vestibular interactions part. The vestibular system part, Chapters 2 to 4, investigates how specific forces induce in humans a tilt and translation percept when there is no visual information. The visual-vestibular interactions part, Chapters 5 to 7, studies the scaling between visual and inertial cues in a simulation environment.

In Chapter 2, we investigated the artifacts that might be present when measuring perceived tilt using a joystick. Subjects were sinusoidally moved around their naso-occipital axis while dynamically indicating their tilt with a joystick. The joystick was either moved against the direction of self-motion, defined as the inside-out (IO) condition, or in the direction of self-motion, defined as the outside-in (OI) condition. Additionally, we also tested whether there was a difference in holding the joystick above, around, or below its rotation point. The results showed a significant difference in the indicated tilt measurement between the IO and OI conditions, but not on the holding positions. This led to the conclusion that the IO condition was related to perceived vertical whereas the OI was related to perceived tilt.

In Chapter 3 we investigated the illusory tilt, known as somatogravic illusion, that subjects perceive when subject to a sustained linear acceleration in the dark. To measure the tilt, we used the OI joystick condition of Chapter 2. To generate the motion profiles, we used a variable-radius centrifugation technique to create a lateral centripetal acceleration where subjects, after some seconds at constant angular velocity, had no angular motion perception. Results showed that the time constant of the somatogravic illusion was in the order of two seconds. Additionally, the illusion was accurately modeled by the self-motion perception model described by Mayne in 1974, defined as Mayne equation.

After studying the tilt percept in Chapters 2 and 3, in Chapter 4 we investigated the translation percept occurring when humans are subject to specific forces in the dark. Participants were subject to lateral sinusoidal profiles at different frequencies and amplitudes and had to indicate their perceived peak-to-peak displacement and maximum velocity. Results showed that the displacement estimates were in the same order of magnitude of the linear velocity estimates, when these were converted to distance units. In most subjects, perceived

velocity was accurately modeled by the Mayne equation whereas perceived displacement required an additional leaky integrator for a better fit. In a small group of subjects, the displacement estimates seemed affected by cognitive processes not included in current self-motion perception models.

Chapters 3 and 4 showed that the Mayne equation can accurately model the tilt-translation ambiguity shown to occur when there is no visual information. The measured time constant for this model was in the same order of magnitude for both studies. However, for a simulation environment this model is only suitable for situations with poor visual motion (e.g., flying in clouds or at night). Therefore, the second part of the thesis focused on visual-vestibular interactions.

Chapter 5 investigated the preferred amplitude scaling between visual and inertial cues. Subjects moved sinusoidally with visual and inertial cues having the same phase and frequency but different amplitude. Their task was to change the inertial amplitude until the best match with the visual amplitude was found. Results showed that the motion gains, defined as the ratio between the inertial and visual amplitudes, decreased when the visual amplitude and frequency increased. Overall, these motion gains were smaller than one, meaning that the preferred inertial amplitude was smaller than the visual amplitude. Additionally, we found that there was not a preferred motion gain value, but a range of values that depended on the initial inertial amplitude. This study confirmed that inertial motion in a simulator environment is overestimated.

The range of inertial values found in Chapter 5, defined here as Optimal Zone (OZ), seemed similar to the Coherence Zone (CZ) described in the literature, defined as a zone where the inertial and visual cues are perceived as coherent, even though their amplitude or phase might be different. Therefore, in Chapter 6 we used sinusoidal lateral motion to compare the Optimal and Coherence Zones. For the OZ, subjects had again to change the inertial amplitude until the best match with the visual amplitude was obtained, whereas for the CZ, subjects had to find the highest and lowest inertial amplitude that was still coherent with the visual amplitude. Results showed that the Optimal and Coherence Zones were different, with the former being located within the latter. The OZ motion gains showed the same amplitude and frequency trends found in Chapter 5, despite the study being conducted in different apparatuses.

The motion gains lower than one found in Chapters 5 and 6 might depend on the visual cues being displayed in the simulator. Therefore, Chapter 7 investigated if the amplitude scaling between visual and inertial cues is affected by the field-of-view (FoV), and size and depth cues. In this study, subjects changed the visual amplitude until the best match with the inertial amplitude was obtained. This was performed for sinusoidal motion in surge, sway, and yaw. The results showed that the visual gains, defined as the ratio between the visual and inertial cues, were affected both by the FoV and scene content. The visual gains

decreased, making them closer to one, when the FoV became wider. Also, the visual gains became closer to one when more size and depth cues were shown in the virtual world.

We concluded that depth perception plays a major role in the measured visual gains. For yaw, where optic flow speed is independent from the distance between the objects in the visual scene and the observer, the visual gains were one and constant across the different visual scenes whereas for surge and sway, where optic flow speed depends on object placement in the virtual world, the visual gains were much higher than one and affected by size and depth cues. The visual gains seem to be a good measurement to evaluate how size and depth cues are interpreted in a simulation environment.

In Chapter 8, the major implications of the results of the previous chapters to the design of MCAs were considered. A self-motion perception model was chosen from the literature and was updated with the findings from the studies conducted in this thesis. Additionally, we proposed a framework, using this self-motion perception model, to design a "perceptual" MCA. Although the perceptual MCA designed here is not yet a solution that might substitute the more classical MCAs, the approach can offer some advantages in specific maneuvers and can be easily updated with new insights in human self-motion perception.

This thesis showed that self-motion perception induced by specific forces in the dark can be accurately modeled by the Mayne equation. It is expected that future studies would confirm that this equation can accurately model self-motion for canal-otoliths interactions. We also showed that self-motion in a simulation environment is different than in real life, mainly due to the lack of proper visual depth cues but also due to cognitive effects like past experience or expectation. Therefore, the role of cognition in self-motion perception should be studied and included in future models. Also important is to study how visual and inertial information is combined at the CNS level to make it consistent across the different solutions used in current self-motion perception models. As a last note, the experiments conducted here were passive, meaning that subjects focused solely on their perception, while the perceptual results should be used to design MCAs for vehicle motion, where subjects focus not only on their perceived motion, but also on a control task. Therefore, future research should investigate the applicability of the current findings on human behavior during active control tasks, to ultimately achieve more immersive and efficient vehicle simulation.

Contents

Chapter 1

Introduction

The history of flight simulation is practically as old as the history of aviation itself. Early on, there was the need to prepare novice pilots for the complex task of flying an aircraft. This created the necessity for flight training and led to the appearance of the first flight simulators. One of the first truly synthetic flight training devices was the Antoinette trainer [1]. This simulator was used to let pilots experience the typical pitch and roll motions of an aircraft. As seen in Figure 1.1, the inertial motion of the Antoinette trainer was generated manually by the flight instructor while the visual motion was given by the area surrounding the flight trainer. Flight simulators have become the most used training tool in aviation.

(a) Front view   (b) Back view

Figure 1.1: *Front and back view of the Antoinette flight trainer.*

Although flight simulators started as a training tool, this is no longer their sole purpose. The flexibility of the simulation environment makes flight simulators a cost-effective and safe design tool. New aircraft technologies, such as

new cockpit interfaces and novel fly-by-wire control systems, were first tested in flight simulators before appearing in the real aircraft. Flight simulators are also used to investigate a pilot's physiology, like tolerance to g-forces [2–4]. Although widely used by the aircraft industry, motion-based simulators are not exclusive to flight simulation and can also be found, for example, in the automotive [5–7] or maritime domains [8–10].

The flight simulator evolved from the Antoinette trainer to the state-of-the-art flight simulators that exist today. Figure 1.2 shows an example of a training and a research motion-based simulator. From Figure 1.2(a), we observe that inertial motion is no longer manually powered by the instructor but by hydraulic or electric motors. The visual system is no longer the simulator surrounding area but a computer-generated display where realistic high resolution images show what pilots would see from a real aircraft cockpit. Current flight simulators also have a one-to-one fully functional replica of a typical aircraft cockpit to create the environmental cues necessary for immersion in the simulation. Another improvement is that current simulators have high-fidelity aircraft models to generate the typical motions of an aircraft so that the behavior of the simulated aircraft is similar to the behavior of the real aircraft.

(a) Training simulators   (b) Research simulator
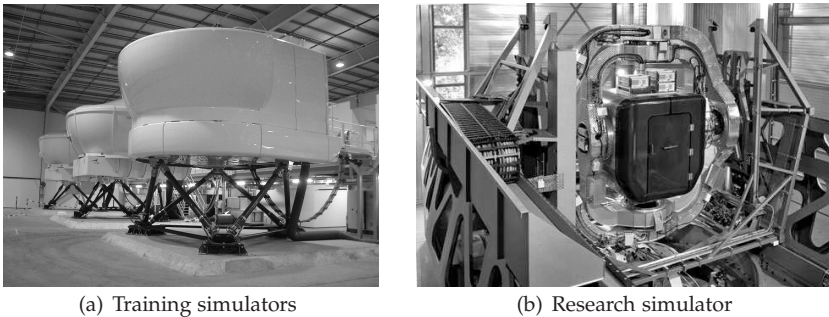
Figure 1.2: *Current state-of-the-art motion-based simulators. Figure 1.2(a)[1]shows typical motion-based training simulators while Figure 1.2(b) shows the DESDEMONA research simulator.*

Despite the numerous advances in flight simulation, the simulator environment does not substitute the real aircraft. The advances in computer graphics made it possible to have a realistic visual scene that is quite comparable with the real situation despite differences in luminance, resolution, and contrast, among other things. However, the inertial motion present in a simulator is not equivalent to the motion generated by the real aircraft, due to the significant physical limitations of the simulator motion system [11]. While a real aircraft has several

---

[1]This photo is a courtesy from FSC.

kilometers of motion space, the simulator is constrained to the few meters of displacement allowed by the actuators. Therefore, the inertial motion of the aircraft has to be transformed into inertial motion that fits the simulator's motion space. This transformation is performed by motion cueing algorithms (MCAs).

1.1 Motion cueing algorithms

Motion cueing algorithms are used to keep the simulator inertial motion platform within its physical limits [11–13]. A typical representation of a MCA is shown in Figure 1.3. Here, the aircraft specific forces are scaled by a gain factor and then transformed from the aircraft body reference frame to the simulator inertial reference frame (R_{B2I}). These inertial specific forces are then transformed into accelerations by removing the gravity component and filtered by a high-pass filter. The high-pass filter ensures that the simulator motion platform only follows the high-frequency linear motions, which have a short duration, but not the low-frequency linear motions, which would quickly drive the simulator out of its limits. The same technique is used to transform the aircraft angular motion into simulator angular motion, where block R_{B2E} transforms aircraft body rates into Euler angular rates [11, 14].
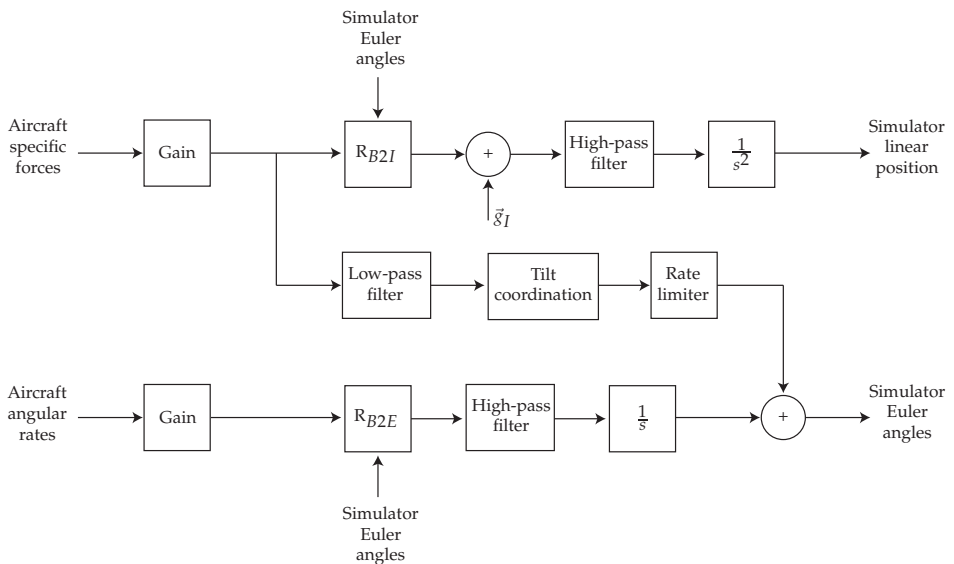
Figure 1.3: *Typical structure from a motion cueing algorithm [11].*

In addition to limit low-frequency motion, the high-pass filters can be designed to make the simulator cabin return to its neutral position, to create significant "motion space" for the inertial motions that may follow. This is known as

"washout" motion. A third-order high-pass filter is sufficient to make the simulator return to its neutral position [11] for linear motion because this input is in acceleration units, whereas for angular motion, a second-order high-pass filter would already be sufficient because the input is in velocity units. However, if the aircraft motion is not severe, lower order high-pass filters can be used [11].

The low-frequency linear motion can be simulated with tilt coordination [13]: tilting the simulator cabin in order to use the gravity vector as a linear acceleration vector, which creates a perception of linear motion. However, the cabin tilt-motion should be slow enough so that the pilot does not perceive the rotation, which would impair the perception of linear motion. Therefore, a rate limiter (Figure 1.3) is normally used to keep the cabin tilt sub-threshold [15]. Normally, a second-order low-pass filter is used here and only for surge and sway motions since tilt coordination cannot be used for vertical motion [11].

With this structure, MCAs aim at minimizing the error between the aircraft motion cues and those generated by the simulator without exceeding the simulator physical limits. This is done by changing the parameters used for scaling and filtering the aircraft motion [14]. Having motion cues in the simulator as close as possible to the ones reproduced by the aircraft is commonly referred to as the objective approach to simulator fidelity [1, 16, 17], where simulator fidelity is defined as the similarity between the aircraft and simulator environmental cues [1]. With this approach, high simulator fidelity can be achieved for inertial motions with small amplitude and short duration since then it is possible to design a MCA with low amplitude and phase errors [18–20]. However, the simulator will not be able to follow the inertial motion when it increases both in amplitude and duration, which decreases the simulator fidelity and might even create noticeable false cues, the inertial motion cues experienced as anomalous by the pilot [21].

An example of a false cue generated by the MCA is the washout motion described before. In a take-off maneuver, for example, the simulator will move forward when the pilot releases the brakes at full throttle, similar to a real aircraft. However, due to the third order high-pass filters used in the MCA, the forward movement will be short and the cabin will return to neutral position. This return motion is not present in the real aircraft since it continues to move forward. Therefore, if the pilot in the simulator perceives this incorrect backward movement, immersion in the task might be lost. In fact, false cues such as this might be more adverse for pilot immersion than fixed-base simulation (i.e., simulators with no inertial motion) [14, 22–24].

A possible way to minimize the simulator physical limitations and false cues from pilots is to use human self-motion perception knowledge. Here, instead of making the simulator motion as close as possible to the aircraft motion, researchers try to make the perceived simulator motion as close as possible to

the perceived aircraft motion, even though the simulator motion might be different from the aircraft motion. An example is the tilt coordination technique described before, where the tilting movement does not occur in the real aircraft during pure linear accelerations but the perception of sustained acceleration in the simulator is similar to the one in the real aircraft. The use of perceptual knowledge in a simulation environment is normally referred to as the perceptual approach to simulator fidelity [1, 16, 17, 25]. This is particularly interesting with linear motion simulation, like with the use of tilt coordination, because pure linear accelerations will quickly drive the simulator to its physical limits [26, 27]. Therefore, this thesis will mainly focus on linear motion. Angular motion, on the other hand, can be performed nearly unconstrained by current simulators [28, 29]. However, the lack of knowledge on how the human central nervous system (CNS) integrates the information obtained from other sensory systems has been argued to be a drawback when using human self-motion perception to improve MCAs [16, 17].

1.2   Human self-motion perception

Humans are able to estimate self-motion based on the information provided by different sensory systems. This estimate is essential for moving actively, for example, through environments or maintain equilibrium. The three body sensory systems that are considered to contribute the most to self-motion perception are the visual, vestibular and somatosensory systems [30, 31]. However, the contribution of the somatosensory system is difficult to measure experimentally since it requires the use of, for example, labyrinthine defective [32–34] or paraplegic [35] patients. For healthy subjects it is difficult and ethically questionable to completely isolate the contributions of the vestibular and somatosensory system since it needs the use of medical procedures that go beyond the scope of this thesis. To overcome this difficulty, any contribution from the somatosensory system to the perception of self-motion was attributed to the vestibular system. This means that in the experimental work conducted in this thesis, we might be attributing characteristics of the somatosensory system to the vestibular system.

1.2.1   Visual system

The visual system responds to optic flow from visual scenes to create a perception of self-motion [36–39]. Optic flow as been defined as "the pattern of motion present at the eye of a moving observer" [40]. For example, if the observer moves toward a certain object, visually, that object is moving closer to the observer. Optic flow delivers information not only from the observer movement but also information of the visual scene 3D layout [38]. This information

given by optic flow is crucial to create vection, which is defined as the perception of self-motion induced by a visual scene [38,41–45]. Self-motion perception obtained by vection can be illusory [38], as shown by the well-known "train illusion", in which a human in a stationary train perceives that his train is moving when the neighboring train starts to move, since this neighboring train is interpreted as a static scene. The illusion disappears as soon the human looks to the opposite window and sees a stationary environment.

Besides the information obtained from visual scene motion, the frame [46,47] and polarity [47] of a visual scene can be used to create an estimate of self-orientation. Polarity information (i.e., objects with an identifiable top and bottom) can be used to identify the vertical direction (i.e., the direction of the earth gravity vector), which gives self-orientation information. Frame information (i.e., distinct horizontal and vertical lines) such as provided by windows and columns of a building is also used by humans to estimate their self-orientation. Therefore, from the visual system alone, one can make an estimate of self-linear motion, self-angular motion and self-orientation. However, in the dark, humans still have perception of self-motion and for that, the vestibular system is used.

1.2.2   Vestibular system

The vestibular system is located in the human inner ear [31,48]. For each inner ear, this system contains an otolith and a semicircular-canal organ, which react to linear and angular motion, respectively. The semicircular-canals respond to head angular accelerations on roll, pitch and yaw. These organs are normally modeled as having high-pass characteristics for angular velocity, meaning that low-frequency angular velocities are attenuated [30,31]. Therefore, when subject to a constant angular velocity, humans will perceive themselves as being stationary [49].

The otoliths respond to head specific forces on surge, sway and heave [30, 31, 48]. Specific force is defined as the vectorial sum of the linear accelerations due to motion and gravity. These organs are normally modeled as having unit gain characteristics [50,51] or a unit gain with high-frequency dynamics [48,52,53]. Because the otoliths respond to specific force, Einstein's equivalence principle [54] shows that they cannot discriminate between linear acceleration due to motion, which would give information about linear self-motion, and acceleration due to gravity, which due to the difference between the head orientation and the gravity vector direction would give information about self-orientation. However, even in the dark, one has an estimate of self-orientation and an estimate of self-motion. If not, humans would perceive forward movement, in the head frame of reference, when lying on their back. Therefore, the CNS has to combine and process the information coming from the different sensory systems to create an estimate of self-motion and an estimate self-

orientation.

1.2.3   Motion perception models

Researchers have been measuring perceived self-motion from different motion profiles to understand how the CNS processes sensory information, which has led to the design of different human self-motion perception models. However, no model in the literature can yet fully explain how this neural processing is done. These human perception models are able to explain isolated percepts, such as the perceived motion from a profile in a single degree of freedom, but fail to correctly estimate perceived motion from complex motion profiles when several sensory information sources are involved.

Another issue is that researchers do not agree on how to model the CNS behavior. For example, Holly et al. [55] developed a Whole-Motion Model to explain human perception during centrifuge runs. This model is based mainly on the laws of physics. On the other hand, some researchers have proposed that the CNS processes the signals from the sensory models in a statistically optimal fashion using Bayesian theory [56–60]. Yet others have used engineering concepts to explain the processes occurring at the CNS [30,50,51,61–63]. For example, the observer model theory was used to explain that the CNS has an internal copy of the sensory organs, the internal model, and estimates self-motion from the errors between the signals from the internal model and the signals from the sensory organs [50,51,64].

To use human self-motion perception to design a MCA, one would have to first understand how humans perceive self-motion in a simulator environment. However, the human perception models developed in the literature were mostly based on motion profiles that are rarely used in such an environment. Therefore, these models might not be able to explain the processing occurring in the CNS when humans are in a flight simulator. Another issue with some of the models found in the literature is their complexity that could result in significant computational effort, which is not desirable for MCAs that run in real time.

As a consequence, we hypothesize that the state of the art in human modeling did not mature to a level such that the insights gained can be used in MCAs. Therefore, in this thesis we conducted experimental work to understand how humans perceive self-motion in a simulator environment. We focused specifically on linear motion, and therefore specific force, since these are the types of motion that are more prone to drive the simulator to its physical limits.

1.3   Thesis goal

The aim of this thesis is to investigate how specific forces affect human self-motion perception in a simulation environment. To achieve this goal, the thesis has two parts. In the first part, we investigate how the CNS estimates tilt and translation from the specific forces signaled by the vestibular system. The sub-goals of the first part are:

- Investigate if the measured tilt percept is affected by different measurement methods.

- Study how specific forces induce a tilt percept when no visual cues are present.

- Study how specific forces induce a linear displacement and linear velocity percept when no visual cues are present.

In the second part of this thesis, we investigate perceived self-motion due to visual-vestibular interactions in the presence of specific forces. We focus mainly on the mismatch between the amplitude of visual and inertial cues. The sub-goals for this second part are:

- Investigate what is the preferred amplitude scaling between visual and inertial cues in a simulation environment.

- Investigate the difference between the preferred amplitude scaling and the amplitude coherence zones between visual and inertial cues in a simulation environment.

- Study how different visual scene characteristics affect the preferred amplitude scaling between visual and inertial cues in a simulation environment.

1.4   Approach

In this thesis, we focused on a perceptual approach instead of an objective approach to address simulator fidelity. Figure 1.4 illustrates the main differences between the two approaches, where the block HMPM in Figure 1.4(b) represents a human self-motion perception model with visual-vestibular interactions.

The main difference between the objective and perceptual approach is the error that these approaches try to minimize. In the perceptual approach, a human self-motion perception model is needed to estimate the difference between the perceived motion in the aircraft and the one in the simulator. Researchers have

(a) Objective approach to simulator fidelity.

(b) Perceptual approach to simulator fidelity [25].
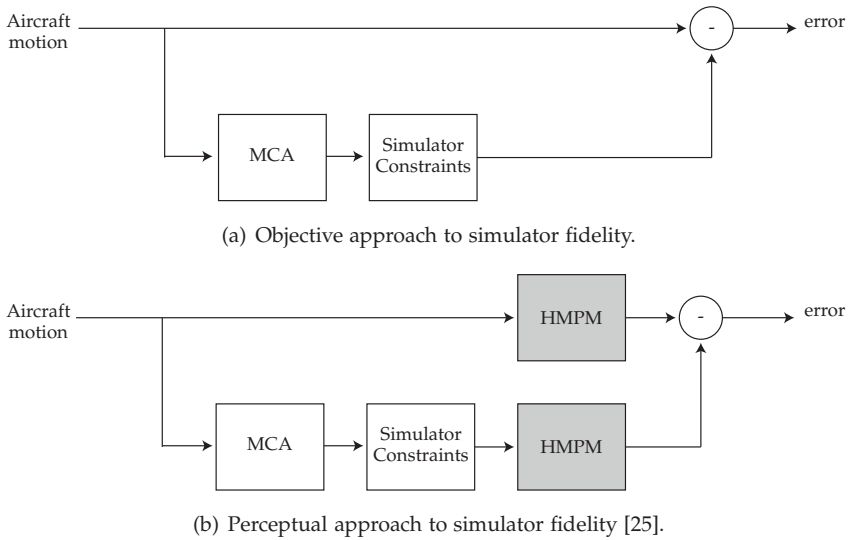
Figure 1.4: *Motion-based simulation problem using an objective (top) or perceptual (bottom) approach to simulator fidelity.*

already used a perceptual approach when designing MCAs [21,25,65,66]. These perceptual MCAs were optimized based on the output of the vestibular system. However, we have seen in Section 1.2 that the vestibular system alone cannot explain the motion illusions experienced by humans sufficiently. Therefore, a self-motion perception model that generates an estimate of perceived motion based on how the CNS fuses sensory information is needed for a perceptual approach.

1.4.1 Visual-vestibular self-motion perception model

In Section 1.2 we observed that there is no consensus yet on how the CNS operates, which led us to conclude that there is not a self-motion perception model that can be directly used with a MCA. However, in order to understand how humans perceive self-motion in a simulator environment, we chose the self-motion perception model described by Bos et al. [63] as a starting point for the experimental work conducted in this thesis. We chose this model since it showed to be a good hypothetical framework [30, 51, 63, 67] on how the CNS operates. However, this model includes assumptions that need to be confirmed experimentally [63]. Figure 1.5 shows the visual-vestibular model shown in Bos et al. [63].

The inputs for this model are visual flow (v in m/s), specific force (f in
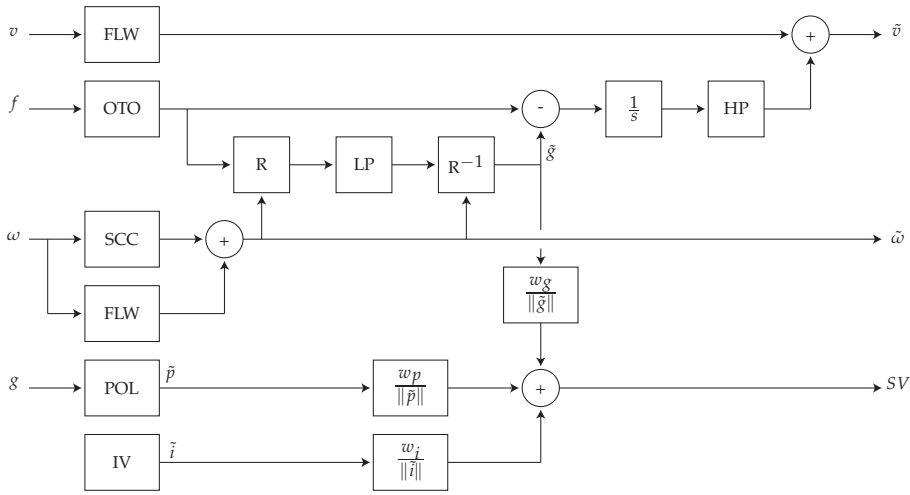
Figure 1.5: *Visual-vestibular model [63].*

m/s^2), angular velocity (ω in $°/s$), the idiotropic vector ($\tilde{i}$ in m/s^2, magnitude irrelevant) (see Mittelstaedt [68]), and the direction of the gravity vector (g in m/s^2, magnitude irrelevant) which is transformed into an estimate of the visual vertical orientation ($\tilde{p}$) by the part of the visual system responsible to detect polarity (POL). The model outputs a linear velocity estimate ($\tilde{v}$ in m/s) that gives information on self-linear motion, an angular velocity estimate ($\tilde{\omega}$ in $°/s$) that gives information on self-angular motion, and the subjective vertical (SV in m/s^2, magnitude irrelevant) that gives information on self-orientation. According to Figure 1.5, to obtain an estimate of linear motion ($\tilde{v}$), the CNS has to process the information obtained from the otoliths (OTO), semicircular-canals (SCC), and optic flow (FLW) by means of low-pass (LP) and high-pass (HP) filters. Although this dynamic behavior of the CNS is accepted in the literature, there is no agreement on the parameters used in these high-pass and low-pass filters. The angular velocity estimate ($\tilde{\omega}$) is obtained from the sum of the information sensed by the semicircular-canals (SCC) and optic flow (FLW). The subjective vertical (SV) is obtained from a vectorial weighted sum of the information given by the vestibular ($\tilde{g}$), visual ($\tilde{p}$), and idiotropic ($\tilde{i}$) estimates. The weights[2] (w_i, w_p, and w_g) used in the summation were obtained based on the experimental data obtained by Groen et al. [69].

---

[2]Originally, w_g is a function depending on $\tilde{p}$ and $\tilde{i}$. This effect is observed especially at large angles. However, because there will be no large angular displacements in the experiments conducted in this thesis (maximum displacement close to 22°), we show w_g in Figure 1.5 as a constant weight. Additionally, in the original model the SV estimate is multiplied by the magnitude of $\tilde{g}$ to explain motion sickness.

The first part of this thesis focuses on assessing whether the dynamic behavior shown in the model of Figure 1.5 can be obtained experimentally in a simulation environment and, if successful, in obtaining the parameters that describe the low-pass (LP) and high-pass (HP) filters used in the model. To limit the number of sensory inputs used by the subjects, the experimental work was conducted in the dark. Therefore, only the vestibular system is used by the CNS when estimating self-motion.

1.4.2   Vestibular system

When in the dark, the model of Figure 1.5 can be simplified to the self-motion perception model described in 1974 by Mayne [30] and later augmented by Glasauer [70] and by Bos and Bles [51] to the 3-dimensional equation below:

$$\frac{d\tilde{g}}{dt} = \frac{1}{\tau}(f_{oto} - \tilde{g}) - \omega_{scc} \times \tilde{g}, \tag{1.1}$$

where f_{oto} is the specific force signal given by the otolith afferents, ω_{scc} is the angular velocity signal given by the semicircular-canal afferents, τ is the time constant of the low-pass filter operating on the otolith afferents, and $\tilde{g}$ is the estimation of acceleration due to gravity as taken by the CNS. The estimation of acceleration due to linear motion can be achieved from Equation (1.1) by subtracting the estimated gravity vector from the specific force signal given by the otolith afferents ($\tilde{a} = f_{oto} - \tilde{g}$).

As stated before, this thesis focuses on the perception of linear motion, meaning that the motion profiles used during the experimental work were based on linear motion. For this type of motion, the output of the semicircular canals (ω_{scc}) is zero. Therefore, when angular motion is not included, the estimated acceleration due to gravity and the one due to motion can be written as Equations (1.2) and (1.3), respectively:

$$\tilde{g}(s) = \frac{1}{\tau s + 1} f_{oto}, \tag{1.2}$$

$$\tilde{a}(s) = \frac{\tau s}{\tau s + 1} f_{oto}. \tag{1.3}$$

Equations (1.2) and (1.3) show that low-frequency specific forces are perceived as tilt whereas high-frequency specific forces are perceived as linear motion. The fact that low-frequency specific forces create a tilt percept is an illusion commonly referred to as the somatogravic illusion [30,31,51,55,61,71,72]. In this thesis, we conducted experimental work to validate the model in Equation (1.2) and, if valid, obtain its time constant (τ) value.

Additionally, we tried to validate Equation (1.3) since we are interested in

studying how to affect linear motion perception. Figure 1.5 shows that the output of the motion perception model should be in velocity units so that it can be combined with the linear motion perception obtained from the visual system. Therefore, Equation (1.3) needs to be transformed to velocity units. However, several researchers [62, 63, 73] argued that the velocity component is not accurately integrated by the CNS, stating that a leaky integrator is needed to perform this operation. This explains the necessity of the high-pass filter added by Bos et al. [63] and shown in Figure 1.5. The perceived linear velocity will then be given by Equation (1.4):

$$\tilde{v}(s) = \frac{\tau s}{\tau s + 1} \frac{\tau_l s}{\tau_l s + 1} \frac{1}{s} f_{oto},$$ (1.4)

where τ_l is the time constant of the leaky integrator.

We conducted experimental work to observe if the leaky integrator is necessary to obtain a correct estimate of linear motion and to obtain the time constant's values (τ and τ_l). Although understanding how the vestibular system affects the perception of self-motion in humans is crucial, in a simulator environment the visual cues shown by the simulator displays will combine with the vestibular cues and affect self-motion perception. Therefore, in the second part of this study we focused in visual-vestibular interactions.

1.4.3   Visual-vestibular interactions

The visual-vestibular interactions in this thesis focus on the scaling between visual and inertial motion cues. A MCA (see Figure 1.3) generally scales down and filters the vehicle inertial cues. However, simulators capable of large displacements can perform some inertial cues one-to-one, meaning that the vehicle inertial cues are neither scaled nor filtered. In one-to-one simulation, the visual motion cues will have the same amplitude as the inertial motion cues. Nevertheless, researchers have found that in a simulation environment, having one-to-one inertial and visual cues is often perceived as "too strong" [74–77]. This inertial motion overestimation was hypothesized to occur due to differences between the simulator and real world visual properties [75], and due to motion distortions imposed by the MCAs and the vehicle model [78].

In driving simulation, two studies [76, 77] found that during a slalom maneuver, the motion gains (i.e., the ratio between the inertial and visual cues) preferred by subjects were approximately 0.6. Similar results were found in flight simulation during take-off [74] and decrab [75] maneuvers. These studies, however, asked subjects to directly compare the cues perceived in the simulator with the ones perceived in a real vehicle. Therefore, this subjective preference to lower motion gains might be related with errors in the vehicle models used to generate the motion cues or in handling differences between the sub-

jects' vehicle and the one simulated by the vehicle model. Additionally, Grant and Haycock [78] suggested that the lower motion gains found at the Groen et al. [74] study could be related to distortions introduced by the MCA used to create the simulator inertial motion.

Therefore, in the second part of this thesis we conducted experimental work to investigate what is the "best match" between the visual and inertial amplitude in a simulation environment. Additionally we investigated if this best match is affected by the characteristics of the displayed visual cues and if the trends found in one simulator were transferable to other simulators.

Based on the results from the first and second part of this thesis, in the last chapters we suggest modifications to the self-motion perception model shown in Figure 1.5 and propose a framework where this perception model is used to improve MCAs.

1.5   Assumptions

This section presents a summary of the main assumptions made:

- In this thesis, a perceptual approach to simulator fidelity was chosen to improve MCAs used in motion-based simulators. This is not the only valid approach to improve MCAs, however. Other known approaches to evaluate flight simulator fidelity include: objective fidelity, and behavioral fidelity [17].

- This thesis focused in the effect of specific force on self-motion perception. This choice was made because the simulation of linear motion is currently the bottleneck in motion-based simulators, whereas angular motion can be performed nearly unconstrained by current simulators. Nevertheless, from a perceptual point-of-view, motion illusions caused by angular motion are still important to investigate and can give further insight that could be helpful in the improvement of MCAs.

- The experimental work conducted in this thesis measured healthy subjects with a functional somatosensory system. However, the self-motion perception model does not model this sensory system, meaning that its effect on self-motion perception might be wrongly attributed to other sensory systems. The lack of the somatosensory system in the visual-vestibular model of Bos et al. [63] is explained by the fact that this model was optimized to study motion sickness, a condition that does not affect labyrinthine defective patients [51], which have a healthy somatosensory system.

- The decision to choose the visual-vestibular model as the self-motion perception model used in this thesis was made on the basis of its accuracy in

estimating the most known motion/orientation illusions. However, there are other self-motion perception models that present similar results when used to estimate self-motion in a simulation environment because of their similar structure and behavior [51].

1.6   Thesis outline

Figure 1.6 shows the outline of this thesis. The thesis is divided in two parts. The first part studies the contribution of the vestibular system to the perception of self-motion. This part consists of Chapters 2 to 4. The second part of the thesis deals with the effects of visual-vestibular interactions for self-motion perception. This part comprises Chapters 5 to 7. The last chapters, chapter 8 and 9, include a general discussion of the findings with its contribution to the design of "perceptual" MCAs and draw the main conclusions of the dissertation.

The chapters included in this thesis (except Chapters 1, 8, and 9) were written as papers for scientific journals or conferences. Therefore, each chapter can be read individually without loss of content. The chapters show minor modifications when compared to the published papers. The first page of these chapters includes a short introduction describing the chapter goal and its connection to the work conducted in the thesis. Additionally, this page contains the original paper title, information on its authors, and the journal/conference where it was published/submitted. A short description of the objective in each chapter is given below. The order of the chapters does not follow the chronological order[3] in which the experiments were conducted.

Chapter 2 - Measuring dynamics of the subjective vertical and tilt

There are several methods to measure perceived tilt. However, these methods might influence the measurement results, meaning that although the perceived tilt might be the same, the measured tilt could differ due to artifacts inherent to the method. To identify these artifacts, this chapter investigates how to measure tilt dynamically with different joystick methods from motion profiles that actively tilt the subjects.

Chapter 3 - Perceived tilt due to specific force in the dark

A sustained linear acceleration in the dark induces two different percepts in humans: a translation and a tilt percept. The translation percept is expected since a linear acceleration normally induces a physical displacement. However, the tilt percept is illusory because humans are not actively tilting when subjected to

---

[3]The experiments' chronological order is the following: Chapter 5, Chapter 2, Chapter 3, Chapter 6, Chapter 7, and Chapter 4.
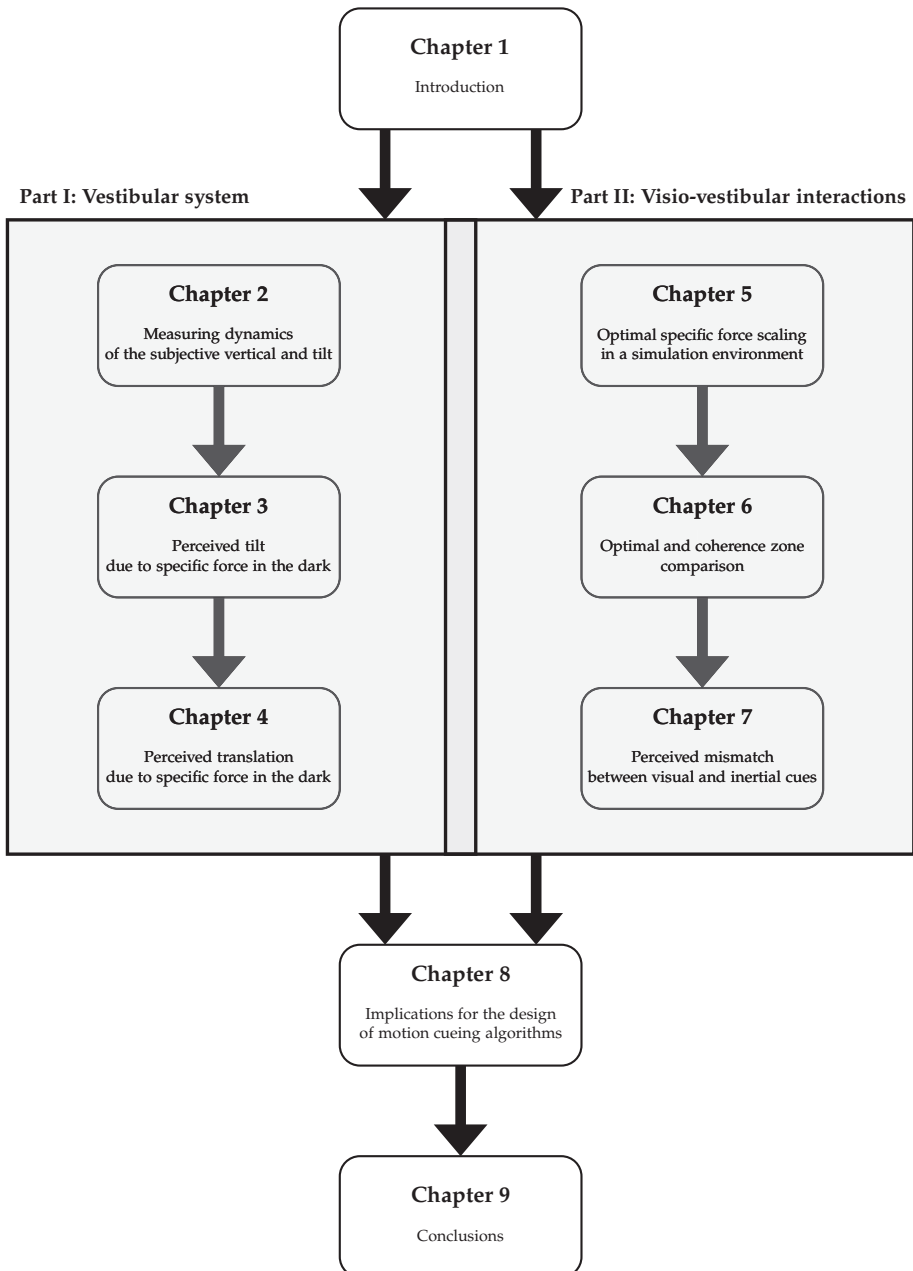
Figure 1.6: *Outline of the thesis.*

a sustained linear acceleration in the dark. In Chapter 2 we investigated how to use a joystick to measure tilt perception dynamically. In this chapter we use the same method to measure the illusory tilt percept induced by a sustained linear acceleration.

Chapter 4 - Perceived translation due to specific force in the dark

Chapter 3 measures how humans perceive tilt when subject to a sustained linear acceleration in the dark. However, this acceleration creates not only a tilt percept but also a translation percept. Therefore, in this chapter we measure how humans perceive linear displacement and linear velocity when subject to a sinusoidal specific force in the lateral direction.

Chapter 5 - Optimal specific force scaling in a simulation environment

Chapters 3 and 4 studied the effects of specific force on self-motion perception when no visual cues were present. However, visual cues are broadly used in flight simulation. Moreover, there are several simulators that only have visual cues due to the high costs of motion platforms. Despite the numerous advances in simulator's displays, the visual cues used in flight simulation are different from the ones available in real flight. This influences not only the perceived but also the amount of inertial motion necessary to induce a correct match between the visual and inertial cues. Therefore, this chapter measures the preferred amplitude scaling between visual and inertial cues in a simulator environment.

Chapter 6 - Optimal and coherence zone comparison

Chapter 5 shows that there is not a preferred scaling value but instead a preferred range of scaling values. This range seems similar to the coherence zones described in the literature. The coherence zone is defined as a zone where inertial and visual amplitudes are perceived as coherent even though their values are different. Therefore, in this chapter we compare the coherence zone with the preferred scaling range found in Chapter 5.

Chapter 7 - Perceived mismatch between visual and inertial cues

In Chapters 5 and 6 we investigated the preferred amplitude scaling between visual and inertial cues. This preferred scaling might, therefore, depend on the quality of the visual and inertial cues presented to subjects. This chapter investigates the effect of visual quality on the preferred scaling between visual and inertial cues.

Chapter 8 - Implications for the design of motion cueing algorithms

The previous chapters all investigated how humans perceive self-motion in a

simulator environment. This chapter addresses the consequences of those results to the design of "perceptual" motion cueing algorithms.

Chapter 9 - Conclusions

This chapter includes the general conclusions of this work and recommendations for follow-up studies.

Part I

Vestibular system

Chapter 2

Measuring dynamics of the subjective vertical and tilt

To perceive self-tilt, humans have to distinguish between accelerations due to self-motion and those due to gravity. Previous studies on this topic measured perceived self-tilt using a variety of methods which might introduce measurement errors, leading to different tilt angles even though the perceived tilt might be the same. This chapter investigates how to measure tilt dynamically with different joystick manipulations from motion profiles that actively tilt the subjects.

2.1   Introduction

One important characteristic of humans (and animals in general) is their ability to discriminate between acceleration due to motion and acceleration due to gravity. This characteristic is not trivial since according to Einstein's equivalence principle [54] a sensor that measures acceleration cannot discriminate between these two accelerations. If humans would base their acceleration perception solely on an accelerometer, one would perceive being accelerated upward while standing up in an earth fixed reference frame. Therefore, to perform fundamental tasks like walking or balancing objects it is essential to identify which accelerations are generated by gravity and which accelerations are generated by motion. The perception of gravity is obtained by the fusion of information from different sensory systems. The sensory systems believed to mostly contribute to this perception are the visual, vestibular and somatosensory systems [30–33,79]. The orientation of the perceived gravity vector is commonly referred to as the subjective vertical (SV) [68]. Much effort has been taken by researchers to understand the mechanisms behind the human estimation of the SV [30,31,51,80]. Most of these studies were performed during static conditions [31,68,81]. Here, subjects were passively rotated to a certain angle where they had to indicate the direction of their SV. However, there are also certain dynamic aspects of interest, requiring the SV to be measured dynamically [61,72,82]. In the dynamic case, subjects rotated while continuously indicating their SV. In both the static and dynamic studies, different measurement methods were used to determine the SV. The most commonly described measurement methods used verbal responses [31,71,81,83], adjustments of a luminous bar [72,81,84], and adjustments of a joystick or rod [61,72,82]. Verbal estimates require some understanding of angular units (typically degrees), while alignments of the visual vertical may be confounded by ocular responses. In all these measurement methods, the obtained results are a mixture between the actual perception of the vertical direction plus some artifacts introduced by the measurement method itself.

When focusing on tactile/haptic methods to measure the subjective vertical, we encountered several methodological issues not having been addressed previously. In this chapter we focused in the way a joystick can be manipulated when measuring the subjective vertical. In some studies [61,71], researchers asked subjects to indicate their perception of tilt by moving the joystick in the direction of motion, which we define in this chapter as outside-in (OI) modality, i.e., as if the stick were the subject's body as seen from the outside. In other studies [72,83], subjects were asked to indicate their perception of tilt by moving the joystick against the direction of motion, which we define in this chapter as inside-out (IO) modality, i.e., as if the stick were the Earth as seen by the subject from the inside. From a physical point of view, the same angle should result from both modalities. However, from a perceptual point of view this

might not be the case. Studies using other measurement methods (e.g., verbal estimates) showed that there might be a difference between subjective vertical and tilt [85, 86]. On the OI case, the joystick follows the physical motion while on the IO case, the joystick is kept aligned with the vertical direction. Therefore, it is not clear whether the two modalities are measuring the same percept or if the OI is measuring perception of tilt while the IO is measuring perception of verticality. The studies that specifically used the joystick method did not elucidate whether a perceptual difference might be found since, for example, the IO modality has been used to measure both perception of tilt and of verticality [72, 82, 83]. The IO and OI issue has been studied in other research fields, like in the development of tactile vests [87] or in the design of attitude displays for aircrafts [88].

An experiment was designed where subjects oscillated in roll with their eyes open and the joystick shielded. By providing as much veridical information on the motion itself as possible we could thus focus on the characteristics of the measurement method. Magnitude, phase and offset of the perceived roll angle were measured using a joystick moving with or against the motion. In addition, we investigated the effect of having the joystick being held above, at or below its rotation axis.

2.2   Method

The goal of this experiment was to observe the effect of different ways of manipulating a joystick on the subjective vertical.

2.2.1   Apparatus

The experiment used the TNO 3D rotation chair shown in Figure 2.1(a). The chair allows rotations in yaw, pitch and roll with the participant's head centered on the chair's axis of rotation. Here, the rotational chair was configured for roll rotations only. A custom made joystick (Figure 2.1(b)) consisting of a metal stick, 1.5 cm diameter and 13.5 cm long, was capable of rotating about its middle unlimitedly. The stick was gravity neutral, i.e., gravity could not affect the orientation of the stick, nor could inertial acceleration. The stick was attached to and always moved with the chair such that the subjects could manipulate the joystick with their right hand at a comfortable position.

2.2.2   Motion stimulus

The motion stimulus used to rotate the chair was the same for all experimental conditions. It consisted of a sinusoidal oscillation with a frequency of 0.2 Hz

(a) TNO rotational chair   (b) Joystick schematic
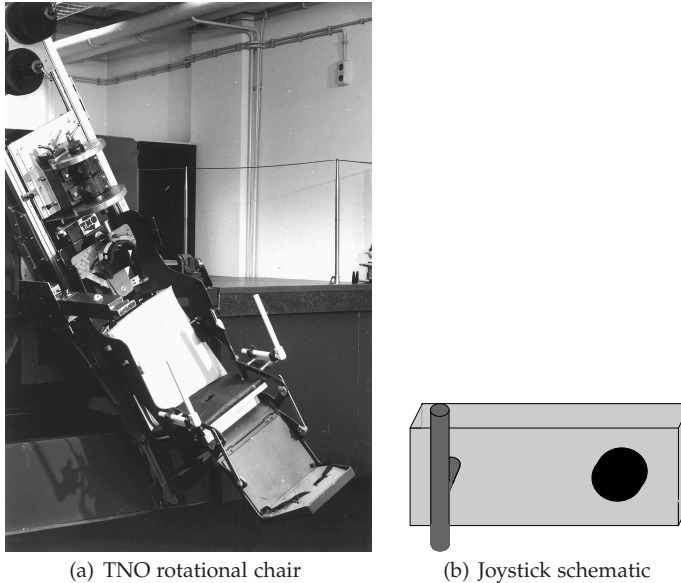
Figure 2.1: *The left figure shows the TNO 3D rotational chair and the right figure shows a schematic of the custom made joystick fixed to the arm rest of the rotational chair.*

and an amplitude of 22 degrees, resulting in a projection of gravity along the interaural axis of 0.4g maximum. The 0.4g was chosen because it is well above threshold [89] without being uncomfortable for subjects. A frequency of 0.2 Hz was chosen because it is close to the 1 rad/s frequency that is normally used in simulator studies to measure motion fidelity [18]. Each motion stimulus lasted for one minute starting and ending in the upright position.

2.2.3   Joystick measurements

The joystick was used in six different ways. Due to the symmetric design, the joystick could first be held in three different positions: at the top above the rotation axis (Top or T), at the rotation axis (Middle or M), and at the bottom below the rotation axis (Bottom or B) as shown in Figure 2.2(a). This can create different strategies by the subjects since the arm rotations are not equal between positions due to the hand distance to the pivot point. Also, the hand on top will have to move leftward to induce a CCW rotation, but rightward at the bottom. Moreover, the effect of gravity and inertia on the hand itself may also differ between the three holding positions. Therefore we decided to test if these different holding positions influenced the measurement of the dependent variables.

The joystick was always manipulated with the right hand. The other difference concerned moving the rod with or against the motion, which we respectively refer as outside-in (OI), as if "looking" from the outside world to oneself, and inside-out (IO), as if one was "looking" from inside to the outside world; analogous to the different design of attitude indicators used in aircraft. In the IO case, subjects were instructed to keep the stick gravity fixed or pointing to the zenith, thus moving against the chair. In the OI case, subjects were instructed to move the joystick with the motion in the same extent as the perceived angle of tilt (see Figure 2.2(b)).

(a) Holding positions

(b) IO and OI modalities
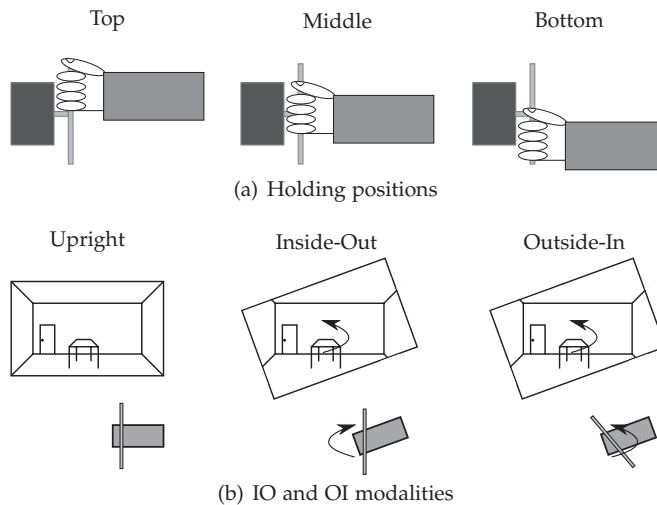
Figure 2.2: *Figure 2.2(a) shows the three different hand-positions (T, M, B) used during the experiment. Figure 2.2(b) shows a schematic of the IO and OI modalities. During a self-roll rotation counterclockwise the joystick in the IO modality has to be rotated clockwise so that it is aligned with the SV. For the OI modality, the joystick has to be rotated counterclockwise as much as the counterclockwise rotation that the subject perceived.*

To prevent mere visual guidance of the joystick tasks, the hand and stick were shielded by a cloth during the dynamic measurements. With their eyes open, subjects could, however, still see their own tilt from the vertical structures present in the laboratory room (e.g., chairs, tables, electric sockets and cables on the wall). This lead to a maximum of sensed information about tilt, while all discrepancies between true and observed tilts are assumed attributable to the measurement method.

2.2.4   Subjects

Twelve subjects (ten males and two females) participated in this experiment. The mean age of the participants was 30 years with a standard deviation of 9 years. None of the subjects had any self known vestibular or motor skill deficit. All experimental conditions had been approved by the local Ethics Committee. Subjects were informed about the purpose of the experiment and their rights according to the Declaration of Helsinki on ethical principles for medical research involving human subjects. The participants were TNO employees without expertise in equilibrium and orientation. An informed consent was signed before starting the experiment.

2.2.5   Experimental design

The experiment had a repeated measures design. This means that all subjects participated in all three (T, M, and B) times two (IO and OI), i.e., six experimental conditions. Half of the subjects started with all the IO measurements and then proceeded to the OI while the other half did the opposite. The holding positions were randomized for each subject yielding different combinations of manual holding positions.

2.2.6   Procedure

Before starting the measurements, subjects were instructed to keep their heads fixed in the head-rest (Figure 2.1) to prevent unintentional head movements in roll. To mask the actuator noise of the rotational chair, white noise was generated and sent to subjects through a headset. To observe which joystick modality (IO or OI) was more intuitive to the subjects, all subjects were positioned at a fixed angle of 22 degrees in advance of the six main conditions. For this static condition, subjects indicated the amount of tilt they perceived with the joystick, however, without any instructions given regarding the methods described above, based on the question "How would you use this joystick to indicate the amount of tilt you are now experiencing?". After returning the chair to the upright position, further instructions were given and the joystick was visually shielded using a cloth. A practice run was performed before both IO and OI measurement sets to ensure that the instructions were understood. After the practice run, the T, M, and B measurements were performed. Each experimental run lasted for one minute during which subjects had to follow the motion stimuli actively using the indicated joystick modality. At the end of the experiment, subjects were asked in addition which joystick modality they preferred.

2.2.7   Data analysis

The joystick data was sampled with a sampling frequency of 50 Hz. The obtained signal was fitted to a single sine with a fixed 0.2 Hz frequency but variable amplitude, phase, and offset using a least squares minimization procedure (see Figure 2.3). The first 20 seconds of all responses were neglected when fitting the sinusoid to minimize initial anomalies. The variance accounted for (VAF) was used as a quality measure of the obtained sine fit. A VAF of 100% means a perfect fit.

A repeated measures ANOVA was used to determine if the independent variables (joystick modality and the manual holding position of the joystick handle) significantly changed the dependent variables (amplitude, phase, and offset). When performing repeated measures ANOVA it may happen that sphericity is violated (see [90] for further insight). When this happens, a correction is needed to prevent wrong p values. In this study we used the Greenhouse-Geisser correction. The corrected p values are more conservative than the uncorrected p values. An additional one-sample t-test was performed to observe whether the obtained averages for the amplitude, phase difference and offset differed from the true values of respectively 22, 0 and 0 degrees. This test was only performed for the independent variables where the repeated measures ANOVA showed a significant main effect. All the statistical analyses were performed using SPSS PASWS 18.0.
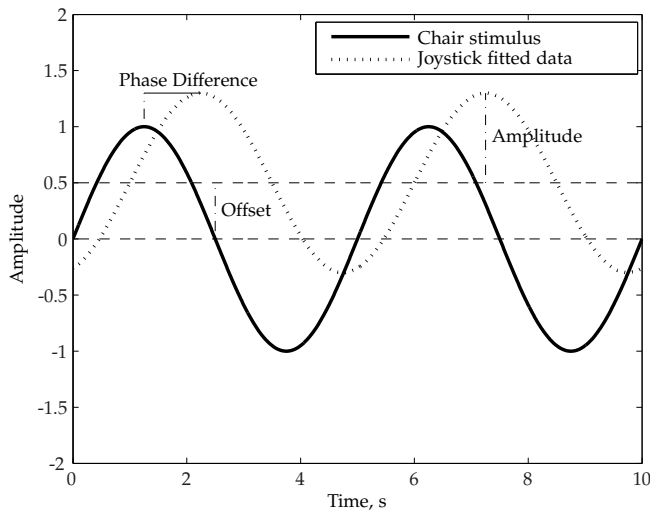
Figure 2.3: *Definition of phase difference, amplitude and offset for the sinusoid obtained from the joystick raw data.*

2.3   Results

2.3.1   Static condition

Initially, seven subjects chose the IO modality against five subjects chosing the OI modality. A Chi-squared test showed no significant difference in the subjective preference of the joystick modality, $\chi^2(1) = 0.33, p = 0.564$. At the end of the experiment, eight subjects preferred the IO modality against four subjects that preferred the OI. The Chi-squared test showed that these differences were not significant either, $\chi^2(1) = 1.33, p = 0.248$.

2.3.2   Dynamic conditions

All subjects completed all six dynamic trials. The subsequently performed sinusoidal fits showed VAFs all above 90% (93.6% on average), indicating that the matching magnitudes, phases and offsets are reliable parameters describing the obtained individual SV behaviors.

The control signal for the rotational chair had an amplitude of 22 degrees. However, the measured data showed that the actual chair movement amplitude was 20.6 degrees. Therefore this value has been considered for the amplitude analysis instead of the commanded 22 degrees. The results for the mean amplitude, phase and offset perceived by the subjects are shown in Figure 2.4. Only the significant effects of the repeated measures ANOVA are shown in Table 2.1.

Table 2.1: *Repeated measures ANOVA significant results for the mean amplitude, phase difference and offset of the perceived sinusoidal signal.*

Dependent Variables	Independent Variables	Corrections	F-ratio	p
Amplitude	J. modality	-	F(1,11) = 5.85	0.034
Phase	J. modality	-	F(1,11) = 15.12	0.003
	J. modality * Hold-pos	G-G	F(1.3,14.3) = 8.10	0.009
Offset	Hold-pos	-	F(2,22) = 5.53	0.011
	J. modality * Hold-pos	-	F(2,22) = 6.15	0.008

For the *amplitude* dependent variable, the OI modality showed significantly higher amplitudes than the IO modality. If we aggregated the data of the holding position, the OI modality has a mean amplitude of 20.13 degrees while that of the IO modality is 15.97 degrees. The different holding positions did not yield different results. A one-sample t-test (Table 2.2) showed that the average amplitude measured with the IO modality differed from the real amplitude of 20.6 degrees. On the other hand, the OI modality did not differ from the real amplitude.

The *phase difference* results showed that the phase difference for the OI modality (-4.65 degrees) was significantly different from the phase difference obtained
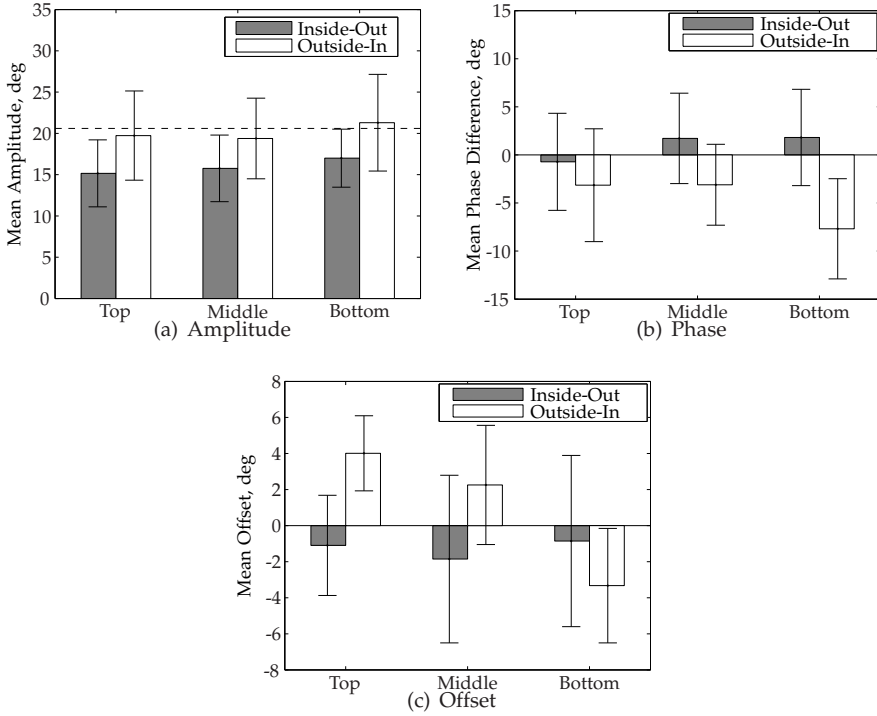
Figure 2.4: *Mean amplitude (top left), mean phase difference (top right), mean offset (bottom) and the respective 95% confidence intervals of the fitted sinusoid for all experimental conditions. The dashed line in Figure 2.4(a) represents the real amplitude of 20.6 degrees.*

Table 2.2: *One-sample t-test results for the mean amplitude, phase difference and offset of the perceived sinusoidal signal. Significant variables have a $p < 0.05$*

Dependent Variables	Independent Variables	t	p
Amplitude	IO	t(11) = -2.72	0.020
	OI	t(11) = -0.20	0.842
Phase	IO	t(11) = 0.48	0.639
	OI	t(11) = -2.36	0.038
Offset	T	t(11) = 2.70	0.021
	M	t(11) = 0.21	0.835
	B	t(11) = -1.90	0.084

for the IO modality (0.94 degrees). A significant interaction between the joystick modality and the holding zone was also found. This significant interaction is shown in Figure 2.4(b) showing different phases when holding the middle or bottom of the joystick for the IO and OI modality. The average phase difference

measured with the OI modality differed from zero as shown in Table 2.2. This means that the signal measured with the OI modality lagged the chair motion.

The mean *offset* data showed significant differences between the manual holding positions. A post-hoc test using a Bonferroni correction to cancel any type I errors [90] showed that when subjects hold the joystick at the top, their offset is significantly higher than when they hold it at the bottom ($p = 0.041$). Like for the phase difference a significant interaction between the joystick modality and the holding zone was found. Figure 2.4(c) shows that when the joystick was held at the top or middle position, the mean offset was positive for the OI modality. The Top holding position was the only condition where the offset differed from zero (Table 2.2). The recorded data showed that the offset value mainly increased during the onset of the rotational movement, i.e., the transition from a steady state (chair stopped) to a dynamic state (chair rotating). For the remaining dynamic state, the offset remained nearly constant.

2.4   Discussion

Subjects did not show a clear preference for a certain joystick modality as is shown by the inconclusive static-tilt results. The same occurred when choosing a preferred joystick modality after concluding all experimental conditions.

When measuring the SV dynamically, we found differences between the joystick modalities for the perceived amplitude and the perceived phase difference. Since the motion stimulus was the same for all experimental conditions, we assume that the perceived tilt was also the same. Therefore, if both modalities would correctly measure the perceived motion, differences between the methods are not expected. For the perceived amplitude, we found that the OI modality gave a measurement closer to the amplitude of the true motion stimulus. The measurement obtained by the IO modality was smaller than the one of the true motion. In the IO modality, subjects had to keep the rod aligned with what they perceived as Earth vertical by moving the rod opposite to the tilt of their body. In the OI modality, they had to move the rod in the same direction as the tilt of their body. Although physically implying an equal tilt, the two modalities may induce different perceptions (i.e., of verticality and tilt). Given the observations that the measurements of both do differ, this seems to be the case indeed. Moreover, the difference may be accounted for by the idiotropic vector.

Mittelstaedt [68] explained that humans tend to orient their SV away from the true gravity vector and in the direction of their own spinal axis. This SV underestimation is also known as the Aubert effect [91]. Here, the idiotropic vector was postulated to be aligned with the longitudinal or spinal axis and the SV was calculated as a weighted vector addition of a gravitational vector determined vestibularly and visually on the one hand and the idiotropic vector

on the other (see also Groen et al. [69], and Bos et al. [63]). Figure 2.5 shows a graphical representation of the underestimation caused by the idiotropic vector, its legend explaining the different components involved.
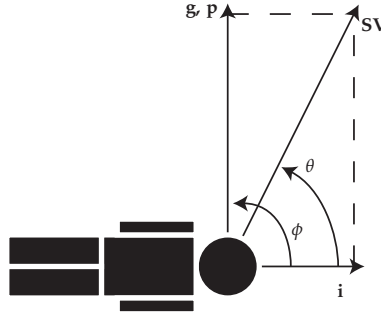
Figure 2.5: *Vector representation of the subjective vertical (**SV**) mechanism as proposed by Groen et al. [69], and Bos et al. [63] for a subject tilted 90 degrees in roll. In the figure, **g** represents the vestibular information, **p** the visual information, **i** the idiotropic vector, θ the subjective vertical rotation, and φ the total tilt.*

The tilt angle measured by the IO modality showed an underestimation not present in the tilt angle measured by the OI modality. Therefore, it seems that the idiotropic vector influences the IO but not the OI modality. From Bos et al. [63], the SV rotation (θ) is given by Equation (2.1). In our study, w_s is the ratio between the weightings of the normalized combined gravitational and visual vectors **p** and **g**, and that of the idiotropic vector **i**.

$$\tan(\theta) = \frac{w_s \sin(\phi)}{w_s \cos(\phi) + 1} \tag{2.1}$$

Using the values of 15.97 degrees for θ and 20.13 degrees for ϕ, taken from our current study, w_s gets the value 3.8. Taking into account that variations of one degree in θ can have a large effect in w_s (e.g., θ = 15 degrees would result in a w_s of 2.9), the w_s obtained in our study is very similar to the w_s of 2.9 reported by Bos et al. [63] in a comparable condition. The difference existing yet may be explained by the different conditions used (90 degrees of tilt versus 20), and quasi-static versus dynamic. As a consequence, we therefore assume that the idiotropic vector affects the perception of verticality but not the perception of tilt. Moreover we suggest to keeping to the term "subjective vertical" when measured inside-out, and "subjective tilt" when measured outside-in.

For the perceived phase difference the results showed that the OI modality lagged the chair motion. Although the average phase difference obtained with the IO modality was positive, the statistical tests showed that this value did not differ from zero. Another study using the IO modality showed a phase

lead tendency for a motion stimulus with similar frequency content [82]. These results indicate that the joystick modality can highly influence the obtained measurement. Therefore, although both IO and the OI methods were used to measure the perceived motion it may happen that the different joystick rotation needed for each method:

- measures different perception, i.e. the IO measures the "subjective vertical" and the OI measures the "subjective tilt", like hypothesized above.

- measures artifacts (e.g. different workload, different arm rotation) with different characteristics for each method.

Therefore, one should be extra careful when choosing a measuring method since the task coupled to that method can yield different results for the same perceived motion. In fact, other studies already showed that different measurement methods can influence the results. Wright and Glasauer [82] found that subjects indicated the gravity direction significantly better when using a glass of water rather than a joystick. This, however, only holds for static conditions, for in dynamic conditions the level of the water will align with the specific or gravito-inertial force, and not perpendicular to gravity. In another study, Merfeld et al. [72] found differences between the visual and somatosensory measurements when measuring perceived tilt, which, as stated in the introduction, may be attributed to eye movements.

The different manual holding positions only influenced the offset. Results showed that the offset value varied mainly at the onset of the chair movement. Therefore we consider that the offset measured with the joystick is not related with the perceived offset but with a joystick error induced by the initial chair movement. The holding zone influenced this initial offset because the acceleration acting on the subjects hand during the onset depends on the hand position.

2.5   Conclusion

In this study, we showed that the measurement method can influence the measurement of the SV. We compared two different joystick modalities, the IO where the joystick moves against the true rotation and the OI where the joystick moves with the true rotation. For the same motion stimuli, the two modalities showed different results of perceived motion. The OI modality lagged the real chair motion while the phase difference obtained with the IO did not differ from zero. To our opinion, the IO method seems closer related with measuring the SV while the OI seems related with the perception of a rotation. To that end we suggest to reserve the term "subjective vertical" to the sense of verticality measured in an inside-out way, i.e., as if 'looking' from inside to the outer world. The sense

of tilt as measured for example by manipulating a joystick as if 'looking' from outside to oneself may then be rephrased into "subjective tilt".

Chapter 3

Perceived tilt due to specific force in the dark

A sustained linear acceleration in the dark induces two different percepts in humans: translation and tilt. Although the translation percept is expected because a linear acceleration induces a physical displacement, the tilt percept is illusory because when subject to a sustained linear acceleration in the dark, humans are not actively tilting. Chapter 2 showed how to use a joystick to measure tilt perception dynamically. In this chapter, the joystick method of Chapter 2 is used to measure the tilt percept induced by a sustained linear acceleration generated using a variable-radius centrifugation technique. Besides being measured experimentally, the tilt illusion is modeled using the Mayne self-motion perception model.

3.1 Introduction

Humans perceive body tilt due to the angular motion being signaled by the semicircular-canals afferents and due to the change of gravity being signaled by the otolith afferents [31, 51, 82, 92]. However, it has also been shown that perception of whole body tilt can result solely from sustained linear accelerations [30,31,51,55,61,71,72]. This illusion is commonly referred to as the somatogravic illusion and originates in the otolith organs of the inner ear because of its incapacity to distinguish between linear acceleration due to self-motion and gravity. In aviation, this illusion has caused fatal accidents. For example, during a catapult launch from an aircraft carrier in poor visual conditions, fighter pilots may misperceive the horizontal take-off acceleration as pitching upward. The tendency to compensate for this pitch-up sensation has caused pilots to crash planes into the ocean [93–95]. Researchers have shown that the dynamic behavior of this pitch-up sensation may be approximated by a first-order low-pass filter [30, 51, 61]. Although the physiological basis of the somatogravic illusion seems to be well understood, the main time constant of the illusion (i.e., the time it takes for the tilt percept to reach 63.2% of its steady stable value) is still subject of discussion [55].

The past studies found a time constant for the somatogravic illusion both on the order of seconds and tens of seconds. This discrepancy between time constants might be explained by the different methods used to generate sustained linear accelerations. Studies using fixed-radius centrifugation generally give time constants of tens of seconds [33,72,96,97]. Based on experimental [51,72] and theoretical [51] arguments, these long time constants have been ascribed to canal stimulation at centrifuge motion onset. These arguments are further substantiated by the fact that lower time constants (on the order of seconds) were also found in studies using a linear sled to generate linear oscillatory accelerations without centrifugation [62,80,98]. To avoid extreme long sled lengths, required to induce sufficient long lasting accelerations (and controlled decelerations thereafter), variable-radius centrifugation has been used to generate sustained linear accelerations without stimulation of the semicircular-canals. Here, subjects are rotated on-centre up to a constant angular velocity. Due to the high-frequency dynamics of the semicircular-canals, the rotation sensation fades out after tens of seconds of rotating at constant velocity [31]. Then, the subject is translated along the radius to an eccentric position, while maintaining constant angular velocity. This generates a centripetal acceleration in the lateral direction without parasitical stimulation of the semicircular-canals. In these studies too, time constants on the order of seconds were found [61,72]. An effect of stimulus frequency on these time constants has, however, never been studied.

In this study, we investigated the time constant of the somatogravic illusion for sustained linear accelerations with onsets characterized by different

frequency content. To achieve this, the Desdemona research simulator [99] was used as a variable-radius centrifuge to prevent stimulation of the semicircular-canals. To obtain the time constant, the experimental data were fitted to two self-motion perception models. We used a simple motion perception model where we expect to find an effect of the frequency on the time constant and a model with improved high-frequency dynamics where we expect the extra dynamics to handle this frequency effect.

3.2 Methods

3.2.1 Subjects

A total of six subjects (three male; mean age 25 years, $SD = 4$) participated in this experiment. All subjects were paid a standard fee and gave their informed consent after general instructions. The institutional Ethical Committee approved all experimental conditions in the study. Subjects were informed about their rights according to the Declaration of Helsinki on ethical principles for medical research involving human subjects. The subjects reported no history of vestibular dysfunction.

3.2.2 Motion platform

The study was conducted at the Desdemona research simulator (Figure 3.1). The simulator has six degrees-of-freedom (DoF) that allow centrifuge-based motion simulation [99]. The simulator cabin is mounted in a three DoF gimbaled system that permits full rotations in pitch, yaw and roll. The gimbaled system itself is mounted on an eight-meter linear track, which is capable of rotating around its central Earth-vertical yaw axis to produce planetary motion. Using the gimbal system, the subjects' naso-occipital axis was perpendicular to the linear sled which generated centripetal acceleration along the subjects' lateral axis. This induced a sensation of lateral self-tilt (roll).

3.2.3 Motion profiles

All motion profiles used in this study had a theoretical centripetal acceleration of 4.1 m/s^2 in the lateral direction causing a (roll) tilt of 22.5 degrees of the specific force away from the gravity vector. To generate such profiles, the centrifuge rotated at a constant angular velocity of 80 deg/s. An acceleration of 5 deg/s^2 was initially used to reach this constant angular velocity. During the 5 deg/s^2 angular acceleration, the centripetal acceleration was zero because the simulator cabin was at the center of rotation. The centripetal acceleration was
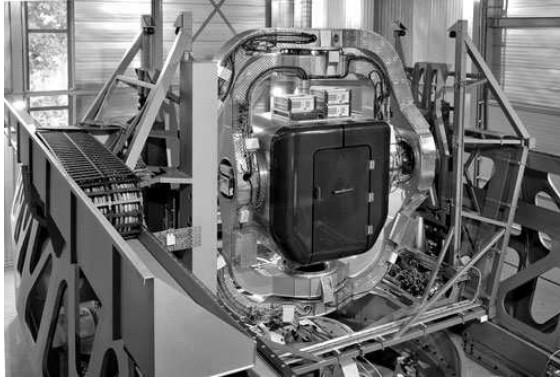
Figure 3.1: *Desdemona research simulator.*

generated only after the subject reported no perception of yaw rotation, which generally happened well within 60 s. To generate the centripetal acceleration, a raised-cosine velocity profile moved the simulator cabin 2.15 m outward. This motion profile guaranteed a smooth movement of the simulator actuator over the radius. Equation (3.1) describes the cabin movement along the centrifuge arm, where d is the final distance of the simulator cabin along the centrifuge arm, t_{start} is the time at which the simulator cabin starts to move, and f_r is the frequency, in Hz, of the raised-cosine leading up to the steady-state acceleration. Using three different frequencies for f_r we generated three different motion profiles. The frequency values were 0.05, 0.1, and 0.2 Hz.

$$
R(t) = \begin{cases} 0 & , t < t_{start} \\[2mm] -df_r\left((t - t_{start}) - \dfrac{\sin\left(2\pi f_r(t - t_{start})\right)}{2\pi f_r}\right) & , t_{start} \leq t < t_{start} + \dfrac{1}{f_r} \\[2mm] -d & , t_{start} + \dfrac{1}{f_r} \leq t \end{cases}
$$

$$(3.1)$$

The generated centripetal acceleration is given by Equation (3.2), where a_c is the centripetal acceleration, ω is the angular velocity of the centrifuge arm and R is the distance, as given by Equation (3.1).

$$
a_c(t) = \omega^2 R(t) \tag{3.2}
$$

Apart from the lateral centripetal acceleration and gravity, a Coriolis acceleration is at issue, acting on the naso-occipital axis of the subject. Together, all linear accelerations compose the gravito-inertial acceleration, or specific force.

Equation (3.3) shows the specific force (f), where f_x is the specific force acting on the subjects' naso-occipital axis, f_y is the specific force acting on the subjects' lateral axis, f_z is the specific force acting on the subjects' vertical axis and g is the magnitude of the gravitational acceleration (9.81 m/s^2). Figure 3.2 shows the time histories of the specific force components for the three different motion profiles.

$$f = \begin{cases} f_x = -2\omega\dot{R} \\ f_y = -\omega^2 R + \ddot{R} \\ f_z = g \end{cases} \tag{3.3}$$

(a) Frequency = 0.05 Hz

(b) Frequency = 0.1 Hz

(c) Frequency = 0.2 Hz
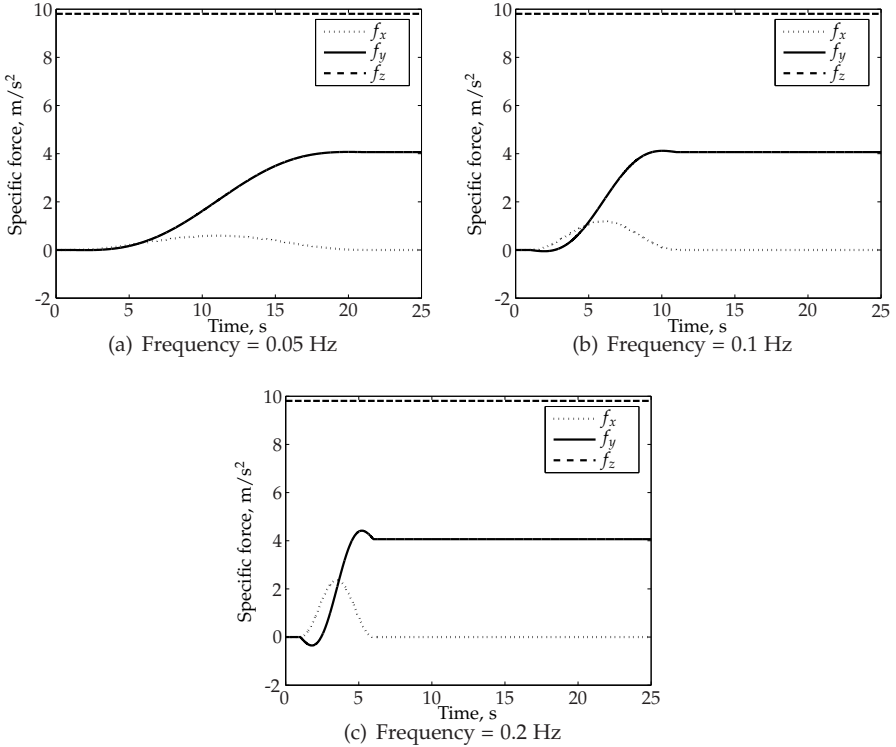
Figure 3.2: *Specific force components acting on the subjects for the four different motion profiles.*

3.2.4   Joystick

For measuring the roll-tilt illusion, we used a custom-made joystick which is not affected by any linear acceleration (i.e., gravity neutral) due to its symmetrical design. A schematic of the joystick is shown in Figure 3.3. This joystick was fixed to the subject's seat. Subjects were asked to indicate their perceived roll-tilt by rotating the rod in the same direction as their perception. Therefore, for a roll-tilt to the right, subjects had to move the rod also to the right (to measure perceived tilt) instead of moving it to the left to keep it aligned with their subjective vertical [82]. Joystick rotation was physically limited to rightward rotations from upright onwards. A button next to the gravity neutral joystick allowed subjects to indicate when they were ready to proceed to the next experimental trial.
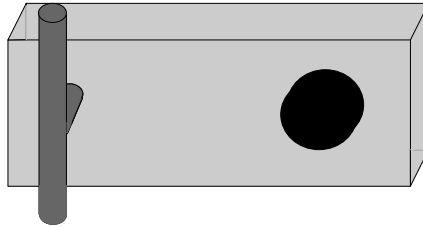
Figure 3.3: *Schematic of the joystick used to measure the roll-tilt illusion. The rod had a diameter of 1.5 cm and a length of 13.5 cm. Both the rod and the knob were operated using the right hand.*

3.2.5   Experimental design

Each subject perceived the roll-tilt illusion seven times for each of the three different motion profiles. This leads to a total of 21 experimental trials for each of the six subjects. The order in which subjects performed the experimental conditions and its repetitions was randomized. Although the experiment consisted of two additional conditions including vision, in this chapter, we only describe the experimental conditions without a visual stimulus.

3.2.6   Procedure and subjects' instructions

Subjects were seated in the simulator cabin and secured by a five-point safety belt. Subjects were instructed not to move their head during the experiment. A headrest provided head support. These measures were intended to minimize the "cross-coupling" effect that occurs when the subjects' head rotates during a constant angular-velocity environment [49]. Subjects wore a headset on which white noise was presented to mask actuator sound. The headset also allowed

for communication between the subject and the experimenter. All experimental trials were performed with eyes closed in a dark cabin. The experimental trials started by rotating the centrifuge arm until a constant angular velocity was reached. During this rotation, the simulator cabin remained in the center of the centrifuge arm. Subjects communicated to the experimenter when the perception of yaw rotation had disappeared. With an additional delay of 6 s, subjects then initiated the lateral motion by pressing the knob next to the joystick. The start of the cabin movement was signaled to subjects by a 1.5 s sound cue via the headset. While the cabin was moving outward, subjects constantly indicated their roll-tilt perception by keeping the rod aligned with the perceived roll angle. Subjects communicated to the experimenter when a steady tilt illusion was obtained. After a verbal signal from the experimenter, subjects pressed the knob again and the cabin returned to the center position. During this period, subjects moved the joystick back to zero tilt. When the simulator cabin was back at the center position, 6 s passed before automatically proceeding to the next experimental trial. This procedure was repeated until all the 21 experimental trials were completed.

3.2.7   Data analysis

The Mayne equation

The input of the otoliths is the three-dimensional specific force $(\vec{f})$, as defined in Equation 3.4 where $\vec{a}$ is the acceleration vector due to motion and $\vec{g}$ is the acceleration vector due to gravity.

$$\vec{f} = \vec{a} + \vec{g} \tag{3.4}$$

From Equation (3.4) it follows that the otoliths alone cannot discriminate between accelerations due to self-motion and accelerations due to gravity. However, the Central Nervous System (CNS) seems to be able to estimate both components [30, 51], otherwise humans would perceive acceleration due to gravity as linear movement which induce a constant percept of moving upwards. Mathematical models have been proposed to explain how the CNS may distinguish between the two different accelerations. An elegant and simple model was proposed by Mayne [30]. Although the original equation was described for two dimensions, Bos and Bles [51] turned these to one 3D coupled equation. This equation is described by Equation (3.5), where f_{oto} is the specific force signal given by the otolith afferents, ω_{scc} is the angular-velocity signal given by the semicircular-canal afferents, τ is the time constant of low-pass filter operating on the otolith afferents, and $\tilde{g}$ is the estimation of the acceleration due to gravity as taken by the CNS.

$$\frac{d\tilde{g}}{dt} = \frac{1}{\tau}(f_{oto} - \tilde{g}) - \omega_{scc} \times \tilde{g} \tag{3.5}$$

Equation (3.5) takes the combined outputs from the otolith and semicircular-canals organs to produce an estimate of acceleration due to gravity ($\tilde{g}$) and the estimation of acceleration due to motion ($\tilde{a} = f_{oto} - \tilde{g}$). Bos and Bles [51] showed that the Mayne equation could predict a large number of motion/orientation illusions, in particular the somatogravic illusion.

Since our method of inducing the somatogravic illusion did not involve stimulation of the semicircular-canals, Equation (3.5) can be simplified into Equation (3.6). Equation (3.6) is equivalent to a first-order low-pass filter with a time constant equal to τ.

$$\frac{d\tilde{g}}{dt} = \frac{1}{\tau}(f_{oto} - \tilde{g}) \Leftrightarrow \tilde{g} = \frac{1}{\tau s + 1}f_{oto} \tag{3.6}$$

We tested two different otolith transfer functions in this study; one is commonly used in literature [50, 51] and is defined by a unit gain, whereas the other has dynamics as described by Hosman [48]. Therefore, we calculated the time constant of the somatogravic illusion based on Equation (3.7) and (3.8), where Equation (3.7) uses the unit gain otolith model and Equation (3.8) uses the otolith model described by Hosman [48].

$$\begin{aligned} f_{oto} = f \Rightarrow \\ \tilde{g}(s) = \frac{1}{\tau s + 1}f \end{aligned} \tag{3.7}$$

$$\begin{aligned} f_{oto} = \frac{(s+1)}{(0.5s+1)(0.016s+1)}f \Rightarrow \\ \tilde{g}(s) = \frac{(s+1)}{(\tau s+1)(0.5s+1)(0.016s+1)}f \end{aligned} \tag{3.8}$$

In terms of model fit, the otolith model described by Hosman should have a better fit since the extra dynamics could allow the fitting algorithm to predict any high-frequency dynamics shown in the measured signal. However, these extra dynamics given by the otolith model were fixed to values suggested by the literature and could not be adjusted by the fitting procedure. Therefore, the fitting procedure used the same number of parameters for both models.

Processing of joystick data

The joystick raw data were sampled at 25 Hz. A second-order low-pass filter with a cut-off frequency of 4 Hz was used to filter the joystick-sampled data. The filter 4 Hz cut-off frequency was well above the important frequencies of the motion profiles. We used a zero-phase forward and reverse digital filtering technique to ensure no phase distortion of the filtered responses. The data of each run were trimmed between the button press to start the cabin movement and the button press that brought the cabin back to the center of the simulator's planetary arm. Therefore, the higher frequency conditions had fewer data points, due to a faster movement in time, than the lower frequency conditions. The predicted response of Equations (3.7) and (3.8) is in gravity components and therefore, not comparable with the roll angle measured by the joystick. Thus, Equation (3.9) transforms the gravity components to the roll angle predicted to be perceived by humans. In Equation (3.9), $\tilde{g}_y$ and $\tilde{g}_z$ are the estimated acceleration due to gravity in the lateral and vertical direction, respectively; and K is the perceived magnitude.

$$\tilde{\phi} = \tan^{-1}\left(\frac{\tilde{g}_y}{\tilde{g}_z}\right) K \tag{3.9}$$

A least squares minimization procedure was used to estimate the two parameters of interest, the time constant and the perceived magnitude. The algorithm calculates the value of the parameters that yield the smallest error between the predicted response and the measured data. A fit was obtained for all experimental trials, which led to a total of 21 model fits. For each fit, we used the Variance Accounted For (VAF) to evaluate the quality of the fit. The VAF is given by Equation (3.10), where u is the recorded data, $\overline{u}$ is the mean of the recorded data and u_m is the model data. A VAF of 100 % means that the measured data and the data generated by the mathematical model are equal.

$$VAF = 1 - \frac{\sum(u - u_m)^2}{\sum(u - \overline{u})^2} \tag{3.10}$$

3.3 Results

Figure 3.4 shows the mean joystick responses and their standard deviation, combined over six subjects. The graphs show that the perceived tilt lags in relation to the true tilt of the specific force vector. After a few seconds, the roll response reaches its steady-state value, close to the true tilt.

Figure 3.5 shows that the overall VAF values for the fits were high (above 95%), meaning that both models were able to accurately describe the measured data. An ANCOVA showed no significant differences between the VAFs ob-

(a) Frequency = 0.05 Hz

(b) Frequency = 0.1 Hz

(c) Frequency = 0.2 Hz
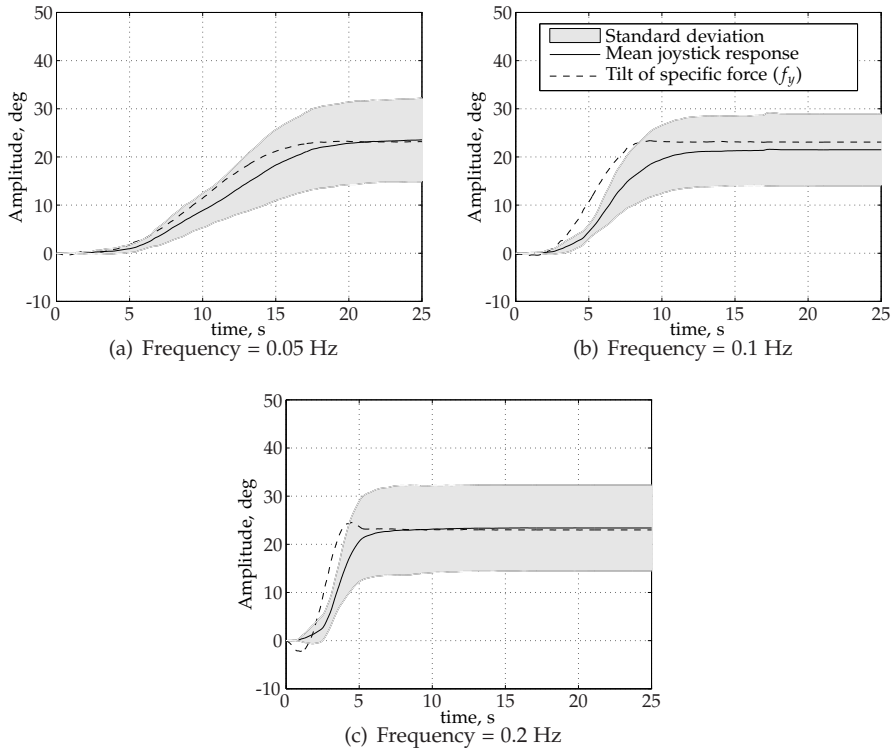
Figure 3.4: *Mean joystick response between the six subjects and the respective roll tilt of the specific force in relation to the subjects' spinal axis for the three different motion profiles. The shaded area represents the standard deviation. The roll response for each subject (used to calculate the between subjects mean response) was obtained by averaging over the seven repetitions.*

tained for the two models. The different frequencies also had no effect on the VAF. The mean VAF was 98.01%.

Figure 3.5 also shows the mean of the estimated parameters (gain and time constant) across subjects for the two tested otolith models. The results show that the time constants obtained for both models are on the order of seconds. An ANCOVA showed a main effect both of the frequency ($F = 16.29$, $p = 0.000$) and otolith model ($F = 15.93$, $p = 0.000$) on the time constant value. The average values for the unit gain otolith model were 2.04, 1.75, and 1.30 s for the 0.05, 0.1, and 0.2 Hz frequencies, respectively. For the model with otolith dynamics, the average time constants were 2.60, 2.36, and 1.90 s for the conditions with 0.05, 0.1, and 0.2 Hz, respectively.

The ANCOVA showed no effects of the otolith model and frequency on the

perceived amplitude gain. Figure 3.5(c) shows that the amplitude gain was around one for all conditions.
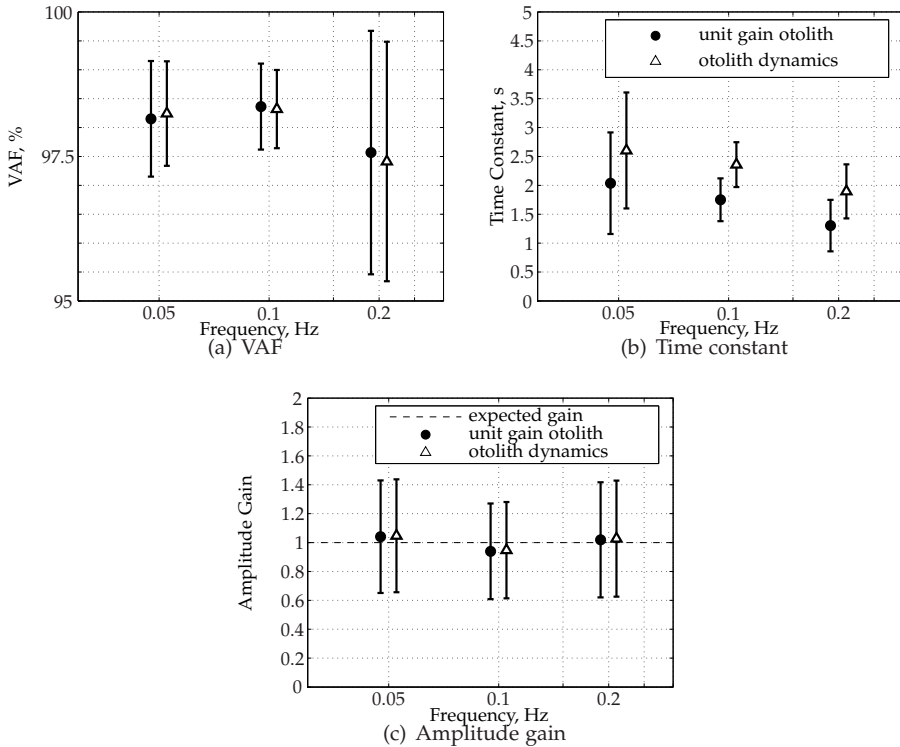
Figure 3.5: *Parameters obtained from the least squares fitting procedure for both tested models. In the plots, we show the mean parameters. The vertical lines represent the 95% confidence intervals. The mean VAFs are also shown in this figure.*

3.4   Discussion

In this study, we investigated the time constant of the somatogravic illusion without confounding by semicircular-canal stimulation. This was achieved by pre-rotating the cabin on the centrifuge axis to constant angular velocity, and subsequently moving the cabin to an eccentric position. We found a time constant on the order of seconds, rather than tens of seconds, as often found in studies using fixed-radius centrifugation (e.g., [31,33,72,96,97,100,101]). In fact, Merfeld et al. [72] showed this experimentally in a study where fixed-radius centrifugation was compared with variable-radius centrifugation for the same

subjects. The sensation of tilt changed more rapidly in the experimental conditions using variable-radius centrifugation, which showed that the semicircular-canals influenced the time constant of the somatogravic illusion during fixed-radius centrifugation. In that study, the observed time constant was between 15 and 28 s (depending on the subject orientation in the centrifuge cabin) for the fixed-radius condition. Although the authors showed that the "sensation of tilt changed substantially more rapidly" for the variable-radius condition, a value for this time constant was not reported. The influence of the semicircular-canals in the time constant of the somatogravic illusion during fixed-radius centrifugation was also shown with a theoretical model by Bos and Bles [51]. Using the Mayne equation, they showed that the somatogravic illusion would take longer if the centripetal acceleration was generated while the yaw canals were still signaling angular motion (like in fixed-radius centrifugation). Therefore, our results support the hypothesis that the angular acceleration inherent to fixed-radius centrifugation may interfere with the pure otolith-induced somatogravic illusion, as suggested in other studies [51, 61, 72].

The estimated time constant of the somatogravic illusion in this experiment was around 2 s. This value is comparable with what was found in other studies in the literature [51, 62, 102]. In Bos and Bles [51], the time constant of Equation (3.5) ranged between 1 and 2.8 s. This value is similar to what was found in our study despite the use of different techniques to generate linear acceleration. Merfeld et al. [62] also used variable-radius centrifugation and a linear sled to obtain the perceived roll-tilt for different sinusoidal profiles. Here, 7 different sinusoidal profiles with a fixed amplitude and frequency ranging from 0.005 to 0.7 Hz were used to generate pure tilt motion and pure linear motion. The motions were used to fit two self-motion perception models. The linear motion data were fitted to a low-pass filter with a time constant of 2.3 s. Although the motion profiles used in Merfeld et al. [62] were sinusoidal, the time constant he found is similar to the one we found with sustained linear accelerations. Seidman et al. [61] measured a time constant of 7 s using variable-radius centrifugation. However, their motion profile was along a different direction, with a different amplitude and frequency. The human ability to detect linear motion was found to depend on the direction of motion [103, 104]; therefore, it is reasonable to consider an effect of the degree of freedom on the time constant of the somatogravic illusion. In all studies referred before, researchers found a single time constant for the somatogravic illusion. However, our study found that this time constant varied with the frequency content of the motion profiles. Implications of this result on current self-motion perception models are shown in the next subsection.

3.4.1   The Mayne equation

The main time constant of the somatogravic illusion was obtained by fitting the Mayne equation [30, 51] to the measured experimental data. We considered two different otolith dynamics when fitting the data: the simplified unit gain dynamics used in some studies [50, 51] and the dynamic model fitted by Hosman [48]. For the three different measured frequencies, the mean VAF of the fitted Mayne equations were above 95%. This means that the models used were able to predict on average more than 95% of the subjects' responses.

When considering the otolith physiology, it is reasonable to consider an otolith model with dynamics [48]. The extra dynamics of this model are used to model high-frequency behavior found in humans and animals [48,52,78,89,105]. In this study, we introduced this model to observe if the frequency dependency of the time constant could be explained by the extra dynamics. However, results showed the same frequency dependency in both models. Although the time constants from the two models have different values, the characteristics of Equations (3.7) and (3.8) are similar around the motion profile frequencies (0.05 to 0.2 Hz). The model of Equation (3.8) needs time constants 0.6 s higher to compensate for the increased gain introduced by the extra dynamics.

These results show that the models used are not yet able to completely describe the somatogravic illusion. The models would describe the roll-tilt illusion if the time constants were equal for the different tested frequencies. However, it seems that the time constant decreases for motion profiles with higher frequency content. Therefore, it is necessary to include a mechanism to update the time-constant value. The data used in this study are not enough to estimate this mechanism since only six subjects participated in the study, the amplitude was fixed for all motion profiles, and the tested frequencies were low. The frequency range should be more than one decade to better understand the model structure in the frequency domain. In the authors' opinion, one option to account for this dependency could be to assume an internal model [50, 51] or a Kalman filter operating in the central nervous system. Then the Kalman gain may be frequency dependent so as to optimize the tilt-translation disambiguation. However, this frequency dependent mechanism is not described yet in current self-motion perception models [55, 60–62, 73, 92].

3.4.2   Practical consequences

The modeling of the somatogravic illusion is crucial for the simulation field where linear accelerations have to be scaled down and are of limited duration due to the physical limitations of motion simulators. Currently, techniques like tilt coordination [13] use the gravity vector to simulate the total specific force vector. In this technique, researchers tilt the simulator cabin to match

the direction of the gravity vector with the direction of the total specific force vector. A rate limiter is used to ensure that the cabin rotations are not perceived by the pilot. However, this rate limiter may create delays perceived by the pilot, which may compromise the simulation realism. Instead of trying to create an unperceived rotation, the technique we propose assumes that humans perceive tilt when subject to linear acceleration and tries to use that knowledge to induce the same tilt perception by tilting the simulator platform without the use of any rate limiter. Therefore, improvements in this self-motion perception model, like including an internal model to deal with the frequency dependency, would directly lead to improvements in motion simulation.

3.5   Conclusion

In this study, we used variable-radius centrifugation to study the time constant of the somatogravic illusion. Our results showed that this time constant is on the order of two seconds for lateral accelerations. This result seems congruent with other studies where linear acceleration was isolated from angular motion. Although the Mayne equation accurately fitted the measured data, it cannot explain the frequency dependency of the time constant. Introducing high-frequency dynamics in the model neither improved the model fit nor explained the frequency dependency. Therefore, this model needs to be augmented with a mechanism to deal with the frequency dependency of the time constant. Implementing an internal model in the Mayne equation could be a solution to deal with this frequency dependency. With this study, we conclude that the time constant of the somatogravic illusion is on the order of seconds and is dependent on the motion profile frequency content. This study not only improved the fundamental knowledge regarding the somatogravic illusion, but also suggested improvements to the self-motion perception models which ultimately will improve applications using these models, like motion cueing research.

Chapter 4

Perceived translation due to specific force in the dark

Chapter 3 measured how humans perceive tilt when subject to a sustained linear acceleration in the dark. However, an acceleration creates not only a tilt percept but also a translation percept. These two percepts are shown to depend on the frequency of the inertial motion profile. The translation percept has not been, however, studied in detail. Therefore, in this chapter we measure how humans perceive linear displacement and velocity when subject to a sinusoidal specific force in the lateral direction.

4.1   Introduction

Perception of linear self-motion is essential for spatial-orientation and loco-motion [31]. To create an estimate of self-motion, the central nervous system (CNS) processes information from different sensory systems such as the vestibular, visual and somatosensory systems [31, 32, 79]. Although the visual and somatosensory systems are important for self-motion perception, in this study we focused solely on modeling the vestibular system. However, in healthy subjects the perception of motion with the somatosensory system cannot be dissociated from the perception of motion with the vestibular system and therefore, the results here obtained might have been influenced by the somatosensory system. The vestibular system is composed of the otoliths, which respond to linear motion [30, 52], and the semicircular-canals, which respond to angular motion [106]. Both the input and output of the otolith organs are related to specific force, defined as the vectorial sum of linear accelerations due to self-motion and those due to gravity [51]. Here, Einstein's equivalence principle [54] implies that the otolith organ cannot, by itself, discriminate between these two types of acceleration. However, humans are able to estimate tilt, which is related to gravity and are able to estimate translation, which is related to linear inertial acceleration [30, 51]. Therefore, to generate these tilt-translation percepts, the CNS cannot solely use the otolith's sensory information. This led to the study and creation of human self-motion perception models explaining how the CNS obtains these tilt-translation responses [30, 51, 55, 61–63, 73, 92].

In 1974, Mayne [30] proposed a two-dimensional model to explain how humans discriminate between gravity and linear self-acceleration. This model was later improved to a three-dimensional model by Bos and Bles [51]. In this model, the signals from the vestibular system are combined and a low-pass filter is used to separate the specific force into a gravity and a self-motion linear acceleration estimate. Several studies measuring tilt perception showed that the tilt estimate could be accurately derived from the gravity estimate predicted by human self-motion perception models [61, 62, 72, 107]. In these studies, researchers measured the perceived tilt (e.g., by using a joystick) and compared it with the model predictions. However, it is unclear if the linear acceleration estimate due to self-motion is correctly derived from this model since, on the one hand, it cannot be directly measured, and on the other hand, there are few studies investigating human translation perception [62].

Although humans do not seem able to estimate their perceived linear acceleration [51, 63], they seem capable to estimate their linear displacement [62, 108]. For example, Wright et al. [108] conducted an experiment where participants estimated their peak-to-peak displacement without any difficulties during an experimental condition without visual displays. Unfortunately, the task was performed with a sinusoidal motion profile with a single frequency so little

can be said about the dynamic behavior of the linear displacement estimation. In another study, Merfeld et al. [62] measured peak-to-peak displacement for motion profiles with different frequencies. The results were surprising because subjects reported peak-to-peak displacement estimates that were qualitatively similar to peak-to-peak acceleration estimates predicted by the self-motion perception model used in their study, as if the acceleration estimates predicted by the model were not integrated to yield the displacement estimates reported by the subjects.

To perceive linear displacement, the self-motion linear acceleration estimate has to be integrated twice, first into a linear velocity estimate, and only then, into a displacement estimate. According to some researchers [62, 63] this displacement estimate is not obtained by simple integrations, but by a leaky integration. However, the studies that measured this leaky integrator used off-vertical-axis rotations [73, 109], which stimulate not only the otoliths but also the semicircular-canals, shown to affect motion perception [51, 72], or fitted the model with experimental data obtained via vestibular-ocular reflex responses [72, 73, 109], shown to differ from verbal responses [62, 92].

The aim of this study is, therefore, to investigate how humans perceive displacement when subject to mere linear motion. Additionally, we will investigate if humans can give an estimate of their linear velocity since, to our knowledge, no study measured this percept experimentally. Moreover, linear velocity is important when being combined with visual cues [63], specifically known to code for velocity [37, 110]. To reach this aim, an experiment was conducted at the Desdemona research simulator where subjects had to estimate the peak-to-peak displacement and maximum velocity of a sinusoidal lateral motion.

4.2   Method

4.2.1   Subjects

Seventeen paid volunteers participated in this experiment (11 male and 6 female). The subjects had an average age of 39 years with a standard deviation of 14 years. None of the subjects had any self-known vestibular or motor skill deficit. The experiment was approved by the local ethics committee, following the Declaration of Helsinki on ethical principles for medical research involving human subjects.

4.2.2   Apparatus

The experiment was conducted at the Desdemona research simulator (see Figure 4.1) located at the TNO institute in Soesterberg, the Netherlands. This simu-

lator features a centrifuge based design with six degrees-of-freedom (DoF) [29]. In this study, only the 8-meter horizontal actuator of the simulator was used to generate lateral sinusoidal motion. The velocity and acceleration limits of this actuator are 3.2 m/s and 4.9 m/s^2, which together with the 8 m displacement limit, constrain the experimental conditions described below.
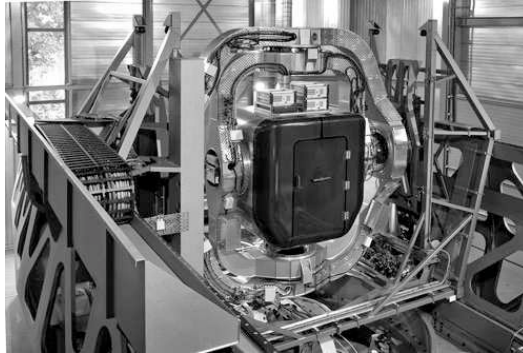
Figure 4.1: *Desdemona research simulator.*

4.2.3 Experimental Design

In previous studies, researchers have kept the linear acceleration constant when studying the effect of frequency on perceived linear motion [51, 62] because the output of the otolith organs is assumed proportional to specific force [52]. However, researchers asked subjects to report their perceived linear motion in terms of displacement. In that case, conclusions on the dynamics of perceived displacement will thus be confounded by the dynamics of the stimulus itself, as shown in Figure 4.2.

Since the main goal of this study is to investigate displacement perception, we therefore kept the displacement amplitude across the different motion profiles constant instead of the acceleration amplitude. As a result, any frequency effect on perceived displacement will be the consequence of a perceptual mechanism. However, these motion signals are difficult to generate in a simulator because for low frequencies, the accelerations used as input by the vestibular system are small and might be sub-threshold [89], whereas for high frequencies, the accelerations will be above the simulator limits. Figure 4.2 shows the accelerations involved when designing a 1 m sinusoidal motion profile over a certain range of frequencies.

Six different motion profiles were used in this experiment. The motion profiles were generated based on lateral sinusoidal profiles with two amplitudes, 0.5 and 1 m, and three frequencies, 0.1, 0.2, and 0.3 Hz. This frequency range
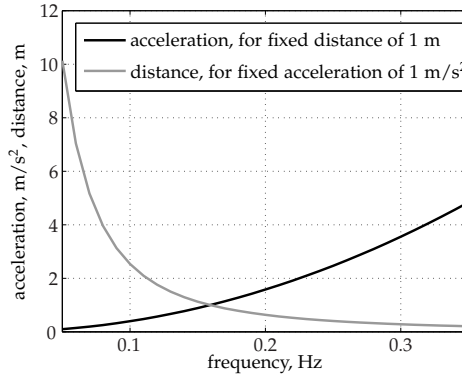
Figure 4.2: *Linear acceleration and displacement across the frequency for constant acceleration and constant displacement profiles.*

encloses frequencies where humans perceive both tilt and translation, as shown previously [107]. Additionally, these amplitude/frequency combinations were above the measured acceleration threshold (0.06 m/s² for lateral motion [89]) and below the simulator linear acceleration limits since the acceleration amplitude of the motion profiles ranged from 0.20 to 3.55 m/s². This means that there were a total of six (2 amplitudes × 3 frequencies) experimental conditions. Each experimental condition was conducted three times, meaning a total of 18 experimental runs per subject. The experimental runs were randomized over all subjects using a latin square design.

4.2.4 Motion profiles

Figure 4.3 shows the six motion signals used in this experiment. To prevent any discomfort, damage, and discontinuities, the simulator started and stopped with zero position, velocity, and acceleration, by means of a fade-in and fade-out phase function, $fade(t)$, as shown below:

$$a(t) = A \sin(2\pi f t) \times fade(t) \tag{4.1}$$

with:

$$fade(t) = \begin{cases} \frac{1}{2} - \frac{1}{2}\cos(\pi f t), & 0 < t \leq T \\ 1, & T < t \leq (N+1)T \\ \frac{1}{2} - \frac{1}{2}\cos\left(\pi f(t-T)\right), & (N+1)T < t \leq (N+2)T \end{cases} \tag{4.2}$$

and T the period of the signal and N the number of periods not affected by

(a) f = 0.1 Hz   (b) f = 0.2 Hz   (c) f = 0.3 Hz
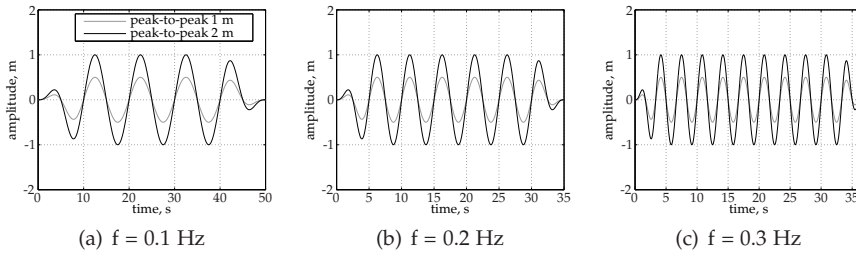
Figure 4.3: *Example of the motion signals for the two different amplitudes and three different frequencies.*

fade-in/out. Per stimulus frequency, a compromise was made between total signal time and number of periods. Keeping one variable fixed would result in an undesirable variation of the other. Therefore, N was 3, 5, and 9, respectively for the 0.1, 0.2, and 0.3 Hz motion signals, as also shown in Figure 4.3.

4.2.5   Procedure

Before entering the motion simulator, subjects were briefed on the purpose of the experiment and an 8 meter line was shown on the floor of the briefing room with 1 meter marks to facilitate their estimates during the experiment. Subjects were not informed of the size of the simulator horizontal actuator.

After reading the briefing and signing the informed consent, subjects were seated inside the simulator cabin and strapped with a 5-point safety belt. A headset with active noise reduction was used to minimize the effect of audio cues due to the simulator's actuators. White noise was added to mask the remaining sound. This headset was also used for communication purposes. Inside the cabin there was a picture displaying a typical road lane-width in the Netherlands (4 meters peak-to-peak) to help subjects during the peak-to-peak estimation task. There was also a scale showing typical vehicles' speeds, as shown in Figure 4.4.
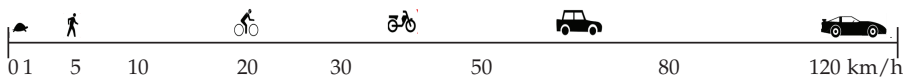
Figure 4.4: *Typical vehicle's speeds scale used to help subjects estimating their maximum linear velocity.*

The experiment started with a reference condition over 2 meters at 0.2 Hz with 7 periods in which subjects were informed of their lateral peak-to-peak displacement (4 meters) and peak velocity (9 km/h). During the experimental

conditions, subjects had to keep their eyes closed and were only allowed to open them when they heard a beep presented at the end of the run. After this beep, they reported their perceived peak-to-peak lateral displacement and their maximum lateral velocity. Additionally, to monitor the subjects' well being, their MIsery SCore (MISC) [9] was reported (see Table 4.1). The experiment stopped when subjects reported their perception for all experimental conditions and their repetitions. Including briefing and debriefing, the experiment took around one hour per subject.

Table 4.1: *The MIsery SCore (MISC) rating scale used to measure motion sickness [9]*

Symptom		MISC
No problems		0
Slight discomfort but no specific symptons		1
Dizziness, warm, headache, stomach awareness, sweating, etc.	Vague	2
	Some	3
	Medium	4
	Severe	5
Nausea	Some	6
	Medium	7
	Severe	8
	Retching	9
Vomiting		10

4.2.6   Data analysis

The reported peak-to-peak displacements and maximum velocities were averaged across subjects for the six different experimental conditions (2 amplitudes $\times$ 3 frequencies). A repeated measures ANOVA was used to test if there was an effect of the frequency or amplitude on these estimates. A Greenhouse-Geisser (G-G) correction was applied whenever sphericity was violated. As a consequence, the corrected p values are more conservative. All statistical tests were performed with SPSS 19.

Additionally, for each subject we averaged their reported peak-to-peak displacement and maximum velocity estimates within each frequency. Then, we divided the higher amplitude condition by the lower amplitude condition to obtain individual motion ratios. These ratios were then averaged across subjects and a one-sample t-test was performed to check if the average motion ratio was significantly different from 2, which was the stimulus ratio between the two amplitudes used to generate the motion profiles. This allows to test if the perceived increase of the motion profiles' amplitude is similar to the actual amplitude increase.

4.3   Results

This section starts with the results for the estimated peak-to-peak linear displacements, which are then followed by those for the maximum velocity. At the end we will compare the displacement with the velocity results.

4.3.1   Perceived linear displacement

When analyzing the peak-to-peak linear displacements across all subjects, we observed a significant main effect of the different stimulus amplitudes but not of the frequency. A frequency effect would be expected due to the effect of the perceptual high-pass filter assumed essential for estimating linear self-motion [30, 51]. Focusing on the individual data revealed that the peak-to-peak estimates increased with the frequency for some subjects and decreased with the frequency for others. To objectively discriminate between these behaviors, we averaged the two different amplitude estimates per frequency and applied a linear regression on these averages for each subject separately. The resulting slopes revealed that 12 subjects had an increasing trend with the frequency, 4 subjects had a decreasing trend with the frequency and 1 subject had a slope close to zero. Figure 4.5 shows the average peak-to-peak displacement estimates for the subjects with increasing and decreasing trends, without the one subject who showed no trend. Two repeated measures ANOVAs were conducted, one for each group, with results shown in Table 4.2.
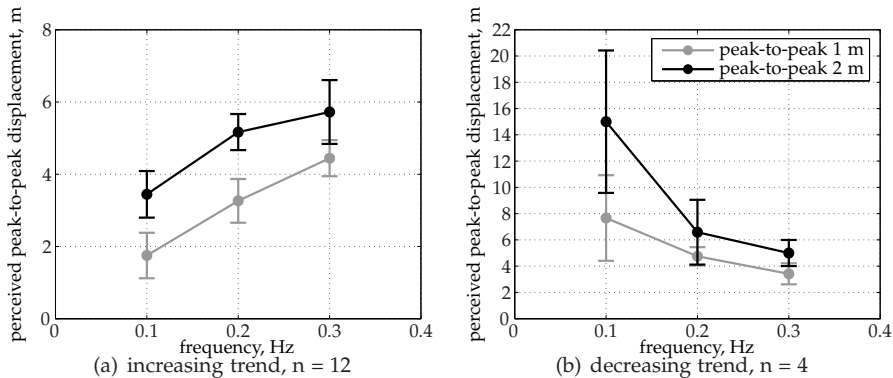
Figure 4.5: *Average peak-to-peak displacement estimates for the two different subjects groups and their 95% confidence intervals.*

Figure 4.5 shows that both groups had higher peak-to-peak estimates during the 2 m peak-to-peak motion profiles. This was statistically significant for both groups as was the frequency effect (Table 4.2). For the subject data shown

Table 4.2: *Repeated measures ANOVA results for the linear displacement estimates for the two different subject's groups*

Trend	Independent Variables	Correction	F-ratio	p
Increasing	Amplitude	-	F(1,24) = 53.13	0.000
	Frequency	G - G	F(1.4,32.6) = 24.83	0.000
Decreasing	Amplitude	-	F(1,8) = 12.80	0.007
	Frequency	G - G	F(1.2,9.4) = 12.59	0.001

in Figure 4.5(a), a post-hoc test using a Bonferroni correction, a method used to account for the statistical errors introduced by multiple comparisons [90], revealed that the 0.1 Hz estimates were significantly lower than the 0.2 Hz ($p = 0.000$) and 0.3 Hz ($p = 0.000$) estimates and that the 0.2 Hz estimates were significantly lower than the 0.3 Hz ($p = 0.008$) estimates. For the data shown in Figure 4.5(b), the 0.1 Hz estimates were significantly higher than the 0.2 Hz ($p = 0.048$) and 0.3 Hz ($p = 0.009$) estimates, with no difference between the 0.2 Hz and 0.3 Hz estimates ($p = 0.151$). For both groups, the ratio between the 1 and 2 m conditions averaged over all frequencies and subjects was approximately 1.7. However, this ratio was not statistically different from the stimulus ratio of 2, both for the increasing trend ($t(11) = -2.06, p = 0.064$) and decreasing trend ($t(3) = -0.817, p = 0.474$) groups.

4.3.2 Perceived linear velocity

The perceived linear velocity results were divided into the same two groups shown in the previous section. Figure 4.6 shows the average maximum velocity estimates for the subjects with increasing and decreasing trends, again without the one subject who showed no trend in the displacement estimate. Two repeated measures ANOVAs were conducted, one for each group, with results shown in Table 4.3.

Table 4.3: *Repeated measures ANOVA results for the linear velocity estimates for the two different subject's groups*

Trend	Independent Variables	Correction	F-ratio	p
Increasing	Amplitude	-	F(1,24) = 50.91	0.000
	Frequency	G - G	F(1.3,31.4) = 187.59	0.000
	Amplitude × Frequency	-	F(2,48) = 6.35	0.004
Decreasing	Amplitude	-	F(1,8) = 31.52	0.001
	Frequency	G - G	F(1.3,10.0) = 21.71	0.001
	Amplitude × Frequency	G - G	F(1.0,8.3) = 6.53	0.032

The maximum velocity estimates were significantly affected by the frequency and amplitude of the motion profiles (Table 4.3). Figure 4.6 shows that for both
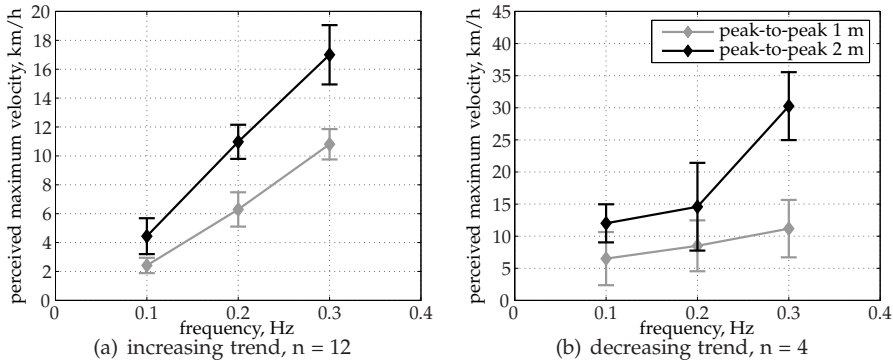
Figure 4.6: *Average maximum velocity estimates for the two different subjects groups and their 95% confidence intervals.*

groups, the velocity estimates were higher for the motion profile with higher amplitude and that they increased with the frequency. For the increasing trend group (Figure 4.6(a)), a post-hoc test using a Bonferroni correction showed that the 0.1 Hz estimates were significantly lower than the 0.2 Hz ($p = 0.000$) and 0.3 Hz ($p = 0.000$) estimates and that the 0.2 Hz estimates were significantly lower than the 0.3 Hz ($p = 0.000$) estimates. For the decreasing trend group (Figure 4.6(b)), there was no significant difference between the 0.1Hz and 0.2Hz estimates ($p = 0.339$) whereas the 0.3 Hz estimate was significantly higher than the 0.1 Hz ($p = 0.000$) and 0.2 Hz ($p = 0.017$) estimates. Additionally, there was a significant interaction between the amplitude and frequency of the motion profiles due to the 2 m velocity estimates increasing more steeply than the 1 m estimates do. The ratio between the 1 and 2 m conditions averaged over all frequencies and subjects was 1.7 and 2.1 for the increasing trend and decreasing trend groups, respectively. The ratio differed statistically from the stimulus ratio of 2 for the increasing trend group ($t(11) = -3.59, p = 0.004$) but not for the decreasing trend group ($t(3) = 0.538, p = 0.628$).

4.3.3   Linear displacement versus velocity

To avoid comparing velocity with distance units, we transformed the velocity estimates into predicted displacement estimates by mere integration over time. Figure 4.7 shows the observed and predicted estimates. For both groups, it can be seen that the observed estimates are in the same order of magnitude as the predicted estimates, which was confirmed by a repeated measures ANOVA showing no significant difference both for the increasing trend ($F(1, 24) = 3.68, p = 0.067$) and decreasing trend ($F(1, 8) = 0.84, p = 0.387$) groups. How-

ever, for both groups we found a significant interaction between the two estimates (predicted and observed) and the frequency ($F(1.2, 28.9) = 6.32, p = 0.014$ for the increasing trend group and $F(1.2, 9.7) = 6.51, p = 0.025$ for the decreasing trend group). This implies that the effect of frequency on the observed estimates is different from that on the predicted estimates.
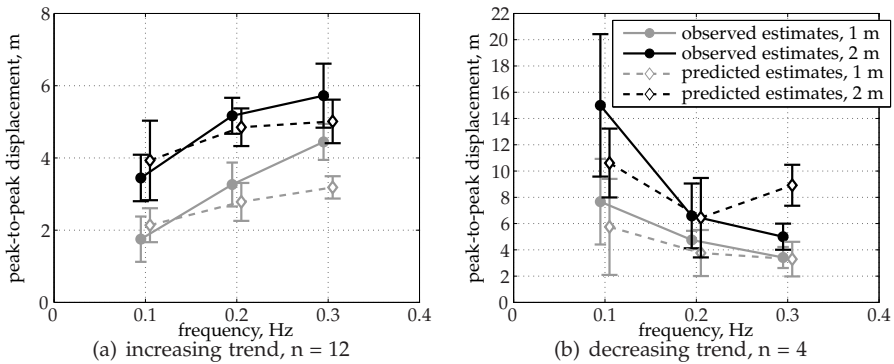
Figure 4.7: *Average observed and predicted displacement estimates for the two different subjects groups. The error bars represent the 95% confidence intervals.*

Due to this significant interaction, we conducted individual repeated measure ANOVAs on the predicted estimates for both groups. For the increasing trend group, a post-hoc test using a Bonferroni correction revealed that the 0.1 Hz estimates were significantly lower than the 0.2 Hz ($p = 0.002$) and 0.3 Hz ($p = 0.005$) estimates but showed no difference between the 0.2 Hz estimates and 0.3 Hz ($p = 0.362$) estimates. For the decreasing trend group, the post-hoc test showed that the 0.1 Hz estimates were significantly higher than the 0.2 Hz ($p = 0.001$) estimates. However, there was no statistically difference between the 0.3 Hz estimates and the 0.1 Hz ($p = 0.506$) and 0.2 Hz estimates ($p = 1.000$).

4.4 Discussion

In this study we investigated how humans perceive linear velocity and displacement during a sinusoidal motion profile in the lateral direction. The subjects' task was to report their perceived sinusoidal peak-to-peak displacement in meters and the perceived maximum velocity in kilometers per hour. The results showed that the frequency of the motion profiles affected the linear displacement estimates differently between subjects since 12 subjects reported estimates increasing with the frequency, 4 subjects reported estimates decreasing with the frequency and 1 subject reported approximately constant estimates with the

frequency. These differences led us to divide the subjects into two groups, one with an increasing trend, and one with a decreasing trend, leaving out of the analysis the one subject with a constant estimate across the frequency.

The data of the group showing an increasing trend seems to confirm what has been reported before, where several studies [30, 51, 62] showed that the perception of linear self-motion follows high-frequency dynamics, which means that translation estimates during low frequency motion are attenuated with respect to high-frequency translation estimates. However, the estimates reported by the decreasing trend group have never been reported. In this group, the estimated low-frequency displacements were higher, instead of lower, than the high-frequency displacement estimates. These results could be related to previous knowledge on vehicle behavior from these subjects. Since the low-frequency motions last longer than the high-frequency motions, these subjects could have cognitively inferred that the displacement for the low frequency motions would also be higher than the displacement for the high frequency motions. An effect of previous knowledge on linear motion perception was already suggested by Wertheim et al. [111]. However, these cognitive effects are difficult to model because they vary considerably from person to person.

For that reason, the remaining of the discussion section will focus in the results of the increasing trend group. The linear displacement results showed that subjects overestimated their peak-to-peak displacement, with the 1 m peak-to-peak motion profile perceived as being approximately 3 meters and the 2 m peak-to-peak motion profile as approximately 5 meters. This contradicts the observations by Wright et al. [108] showing displacement estimates lower than the physical displacements. This, however, concerned vertical motion which may explain the difference since different sensitivities have been found for different degrees-of-freedom [103, 104]. For lateral motion, Merfeld et al. [62] reported underestimated perceived displacements for sinusoidal profiles with frequency ranging from 0.05 to 0.2 Hz and overestimated displacements from 0.5 to 0.7 Hz. However, only the 0.7 Hz motion profile was generated with lateral linear motion, similar to the motion profiles shown in this study, whereas all the other motion profiles were generated using a variable-radius centrifuge technique, which can introduce motion percepts in different degrees-of-freedom due to the coriolis acceleration. Additionally, the diameter of the centrifuge used to generate the motion profiles in the study of Merfeld et al. [62] was much smaller than the peak-to-peak displacement integrated from the total lateral acceleration, which in that case was the sum of the centripetal and radial accelerations. Similar to what we found in the decreasing trend group, or as found by Wertheim et al. [111], the results of Merfeld et al. [62] may have been affected cognitively by knowledge on the apparatus, for example.

Both the perceived peak-to-peak displacement and maximum velocity had

ratios between the 1 and 2 m conditions smaller than 2, which is the stimulus ratio. This difference was significant for the maximum velocity estimates and on the verge of significance for the peak-to-peak displacement estimates. This could indicate that the perceived intensity does not increase in the same proportion as the physical intensity, as showed by Stevens for brightness [112] and heaviness [113], where the intensity could be accurately modeled by a power law. This leads to the need of studies investigating the relation between the inertial amplitude and its perceived intensity, like for example, the study conducted by Zaichik et al. [103].

Surprisingly, the displacements calculated by integrating the estimated velocities over time, defined as predicted displacement estimates, were all in the same order of magnitude as were the actually observed displacements. Although these peak-to-peak displacements were similar in amplitude, their frequency behavior is different as shown by the significant interaction between the estimates (observed and predicted) and the frequency. The observed displacements increased with the frequency whereas the predicted displacements showed an increase from the 0.1 to the 0.2 Hz motion profiles but remained constant from the 0.2 to the 0.3 Hz motion profiles, showing that humans do not conduct a simple integration from linear velocity to displacement. This behavior was modeled in the next subsection.

4.4.1   A perception model

Following the work of Mayne [30], Bos and Bles [51] developed a 3-dimensional equation to describe how the central nervous system (CNS) discriminates from linear accelerations due to self-motion and those due to gravity:

$$\frac{d\tilde{g}}{dt} = \frac{1}{\tau}(f_{oto} - \tilde{g}) - \omega_{scc} \times \tilde{g}, \tag{4.3}$$

where f_{oto} is the specific force signal given by the otolith afferents, ω_{scc} is the angular velocity signal given by the semicircular-canal afferents, τ is the time constant of a low-pass filter operating on the otolith afferents, and $\tilde{g}$ is the estimate of acceleration due to gravity as taken by the CNS. The estimation of the linear acceleration due to self-motion can then be given by the difference between the otolith-measured specific force and the estimated acceleration due to gravity ($\tilde{a} = f_{oto} - \tilde{g}$). Since in this experiment there was no stimulation of the semicircular-canals, the perception of linear self-motion in the dark can be modeled by the block diagram in Figure 4.8.

Although it seems accepted in the literature [30,51,61,62,72] that humans create a self-motion linear acceleration estimate ($\tilde{a}$), it is unclear how this estimate is transformed into a velocity ($\tilde{v}$) and displacement ($\tilde{D}$) estimate. It is unknown whether the velocity estimate is obtained by simple integration or by leaky in-
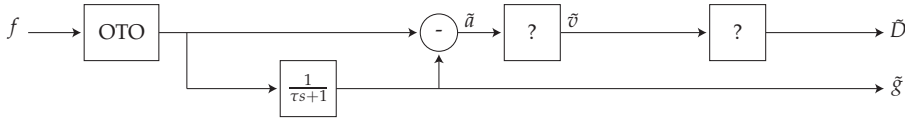
Figure 4.8: *Self-motion perception model for linear motion in the dark.*

tegration as suggested in the literature [62,63,73,114]. The same questions arise when transforming the velocity in a displacement estimate. These unknowns are illustrated in Figure 4.8. Using the predicted and observed displacement estimates, we will propose a model on how the perceived linear acceleration is transformed in perceived velocity and displacement. The predicted estimates, which are related to linear velocity, seem to have high-pass filter characteristics since the low frequency estimates are attenuated when compared to the higher frequency estimates, which remain constant. This seems to indicate that the predicted estimates are obtained from mere integrations over time of the linear acceleration estimates. Based on this and if we assume no otolith end-organ dynamics (represented by a unit gain [50,51]), the perceived lateral linear acceleration of Figure 4.8 can be written as:

$$\tilde{a}_y = \frac{\tau s}{\tau s + 1} a_y \quad \leftrightarrow \quad \tilde{D}_y = \frac{\tau s}{\tau s + 1} D_y, \tag{4.4}$$

where a_y is the physical lateral acceleration, and $\tilde{a}_y$ is the perceived lateral acceleration. By integrating the perceived and physical accelerations over time we obtain D_y, which is the stimulus peak-to-peak displacement used in the experiment ($a_y = s^2 D_y/2$), and $\tilde{D}_y$, which is the perceived peak-to-peak displacement ($\tilde{a}_y = s^2 \tilde{D}_y/2$), in this case represented by the predicted displacement estimates[1]. Because the predicted displacements behaved linearly with stimulus amplitude, as they should according to Equation (4.4), we averaged the predicted displacement estimates over the two amplitudes of the motion profiles. Equation (4.5) shows the transfer function used to estimate the time constant from the predicted data, where a gain K is used to compensate for the amplitude errors introduced by averaging the data. The estimate of τ (and K) was obtained by minimizing the error between the averaged predicted estimates and the peak-to-peak displacements given by the model. The Variance Accounted For (VAF) was used to evaluate the quality of the fit.

$$\frac{\tilde{D}_y}{D_y}(s) = H_{Dv}(s) = \frac{\tau s}{\tau s + 1} K \tag{4.5}$$

---

[1]The reader should note that the same analysis could be done by using the velocity data of Figure 4.6(a) and $\tilde{a}_y = s\tilde{v}_y$. However, to keep everything in displacement units, we used the predicted displacement estimates.

Figure 4.9 shows the magnitude plot of H_{Dv}, with the parameters obtained from the minimization procedure listed in Table 4.4. The magnitude of Figure 4.9 was obtained by applying a logarithm transformation to the model magnitude ($20 \log(|H_{Dv}|)$).

Figure 4.9: *Model fitted to the average peak-to-peak linear displacements obtained from the predicted displacement estimates.*

Table 4.4: *Parameters obtained for the $H_{Dv}(s)$ model*

K	τ [s]	VAF [%]
4.31	1.57	99.83

The time constant obtained in this fit is in the same order of magnitude of the one we found for tilt perception induced by a sustained linear acceleration [107], which ranged from 1.30 to 2.04 seconds. This therefore seems to confirm that the mechanism responsible for disambiguating the tilt-translation percept is the same, as hypothesized by Mayne [30], and shown to be plausible by Bos and Bles [51]. Additionally, it seems to indicate that our central nervous system (CNS) transforms the perceived acceleration ($\tilde{a}_y$) into a perceived velocity by a simple integration. This model, however, predicts that humans would perceive a lasting velocity percept when subject to a constant linear acceleration, like with a centripetal acceleration generated by a centrifuge. This lasting velocity percept was never observed before in centrifuge studies [63]. Still, this result is based on personal observation since this percept was not studied in detail. Because the model developed here seems to correctly explain the measured data and other observed motion profiles, like the acceleration pulse example discussed in Bos et al. [63], we assume for now that a simple integrator suffices when transforming perceived linear acceleration into perceived linear velocity in dynamic conditions as studied here.

Our results also showed that the predicted displacement estimates were different from the observed displacement estimates. This means that the linear displacement percept cannot be obtained by simply integrating the velocity percept. Therefore, we hypothesize that the displacement percept is obtained by leaky integration from the velocity percept, as shown in Figure 4.10, where a first order high-pass filter is used to describe this leaky integration.
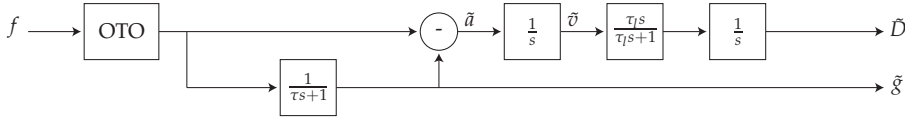
Figure 4.10: *Self-motion perception model for linear motion in the dark.*

Using the structure of Figure 4.10, the perceived peak-to-peak displacement is given by Equation (4.6), where τ_l is the time constant of the leaky integrator.

$$\tilde{D}_y = \frac{\tau s}{\tau s + 1} \frac{\tau_l s}{\tau_l s + 1} D_y \tag{4.6}$$

We can estimate the leaky time constant by fitting the observed displacement estimates. Similar to what was done to the predicted estimates, we averaged the observed displacement estimates over the two amplitudes of the motion profiles and fitted the transfer function of Equation (4.6), shown by Equation (4.7), where τ and K are fixed parameters with the values shown in Table 4.4, and τ_l and K_l are the parameters obtained from the minimization procedure.

$$\frac{\tilde{D}_y}{D_y}(s) = H_{Dd}(s) = \frac{\tau s}{\tau s + 1} K \frac{\tau_l s}{\tau_l s + 1} K_l \tag{4.7}$$

Figure 4.11 shows the magnitude plot of H_{Dd}, with the obtained parameters listed in Table 4.5. This magnitude was again obtained by applying a logarithm transformation to the model magnitude ($20 \log(|H_{Dd}|)$).
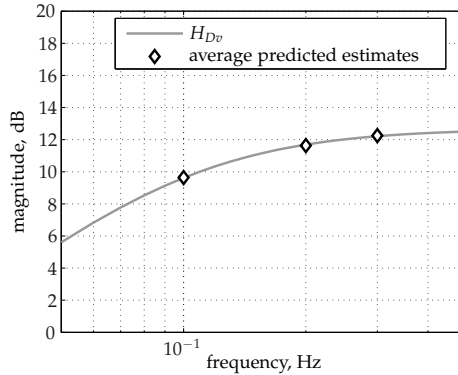
Table 4.5: *Parameters obtained for the $H_{Dd}(s)$ model*

K_l	τ_l [s]	VAF [%]
1.32	1.30	99.19

The lead time constant was similar to τ, which is in line with the study of Bos et al. [63] where they predicted a τ and τ_l of similar values. Our results show that a leaky integrator would accurately model the differences we found experimentally between the observed and predicted displacement estimates. However, the time constant found here is higher than what was found previously. For example, Merfeld and Zupan [114] used a leaky integrator with a time
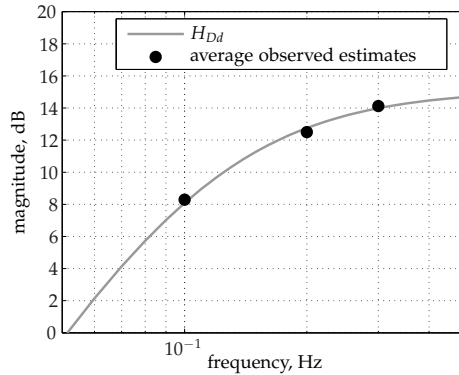
Figure 4.11: *Model fitted to the average peak-to-peak linear displacements obtained from the the observed displacement estimates.*

constant of 0.1 seconds to explain translational vestibulo-ocular reflex (VOR) responses. Vingerhoets et al. [73] found that the 0.1 seconds time constant had to be even smaller (i.e., 0.04 seconds) in order to fit their data. However, these time constants were obtained for a self-motion perception model different from the one presented here (see Figure 4.10). For a similar self-motion perception model, Vingerhoets et al. [73] found a $\tau = 0.05$ and $\tau_l = 0.68$. If we used these smaller time constants, the model would predict a displacement of approximately zero for all experimental conditions, which does not correspond with what we measured experimentally. The difference may be explained by the difference in the used measurements since self-ratings were used in this study whereas Vingerhoets et al. [73] used VOR responses, which were measurement methods already shown by other studies [62, 92] to give different results. Moreover, Vingerhoets et al. [73] used off-vertical axis rotation, which includes angular motion shown to affect motion perception [51, 72], while we used pure linear translation. We therefore assume the time constants derived from our experiment to be representative for dynamic behavior of human motion perception leading to verbal judgments in particular when perceiving translation in the dark.

4.5   Conclusion

In this study we investigated how humans perceive linear velocity and linear displacement for sinusoidal motion profiles with two fixed peak-to-peak amplitudes (1 and 2 m) and three frequencies (0.1, 0.2, and 0.3 Hz). For linear motion perception, the central nervous system has to transform the acceleration signaled by the otoliths organ into a linear velocity and displacement estimate.

This study shows that this transformation is not obtained by simply integrating the acceleration signal, as one would expect physically. The linear displacement estimate significantly increased with the amplitude and frequency of the motion profiles. Physically, one would expect the displacement to increase with the amplitude but not with the frequency since the actual simulator displacement was constant across the frequency. Similarly, the velocity estimates significantly increased with the amplitude and frequency of the motion profiles. Integrating the velocity estimates created displacements that were in the same order of magnitude of the measured displacement estimates, but with a different frequency effect. The Mayne equation could accurately model the velocity estimates, whereas for the displacement estimates a leaky integrator needed to be added to better model the transformation from velocity to displacement estimates. The fitted parameters of the Mayne equation were in the same order of magnitude as those previously found for the tilt percept induced by sustained accelerations, suggesting that this self-motion perception model can accurately describe the tilt-translation ambiguity. Additionally, we found that the linear displacement estimates of some subjects were cognitively biased. This study showed how humans perceive linear motion in the dark and presented a possible self-motion perception model to describe it. This result is a crucial first step before studying, for example, how linear motion estimation is affected by visual cues.

Part II

Visual-vestibular interactions

Optimal specific force scaling in a simulation environment

Chapters 3 and 4 investigated how self-motion perception in the dark is affected by inertial motion cues, particularly by specific forces. However, in a simulation environment humans are subject not only to the inertial but also to the visual cues delivered by the simulator displays. Previous simulator studies showed that having the same amplitude for inertial and visual cues is not always the preferred choice by subjects. Therefore, this chapter investigates what is the optimal amplitude scaling between visual and inertial cues in a simulation environment, for motion profiles with different amplitude and frequency combinations.

Authors B. J. Correia Grácio, M. M. van Paassen, M. Mulder, and M. Wentink

5.1   Introduction

In motion simulators subjects can be presented with sensory cues that represent the sensory stimulation that is experienced in a real vehicle. Part of this sensory information is provided by inertial cues generated by a motion platform. However, most vehicle motions cannot be generated in the simulator because of its physical limits. Therefore, algorithms are needed to transform vehicle inertial motion into simulator inertial motion. Such algorithms are usually referred to as Motion Cueing Algorithms (MCAs). New high fidelity motion platforms make it possible to simulate certain maneuvers one-to-one, i.e. the simulator inertial motion amplitude is equal to the vehicle inertial motion amplitude. Examples of these large amplitude platforms are the Desdemona Research simulator at TNO Human Factors in the Netherlands and the KUKA simulator at Max Planck Institute in Germany. However, several studies [74–77] showed that subjects perceive one-to-one motion in a simulator differently than in real life. Subjects in these studies reported motion to be too strong. Feenstra et al. [76] and Pretto et al. [77] conducted a car driving study where subjective measurements showed that simulator inertial motion needed to be scaled down in order to subjectively match "what was seen with what was felt". In these studies a preferred scaling factor of the inertial motion between 0.5 and 0.7 was reported. These values were obtained from paired comparisons between MCAs with different characteristics. Groen et al. [74] showed that a simulated take-off maneuver was experienced as more realistic when translational inertial accelerations were scaled down. Again a preferred motion gain of 0.7 was found. In another study by Groen et al. [75], it was shown that for a correct percept of a decrab maneuver in a simulator, the simulated sway motion had to be smaller than the actual aircraft motion. These studies directly compared the motion cues in the simulator with the motion cues of the real vehicle. Therefore, errors in the vehicle model used to generate the correct motion could influence the perceived motion cues in the simulator. Another factor that can influence the subjects' motion judgment is that the vehicle model handles differently than the vehicle subjects are used to in real-life. In the studies mentioned above, the authors did not have the objective to find a relation between the motion gain and the amplitude and frequency of the vehicle motion signal. The goal of this study is to investigate whether the motion gain used in MCAs for linear accelerations depends on the frequency and amplitude of the input motion signal.

The Desdemona research simulator was used as a platform to study which motion gain would give the best match between visual and inertial cues. Subjects were presented with lateral translational movements and they had to match the inertial information with the visual information. The use of lateral cues allows for the comparison of the obtained scaling values with previous experiments conducted in Desdemona [76,115,116] where similar motion profiles were

used. The visual information was displayed via the simulator's projectors while the inertial information was generated using the motion platform. Both signals were sinusoids with matching phase and frequency, but different amplitudes. We used six different visual profiles, each with a different combination of frequency and amplitude. The amplitude/frequency values were a compromise between the simulator limitations and human motion perception ranges that are of interest for vehicle simulation. In order to decrease the experiment duration, we developed an online tuning method where subjects could change the inertial motion amplitude in-the-loop. Classically, tuning of MCAs is conducted with an experienced subject that verbally indicates to the MCA designer how the motion is being perceived, while the designer tries to achieve the experienced subject requirements by changing values in the MCA. Our method gives full control of the tuning to the subject inside the cabin by means of a joystick. A joystick's deflection would change the inertial amplitude while the subject is experiencing it, making it easier to decide whether the experienced motion is too strong or too weak. The controlled signal was the acceleration of the motion platform since it is the signal sensed by the vestibular system [31].

The following sections describe in more detail the experimental protocol and present the experimental results. At the end, we discuss the results and present the conclusions of this study.

5.2   Method

The experimental goal was to study the relation between the inertial and visual motion amplitude that creates a realistic percept in the Desdemona simulator. The dependent variable of this study was the motion gain, which is defined by the ratio between the inertial and visual amplitude. The visual signals were designed with different frequencies and amplitudes to determine whether there was an effect of these variables on the motion gain. Therefore, the independent variables for this study were the visual amplitude, the visual frequency and the initial motion gain, which could be higher or lower than one.

5.2.1   Apparatus

We used the Desdemona research simulator (Figure 5.1) located at the TNO institute in Soesterberg, the Netherlands. The simulator features a centrifuge based design with six degrees-of-freedom (DoF). More details regarding the motion platform can be found in Roza et al. [29]. For this study, we only used the 8-meter horizontal track of the simulator to generate lateral motion cues. The lateral motion stimuli were sinusoidal acceleration profiles.
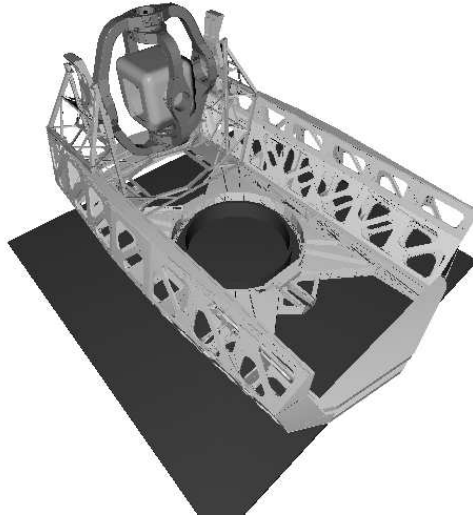
Figure 5.1: *Schematic of the Desdemona research simulator developed by AMST Systemtechnik (Austria) and TNO Human Factors (Netherlands).*

The simulator cabin contains a generic F-16 cockpit with realistic throttle, side-stick and rudder pedals. For this study only the side-stick was used. Three beamers projecting on a three part flat screen generate the Out-The-Window (OTW) visual. The Field-of-View (FOV) was 120 degrees horizontal and 32 degrees vertical. The participants were seated approximately at 1.5 meters from the simulator screens. The OTW view showed the aircraft-parking zone of the Innsbruck airport in Austria. A yellow car was parked in front of the terminal as shown in Figure 5.2. A realistic visual scene was chosen because it resembles the type of scenes normally displayed in vehicle simulation.

5.2.2   Subjects

Twelve subjects, five males and seven females, participated in this experiment. Their average age was 28 years with a standard deviation of 11 years. All subjects were TNO employees. An informed consent was signed before participation. Subjects sat in the chair and wore a headset that outputted white noise to mask actuator sound. This headset was also used for communication between the participant and the experimenter. Participants had to adjust the motion amplitude online using the side-stick inside the cabin until the best match between "what they were feeling and what they were seeing" was achieved. When finished, they communicated to the experimenter how confident they

Figure 5.2: *Visual scene showing part of the Innsbruck airport in Austria.*

were that the motion gain they chose was the best match they could achieve with the visual being displayed.

5.2.3   Experimental design

The experiment had a repeated measures design. The amplitude of the inertial acceleration signal was measured for six different visual signals. The visual signals were combinations of sinusoids with amplitudes of 1 and 2.5 m/s^2 and frequencies of 0.2, 0.4 and 0.8 Hz. The frequency values were chosen near the zone where there is an increase of sensitivity of the otolith model described by Hosman [48]. Each visual signal was measured two times, one for initial inertial amplitudes higher than the visual amplitude and other for initial inertial amplitudes lower than the visual amplitude. This was done to test whether a different initial condition would produce different motion gains for the same visual signal. This led to initial motion gains of 1.4 and 0.6 that were obtained based in the motion platform limitations. The frequency of the inertial signal was always equal to the one of the visual signal. The independent variables combinations make a total of twelve different experimental conditions. Each experimental condition was repeated three times, meaning that subjects performed 36 simulator runs. A Latin squares design was used to randomize the experimental conditions for each repetition. This means that for each repetition, all twelve experimental conditions were performed in a different order for all twelve subjects. With this we expect to reduce any order effect that may affect the motion gain.

5.2.4   Procedure

Subjects had to adjust the motion gain of the simulator until the best match between the visual and inertial cues was obtained. After being seated in the simulator, practice conditions were run to ensure that the subjects understood the task. Each experimental run started by pressing the trigger-button of the side-stick. Then, the visual moved with the same frequency of the motion platform but with different amplitude. The initial motion gain depended of the experimental condition. The visual amplitude remained constant during the experimental run but the inertial amplitude could be changed. The side-stick was used to actively change the inertial amplitude. A deflection to the left would decrease the inertial amplitude while a right-deflection would increase it. Subjects were instructed to adjust the inertial amplitude to the visual amplitude until the cues matched optimally. Subjects were encouraged to try out different inertial values before settling for one. When satisfied with their adjustment, the trigger-button was pressed to stop the experimental run. Subjects were then asked to rate how confident they were that the obtained inertial amplitude was optimal. A value ranging from one to ten was assigned, where one is not confident and ten is highly confident. Each participant performed the 36 experimental runs such that the experimental conditions order was not repeated between subjects.

5.2.5   Data analysis

We defined the motion gain as the ratio between the motion and visual acceleration signal[1]. A gain of one represents the real life situation where the visual cues are equal to the inertial cues. A motion gain higher than one shows that subjects wanted inertial cues stronger than the visual cues. A gain lower than one shows a preference for inertial cues weaker than the visual cues.

To analyze the data, we calculated for every subject the mean gain of every experimental condition. After, we used these individual means to calculate the total mean for every experimental condition. A repeated measures ANOVA was used to determine if the mean motion gains obtained for every experimental condition were statistically different from each other. The statistical analysis were performed using SPSS PASWS 18.0.

---

[1]Although we defined the visual signal in acceleration, humans perceive visual velocity and not visual acceleration [37]

5.3   Results

5.3.1   Motion gain

Figure 5.3 shows the mean motion gain values for all experimental conditions. The results were pooled for the three repetitions since no significant differences were found between them. The results from the statistical analysis are shown in Table 5.1. The mean motion gain was higher when the experimental trial started with a motion gain higher than one. A repeated measures ANOVA showed that this difference between initial conditions was significant. The added mean motion gain for the initial condition dependent variable were respectively 0.89 and 0.65 for the initial motion gain higher than one and initial motion gain lower than one.

The motion gain was also dependent on the visual amplitude. A repeated measures ANOVA showed that the condition with lower visual amplitude had significantly higher motion gains than the condition with higher visual amplitude. The added means showed a motion gain of 0.90 and 0.65 respectively for the 1.0 m/s^2 and 2.5 m/s^2 visual amplitudes.

The statistical tests showed a significant main effect of the frequency in the motion gain. The pooled mean motion gains were 0.90, 0.81 and 0.61 respectively for the 0.2, 0.4 and 0.8 Hz experimental conditions. A post hoc test using a Bonferroni correction showed that the mean gains for the 0.8 Hz experimental conditions were significantly higher than the 0.2 Hz ($p = 0.011$) and the 0.4 Hz ($p = 0.008$) experimental conditions.

A significant interaction between stimulus amplitude and initial condition on the motion gain was observed. Figure 5.3 shows that the effect of the initial condition on the motion gain was higher for the low amplitude signals than for the high amplitude signals. For the low amplitudes, we obtained a motion gain with a grand mean of 1.1 and 0.74 respectively for an initial condition higher and lower than one. For the high amplitudes, the total means were 0.73 for an initial condition higher than one and 0.57 for an initial condition lower than one.

A significant interaction was also found between the initial conditions and the frequency content of the signal. From Figure 5.3, one can observe for the conditions starting with motion gain higher than one, a greater decrease of the obtained mean motion gain from the lower to the higher frequencies than for the conditions starting with a motion gain lower than one. This is especially visible for the conditions with a frequency of 0.2 Hz when compared with the conditions with a frequency of 0.8 Hz. For the conditions starting with a motion gain higher than one, the mean values were 1.06, 0.94 and 0.68 respectively for the 0.2, 0.4 and 0.8 Hz conditions. For the conditions with an initial motion gain lower than one, the mean values were 0.74, 0.69 and 0.53 respectively for the 0.2,

(a) Visual Amplitude = 1m/s^2 (b) Visual Amplitude = 2.5m/s^2

Figure 5.3: *Mean motion gain for the 1 m/s^2 amplitude visual signal (left) and 2.5 m/s^2 amplitude visual signal (right). The vertical bars represent the 95% confidence intervals.*

0.4 and 0.8 Hz conditions.

Table 5.1: *Repeated measures ANOVA results for the mean phase difference ($**= p < 0.01; * = 0.01 \le p < 0.05$).*

Independent Variables	Correction	F-ratio	p	sig.
Amplitude	-	F(1,11) = 19.61	0.001	**
Initial Condition	-	F(1,11) = 23.33	0.001	**
Frequency	Greenhouse-Geisser	F(1.20,13.16) = 12.66	0.002	**
Amplitude $\times$ Initial Condition	-	F(1,11) = 15.48	0.002	**
Initial Condition $\times$ Frequency	-	F(2,22) = 4.85	0.018	*

5.3.2   Confidence values

Figure 5.4 shows the mean confidence values obtained after each experimental condition. The results show that subjects were quite confident in their reports. Nevertheless, a small decay in the confidence values for the highest frequency conditions was noticeable. A repeated measures ANOVA was used as an indication of the statistical significance of this drop in the subjects' confidence. We found a significant main effect of the frequency on the confidence levels, $F(2,22) = 13.40, p = 0.000$. The post hoc tests revealed that the 0.8 Hz conditions had a mean confidence level significantly lower than the 0.2 Hz ($p = 0.004$) and 0.4 Hz ($p = 0.004$) conditions. The pooled mean confidence values were 7.6, 7.4 and 6.7 respectively for the 0.2, 0.4 and 0.8 Hz conditions.

(a) Visual Amplitude = 1m/s^2 (b) Visual Amplitude = 2.5m/s^2

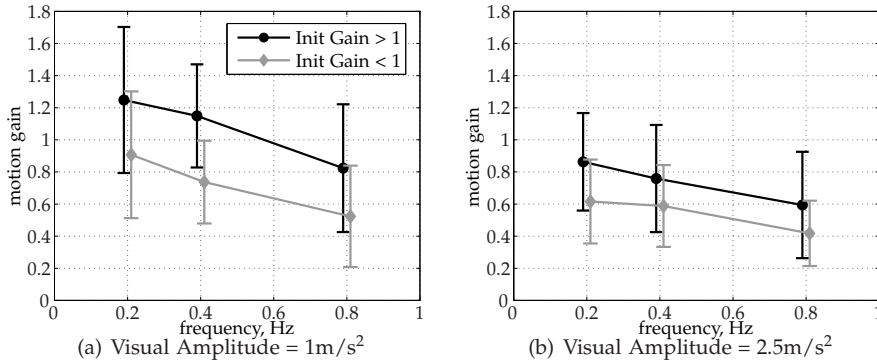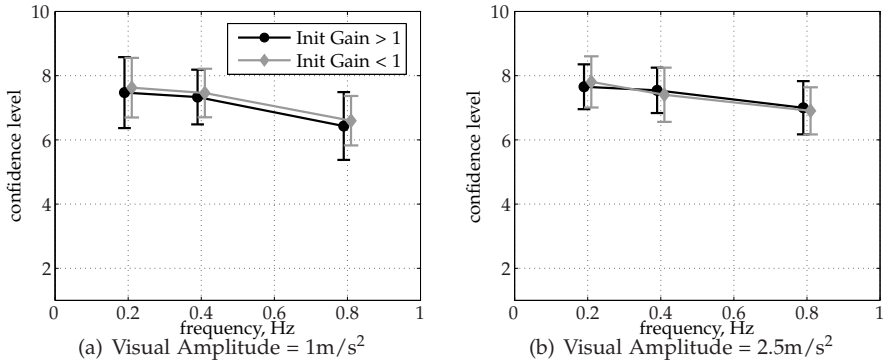**Figure 5.4:** *Mean confidence levels for the 1 m/s^2 amplitude visual signal (left) and 2.5 m/s^2 amplitude visual signal (right). The vertical bars represent the 95% confidence intervals.*

5.4   Discussion

5.4.1   Motion gain dependence on stimulus amplitude

The results showed that with an increase of the stimulus amplitude, the subjective motion gain decreased. We do not know how the motion gain varies as a function of the stimulus amplitude, it can be a linear/non-linear dependence; it can saturate for stimuli with higher amplitudes. However, we can state that these results are interesting for the development of MCAs. From a MCA design point of view, it is beneficial that for higher amplitudes subjects prefer a motion gain lower than one. This means that smaller simulator excursions could be used for stimuli with higher amplitude without loss of perceived realism to the subject. Based on these results, a scaling algorithm can be designed where the used motion gain decreases with the increase of the reference motion stimuli. This reduction of the necessary simulator motion envelope is valuable for generating motion cues that could not be produced before due to the use of a constant scaling algorithm. To the authors' knowledge, there are no MCAs that dynamically scale the motion information based in the amplitude of the reference motion stimuli.

The mean motion gain values obtained are close to the values obtained in literature [74,75,77] and on previous Desdemona studies [76,115,116]. Groen et al. [74] when simulating a take off run found a preferred motion gain of 0.2 for the surge motion of the simulator. The amplitude of the reference signal was 3.5 m/s^2, which is higher than what was used in this experiment. The low value found for their surge motion filter may be explained by the present observation that the higher the amplitude of the motion signals, the lower the motion gain

preferred by subjects. Feenstra et al. [76] found that subjects preferred a motion gain of 0.7 when driving trough a slalom course that delivered a theoretical lateral specific force of approximately 1.2 m/s^2. Their results are also within the range of our findings.

5.4.2 Motion gain dependence on stimulus frequency

The subjective motion gain was affected by the frequency of the motion signal. Signals with higher frequency tended to have a motion gain smaller than signals with lower frequencies. For a sinusoidal motion profile, an increase in frequency also means an increase in the signal jerk. This means that for profiles with the same acceleration amplitude but different frequencies, the jerk will be higher for the stimulus with the highest frequency. The decrease of the motion gain with the frequency indicates that humans are sensitive to high jerk, rating then motion as too strong [78]. Human sensitivity to jerk was already discussed to be an important motion perception issue in other studies [78,117,118]. Grant et al. [78] showed that the concept of motion strength depended not only on the acceleration value of the motion signal but also on the jerk value. Therefore, it is incorrect not to consider the jerk sensitivity when modeling the linear motion perception system. The otolith is normally modeled as a unit gain block where the input is specific force [50,51], which does not take into account a jerk sensitivity. On the other hand, Hosman [48] included high frequency sensitivity in the otolith model. However, it is yet not clear whether the jerk sensitivity comes from the otolith, from the somatosensory system or from the central nervous system processing.

Just as a qualitatively measurement, we decided to plot the obtained motion gains against the transfer function of the otolith proposed by Hosman [48]. Equation (5.1) shows the otolith transfer function, where τ_L is the lead-time constant, and τ_1 and τ_2 are the time constants that give overdamped mass-spring-dashpot characteristics to the otholiths [48]. Wentink et al. [53] set these time constants in their motion perception toolbox as 0.3, 0.12 and 0 respectively for τ_L, τ_1 and τ_2.

$$H_{OTO}(s) = \frac{(1 + \tau_L s)}{(1 + \tau_1 s)(1 + \tau_2 s)} \tag{5.1}$$

The motion gain values were inverted to be compatible with the information given by the transfer function, i.e. if the motion gain is 0.8, the sensitivity value would be 1.25. This means that subjects decreased the motion gain when they felt that the perceived motion was too strong when compared with the visual information being displayed. Figure 5.5 shows the mean sensitivity plotted against the otolith model. We noticed that for both signal amplitudes, the
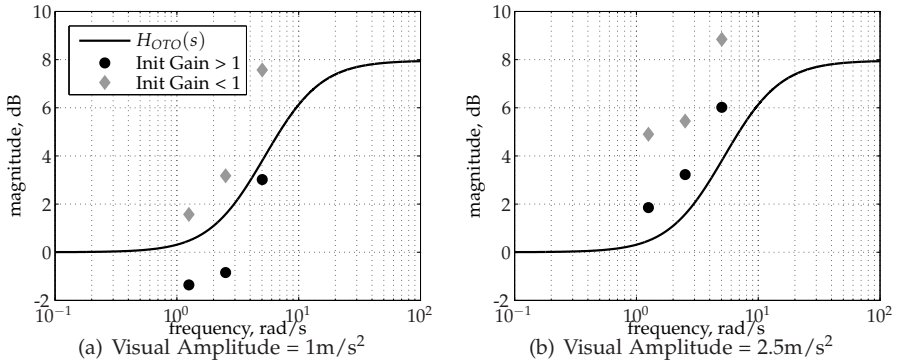
Figure 5.5: *Otolith dynamics with sensitivity indication for the conditions with visual amplitude of 1 m/s² (left) and conditions with 2.5 m/s² (right).*

obtained subjective sensitivity increases with a trend similar to the one of this otolith model.

This frequency dependency can be used to improve the design of current MCAs. A motion filter that included an inverse model of the otolith could be used to filter the accelerations that are used as input for the motion platform. This means that high frequency accelerations would be scaled down more than low frequency accelerations. A filter like this decreases the jerk during motion simulations, which might decrease the overestimation of inertial motion normally found in a simulator environment [75].

However, one should consider in the results the fact that there were reports of a motion artifact being felt especially during the high frequency condition. These motion artifacts are created due to the mechanical limitations of motion platforms when dealing with higher derivatives of the motion signal such as jerk. For example, Grant et al. [78] had to develop a compensation algorithm to eliminate non-linearities created by the motion platform. In our case, 'stick-slip' was detected for the higher frequency motion profiles. Such mechanical artifact will be solved in the near future and it will then be investigated whether this could have an influence in the preferred motion gains.

5.4.3 Motion gain dependence on initial condition

Although subjects were asked to find the best motion gain for the displayed visual information, this value was still dependent on the initial inertial condition. The differences found in the initial conditions showed that an initial motion gain higher than one would yield motion gain values higher than the ones obtained from an initial motion gain lower than one. We were expecting

to get similar results for the conditions with the same visual amplitude but the results were statistically different. Nevertheless it seems that subjects tended to a sort of inner-coherence zone where the motion already felt optimal. This inner-coherence zone is different than what is referred to as coherence zone [45, 119] in the literature. In coherence zone studies, subjects are asked to adjust the motion gain such that the motion gain is coherent with the visual. In this way, an upper threshold and a lower threshold define the coherence zone. The upper threshold is defined as the highest motion gain one can have before the inertial cue is perceived incongruent when compared with the visual cue. In contrast, the lower threshold is defined as the minimal motion gain one can have before the visual and inertial cues are perceived as incongruent. In this study, we did not ask subjects to look for this boundary that divides congruent cues from incongruent cues but for the optimal value between the inertial and visual information. Therefore, we define the inner-coherence zone by an upper and lower threshold that are perceptually indistinguishable from each other when these are measured from different initial inertial amplitudes. We expect the optimal gain to be within the inner-coherence zone. Figure 5.6 illustrates the concept of inner-coherence zone.
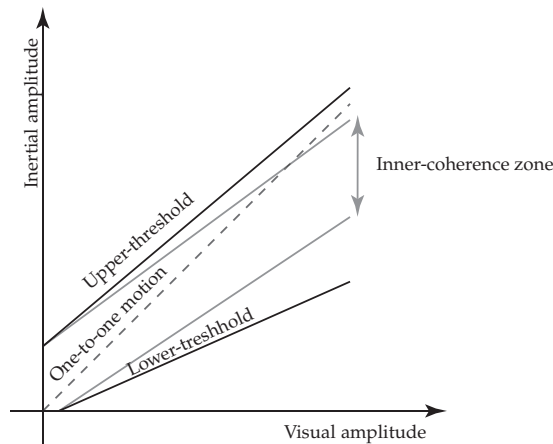
Figure 5.6: *Schematic of the Inner-coherence zone for a simulation environment. The upper boundary of the inner-coherence zone crosses the one-to-one motion line suggesting that for higher amplitudes, the optimal motion gain zone needs a motion gain lower than one. This trend was found during this experiment.*

5.5   Conclusion

With this experiment we showed that in the Desdemona simulation environment, the optimal motion gain is not one. This was already observed in other studies where a one-to-one inertial/visual ratio was not the preferred motion condition. We conclude that the subjective motion gain depends of the amplitude and the frequency of the stimuli. We found that the preferred motion gain decreases with the increase of the stimuli amplitude. However, we need more data points to define the exact nature of this relation. The results also showed that the motion gain decreases with the increase of the motion frequency. This increase seems to follow the same trend of the otolith models that include jerk sensitivity, like the model of Hosman [48]. Contrary to initial expectations, we found that the optimal gain depended on the initial motion gain. When the initial motion cue was higher than the visual cue, the subjective motion gain was higher than in the conditions where the initial motion cue was smaller than the visual cue.

This study showed that there are still improvements that can be made to the MCAs of current motion simulators. To date, the motion gain in a classical MCA is constant. However, the results showed that a dynamic motion gain algorithm would improve the perception of motion cues in the simulator. By using such an algorithm, we expect to improve the subjective realism of motion simulation and decrease the used motion envelope.

Optimal and Coherence Zone comparison

Chapter 5 showed that there was not a single value but a range of values of preferred visual-inertial amplitudes. This range seemed similar to the coherence zones, described in the literature as a zone where inertial and visual cues are coherent even though their amplitude or phase are different. This chapter compares the range of optimal amplitudes described in Chapter 5 with the coherence zones described in the literature within and between two different flight simulators.

6.1   Introduction

Ideally, flight simulators would expose pilots to visual and inertial cues indistinguishable from those experienced during real flight. However, the visual and inertial cues in the simulator have limitations not encountered during real flight. For example, visual cues are limited by the projection system (e.g., resolution, luminance, contrast), transport delay, low spatial frequency, and no stereoscopic cues. Nonetheless, the visual amplitude can be reproduced one-to-one in most flight simulators. The inertial cues, however, have to be scaled down to guarantee that the simulator is kept within its physical limits. Motion Cueing Algorithms (MCA) are used to filter the aircraft motion, which creates a difference between the inertial and visual cues of the simulator over a range of frequencies. This difference should be small, or at least remain imperceptible to the pilot [45, 48, 120]. Surprisingly, however, as shown in various driving [76, 77] and flying studies [74, 75], simulations where magnitudes of the visual and inertial cues are equal, are not preferred by subjects. In these studies, the amplitude of the inertial cues was lowered because subjects perceived motion as "too strong". This overestimation of inertial motion was hypothesized to occur due to the differences between the simulator and real world visual properties [75], and due to motion distortions imposed by the MCAs and the vehicle model [78]. Much research [18–20, 45, 48, 120–125] has been conducted on the effects of visual-inertial interactions in flight simulation. In this chapter we focus on the effects of amplitude discrepancies using two approaches: the Coherence Zone (CZ) [45, 120, 123, 124], and the Optimal Zone (OZ) [125].

The CZ is a concept first introduced by Van der Steen [45, 120] when studying amplitude errors between visual and inertial cues. He defined the CZ as a zone where inertial and visual amplitudes are perceived to be coherent although their values are different. In this study, the CZ measurement focused on the particular case where a range of inertial amplitudes is perceived by subjects to be coherent with a certain visual amplitude. To obtain this CZ, the maximum and minimum inertial amplitudes that are still coherent with a certain visual amplitude are measured. These maximum and minimum coherent amplitudes are referred to hereafter as the upper and lower thresholds, respectively. The CZ is then defined by the inertial amplitudes within the upper and lower thresholds. The CZ as defined by Van der Steen has been used in recent studies [123, 124]. Although the CZ has been defined for amplitude differences, it can also be used to identify phase differences between the inertial and visual signal that are still perceived as coherent [122, 126].

The Optimal Zone (OZ) was introduced in a previous study [125] to find the optimal inertial amplitude for a certain visual amplitude. Although researchers expected to find a single inertial amplitude matching the visual amplitude, results showed that the optimal inertial amplitude depends on the *initial* value of

the inertial amplitude. That is, when the initial inertial amplitude was set higher than the visual amplitude, the value selected by subjects as the 'optimal' inertial amplitude was higher than the 'optimal' inertial amplitude obtained when starting with an initial inertial amplitude that was set lower than the (same) visual amplitude. These findings might indicate that there is not just one optimal inertial amplitude for a certain visual amplitude but rather a range, or zone, of inertial motion amplitudes that are considered optimal by subjects. This is indeed very similar to what was found in the CZ experiments. Theoretically, the CZ contains visual and inertial amplitudes that are perceived as coherent. However, it is not known if the inertial amplitudes inside this zone are perceived equally. For example, a coherent inertial amplitude close to the upper threshold might be perceived stronger than a coherent inertial amplitude close to the lower threshold. Therefore, within a CZ, there could still be a subset of inertial amplitudes perceived as a "better match" for a certain visual amplitude. In theory, the OZ would identify such subset. However, it is unknown if this best match is perceived differently than a coherent match. The fact that the relation between the CZ and the OZ is unknown and that they were never obtained in a single study motivated the present research.

The main goal of the present study was therefore to investigate the relation between the concepts of coherence and optimal zone. A second goal was to investigate whether these metrics can be used to measure differences in the perceived motion between simulators with different configurations. An experiment was conducted at the NASA Langley Research Center in Hampton, Virginia, where both the Cockpit Motion Facility (CMF) and the Visual Motion Simulator (VMS) were used. In both simulators, the OZ and the CZ were measured. Both zones were measured for two different stimulus amplitudes and two different frequencies. The measurements were performed in sway, so that the results can be compared to previous studies [76, 77, 125].

The chapter will discuss the results of the experiment and is structured as follows. In Section 6.2 we will briefly discuss the concepts and earlier results obtained regarding the coherence and optimal zone experiments. Section 6.3 describes the experimental method used, the results are given in Section 6.4 and discussed in detail in Section 6.5. The chapter ends with conclusions and recommendations for future work.

6.2   Background

6.2.1   Coherence Zone

When humans walk or control a vehicle, the visual information is coherent with the inertial information. To detect self-motion, the human body integrates

information from the visual, vestibular, and somatosensory systems, and combines it with the expectation derived from bodily actions. In the real world, the visual information is always matched to the vestibular information one-to-one. However, this might not be the case in a simulation environment, where the visual information can be completely different from the inertial information. For example, a simulator visual could be displaying a 10 meter movement while the motion base only moved 1 meter.

If the difference between the visual and inertial information is too large, humans will detect that the perceived inertial movement is incongruent with the visual scene. To study these types of visual-inertial interactions, Van der Steen [45, 120] introduced the concept of coherence zone (CZ). The CZ defines a perceptual zone where the visual and inertial cues are perceived as "coherent". In this chapter, the coherence zones are studied in terms of amplitude differences between visual and inertial cues. However, the concept of CZ can also be extended to include other stimulus properties such as phase differences [122, 126].

To define a CZ, one needs to measure the maximum and minimum inertial amplitudes that are still considered by subjects to be coherent with a particular visual amplitude. The maximum coherent amplitude is defined as the upper threshold (th_{up}), whereas the minimum coherent amplitude is defined as the lower threshold (th_{lo}). To capture the CZ, the coherence zone width (CZW) and the point of mean coherence (PMC) metrics can be defined using Equations (6.1) and (6.2), respectively.

$$CZW = th_{up} - th_{lo} \tag{6.1}$$

$$PMC = th_{lo} + \frac{CZW}{2} \tag{6.2}$$

In Ref. [124], three experiments are described that aimed at extending the knowledge on the CZs first measured by Van der Steen [45]. In the first experiment, the CZ measured by Van der Steen [45] was extended to higher amplitudes. The CZs were measured for visual amplitudes of 0, 4, 12, 18, 22, 26, and 30 deg/s^2. The motion profile used for the visual and inertial motion was based on smoothed steps in acceleration. An up-down staircase procedure was used to obtain both the upper and lower thresholds. Subjects had to answer affirmatively or negatively the following question: "Did the amplitude of the visual movement correspond with the magnitude of the motion?". Then, using a staircase algorithm, the inertial motion of the next run would change, while the visual motion would remain constant. Based on the subjects' successive answers, the inertial motion would then converge to a certain value, later used to calculate the upper and lower thresholds.

Results showed that, up to a visual amplitude of 12 deg/s^2, the obtained CZs were very similar to the ones measured by Van der Steen [45]. The PMC showed values close to the corresponding visual amplitudes while the CZW increased with the visual amplitude. However, for higher visual amplitudes the PMCs became smaller than the corresponding visual amplitudes; the CZW remained approximately constant with the increase of the visual amplitude.

In a second experiment, the staircase measurement method was compared with a self-tuning method where subjects could decide the amount of inertial motion they would like to experience in the next run. This was done because the staircase method was time consuming and the task proved to be difficult for the subjects. Details on the latter self-tuning method are discussed in Section 6.3 of this chapter. Using the two methods, the CZ was measured for the 12 and 30 deg/s^2 amplitudes. The motion profiles were again based on smoothed steps in acceleration. For both the PMC and CZW measurements, the results obtained with the two measurement methods were very similar, and the small differences in the data obtained with both methods were not statistically significant. This does not mean, however, that both methods are equal and that their use would always yield the same results. Since the experiments presented in this chapter are very similar to those with which the measurement methods yielded similar data, we were confident however that in this particular case the self-tuning method would lead to the same trends as the more task-demanding staircase method. It is recommended to study the wider validity of this claim in later experiments.

In a third experiment, the effect of the frequency of the motion stimulus on the CZ was tested. The chosen visual amplitudes were again 12 and 30 deg/s^2. In this experiment there were three different motion profiles: a sinusoid with a frequency of 2 rad/s, a sinusoid with a frequency of 10 rad/s, and the smoothed step in acceleration used in the previous experiments. The self-tuning method was used to measure the CZs. Results showed that the PMC as well as the CZW increase with the stimulus amplitude (similar to the first experiment) but decreased with the stimulus frequency. The frequency dependency of the results was hypothesized to be related to the dynamics of the semicircular-canals [124].

6.2.2   Optimal Zone

In theory, one-to-one simulation (i.e., when inertial cues are equal to visual cues) should result in the best perceived match between visual and inertial information. However, recent studies have shown that one-to-one motion in a simulation can be perceived as too strong [74–77]. In driving simulation, Feenstra et al. [76] studied the effect of providing drivers with different motion conditions during a slalom maneuver. They tested motion gains, the ratio between

inertial and visual motion, of 0, 0.4, 0.7, and 1. A motion gain of 0 means that only visual information was displayed while a motion gain of 1 means that the visual information corresponded to the inertial information. Surprisingly, results showed that 0.7 was the preferred motion gain. The Motion Cueing Algorithm (MCA) used in this experiment cued the lateral road position one-to-one. However, longitudinal specific force was not cued because the car travelled at constant speed. All the other degrees-of-freedom (DoF) where cued one-to-one. In all DoFs a limiter block was used to prevent damage of the simulator whenever the actuators were close to their limits. Pretto et al. [77] conducted a similar study in a different simulator. The authors stated that in this experiment, the vehicle dynamics from the simulated car were directly mapped to the simulator motion. The motion system had a transport delay of 41ms. They tested motion gains of 0.5, 0.75, 1, and 1.25. Results showed that the value 0.5 and 0.75 were most preferred by subjects. Similar trends in the motion gain were also found in flight simulation. Groen et al. [74] tested different motion filters configurations to simulate a take off maneuver. The preferred motion filter conditions involved a motion gain of 0.2 for the surge filter and a motion gain of 0.6 for the pitch filter. Groen et al. [74] stated in the study that, "Remarkably, unity gains were rejected as [being] too powerful." However, in this study the MCA cued high-frequency longitudinal cues with simulator surge and low-frequency longitudinal cues with simulator pitch (tilt-coordination). This classical way of cueing might have introduced distortions in the motion profiles [78]. In another study, pilots reported that the lateral motion experienced during a decrab maneuver was too strong, even though the motion gain was 0.7 [75]. According to the authors, in this condition the motion from the aircraft model was sent directly to the motion platform without involving any MCA in the process. The visual delay was about 50 ms.

To determine if these reported motion gains were being influenced by the vehicle model, an experiment where subjects were asked to find the "best match" between the visual and inertial amplitude was conducted [125]. This best match is hereafter referred to as Optimal Zone (OZ). The OZ was measured in sway for sinusoidal motion profiles in acceleration with amplitudes of 1 and 2.5 m/s^2 and frequencies of 0.2, 0.4 and 0.8 Hz. Subjects were given a visual stimulus with constant amplitude and were asked to change the inertial amplitude until they decided that the 'best match' between the visual and inertial acceleration was obtained. A side-stick was used to change the inertial amplitude while experiencing the constant visual amplitude. A left-deflection reduced the inertial amplitude while a right deflection increased it. At the start of a measurement, an initial inertial amplitude was provided that was either higher or lower than the corresponding visual amplitude. Results showed that this initial inertial amplitude influenced the optimal zone. An initial inertial amplitude set higher

than a certain visual amplitude led to inertial amplitudes that were higher than those obtained when the initial inertial amplitude was set lower than the same visual amplitude. As a result, each visual amplitude had two values where the inertial motion was perceived to be 'optimal', thus resulting in an optimal *zone*. The upper boundary of the optimal zone is referred to as the upper optimal amplitude; the lower boundary of the optimal zone is referred to as the lower optimal amplitude.

In the same study it was found that the inertial amplitude chosen by subjects decreased for stimuli with higher frequency, suggesting a sensitivity to the acceleration derivative (i.e., jerk) as reported in previous research [52, 78, 105]. There was also an effect of the visual signal amplitude. The visual signal with an amplitude of 2.5 m/s^2 led to lower motion gains than the conditions using a visual signal with an amplitude of 1 m/s^2.

When comparing the OZ with the CZ, it is convenient to use similar metrics. Therefore, new metrics for the OZ are hereby introduced which characterize the width and the mid point of the OZ. The width of the OZ is defined by the optimal zone width (OZW) while the mid point is defined by the point of mean optimal (PMO) zone. The OZW and PMO are given by Equations (6.3) and (6.4), respectively, where up_{OZ} is the upper optimal amplitude and lo_{OZ} is the lower optimal amplitude:

$$OZW = up_{OZ} - lo_{OZ} \tag{6.3}$$

$$PMO = lo_{OZ} + \frac{OZW}{2} \tag{6.4}$$

Summarizing, for both zones we defined metrics to characterize the mid point of the zone, the PMC and PMO, for the CZ and the OZ respectively. In the following, the PMC and the PMO will be referred to as "point of mean zone" (PMZ) measures. Similarly, the CZW and the OZW will be referred to as "zone width" (ZW) measures. Although the PMC may be different from the PMO, we consider the concept behind these measures to be the same, thus allowing us to define both measures as PMZs. The same applies to the concept behind the CZW and the OZW.

6.3   Method

Previous studies lack comparable data between the optimal zone (OZ) and the coherence zone (CZ) because these were measured using different degrees-of-freedom, different amplitudes, and different frequencies. Therefore, in this experiment the OZ and the CZ were compared for the same motion profiles in lateral acceleration (sway) using the simulators at the Flight Simulation Facility

of NASA Langley Research Center (LaRC) in Hampton, Virginia. This section describes the methods used in this experiment. For comparison purposes, this study used the same methodology as in Valente Pais et al. [124].

6.3.1 Apparatus

The Cockpit Motion Facility (CMF), and the Visual Motion Simulator (VMS) located at NASA LaRC were used in this study. To compare with the data of previous experiments [76, 77, 125], the motion bases were driven in the sway axis only. The visual scene was the same in both simulators and consisted of an airport scenario where the subject was placed near an hangar entrance (Figure 6.1).

Figure 6.1: *Example of the visual scene displayed on the CMF and VMS.*

CMF

The LaRC CMF (Figure 6.2) is a new facility with one motion base and three interchangeable cockpits. The motion base is a high performance, 1.9 m stroke, six degree-of-freedom, hydraulic motion system. For this study, the Generic Flight Deck (GFD) Cockpit was mounted on the motion base. The GFD cockpit is an all-glass instrument, easily reconfigurable transport type cockpit with interchangeable and programmable control inceptors. The performance limits of the CMF in the sway axis are +/- 1.4 m, +/- 1.0 m/s, and +/- 6.9 m/s^2. The GFD cockpit is equipped with four Wide Angle Collimated (WAC) window displays with a horizontal field of view of 46 degrees, a vertical field of view of 34 degrees, a resolution of 1280 x 1024 pixels per display, and an update rate of 60 Hz. The visual system has a maximum transport delay of 70 ms and a minimum transport delay of 20 ms.

(a) CMF with GFD cabin

(b) GFD cockpit
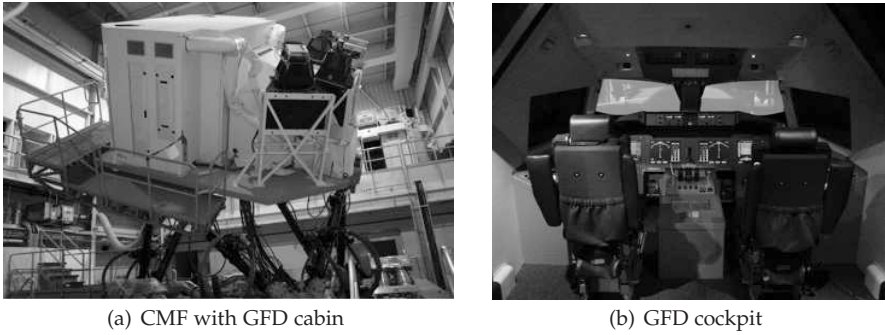
Figure 6.2: *The LaRC Cockpit Motion Facility with the Generic Flight Deck Cockpit.*

VMS

The LaRC VMS, shown in Figure 6.3, is a generic three pilot transport type cockpit permanently mounted on a 1.5 m stroke, six degree-of-freedom, hydraulic motion platform. The performance limits of the VMS in the sway axis are: +/- 1.2 m, +/- 0.6 m/s and +/- 5.9 m/s^2. The VMS is equipped with four WAC window displays, with a horizontal field of view of 66 degrees, a vertical field of view of 45 degrees, a resolution of 1024 x 944 pixels per display, and an update rate of 60 Hz. The visual system has a maximum transport delay of 141 ms and a minimum transport delay of 29 ms.
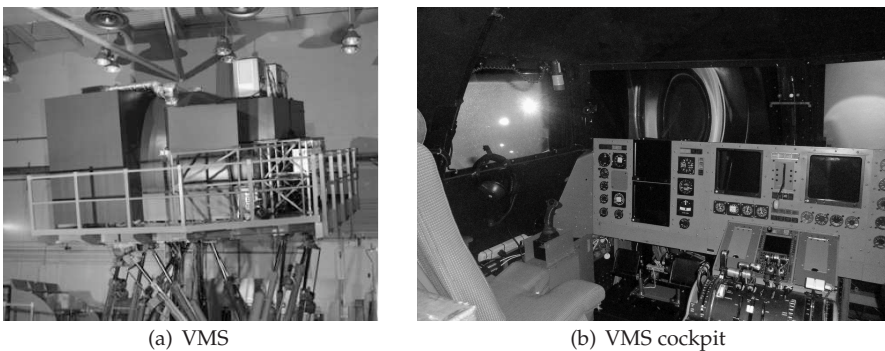

(a) VMS

(b) VMS cockpit

Figure 6.3: *The LaRC Visual Motion Simulator.*

6.3.2   Experimental design

The experiment had a four way repeated measures design. The independent factors considered were the two simulators described above, the two types of instructions given to subjects (either optimal or coherence zone tuning), two visual stimulus amplitudes, and two stimulus frequencies. The visual stimulus amplitudes used were 0.5 and 1 m/s^2. These amplitudes were chosen such that the results could be directly compared to previous studies on optimal tuning performed in other simulators [125].

The choice of frequencies was less straightforward. Initially three frequencies of 2, 3, and 5 rad/s were chosen for the CMF part of the experiment. The lowest frequency of 2 rad/s was the lowest possible frequency to be tested while still remaining within the motion base limits. For the VMS the minimum frequency was 3 rad/s, so only two frequencies would be tested in this simulator. During preliminary tests it became clear that the experimental sessions were too long and there was the risk that subjects would become too fatigued. For this reason, one of the frequencies was eliminated from the tests in the CMF. To maintain symmetry with respect to the tests in the VMS, it would have been better to eliminate the 2 rad/s condition. However, it was thought that maintaining this low frequency would allow for a more direct comparison to results from other studies [124,125] that used frequencies of 1.3, 2, and 2.5 rad/s. Moreover, it was thought that the larger the differences between tested frequencies the easier it would be to observe the effect of frequency on the coherence and optimal zone measurements. It was then decided to maintain the 2 and 5 rad/s conditions for the CMF and test the 3 and 5 rad/s conditions in the VMS. With this design, comparison between the two simulators can be done only at the frequency of 5 rad/s.

In each simulator and for each of the conditions, two measurements were taken: during the optimal tuning, one measurement for each of two initial amplitudes of the inertial motion cue; and during the coherence zone measurements, one for the upper thresholds and one for the lower threshold. For each of these measurements three repetitions were made, resulting in a total of 48 experimental trials in each simulator.

6.3.3   Motion profiles

The visual and inertial motion stimuli consisted of sinusoidal signals with amplitude and frequency defined by the experimental conditions described above. The signals were designed such that experimental runs of different frequencies would last the same amount of time when fade-in and fade-out were included, which takes in total two extra periods. Therefore, without fade-in and fade-out, the experimental conditions for the motion signals with frequencies of 2, 3, and

5 rad/s lasted for 2, 4 and 8 periods, respectively. These sinusoidal signals were faded in and out to guarantee that the acceleration, velocity and position signals always started and ended at zero. The fade in and fade out parts of the signal are described by Equation (6.5), where A is the amplitude in m/s^2, w is the signal frequency in rad/s, and w_s and w_c are the smoothing and compensation frequencies, respectively, also in rad/s. A_c is a compensation amplitude used to make the velocity signal start at zero. This compensation amplitude is equal to $A/12$. Both the smoothing and the compensation frequencies equalled half of the signal frequency.

$$f(t) = \frac{1}{2} A \sin(wt) - \frac{1}{2} A \sin(wt) \cos(w_s t) + A_c \sin(w_c t) \tag{6.5}$$

The complete motion signal is given by Equation (6.6) where T is the period of the signal and N is the number of periods in one run. The number of periods does not include the two periods that are necessary to perform the fade in and fade out. Including the fade in and the fade out, the total length of one run was 12.57 seconds. Figure 6.4 shows examples of complete runs for all three frequencies at an amplitude of 1 m/s^2.

$$a(t) = \begin{cases} f(t), & 0 < t \leq T \\ A \sin(wt), & T < t \leq (N+1)T \\ f(t-T), & (N+1)T < t \leq (N+2)T \end{cases} \tag{6.6}$$

(a) 2 rad/s   (b) 3 rad/s   (c) 5 rad/s
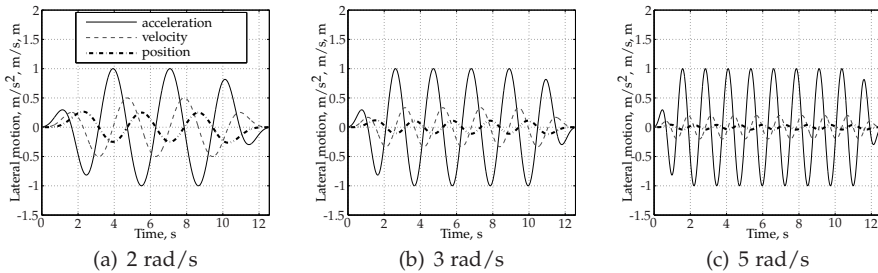
Figure 6.4: *Example of the motion signals during one run for the three different frequencies and an amplitude of 1 m/s^2.*

To further investigate the differences between the inertial motion of the two simulators, the motion signals measured by the simulators' accelerometers were analyzed. Figures 6.5 and 6.6 show the sinusoidal motion profiles generated by the CMF and VMS simulators, respectively. The motion profiles were taken from experimental runs conducted by one of the participants. The displayed motion profiles show examples of a very small inertial amplitude, an amplitude close to 0.5 m/s^2, an amplitude close to 1.0 m/s^2, and a large inertial amplitude.

These amplitudes show the typical inertial motion provided to the subjects during the experiment. Only the motion profiles with a frequency of 5 rad/s are shown, as this is the only frequency that was used by both simulators. In the CMF simulator, the measured data were obtained from Q-Flex Model QA-700 accelerometers manufactured by Honeywell. In the VMS simulator, the measured data were obtained from Sundstrand QA-900 accelerometers.

No effort was made to correct for any simulator non-linearities, such as time delays, overshoot, by means of an offline control algorithm. By not correcting for any distortions created by the different motion bases, we included the possibility for the optimal and coherence zone measurements to show differences between simulators. Also, the correction algorithms employed to correct for motion base distortions are normally used during passive profiles and not during active flight simulation. This is another reason for leaving out any correction algorithms since one of the objectives of this study was to observe if the CZ and/or OZ can be used as a measurement to discriminate between simulators when these are used during normal flight simulation configurations. However, the reader should be aware that the results obtained in this study will only apply to the CMF and VMS simulators.

Signal-to-Noise ratios (SNR) were calculated for the four motion profiles shown in Figures 6.5 and 6.6. This analysis was based on the AGARD-AR-144 report [127]. The SNR was calculated using Equation (6.7), where σ_f^2 is the variance of the measured signal at the fundamental frequency F_f (in this case, 5 rad/s), and σ_n^2 is the variance of the computed noise signal.

$$SNR = \frac{\sigma_f}{\sigma_n} = \sqrt{\frac{\sigma_f^2}{\sigma_n^2}} \tag{6.7}$$

The variance of the measured signal at the fundamental frequency was calculated from Equation (6.8), where X is the Fast-Fourier Transform (FFT) of the measured signal, X^* is the complex conjugate of X, and N is the sample size. The fade-in and fade-out were removed from the time signals used in the FFT calculation.

$$\sigma_f^2 = \frac{2}{N^2} X^*[F_f] X[F_f] \tag{6.8}$$

The variance of the noise signal was calculated from Equation (6.9)

$$\sigma_n^2 = \left(\sum_{i=0}^{N/2-1} \frac{2}{N^2} X^*[i] X[i] \right) - \sigma_f^2 \tag{6.9}$$

The SNRs for the different motion profiles are shown in Table 6.1. Since the VMS has lower SNRs than the CMF, we expect both the Optimal and Coherence
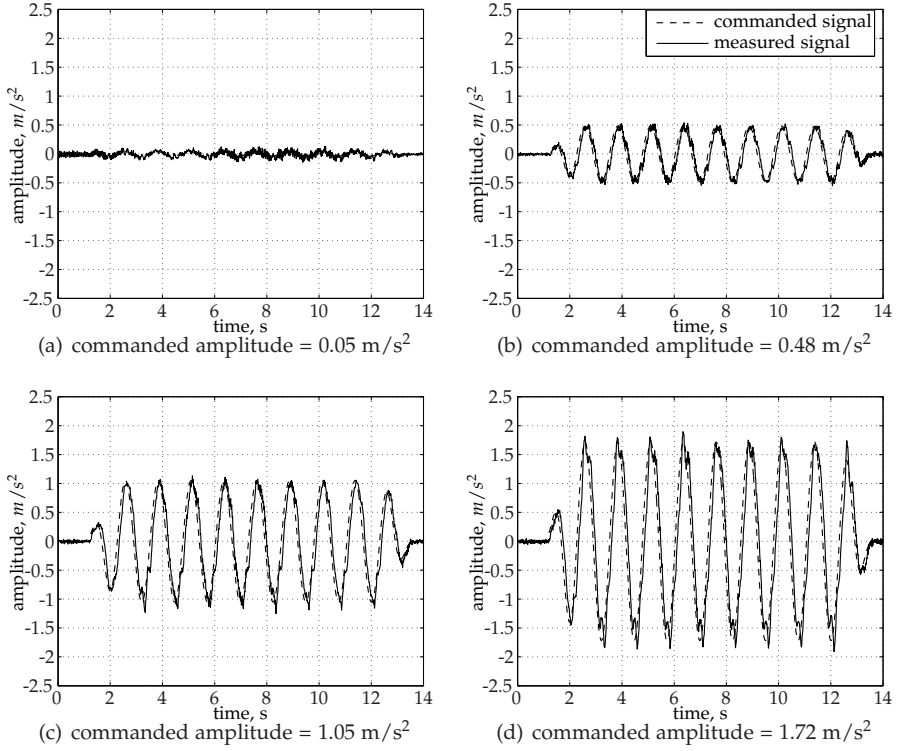
Figure 6.5: *Inertial motion at 5 rad/s for different commanded amplitudes in the CMF.*

Zones in the VMS to be farther away from the one-to-one line.

Table 6.1: *Signal-to-Noise ratio for the CMF and VMS simulators (at 5 rad/s)*

Simulator	commanded amplitude (rad/s)	SNR
CMF	0.05	0.973
	0.48	6.457
	1.05	8.998
	1.72	8.241
VMS	0.04	0.597
	0.50	2.793
	1.10	4.789
	1.60	5.867
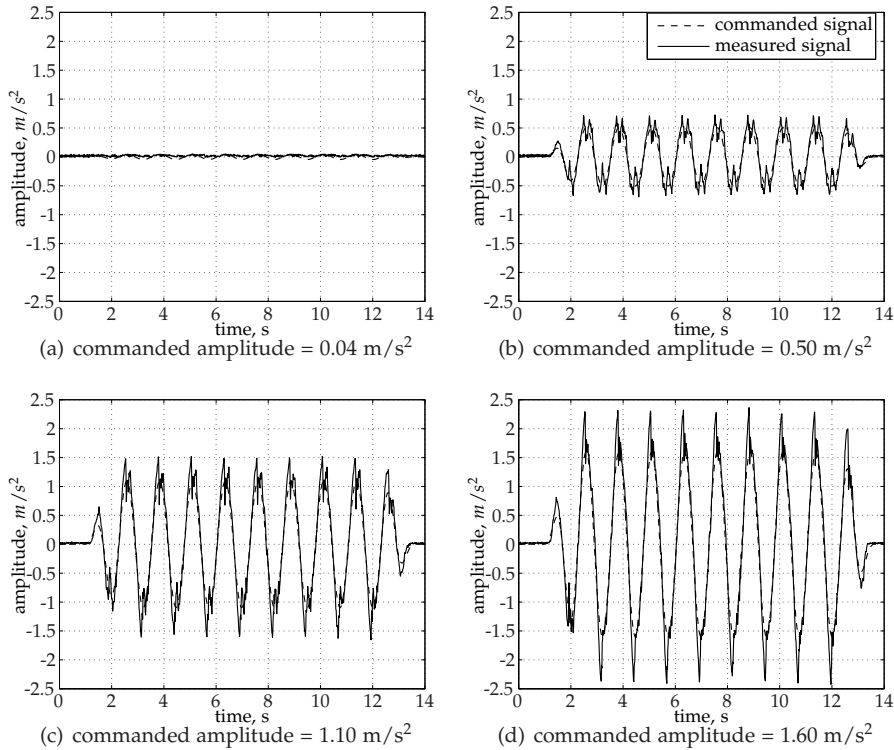
Figure 6.6: *Inertial motion at 5 rad/s for different commanded amplitudes in the VMS.*

6.3.4 Procedure

Subjects were seated in the left-hand chair of the simulator cabin. The subject wore a headset with active noise cancellation which allowed communication with the experiment supervisor and masked any noise from the motion system. Three buttons located on the side-stick, on the left side of the participants, were used to record their answers throughout the experimental runs.

The experiment was divided into two parts. The first part was conducted in the CMF, the second part in the VMS. Due to simulator scheduling it was not possible to have both simulators available at the same time, and randomization between simulators was not conducted. The VMS experiment was performed two months after the CMF experiment. The same subjects were used in the VMS experiment and the experimental order they followed was the same as was used in the CMF. Each experiment part was further divided in two blocks. Figure 6.7 illustrates the experimental design.

In the first block, all the optimal zone measurements were conducted, and
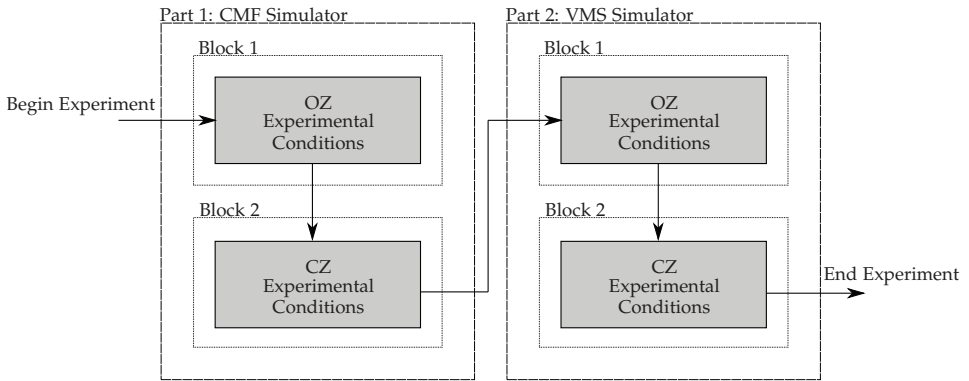
Figure 6.7: *Block diagram of the experimental design.*

in the second block the coherence zones were measured. The measurement method used was the same for both the optimal and the coherence zone measurements. The difference between these measurements was in the instructions given to subjects with regard to how they should choose the amplitude of the inertial motion signal, and in the starting condition of the initial inertial motion signal. Before each block, subjects were given instructions specific to either the optimal zone or the coherence zone. Between each block there was a short break. Each experimental block lasted approximately two hours.

In both simulators, the optimal zone experimental block was performed before the coherence zone experimental block for all subjects. This was done to ensure that knowledge regarding a "coherence zone", which is a necessary part of the coherence zone instructions, did not negatively influence subjects' strategy during the optimal zone measurements. After being told that a range of amplitudes exist where motion and visual cues are perceived as coherent although they are not a physical match, subjects could reject the concept of an optimal zone, and the idea that it could be found by further tuning the inertial amplitude of a simulator. This could hinder their motivation to find the "best match" during the optimal zone measurements. Obviously, for the experimental trial in the second simulator, subjects were already familiar with both concepts. However, in this case, they have already experienced that indeed both tasks, optimal and coherence zone measurements, are possible to accomplish using the same tuning method.

The order of the experimental conditions was randomized for every subject within each block. For each experimental trial, the visual motion amplitude was kept constant and the inertial motion amplitude was varied throughout a set of runs. An example of an experimental run is shown in Figure 6.4. In each trial, the amplitude of the first run was randomly selected at an amplitude between

1.4 and 1.6 times the visual amplitude for runs that approach the optimal zone from above or random value between 0.4 and 0.6 times the visual amplitude for approaching the optimal zone from below. For the coherence zone measurements, the initial inertial amplitude was a random value between 1.1 and 0.9 times the visual amplitude. Before each coherence zone trial started, subjects were informed whether that trial corresponded to a lower or an upper threshold measurement.

At the end of each run within a trial, subjects could change the inertial motion amplitude of the next run. They did this by pushing a switch button one or more times up or down to indicate a desired number of increments or decrements. The chosen number was shown on a head-down display placed directly in front of the subjects. A positive number meant that the next run would have a higher amplitude motion, and a negative number meant a lower amplitude motion. After giving their answer, subjects pressed a second button to signal that they were ready for the next run. The trial ended when subjects' answers had two consecutive reversals of one increment or decrement, i.e., a sequence of 1, -1, 1, or -1, 1, -1, or reached 30 runs; however, the eight subjects always converged within the allowed 30 runs. The consecutive reversals indicated that subjects converged to a certain amplitude of motion that could not be increased or decreased anymore. The size of each increment or decrement was 0.025 times the visual amplitude, which corresponded to 0.0125 m/s^2 for the lowest amplitude condition and 0.050 m/s^2 to the highest amplitude condition.

Before starting the experiment, subjects performed three randomly chosen experimental trials for training purposes.

6.3.5   Subjects and subjects' instructions

Eight volunteers, all employees of the LaRC Flight Simulation Facility performed the experiment. There were seven male and one female participants. The subjects' average age was 49 years, ranging between 31 and 64 years old. All subjects were able to complete the experiment, and there were no complaints of motion sickness.

The participants were instructed to sit upright and refrain from making head movements throughout the experiment. They were, however, allowed to gaze over the visual scene at will.

Participants were told they were to perform a series of experimental trials which consisted of several runs. In each trial the visual scene would move the same way but the amplitude of the simulator inertial motion would vary between runs depending on their input.

For the optimal zone measurements, subjects were not informed whether the trial was an upper or a lower optimal amplitude measurement. Participants

were instructed to find the inertial motion amplitude that, in their opinion, matched the visual amplitude cue the best.

For the coherence zone measurements, subjects were told at the beginning of the trial whether an upper or a lower threshold measurement was being performed. For an upper threshold measurement, subjects were asked to find the strongest inertial motion amplitude that was still perceived as coherent with the visual cue. For a lower threshold measurement they were asked to find the weakest inertial motion amplitude that was still coherent with the visual cue.

For both optimal and coherence zone measurements subjects were instructed to decrease and increase the inertial motion amplitude as many times as needed until they were satisfied with their choice. Subjects were advised to start with increments of 10 or more and decrease the number of increments or decrements at every direction reversal. They were informed of the stopping criteria of the trials.

6.3.6 Data analysis

The amplitude level of the inertial motion in the last run was used as the amplitude chosen by the subject. This amplitude level was then averaged across repetitions of the same condition, for each subject.

From the optimal zone measurements we obtained inertial amplitudes for the upper (up_{OZ}) and lower (lo_{OZ}) optimal amplitudes. With these, we calculated the point of mean optimal (PMO) zone and the optimal zone width (OZW) as defined by Equations (6.3) and (6.4), respectively. For the data analysis of the optimal zone, the dependent measures were the PMO and the OZW; the independent variables were the visual amplitude and frequency.

From the coherence zone measurements we obtained inertial amplitudes for the upper (th_{up}) and lower (th_{lo}) thresholds. From these thresholds we obtained the coherence zone width (CZW) and the point of mean coherence (PMC), as defined by Equations (6.1) and (6.2), respectively. For the data analysis of the coherence zone measurements, the dependent measures were the PMC and the CZW; the independent variables were the visual amplitude and frequency.

To compare the OZ with the CZ we calculated their respective 'point of mean zone' (PMZ) and 'zone width' (ZW) metrics. The PMZ for the OZ is given by the PMO while for the CZ it is given by the PMC. Similarly, the ZW for the OZ is given by the OZW while for the CZ it is given by the CZW. The PMZs and the ZWs were then used as the 'dependent measures' when comparing the coherence zone with the optimal zone. The independent variables were then the visual amplitude, the frequency, and the instructions that the subjects got. That is, the difference between the OZ and CZ measurements is examined as a function of the different instructions that the subjects got before conducting the experiment. With the CZ instructions, subjects are expected to converge to

inertial amplitudes that are higher or lower than the corresponding visual amplitude. Conversely, for the OZ instructions, subjects are expected to converge to inertial values closer to the visual amplitude. Therefore, it is expected that the inertial amplitudes obtained with the OZ instructions lie within the inertial amplitudes obtained with the CZ instructions.

When comparing both simulators we again used the PMZs and ZWs as dependent measures and the simulator, instructions and visual amplitude as independent variables.

For the statistical analysis we conducted repeated measures analysis of variance (ANOVAs). We considered as highly significant the main effects with a p value lower or equal to 0.01, and as significant the main effects with a p value between 0.01 and 0.05. The statistical analysis were performed with SPSS PASWS 19.

6.4   Results

This section starts by presenting the optimal zone (OZ) and coherence zone (CZ) results separately for the CMF simulator. This allows for an initial analysis of the effect of the stimulus amplitude and frequency on the OZ and CZ. Then, the OZ and the CZ are compared, first for the CMF simulator and then for the VMS simulator. Section 6.4 ends with the comparison between the CMF and VMS simulators both for the OZ and CZ.

6.4.1   The CMF simulator

Optimal Zone

Figure 6.8 shows the inertial amplitude values averaged between subjects obtained during the optimal zone measurements. As explained before, the first inertial amplitude provided to the subjects was either higher (upper optimal amplitude) or much lower (lower optimal amplitude) than the visual amplitude. In Figure 6.8 the upper and lower lines in each plot represent the upper and lower measurements, respectively.

To analyze the optimal zone, we calculated the point of mean optimal zone (PMO) and the optimal zone width (OZW) given by Equations (6.4) and (6.3), respectively. We also normalized the PMO by dividing it by the visual amplitude. These normalized PMOs (or gains) were used to observe if the PMO distance to the one-to-one line was affected by the visual amplitude. Figure 6.9 shows the mean values of the obtained PMO, normalized PMO and OZW. A repeated measures ANOVA was conducted to observe the effect of the visual amplitude and frequency on the PMO, normalized PMO and OZW, see Table 6.2.

(a) frequency = 2 rad/s   (b) frequency = 5 rad/s
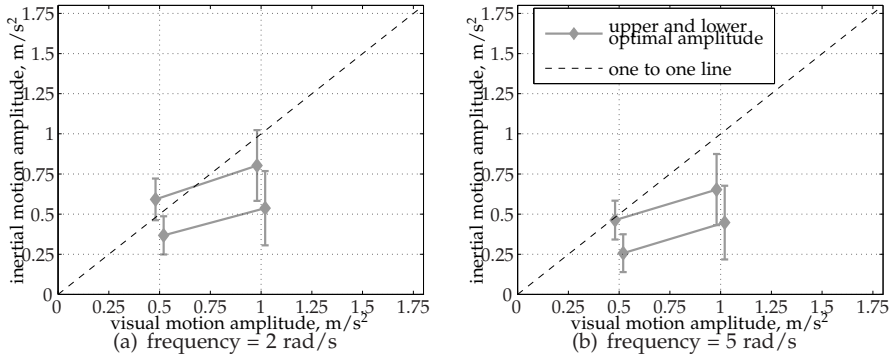
Figure 6.8: *Optimal zone for both frequencies in the CMF simulator. The error bars represent the 95% confidence intervals.*

Table 6.2: *Repeated measures ANOVA results for the point of mean optimal, the normalized point of mean optimal and the optimal zone width in the CMF simulator. ($* = 0.01 < p < 0.05$, $** = p \leq 0.01$)*

Dependent measures	Independent variables	F-ratio	p	sig.
PMO	Amplitude	F(1,7) = 14.87	0.006	**
	Frequency	F(1,7) = 13.07	0.009	**
Normalized PMO	Amplitude	F(1,7) = 30.65	0.001	**
	Frequency	F(1,7) = 14.42	0.007	**
OZW	Amplitude	F(1,7) = 0.19	0.676	-
	Frequency	F(1,7) = 1.27	0.298	-

Figure 6.9(a) shows that the PMO was higher for the conditions with a visual amplitude of 1 m/s^2, considered a significant effect. The PMO of the conditions with a visual frequency of 2 rad/s were higher than the PMO of the 5 rad/s condition, also a significant effect.

The normalized PMOs (Figure 6.9(b)) showed that the gains obtained for the visual amplitude of 1 m/s^2 were significantly lower than the ones obtained for the 0.5 m/s^2 amplitude. Therefore, the 1 m/s^2 PMOs were farther away from the one-to-one line than the 0.5 m/s^2 PMOs'. Similar to the PMO, the normalized PMOs were significantly higher for the visual frequency of 2 rad/s.

The OZW was not affected by the different visual amplitudes and frequencies (see Table 6.2). Figure 6.9(c) shows that the mean OZW remains at the same level, around 0.23 m/s^2, for the tested inertial amplitudes and frequencies.

Figure 6.9: *Mean PMO, Normalized PMO and OZW in the CMF simulator. The error bars represent the 95% confidence intervals.*

Coherence Zone

Figure 6.10 shows the mean upper and lower thresholds obtained during the coherence zone measurements. The upper threshold is represented by the inertial accelerations above the one-to-one line while the lower threshold is represented by the acceleration values below the one-to-one line.

From the upper and lower thresholds we obtained the point of mean coherence (PMC) and the coherence zone width (CZW), see Equations (6.2) and (6.1). The normalized PMCs were calculated by dividing the PMC by the respective visual amplitude.

Figure 6.11 shows the obtained PMC, normalized PMC and CZW. A repeated measures ANOVA was performed to observe the effects of the visual amplitude and frequency of the stimulus in both dependent measures. The repeated measures ANOVA results are shown in Table 6.3. The PMCs increase significantly with the amplitude of the visual stimulus. Also, the PMCs of the
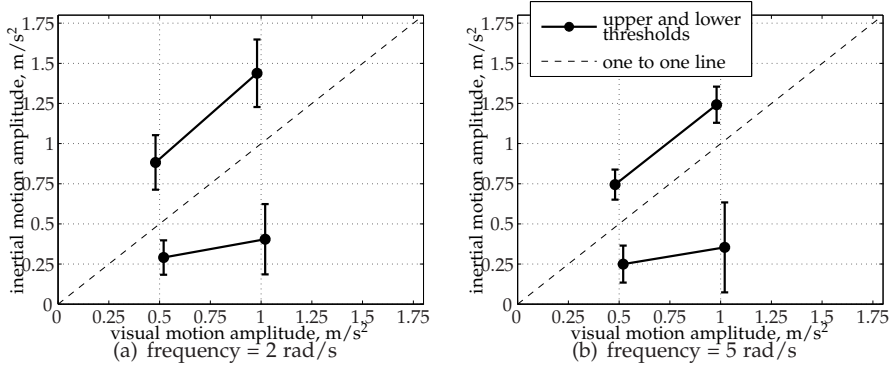
Figure 6.10: *Coherence zone for both frequencies in the CMF simulator. The error bars represent the 95% confidence intervals.*

conditions with higher frequencies were significantly lower than the PMCs of the conditions with lower frequencies. The normalized PMCs decreased significantly with the amplitude and frequency of the visual stimulus. The CZWs had a similar trends to the PMCs. The CZW were significantly higher for the conditions with higher amplitude and significantly lower for the conditions with higher frequency.

Table 6.3: *Repeated measures ANOVA results for the point of mean coherence, the normalized point of mean coherence and the coherence zone width in the CMF simulator. ($* = 0.01 < p < 0.05$, $** = p \leq 0.01$)*

Dependent measures	Independent Variables	F-ratio	p	sig.
PMC	Amplitude	$F(1,7) = 101.20$	0.000	**
	Frequency	$F(1,7) = 7.08$	0.032	*
Normalized PMC	Amplitude	$F(1,7) = 21.22$	0.002	**
	Frequency	$F(1,7) = 7.02$	0.033	*
CZW	Amplitude	$F(1,7) = 17.66$	0.004	**
	Frequency	$F(1,7) = 9.60$	0.017	*

Optimal Zone versus Coherence Zone

Figure 6.12 shows the mean upper and lower thresholds combined with the mean upper and lower optimal amplitudes. Here, we observe that the lower threshold seems similar to the lower optimal amplitude. However, the upper threshold is higher than the upper optimal amplitude. As explained before, we used the point of mean zone (PMZ) and the zone width (ZW) measures to statistically compare the coherence zone with the optimal zone, so PMO is

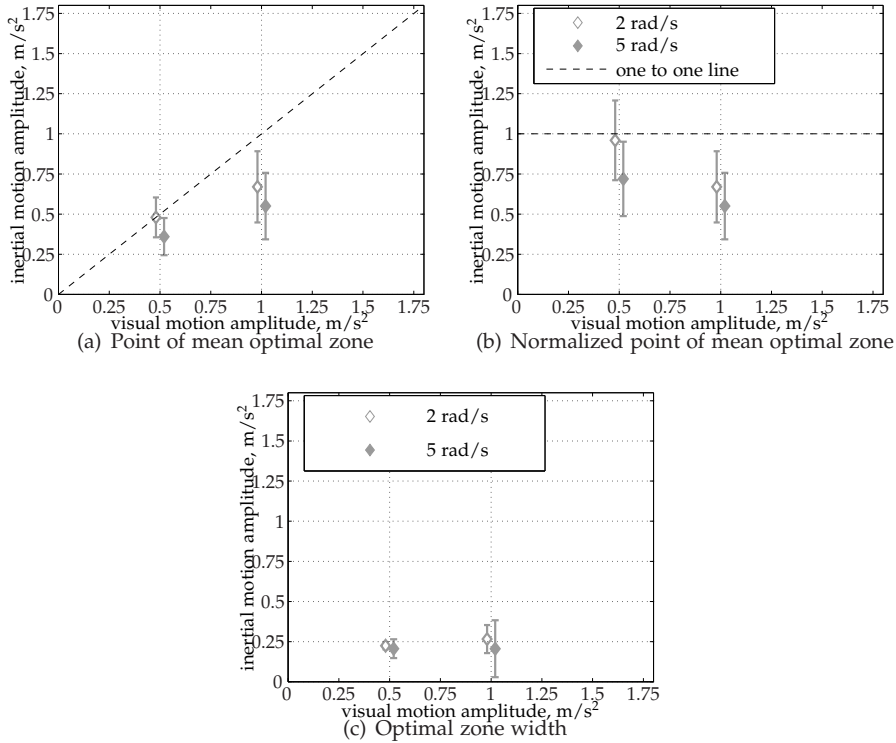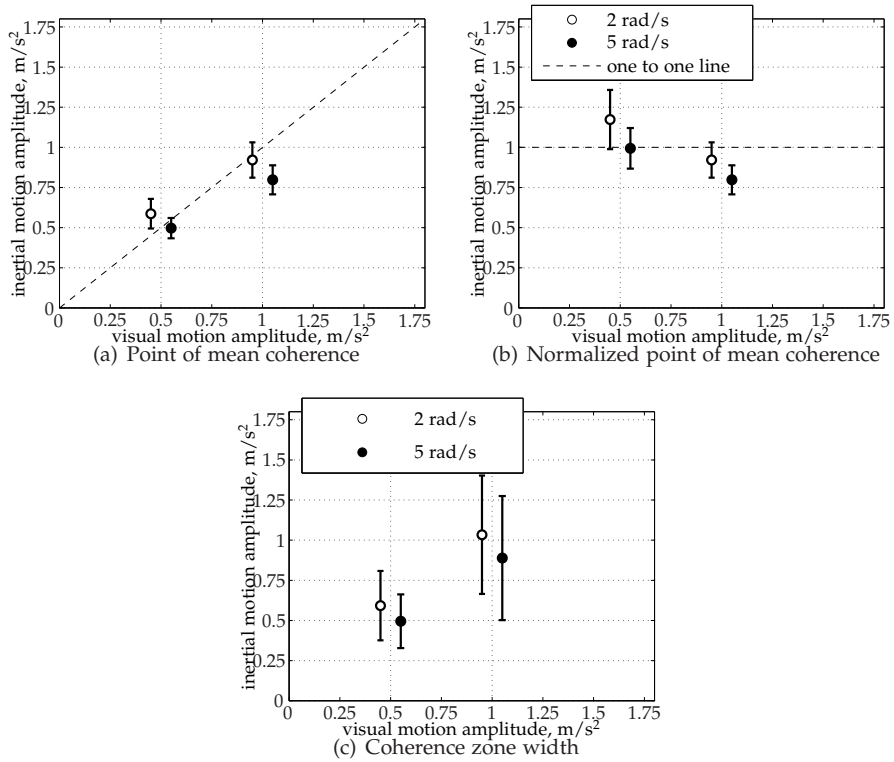**Figure 6.11:** *Mean PMC, Normalized PMC and CZW in the CMF simulator. The error bars represent the 95% confidence intervals.*

Figure 6.12: *Coherence and Optimal Zones in the CMF simulator. The error bars represent the 95% confidence intervals.*

compared to PMC, and OZW is compared to CZW.

Figure 6.13 shows the mean PMZ and the ZW obtained from both the coherence and optimal zone. A repeated measures ANOVA was conducted to test whether the PMZ and ZW were different between the coherence and optimal zone. The results of the statistical analysis are shown in Table 6.4.

The PMZ was significantly influenced by the three tested independent variables (instructions, visual amplitude and stimulus frequency). The PMZ values obtained during the coherence zone instructions were significantly higher than the PMZ values obtained during the optimal zone. Overall, the PMZ was higher for the experimental conditions with higher visual amplitude and lower for the conditions with higher frequency content. A significant interaction was found between the instructions and the visual amplitude (Table 6.4). In Figure 6.13(a) it can be seen that the PMZ from 0.5 to 1 m/s^2 is more pronounced for the CZ than for the OZ conditions.

The ZW was significantly higher for the coherence zone than for the optimal zone measurements. Overall, the ZW was higher for the experimental conditions with higher visual amplitude and lower for the conditions with higher frequency content. The ZW was affected by a significant interaction between the instructions and the amplitude. Figure 6.13(b) shows that the ZW increases with the visual amplitude for the coherence zone instructions whereas it remains constant for the optimal zone. There were no other significant interactions.
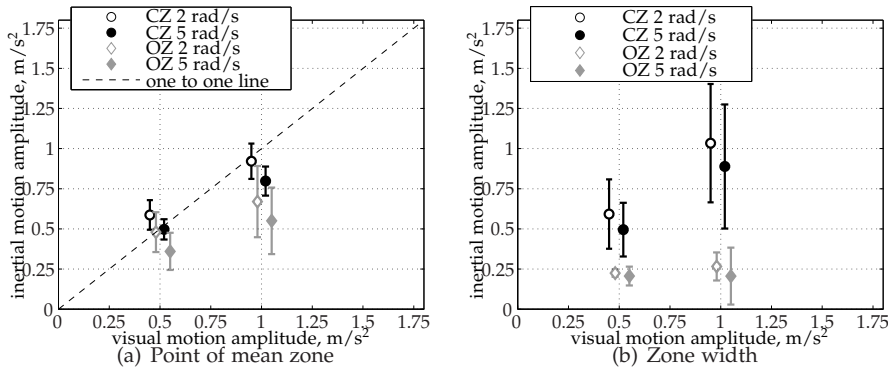
Figure 6.13: *Mean PMZ and ZW in the CMF simulator. The error bars represent the 95% confidence intervals.*

Table 6.4: *Repeated measures ANOVA results for the point of mean zone and the zone width in the CMF simulator. ($* = 0.01 < p < 0.05$, $** = p \leq 0.01$)*

Dependent measures	Independent Variables	F-ratio	p	sig.
PMZ	Instruction	$F(1,7) = 12.07$	0.010	*
	Amplitude	$F(1,7) = 54.76$	0.000	**
	Frequency	$F(1,7) = 13.54$	0.008	**
	Instruction * Amplitude	$F(1,7) = 7.59$	0.028	*
ZW	Instruction	$F(1,7) = 16.78$	0.005	**
	Amplitude	$F(1,7) = 16.08$	0.005	**
	Frequency	$F(1,7) = 7.97$	0.026	*
	Instruction * Amplitude	$F(1,7) = 12.81$	0.009	**

6.4.2 The VMS simulator

Optimal Zone versus Coherence Zone

Figure 6.14 shows the mean inertial accelerations obtained with the optimal and coherence zone methods in the VMS simulator. The trends found are very similar to those found in the CMF simulator (Figure 6.12). Again, the lower threshold seems comparable to the lower optimal amplitude. The upper threshold values are higher than the upper optimal inertial accelerations.

The PMZ and the ZW were used to compare the different instructions. Figure 6.15 shows the PMZ and the ZW for the optimal and coherence zone obtained in the VMS simulator. A repeated measures ANOVA was conducted to test the effect of the independent variables on the PMZ and ZW. The results are shown in Table 6.5. The effects of the instructions, amplitude and frequency on the PMZ for the VMS simulator were the same as in the CMF simulator. Again, the PMZ was significantly higher during the coherence zone measurements.
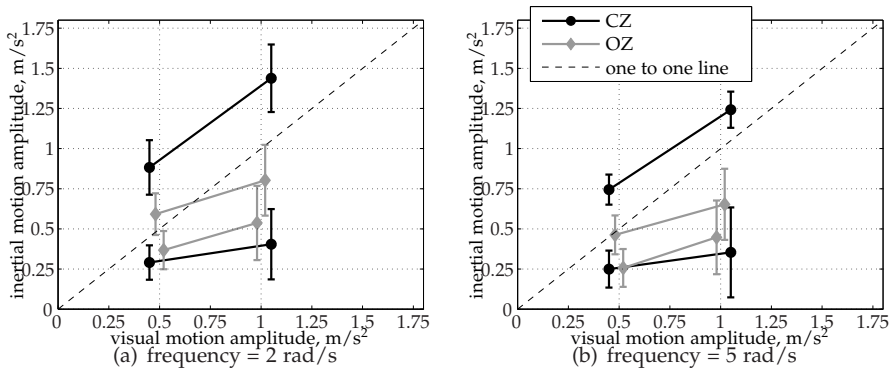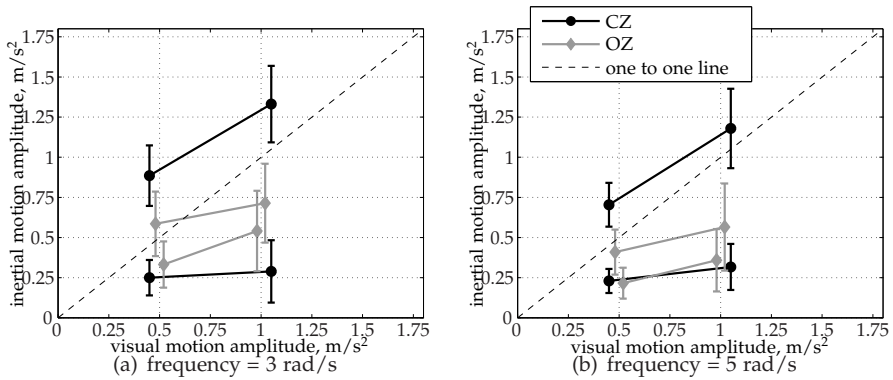
Figure 6.14: *Coherence and Optimal Zones in the VMS simulator. The error bars represent the 95% confidence intervals.*

Overall, the higher visual amplitudes increased the PMZ values whereas the higher frequency stimuli cause a decrease in the PMZ. Again, there was a significant interaction between the measurement method and the visual amplitude.

The ZW was significantly higher for the coherence zone measurements than for the OZ measurements. Overall, the inertial acceleration values were higher for the conditions with a higher visual amplitude and lower for the conditions with a higher frequency content. As was seen in the CMF, there was also a significant interaction between the instruction and the visual amplitude in the VMS. Additionally, in the VMS we found a significant interaction between the instruction and the frequency of the stimulus. If the average across the amplitudes for the ZWs of Figure 6.15(b) is taken, the ZW of the coherence zone is higher for the 3 rad/s (0.84 m/s^2) than for the 5 rad/s (0.67 m/s^2). For the ZW of the optimal zone the value of the 3 rad/s (0.21 m/s^2) condition is approximately the same as that of the 5 rad/s (0.20 m/s^2) condition. There were no other significant interactions.

6.4.3   CMF versus VMS

Figure 6.16 shows the mean PMZ and ZW in both simulators. Only the results of the 5 rad/s experimental conditions are shown since this was the only condition that was performed in both simulators. A statistical analysis was performed to test whether the simulator had any effect on the PMC or the CZW. Table 6.6 shows the repeated measures ANOVA results.

The statistical analysis showed no difference in the PMZ and the ZW results found in the different simulators. From Figure 6.16 it is observed that the PMC and the CZW were approximately the same between simulators. The significant
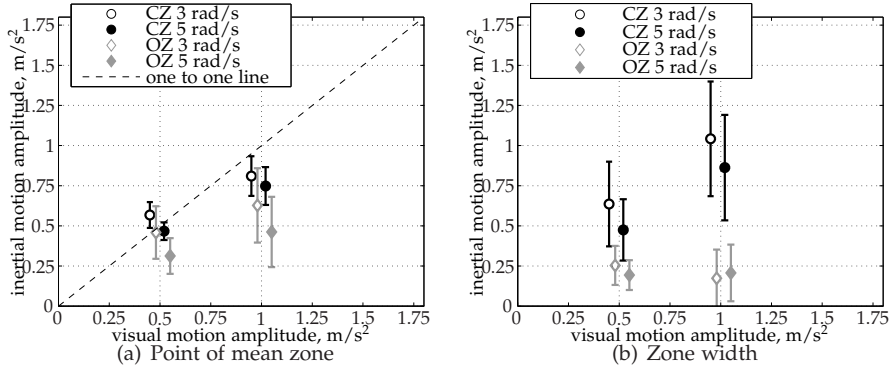
Figure 6.15: *Mean PMZ and ZW in the VMS simulator. The error bars represent the 95% confidence intervals.*
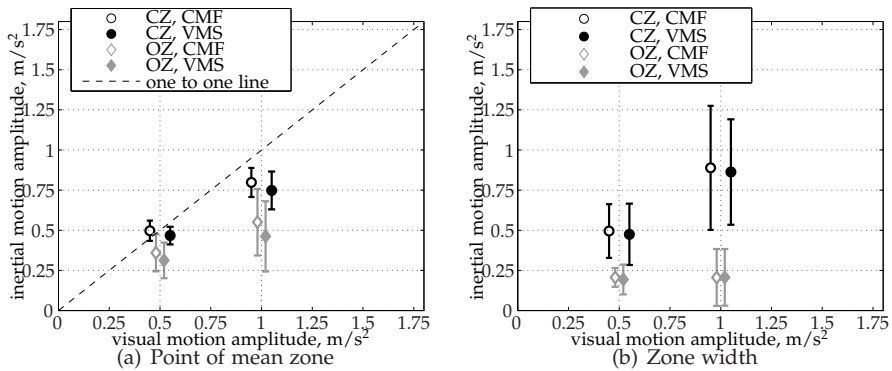
Figure 6.16: *Comparison of the mean PMZ and ZW between the CMF and VMS simulators at 5 rad/s. The error bars represent the 95% confidence intervals.*

Table 6.5: *Repeated measures ANOVA results for the point of mean zone and the zone width in the VMS simulator.* ($* = 0.01 < p < 0.05$, $** = p \leq 0.01$)

Dependent measures	Independent Variables	F-ratio	p	sig.
	Instruction	$F(1,7) = 8.59$	0.022	*
PMZ	Amplitude	$F(1,7) = 32.61$	0.001	**
	Frequency	$F(1,7) = 16.68$	0.005	**
	Instruction * Amplitude	$F(1,7) = 6.85$	0.035	*
	Instruction	$F(1,7) = 12.98$	0.009	**
	Amplitude	$F(1,7) = 19.70$	0.003	**
ZW	Frequency	$F(1,7) = 8.98$	0.020	*
	Instruction * Amplitude	$F(1,7) = 33.32$	0.001	**
	Instruction * Frequency	$F(1,7) = 7.90$	0.026	*

effects of the other independent variables, shown in Table 6.6, are very similar to what was reported in the previous sections and therefore will not be described any further.

Table 6.6: *Repeated measures ANOVA results for the point of mean zone and the zone width between the CMF and VMS simulators.* ($* = 0.01 < p < 0.05$, $** = p \leq 0.01$)

Dependent measures	Independent Variables	F-ratio	p	sig.
	Simulator	$F(1,7) = 3.41$	0.107	-
PMZ	Instruction	$F(1,7) = 17.44$	0.004	**
	Amplitude	$F(1,7) = 41.42$	0.000	**
	Instruction * Amplitude	$F(1,7) = 9.97$	0.016	*
	Simulator	$F(1,7) = 0.184$	0.681	-
ZW	Instruction	$F(1,7) = 11.95$	0.011	*
	Amplitude	$F(1,7) = 14.46$	0.007	**
	Instruction * Amplitude	$F(1,7) = 11.47$	0.012	*

6.5   Discussion

6.5.1   Coherence versus Optimal Zone

In this experiment we measured perception coherence zones and the perceived optimal zone. As was also found in a previous study [125], the optimal zone measurements did not result in one single value, but in a zone bounded by an upper and a lower limit. For comparison purposes, this optimal zone was defined in terms of point of mean optimal (PMO) zone and optimal zone width (OZW), similar to what was done in other studies [123, 124], for coherence zones which were defined in terms of point of mean coherence (PMC) and coherence zone width (CZW).

The perception coherence zones were different from the optimal zones. In general, the optimal zone was contained within the coherence zone, as if there

was a subset of coherent inertial and visual cues that was perceived as a "better match". Together, the coherence and optimal zones define three regions: within the optimal zone, outside the optimal zone and within the coherence zone, and outside the coherence zone. These regions can be considered as a gradient of accepted motion ranging from best (within the optimal zone) to worst (outside the coherence zone) motion. Nevertheless, it is not clear what perception mechanism allows subjects to distinguish between a coherent and an optimal region. Two different assumptions can be given to explain the differences.

First, the different initial inertial amplitudes could have created different paradigms when measuring the two zones. For the coherence zone measurements, subjects start with similar inertial and visual amplitudes and their objective is to increase or decrease the inertial amplitude until a difference between the inertial and visual amplitude is noticed. Conversely, for the optimal zone measurements, subjects start from different inertial and visual amplitudes and their objective is to change the inertial amplitude until the two stimuli are perceived as equal. Although both tasks sound similar, asking for differences between two stimuli appears to create a different result than asking whether two stimuli are equal. Different results for similar tasks were also found when measuring thresholds for linear motion [48,103,104]. Here, subjects were asked to indicate when they perceived motion and when they stopped perceiving motion. In the first case, the motion profile was a sinusoid with amplitude increasing from zero to a supra-threshold value while in the second case the motion profile was a sinusoid with its amplitude decreasing from a supra-threshold value to zero. The amplitude at which motion was detected was significantly higher than the value at which subjects stopped perceiving motion.

Second, what could also have led to the differences between the two zones was what may be referred to as "tuning for comfort". Higher inertial amplitudes can be more uncomfortable for the subjects than lower inertial amplitudes. For the optimal zone, subjects were asked to find the best match between visual and inertial information. It could happen that the best match is not where the visual amplitude is equal to the inertial amplitude but rather the one that feels to be the most comfortable, that is, 'less arousing' inertial amplitude which is *still* perceived as coherent with the visual motion. Such an approach would lead to a PMO lower than the PMC, since for the coherence zone measurements subjects were looking for the boundary of the coherence and not for the most comfortable motion.

This second explanation agrees with the results: PMOs were significantly lower than the PMCs. The PMC was generally closer to the one-to-one line than the PMO. Careful observation of the limits for both zones shows that this difference was caused mainly by the upper threshold and upper optimal amplitude since the lower bounds of both zones were similar. The coherence zone

upper threshold is always above the one-to-one line, whereas the upper optimal amplitude crosses the one-to-one line for the 2 rad/s conditions and is below the one-to-one line for the 5 rad/s conditions. It appears that the optimal zone excludes only the higher inertial amplitudes within the coherence zone.

The PMO and PMC both increase with the visual stimulus amplitude and decrease with the visual stimulus frequency. These trends agree well with those reported for optimal zone measurements in sway [125] and coherence zone measurements in yaw [123, 124]. A possible explanation for the effect of stimulus frequency on the coherence zone, stated in Refs. [123] and [124], is that the semi-circular canals dynamics have a higher gain in velocity at higher frequencies. This higher gain may not be (fully) accounted for during the internal comparison of inertial and visual cues, leading subjects to down tune the inertial cues at higher frequencies. In the present study, since the tested motion was sway, a similar explanation might be found in the sensitivity to jerk (i.e., the derivative of acceleration). For the same acceleration amplitude, when the frequency increases the jerk also increases. Grant and Haycock [78] stated that the subjective notion "motion strength" may be a function of the jerk and acceleration of an inertial motion signal. It could have happened that subjects lowered the upper threshold of the conditions with the higher frequency so as to lower the jerk and therefore lower the perceived "motion strength".

The PMO and PMC both increase with visual stimulus amplitude, but not as much as would be expected. For the lowest amplitude the PMCs and PMOs are close to the one-to-one line and for the highest amplitude they are both below this line. This decrease with respect to the one-to-one line is more evident for the PMO. If these results were to be used in motion filter tuning, the motion gain (i.e., the ratio between the inertial and visual motion), should generally be less than one, especially for the highest amplitude. This supports the findings of other studies [74–77, 125] where a motion gain of one was judged as too strong. One reason why the one-to-one motion may be judged too strong in a simulation environment may be the quality of the visual display [74, 75]. Such hypotheses still need to be validated.

The OZW was significantly lower than the CZW. The CZW was affected by the visual amplitude and frequency and, as was found previously for yaw motion [123, 124], was coupled to the PMCs. A higher PMC corresponds to a higher CZW value and vice-versa. Unlike the CZW, the OZW was unaffected by these two independent variables. The OZW remained approximately the same (around 0.23 m/s^2) for all the experimental conditions. This is perhaps the most remarkable difference found between the optimal and the coherence zone. Since the lower thresholds of the coherence and optimal zones varied comparatively less with frequency than the upper thresholds, the main difference in the zones' width may be related to the upper limits. As seen before, the upper limits of the

optimal zone were significantly lower than those of the coherence zone. Again, this result may be related to a "tune for comfort" effect, although no reason could be found as to why this would lead to an OZW which is unaffected by visual stimulus amplitude or frequency.

Further research should be done to investigate if the constant OZW results found for the tested amplitudes also occur at higher amplitudes, and whether comfort has an effect on the optimal zone measurements. In this study, the optimal zone measurement always started with initial inertial amplitudes that were higher or lower than the visual amplitudes whereas the coherence zone measurements had an initial inertial amplitude that was close to the amplitude of the visual stimulus. As stated previously, these different initial conditions could have biased the differences we found between the two zones. Therefore, the effect of these initial conditions on the zones we obtained should be further investigated. For example, the coherence and optimal zone could be measured in the same experimental trial. Subjects could then indicate optimal amplitude first and thereafter the boundaries of the coherence zone, or the other way around. For applications in motion simulation, it is also important to determine what the impact on perception and behavior is when moving out of the optimal zone while remaining within the coherence zone.

This study showed that the inertial amplitudes inside the coherence zone are not perceived equally. In fact, the lower inertial amplitudes of the coherence zone seemed to be perceived as the best match for the tested visual amplitudes. This might indicate not only that the use of lower inertial amplitudes is acceptable in flight simulation but also that these are optimal to use in such environment. Actually, previous studies [74–77] already showed that one-to-one motion (which is within the coherence zone) was perceived as being too strong. Theoretically, one would expect to have the best perception during one-to-one motion since this would deliver motion cues closer to the ones available in a vehicle. However, one-to-one simulation in current simulators is not possible, not only due to limitations in the motion and visual systems of the simulator but also due to different expectations that subjects might have when in a simulator. Therefore, a visual amplitude in a simulator environment could be perceived differently than in the real world. For example, Kemeny and Panerai [6] mentioned that in driving simulators, observers underestimate driving speed when image contrast, luminance or texture are reduced. They also observed that drivers underestimate distances to a lead vehicle when compared to a similar situation in a real road. Therefore, instead of matching the inertial amplitude with the expected displacement in the real world, the inertial amplitude should be matched to the displacement perceived from the virtual world. Current self-motion perception models do not make a distinction whether the motion was felt in the aircraft or in the simulator. Therefore, when minimizing

the error between the motion perceived in the aircraft from that perceived in the simulator, both perception models have the same structure and parameters. However in this experiment, the preferred inertial amplitude was lower than the visual amplitude, which might indicate that one-to-one motion was perceived as too strong. Therefore, by acknowledging this inertial overestimation, we could use a MCA that tries to minimize the error between the perception in the simulator, which includes an overestimation of inertial cues, and the perception in the aircraft, where inertial cues are not overestimated due to correct visual-inertial information. This would basically mean that the self-motion perception model applied to the simulator motion would be different from the self-motion perception applied to the aircraft motion.

6.5.2   CMF versus VMS

The measurements of the coherence and optimal zone did not differ much between the VMS and CMF simulators. The effects found in the PMZs and ZWs were small and not significant. In terms of visual systems, both simulators had WAC windows but the VMS had lower resolution. Regarding the motion platforms, the VMS had a lower signal-to-noise ratio (SNR). However, the inertial amplitudes obtained for the optimal and coherence zone measurements were very similar for both simulators. The PMZ data, especially the PMO, were slightly lower for the VMS simulator, however this effect was not significant. Nevertheless, final conclusions should not be made based only on the 5 rad/s conditions that were tested in both simulators.

Two factors were expected to influence the PMZ value [75], the quality of the visual cues and the quality of the inertial cues. A simulator that is able to deliver visual and inertial cues as close as possible to the real situation is expected to have PMZ values close to the one-to-one line. When comparing the simulators, we expected the simulator with better motion quality to have PMZs closer to the one-to-one line. In this experiment, the visual system type was similar in both simulators and the visual scene content was the same. Therefore, we expected that any influence in the PMZs and ZWs to be attributed to the inertial cues.

In this experiment, we expected a down-tuning of the inertial motion in the VMS, since the motion platform has lower SNRs which can induce subjects to lower the inertial amplitude in order to lower the inertial noise. On the other hand, one could also expect subjects to increase the inertial amplitude to facilitate the detection of the sway motion, in the presence of the noise in the platform. The slightly lower PMZ for the VMS simulator indicates support for the down-tuning hypothesis. However, one should be careful when drawing any conclusions from the data since this trend was not statistically significant.

To test whether the PMZs and ZWs are affected by "bad motion" one should have a substantial difference between the motion quality of both platforms. Ap-

parently, the SNR difference between the simulators in this study was not large enough or there are other factors related to motion quality that are not captured by SNRs. Alternatively, one could use the same motion base and try to artificially degrade its quality so that a comparison between "different" motion bases could be done, similar to the approach developed by Nieuwenhuizen et al. [128].

6.6 Conclusion

This study compared coherence in the perception of a combination of inertial and visual motion with the tuning that a subject in a simulator arrives at when given the opportunity to select an optimal inertial motion amplitude matching a visually presented motion.

The preferred motion amplitude when selecting an optimal inertial motion amplitude to match a visual motion amplitude depends strongly on the initial motion applied; when starting with a higher inertial amplitude, the finally selected amplitude is higher, and vice versa.

This leads to a zone of amplitudes selected as optimal. When comparing this zone to the coherence zone, it appears that the optimal amplitude zone is a zone *within* the coherence zone. Apparently, even though all motions within the coherence zone are perceived as coherent, some motion amplitudes are preferred over others within that zone. The point of mean coherence was significantly higher than the point of mean optimal zone. This could be an indication that the optimal amplitude instructions are related to "tuning for comfort".

The study was performed on two different simulators, with a partial overlap of the experimental conditions on the two simulators. No significant differences were found between results produced in the different simulators.

Perceived mismatch between visual and inertial cues

In Chapters 5 and 6 we showed that in a simulation environment, a visual amplitude equal to the inertial amplitude does not always provide the best perceived match between visual and inertial motion. This result might be caused by the quality of the visual and inertial cues presented to subjects. This chapter investigates the effect of different visual cues, like field-of-view and scene content, on the preferred scaling between visual and inertial cues.

7.1   Introduction

Motion simulators provide pilots and drivers with inertial and visual cues similar to the ones experienced in a real vehicle. Generally, the inertial cues used in motion simulators are scaled and filtered versions of the vehicle inertial cues [11]. However, simulators capable of large displacements are able to perform certain maneuvers one-to-one (i.e., without scaling or filtering the original inertial cue). When using one-to-one motion, the amplitude of the visual cue displayed in the virtual world should be equal to the amplitude of the simulator inertial cue. Although one-to-one simulation is possible for specific maneuvers, it is often perceived as incorrect by subjects [74–77].

Studies have found that the amplitude of the inertial cue has to be lowered to prevent subjects from perceiving motion as "too strong" [74–77]. Two driving studies [76, 77] using a slalom maneuver showed that the preferred inertial condition had a motion gain (i.e., the ratio between the inertial and visual cues) of approximately 0.6. Similar results were found by Groen et al. [74] when simulating a take-off maneuver, where a motion gain lower than one was used since pilots perceived one-to-one motion as unrealistic. In two other experiments [125, 129], subjects had to choose the inertial amplitude of a sinusoidal motion profile that best matched the movement being displayed via the simulator projectors. In both studies, subjects chose an inertial amplitude lower than the visual amplitude. In all these studies, researchers found that in order to have a realistic simulation, the motion gain had to be lower than one, independently of the type of task (flying or driving). This necessity to lower the motion gain occurred for surge and sway motion but not for yaw motion [75, 120]. However, this difference between the motion gains for linear motion and the ones for angular motion was not shown on the same experiment, using the same subjects, visual characteristics, and apparatus.

Another issue that seems to be ignored is the effect that visual characteristics or scene content may have on the motion gains. For example, visual characteristics are neglected when using the Sinacori Motion Fidelity Criteria [18, 20] to measure motion fidelity. When measuring a motion gain, subjects infer self-motion from the simulator visuals, and then tune the inertial motion until it matches the visual motion. Therefore, the perceived visual motion might be affected by the "quality" of the visual information being displayed. Consequently, if the perceived visual motion is affected by the visual "quality", the motion gain value will also be affected.

Visual characteristics like field-of-view (FoV) or scene content have been shown to influence the perception of self-motion [130–135]. For example, Duh et al. [132] showed that a larger FoV increased the perceived self-motion. However, the effect of the FoV in self-motion perception seems to depend on the degree-of-freedom. Pretto et al. [135] showed that large FoVs are not necessary to

estimate the amplitude of visual rotations in yaw but that horizontal FoVs of at least 60 degrees are advisable for speed perception in surge. In another study, Berger et al. [134] showed that changing scene content by including visuals with extra information (e.g., optic flow and horizon) helped pilots to stabilize a simulated helicopter. Therefore, we expect that a change in FoV and scene content might affect the motion gain. As suggested (but not studied) by Groen et al. [75], having visual characteristics closer to the ones available in real-life should then increase the motion gain to values closer to one.

The goal of this study is to test whether different visual characteristics like FoV and scene content influence the scaling between visual and inertial amplitude. An experiment was conducted where subjects had to match the visual amplitude with the perceived inertial amplitude. This is different than what we did in our previous studies [125, 129] where subjects had to match the inertial amplitude with the perceived visual amplitude. Changing the task in this experiment allowed us to, on the one hand, compare the differences between the two approaches and, on the other hand, create experimental conditions independent from the inertial amplitude that might be chosen by subjects. The amplitude matching task in this experiment was performed for two FoVs, three visual scenes, and three degrees-of-freedom of inertial motion. The results help to understand the influence of different visual characteristics on the motion gain. The simulator visual and inertial systems can then be adjusted to make the perceived motion gain closer to one, which may improve the realism of the simulation. Alternatively, the visual gain may be used to quantify the realism or image quality of the visuals displayed in the simulator.

7.2   Method

7.2.1   Subjects

Nineteen subjects participated in this experiment (11 male and 8 female). The subjects had an average age of 29 years with a standard deviation of 11 years ranging between 18 and 63 years. None of the subjects had any vestibular or motor skill deficit. All experimental conditions had been approved by the local ethics committee. Subjects' rights were based on the Declaration of Helsinki on ethical principles for medical research involving human subjects. One subject was not able to finish the experiment due to scheduling constraints.

7.2.2   Apparatus

The experiment was conducted at the Desdemona research simulator (see Figure 7.1) located at the TNO institute in Soesterberg, the Netherlands. This simu-

lator features a centrifuge based design with six degrees-of-freedom (DoF) [29]. In this study, the 8-meter horizontal actuator of the simulator was used to generate surge and sway motion. Yaw motion was also used in this experiment and was performed by the simulator yaw gimbal which has an unlimited angular displacement.
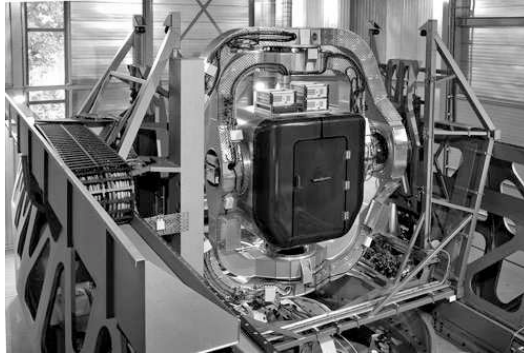
Figure 7.1: *Desdemona research simulator.*

The simulator visual system has three DLP beamers projecting on a three-part flat screen. The total field-of-view (FoV) is 120 horizontal degrees and 32 vertical degrees. Each beamer displays a resolution of 1400 x 1050 pixels and has a refresh rate of 60 Hz. Besides the visual system, the simulator cabin contains an F-16 cockpit with realistic throttle, side-stick and rudder pedals. The side-stick was the only control input used in this experiment.

7.2.3   Experimental design

The experiment had three different experimental blocks, one for each degree-of-freedom. The DoFs tested were surge, sway and yaw. The order in which the experimental blocks were performed by subjects was randomized using a Latin square design. In each block we tested two FoVs, three visual scenes, and two different initial conditions. A Latin squares design was also used to randomize the order in which the FoVs, visual scenes, and initial conditions were conducted by each subject.

The two FoVs were generated using one or three flat-screens. For one screen, the horizontal FoV was 41 degrees while for three screens, the horizontal FoV was 120 degrees. The vertical FoV was kept at 32 degrees for both FoV configurations. We expect the wider FoV condition to induce an increased perception of self-motion.

The three visual scenes are shown in Figure 7.2. Visual content was varied by changing the location or number of objects in the virtual world. The first

visual scene is located near a rural road outside a city (OC), the second scene
is located in a city center (CC), and the third scene is located in a city center
with balloons randomly placed in the air (CCB). In the OC scene, subjects could
only see a road, a city at a large distance, and a tree. In this scene, movement
is mainly perceived by the movement of the ground and sky textures. The CC
scene contained objects that can be easily found in a city like buildings, road,
garbage bins, advertisement posters, among others. These objects help to scale
the perceived movement. The CCB visual scene had balloons to create extra
optic flow. This additional optic flow is expected to increase perception of self-
motion.

(a) OC

(b) CC

(c) CCB
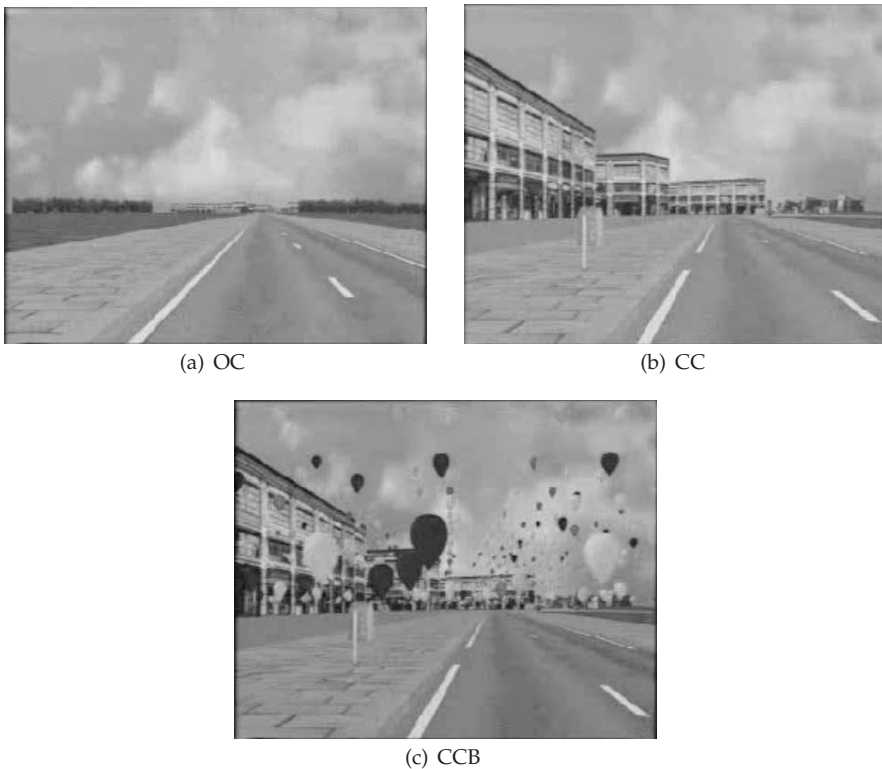
Figure 7.2: *Visual scenes where OC is the scene outside the city, CC is the city centre scene, and CCB is the city centre scene but with balloons randomly placed in the air.*

Two different initial conditions were used in this experiment. In one initial
condition, the visual amplitude was higher than the inertial amplitude (high ini-
tial condition) whereas in the other the visual amplitude was smaller than the
inertial amplitude (low initial condition). In our previous studies [125, 129] we

found that different initial conditions led to motion gains statistically different from each other, which means that the preferred motion gain did not converge to a single value, but rather formed an interval or zone, bounded by the motion gains obtained from the two different initial conditions. Therefore, for methodological reasons it would be incorrect to have only one initial condition in this experiment since it would bias the results. For this study, the visual input in the high initial condition was a random value between values 40% and 60% higher than the inertial amplitude. The visual input in the low initial condition was a random value between values 40% and 60% lower than the inertial amplitude.

For the surge and sway DoFs, the inertial motion profile was a sinusoid with an amplitude of 2 m and a frequency of 1 rad/s. For the yaw DoF, the inertial motion profile was a sinusoid with an amplitude of 20 degrees and a frequency of 1 rad/s. All sinusoids had fade-in and fade-out periods to guarantee that the motion platform started and finished with zero position, velocity and acceleration. Both the fade-in and fade-out lasted for one size period (2π seconds). The total duration of the motion sinusoids was variable and depended on the time it took the subjects to complete the task. In summary, there were 36 experimental conditions (3 DoFs x 2 FoVs x 3 visual scenes x 2 initial conditions) divided in three experimental blocks of 12 conditions each.

7.2.4   Procedure

Subjects started the experiment by reading the briefing form and signing an informed consent. Then, they were seated in the simulator and secured by a five-point safety harness. They wore an active noise cancelation headset where white noise was played to mask the sound of the simulator's actuators. This headset was also used for communication with the experiment supervisor. Before starting with the experimental measurements, each subject had several practice runs in the three different DoFs until they felt acquainted with the task. Their task was to obtain the best match between the visual and inertial amplitude. For that, they had to vary the visual amplitude by means of two directional buttons in the side-stick while perceiving the inertial amplitude. One directional button was used to increase or decrease the visual amplitude by 15% while the other was used to increase or decrease the visual amplitude by 5% (finetuning).

The measuring phase started with one of the three experimental blocks: surge, sway, and yaw. The initial visual amplitude depended on whether it was a high or low initial condition. Subjects were neither informed about the different initial conditions, nor that the inertial amplitude was in fact constant between experimental conditions within the same DoF. Each experimental condition started by pressing the "fire" button of the side-stick, which made the simulator move visually and inertially with the same phase and frequency but different amplitude. Then, subjects used the directional buttons to obtain the

best match between the visual and inertial amplitude. When satisfied with
the amplitude value, subjects pressed the "fire" button to stop the simula-
tion. At this moment, subjects told the experimenter their current MIsery SCore
(MISC) [9] according to Table 7.1. This scale was visible in the cabin interior. The
experiment was aborted if subjects reported a MISC higher than six. After com-
pleting all 12 experimental conditions for the first experimental block, subjects
proceeded in the experiment by conducting the same task for the two remaining
experimental blocks. The experiment took approximately 90 minutes. Subjects
were allowed to take a 5 to 10 minutes break between experimental blocks if
needed.

Table 7.1: *The MIsery SCore (MISC) rating scale [9] used to measure motion sickness*

Symptom		MISC
No problems		0
Slight discomfort but no specific symptons		1
Dizziness, warm, headache, stomach awareness, sweating, etc.	Vague	2
	Some	3
	Medium	4
	Severe	5
Nausea	Some	6
	Medium	7
	Severe	8
	Retching	9
Vomiting		10

7.2.5   Data analysis

The subjective visual amplitudes measured during the experiment were divided
by the corresponding simulator inertial amplitudes to yield (what we define as)
visual gains. Although differences between visual gains obtained with high and
low initial settings were observed in other studies [125, 129], we just defined
"the" visual gain per subject and condition to be the average of each pair of
matching high and low settings. This was done because the main objective of
this research is not to study a visual gain zone but the effect of different visual
characteristics on the visual gains. Therefore, for every subject we averaged the
values between the high and low initial conditions. We then averaged over sub-
jects for each experimental condition (DoF, FoV, Scene content). The visual gain
values that were higher than the 75th percentile plus three times the interquart-
ile range or lower than the 25th percentile minus three times the interquartile
range of their experimental condition were considered extreme outliers and
were discarded from the analysis. As a result, the data of two subjects were not

used in the analysis. A repeated-measures ANOVA was conducted to test if the DoF, FoV or scene content had an effect on the visual gains. A Greenhouse-Geisser (G-G) correction was applied whenever sphericity was violated, resulting in corrected p values that were more conservative. All statistical tests were performed with SPSS 19.

7.3   Results

7.3.1   Motion sickness

Besides the two subjects considered outliers and the subject that was not able to finish the experiment due to time constraints, another four subjects felt motion sick during the experiment and were not able to finish all experimental conditions. These four subjects felt motion sick during the surge condition. The remaining twelve subjects were able to conduct the experiment without serious motion sickness. The total mean MISC for these subjects was of 0.55.

7.3.2   Visual gains

Figure 7.3 shows the average visual gains for all experimental conditions. A visual gain of 1 means that the selected visual amplitude is equal to the inertial amplitude. Therefore, a visual gain higher than 1 means that the visual amplitude is higher than the inertial amplitude, whereas a visual gain lower than 1 means that the visual amplitude is lower than the inertial amplitude. The results from the repeated measures ANOVA are shown in Table 7.2.
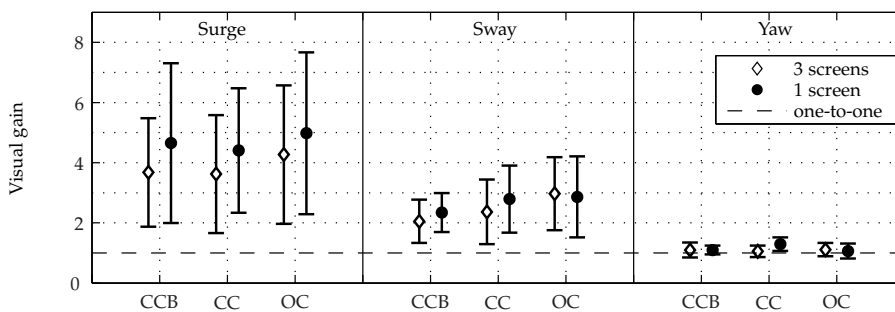

Figure 7.3: *Average visual gains for the three degrees-of-freedom. The error bars indicate the 95% confidence intervals.*

The results of the repeated measures ANOVA (Table 7.2) showed a significant main effect of the DoFs on the visual gains. From Figure 7.3 we observe

Table 7.2: *Repeated measures ANOVA results for the three degrees-of-freedom. (** is highly significant ($p \leq 0.01$), * is significant ($0.01 < p \leq 0.05$))*

Independent variables	Correction	F-ratio	p	Significance
DoF	G-G	$F(1.19,13.08) = 7.94$	0.012	*
FoV	-	$F(1,11) = 11.55$	0.006	**
Visual scene	-	$F(2,22) = 4.09$	0.031	*
DoF $\times$ FoV	-	$F(2,22) = 5.77$	0.010	**

that the surge has the highest visual gains, while yaw has the lowest. The average visual gains between DoFs were 4.27, 2.56 and 1.12 respectively for surge, sway and yaw. A post-hoc test using a Bonferroni correction showed that the yaw visual gains were significantly lower than the surge ($p = 0.036$) and sway ($p = 0.028$) visual gains. A one sample t-test (Table 7.3) showed that these surge and sway visual gains were statistically different from 1, but also that the yaw visual gain was not statistically different from 1.

Table 7.3: *One sample t-test to compare the average degrees-of-freedom with one. (** is highly significant ($p \leq 0.01$), - is not significant ($p > 0.05$))*

Independent variables	t	p	Significance
Surge	$t(11) = 3.24$	0.008	**
Sway	$t(11) = 3.56$	0.004	**
Yaw	$t(11) = 1.41$	0.187	-

There was also a significant main effect of the FoV on the visual gains. The condition with three screens had significantly lower visual gains than the condition with one screen. The average absolute difference between these conditions was 0.36. Figure 7.3 shows that this difference is mainly caused by the surge visual gains. The statistical analysis (Table 7.2) also revealed a significant interaction between the DoF and the FoV. This effect can be seen on Figure 7.3, where the visual gain differences between the experimental conditions with different FoVs are higher for surge motion. Using contrasts to break down the significant interaction, we found that the interaction between surge and yaw motion for different FoVs is significant; $F(1,11) = 12.63, p = 0.005$. This means that the differences in visual gain between the FoV conditions are higher for surge than for yaw motion. On the other hand, we did neither find significant differences between surge and sway motion for different FoVs ($F(1,11) = 4.23, p = 0.064$) nor between sway and yaw motion for different FoVs ($F(1,11) = 0.58, p = 0.462$).

From Figure 7.3, we observe an increasing trend in visual gain from the visual scenes with more content to the visual scenes with less content. The repeated measures ANOVA (Table 7.2) showed a significant main effect of scene

content on the visual gains. The average visual gains were 2.49, 2.59 and 2.86 for the city center balloons (CCB), city center (CC) and outside city (OC) scenes, respectively. However, a post-hoc test using a Bonferroni correction revealed no significant differences between the three levels of scene content.

7.4   Discussion

The main objective of this chapter was to study the effect of field-of-view (FoV) and scene content on the visual gains (i.e., the ratio between the visual and inertial amplitudes) for surge, sway and yaw. Results showed a significant main effect of the FoV on the visual gains. The condition using three screens showed visual gains closer to unity than the condition with one screen. This means that the visual amplitudes chosen for the three screens experimental condition were closer to the simulator inertial amplitude. It may be assumed that the visual amplitude will be closer to the inertial amplitude when the visual characteristics are closer to the ones encountered in the real world, where the human effective FoV is approximately 200 degrees horizontally and 150 degrees vertically [136]. It was shown before [131, 133–137] that a narrower FoV degrades human performance in navigation, perception of size and space, and spatial awareness. This is related to the role of the peripheral view in the perception of self motion. By narrowing the FoV, we are limiting the amount of visual flow used by the peripheral vision and therefore, reducing perceived self-motion [110, 130, 132]. In our study, the wider FoV made subjects perceive themselves as moving faster which made them lower the visual amplitude to values closer to the inertial amplitude.

In this experiment, subjects were also exposed to three different visual scenes: a city center scene containing random balloons in the air (CCB), the same city center scene but without the balloons (CC), and a visual scene in a grass field where the city is seen at a large distance (OC). Since the CC had more recognizable objects than the OC, it was expected a scaling of the visual amplitude closer to the perceived inertial amplitude. In fact, Monen and Brenner [37] showed that without recognizable objects for proper scaling, it is difficult for humans to detect changes in their own velocity. The CCB scene had extra optic flow cues when compared with the CC scene. Optic flow has been repeatedly shown to increase perception of self-motion and control performance [131, 134]. In our study, we found a significant increasing trend showing a smaller visual gain for the CCB scene and a higher visual gain for the OC scene. The CCB visual gains were also closer to one, meaning that they were in the vicinity of the simulator's inertial amplitude. Therefore, when the visual scene contains cues similar to what is experienced in reality, subjects tune their visual amplitude closer to the platform inertial amplitude. However, the post-hoc tests

revealed that there were no significant differences between the different scenes. This could be due to the road displayed in all scenes. In all conditions, the initial position in the virtual world was not random. Therefore, subjects could have used the road as a cue to chose their visual amplitude based on their distance to it. Having a random position in the virtual world might have prevented such strategies from being used.

When comparing the visual gains between the different DoFs, we found that the yaw visual gain was much lower than the sway and surge visual gains. The yaw visual gain was not statistically different than one, which means that subjects chose a visual amplitude very close to the inertial amplitude generated by the motion-platform. Therefore, the best match between visual and inertial motion for the yaw case is when these are approximately the same. On the other hand, for the sway and surge case, the visual gain was higher than one, meaning that subjects considered the best match between visual and motion when the visual amplitude was higher than the inertial amplitude. Previous studies found that the motion gain (which is the inverse of the visual gain used in this study) was underestimated for lateral [75–77, 125] and longitudinal [74, 121] linear motion but not for angular motion [120]. By converting our mean visual gains to motion gains we found a motion gain of approximately 0.23, 0.39 and 0.89, respectively, for surge, sway and yaw. The surge results are similar to what Harris et al. [121] found when subjects matched visual motion to a target distance presented physically, whereas the yaw results are in line with what Van der Steen [120] and Valente Pais et al. [124] found when measuring coherence zones, which are defined as zones where inertial and visual amplitudes are perceived as coherent although their values are different. However, in these studies, the different degrees of freedom were studied in separate environments impeding their comparison. In our study, the same subjects and apparatus were used, allowing for a valid comparison.

The sway motion gains found in this study are smaller than what we found previously [125, 129]. The differences in the motion gains were possibly caused by differences in the measuring task. In our previous studies, subjects tried to find an inertial amplitude that would match their visual perception. In this study, however, subjects tried to obtain a visual amplitude that matched their perception of inertial motion. Therefore, it seems that the perceptual information taken from reference visual cues is different than the perceptual information taken from reference inertial cues even if both the inertial and visual cues have the same physical amplitude. This hypothesis needs, however, to be validated experimentally since it is based on results taken from different studies. Nevertheless the study from Harris el al. [121] seems to show that there is indeed differences between using visual or inertial motion as a reference. Although using a measuring task different from the one used in our studies,

Harris el al. [121] found differences in distance estimation when, in one condition, subjects had to match physical motion to a visual target, whereas in other condition, subjects had to match visual motion to a physical target.

The overestimation of the linear motion visual gains (surge and sway) might be related with the different optic flows shown for each DoF and its connection to depth perception. Figure 7.4 shows an example of optic flows produced for surge, sway, and yaw self-motion. For surge and sway, the optic flow depends on the distance between the observer and the objects shown in the visual scene. The optic flow will then be a cue that subjects can use to interpret depth. For yaw, on the other hand, the optic flow is constant and independent from the distance between the observer and the objects shown in the visual scene. This means that for yaw motion, the self-motion information taken from a generic visual scene might be the same as the information taken from a realistic visual scene because yaw optic flow presents no depth perception cues [38]. Therefore, it is less probable that yaw self-motion information is interpreted incorrectly from the visual scene. This would explain why the yaw visual gains are approximately one and why Valente Pais et al. [123] found no differences between the coherence zones obtained for a star-field visual scene or the ones obtained for an airport visual scene. For surge and sway, on the other hand, depth perception is crucial for the perception of self-motion from visual information [38]. Depth perception depends on visual cues that can be grouped into three categories [138]:

- Primary depth cues, like accommodation, convergence, and stereopsis.

- Pictorial depth cues like perspective, texture gradient, relative sizes, occlusion, atmospheric perspective, lighting and shading, and blur.

- Motion-induced cues like motion parallax and optic flow.

In the real world, these depth perception cues exist naturally and although some might be impoverished or absent, they are never in conflict [138]. In a virtual world, on the other hand, these depth cues might conflict with each other due to the properties of synthetic displays [138]. For example, the displays used in this study provided incorrect accommodation and convergence since far away objects were not focused at infinity. Examples of other missing cues in this study were stereopsis, the lack of shadows, and motion parallax. Therefore, a conflict in depth perception cues could create uncertainties in the self-motion information extracted from the displays, influencing then the surge and sway visual gains as shown by the high confidence intervals found for these DoFs. Thus, reducing the conflicts in the depth perception cues is hypothesized to create visual gains of approximately one, similar to what we found in yaw where there is no conflict. This also shows that the visual gain seems to be a

reliable variable to measure visual realism or image quality. With the visual gain, it is possible to mutually compare different visual aspects and access their effect on simulation realism. This makes the visual gain an important tool in investments aiming at improving virtual reality since it can be used as a decision factor when there is a trade-off between different visual aspects.
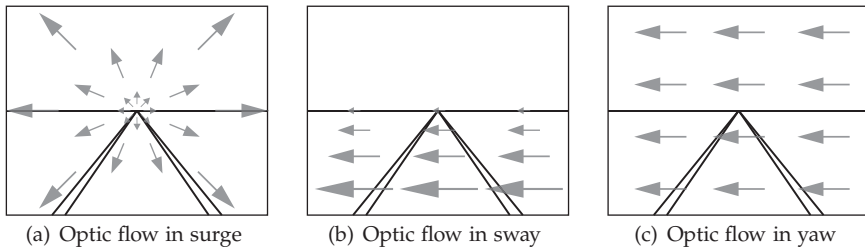

(a) Optic flow in surge   (b) Optic flow in sway   (c) Optic flow in yaw

Figure 7.4: *Example of the optic flow field for surge, sway, and yaw. For surge and sway the image velocity varies with the distance to a certain point in the visual scene.*

In this study, there were also some subjects that could not finish the experiment due to motion sickness. Interestingly, these dropouts occurred all during the surge conditions. According to Bos and Bles [139], it is expected to have motion sickness during motion conditions that affect the subjective vertical, which happens during the surge and sway, but not during yaw, especially for frequencies around 1 rad/s. However, their model predicts the same amount of motion sickness for surge and sway while in our experiment, the motion sickness issues we had occurred during surge. Even so, there could be ecological reasons making humans more prone to motion sickness induced by surge motion than sway motion. Lateral falls, for example, can be prevented more easily than forward and especially backward falls.

7.5   Conclusion

In this study we tested whether the field-of-view and scene content influenced the perceptual scaling between visual and inertial surge, sway and yaw motion. Results showed that a wider field-of-view of an artificial imagery led to visual amplitudes closer to the inertial amplitudes of a motion platform. We also found that the visual scene with the most salient visual cues showed visual amplitudes closer to the inertial amplitude. When comparing degrees-of-freedom, yaw showed visual amplitudes closer to the real inertial amplitude, while sway and especially surge were largely overestimated, with surge also leading to simulator sickness. This difference between degrees-of-freedom was possibly caused by the different optic flows shown in each visual scene and their

relation to depth perception. With this study we can conclude that visual characteristics affect the perceived motion and therefore affect the scaling between visual and inertial amplitude. This result is very important for motion simulation since it shows that poor visual characteristics may influence motion perception even when a high-fidelity motion platform is used. The visual gains (i.e., the ratio between the visual and inertial amplitudes) revealed to be a good metric to take into account when measuring realism or "image quality" in motion simulators.

Chapter 8

Implications for the design of motion cueing algorithms

The previous chapters investigated human self-motion perception in a simulation environment. The experimental results showed not only how specific forces affect human self-motion perception in the dark but also how visual and inertial cues interact with each other to form a percept of self-motion. This chapter proposes a framework using the perceptual knowledge investigated in this thesis to design better motion cueing algorithms (MCAs). The chapter starts with an initial perceptually optimized MCA design using the canal-otolith interaction model from the vestibular system part of the thesis. Due to the limitations imposed by this model, the initial design is then extended with the results from the visual-vestibular interaction part. We show that, although this framework seems promising in decreasing the gap between vehicle and simulation motion perception, in its current form, similar results could be achieved with classically tuned MCAs. The chapter concludes with recommendations to test and further improve these "perceptual" MCAs.

8.1   Including knowledge of the vestibular system

Based on previous knowledge [30, 51, 63, 67, 70] and the results of Chapters 3 and 4 of this thesis, vestibular self-motion perception can be represented by the block diagram of Figure 8.1. This model uses a mere integration over time to transform perceived acceleration ($\tilde{a}$) into perceived velocity ($\tilde{v}$), whereas Bos et al. [63] uses a leaky integration. This difference is justified by the results of Chapter 4 where we showed that for the majority of the subjects, the leaky integ-

ration seems to be at issue when transforming perceived velocity to perceived displacement, but not when transforming perceived acceleration to perceived velocity.
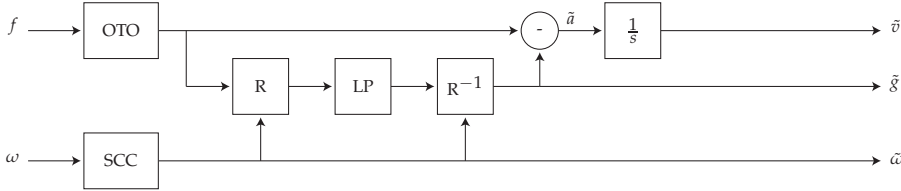

Figure 8.1: *Self-motion perception model with vestibular information and without leaky integration on linear velocity [51, 63].*

The inputs for this model are the specific force (f) and the angular velocity (ω) acting at the subjects' head. The outputs are perceived linear velocity ($\tilde{v}$), perceived angular self-motion ($\tilde{\omega}$), and perceived acceleration due to gravity ($\tilde{g}$). The blocks OTO and SCC represent the dynamics of the otoliths and the semicircular-canals, respectively. From Figure 8.1 we observe that while $\tilde{g}$ is both affected by f and ω, $\tilde{v}$ is mainly affected by f and $\tilde{\omega}$ is only affected by ω. The Human Motion Perception Model (HMPM) of Figure 8.1 will be used as the starting point to create a framework to develop perceptual MCAs.

8.1.1   Framework for perceptual MCAs

In Chapter 1, the perceptual approach [1, 16, 17, 25] to simulator fidelity was presented. Here, the simulator fidelity is improved by minimizing the error between the motion perceived in the real vehicle and the one perceived in the motion-based simulator [25, 65]. Figure 8.2 shows a possible framework where the perceptual error is minimized. Here, instead of using the aircraft motion as input for the MCA, one uses the error between the self-motion perception in the aircraft and in the simulator. Then, optimally, both HMPMs will give the same output causing the perception of the simulator motion to equal that of the real aircraft. The gain K is used to control the error value.

The framework shown in Figure 8.2 is similar to the Optimal Control (OC) algorithm [11, 25, 65], which also follows a perceptual approach to simulator fidelity. However, the OC algorithm uses the aircraft motion as input to the MCA (see Figure 1.4(b) in Chapter 1) and an offline optimization that calculates the MCA parameters that give the smallest error between the motion perceived in the aircraft and in the simulator. The cost function used in this optimization includes not only the perceived error, but also variables that account for the linear and angular motion of the simulator [25]. For the framework shown in Figure 8.2, we used a feedback loop structure instead of an open loop like in

the OC algorithm. Similar to the OC algorithm, an offline optimization can also be used to calculate K and the MCA parameters that give the smallest error between the motions perceived in the aircraft and in the simulator without violating the simulator limits. However, since this would calculate the parameters for the worst-case scenario, in the remaining of this chapter we estimated K and other MCA parameters without resorting to an offline optimization procedure.
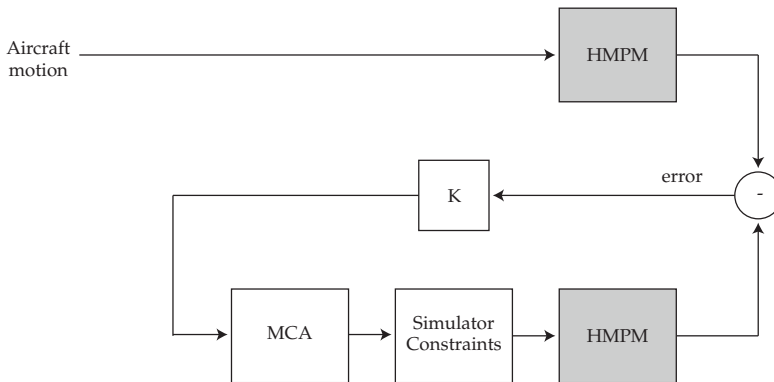

Figure 8.2: *Motion cueing algorithm framework using self-motion perception models.*

This technique was used in a driving simulation study [140], included in this thesis as Appendix A, where we tried to improve tilt coordination [11, 15] during a braking maneuver. Figure 8.3 shows how tilt coordination is used in a typical MCA [11, 14]. Here, the specific forces are scaled and low-pass filtered in the Gain and Low-pass filter blocks, respectively, before being converted to an angle on the Tilt coordination block. This angle conversion is obtained by calculating the direction of the specific force vector obtained from the low-pass filter output. The rate limiter is used to guarantee that the simulator rotations are below the human detection threshold [15] for angular motion.

Figure 8.4 shows the algorithm used to simulate sustained linear accelerations in the driving study [140]. Here, we assume that the gravity estimate from Figure 8.1 is an estimate of sustained linear acceleration whereas $\tilde{a}$ is an estimate of onset linear acceleration. This algorithm contains two self-motion perception models, one to estimate what drivers would perceive in the real vehicle and one to estimate what drivers would perceive in the simulator. The vehicle self-motion perception model only contains a low-pass filter because we considered the braking maneuver as a linear acceleration step with no angular motion. The block "$\tilde{g}$ to $\tilde{\theta}$" was used to obtain the direction of the estimated gravity vector ($\tilde{\theta}_v$), similar to the "Tilt coordination" block in Figure 8.3.

The direction of the estimated gravity in the vehicle ($\tilde{\theta}_v$) cannot be directly fed to the simulator tilt angle, similar to what is done in a typical MCA, be-
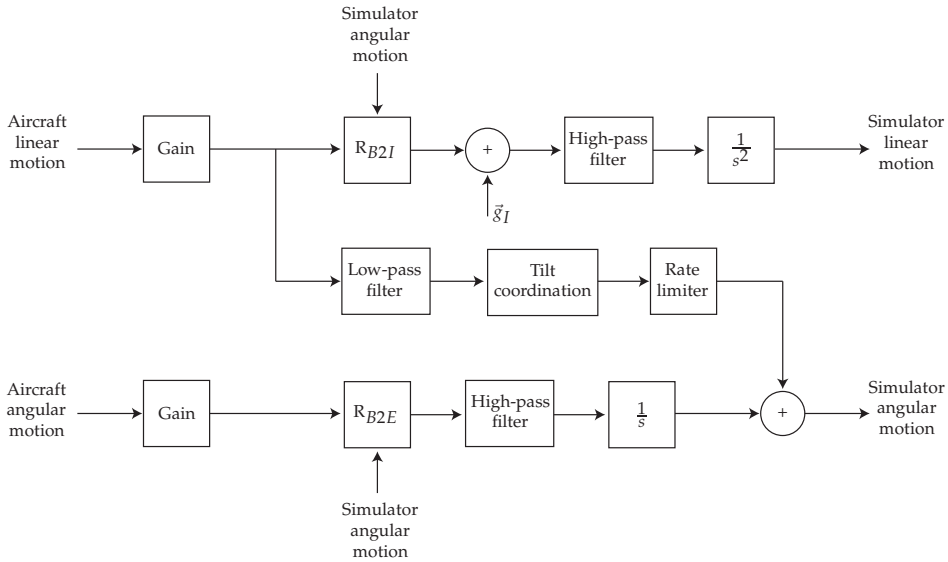
Figure 8.3: *Typical structure from a motion cueing algorithm [11].*
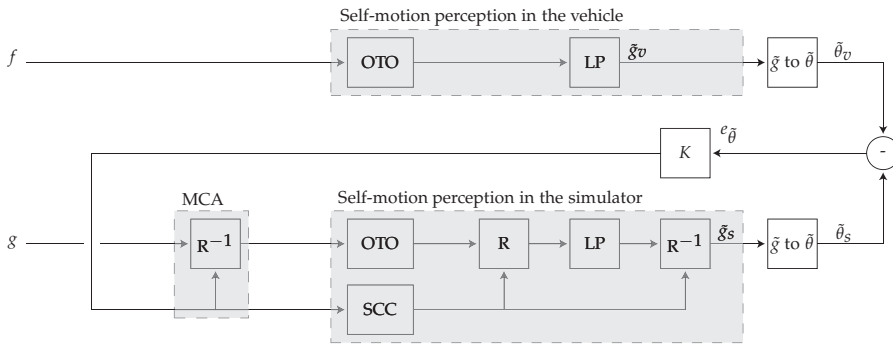
Figure 8.4: *Perceptual motion cueing algorithm used in [140].*

cause then the direction of the estimated gravity in the simulator ($\tilde{\theta}_s$) would be different from the one in the vehicle ($\tilde{\theta}_v$). This happens because, in the simulator, the estimated gravity is affected by the output of the semicircular-canals (SCC) [106]. Therefore, instead of feeding $\tilde{\theta}_v$ to the simulator, we feed the error between the two directions ($\tilde{\theta}_v - \tilde{\theta}_s$). We only match the direction of the two estimated vectors, and not the magnitude, because a non-centrifuge simulator can only generate a gravity estimate of approximately 9.81 m/s^2. The gain K was used to control this error value. A higher K would create a smaller error between the two percepts. However, if K is too high, the system becomes unstable. By feeding $Ke_{\tilde{\theta}}$ to the simulator instead of $\tilde{\theta}_v$, the perceived gravity

direction in the simulator is similar to the perceived gravity direction in the vehicle.

The MCA block in Figure 8.4 was used to rotate the simulator cabin according to $Ke_{\tilde{\theta}}$. Because rotation of the simulator causes rotation of the gravity vector in the subjects' head frame of reference, a rotation matrix (R^{-1}) was used to calculate the specific force components at the subjects' head, one of the inputs necessary by the self-motion perception model in the simulator.

Besides the design of this "perceptual" MCA, the driving study [140] also included an experiment comparing this algorithm with a classical MCA and a rumble-only algorithm. Both the classical and the perceptual MCAs used high-pass filters with the same characteristics to generate onset cues. The results showed no clear preference between the perceptual and the classical MCAs even though both MCAs were preferred to the rumble-only MCA. This perceptual MCA, however, only minimized the error in estimated gravity direction, leaving other perceptual outputs untouched ($\tilde{\omega}$ and $\tilde{v}$ in Figure 8.1).

8.1.2   Perceptual MCA using a vestibular HMPM

The concept presented in the braking study [140] can be further expanded with the vestibular model shown in Figure 8.1. Figure 8.5 shows how this self-motion perception model is then used in the perceptual MCA framework. Again, the algorithm has two self-motion perception models, one representing the subjects in the real vehicle and one representing the subjects in the simulator. The outputs of the vehicle's self-motion perception model are perceived linear velocity ($\tilde{v}_v$), perceived acceleration due to gravity ($\tilde{g}_v$), and perceived angular velocity ($\tilde{\omega}_v$) in the vehicle. Similarly, the outputs of the simulator's self-motion perception model are perceived linear velocity ($\tilde{v}_s$), perceived acceleration due to gravity ($\tilde{g}_s$), and perceived angular velocity ($\tilde{\omega}_s$) in the simulator. The error between the two percepts is fed to the MCA after being multiplied with gains $K_{\tilde{v}}$, $K_{\tilde{\theta}}$, and $K_{\tilde{\omega}}$.

The MCA block in Figure 8.5 is where the designer decides which variables should be optimized. Using the braking maneuver as an example, if the simulator had no physical constrains, we could develop a MCA where $K_{\tilde{v}}e_{\tilde{v}}$ would be connected to the simulator linear motion actuators. We could also integrate $K_{\tilde{\omega}}e_{\tilde{\omega}}$ and sum it with $K_{\tilde{\theta}}e_{\tilde{\theta}}$ before feeding it directly to the simulator angular motion actuators. However, by doing this, the algorithm would generate an f_s in the simulator equal to the one of the real vehicle f, meaning that the simulator would behave as a car and would require the same motion space needed by a car conducting this braking maneuver. This situation is not possible due to the simulator physical constraints.

Therefore, in the MCA (or by changing the gains $K_{\tilde{v}}$, $K_{\tilde{\theta}}$, and $K_{\tilde{\omega}}$) we would need to assign weights to the percepts that are more important to this man-
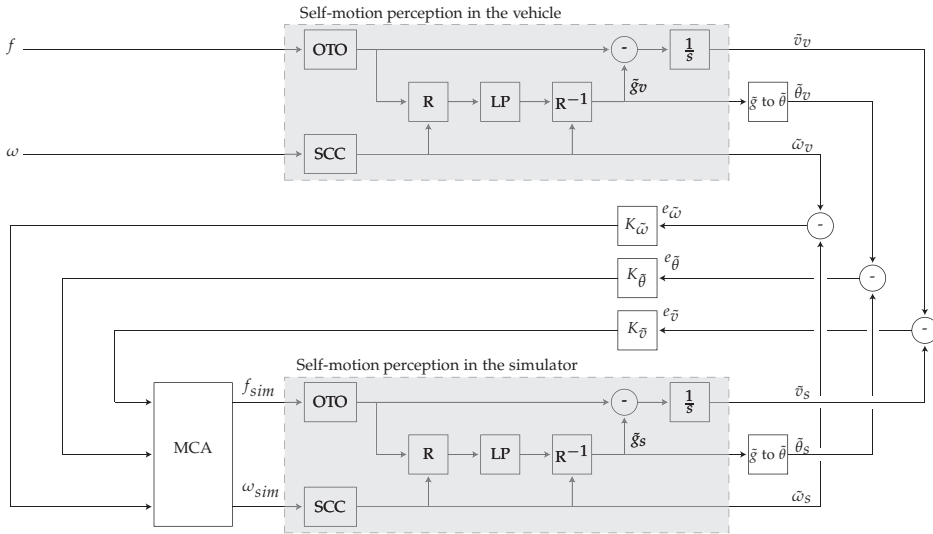
Figure 8.5: *Perceptual motion cueing algorithm using a vestibular self-motion perception model.*

euver, to allow the simulator to move within its physical limits. Additionally, we would need to high-pass filter $K_{\tilde{v}}e_{\tilde{v}}$ to prevent the simulator to exceed the linear motion limits. This means that we might have to use a typical MCA structure (Figure 8.3) in the MCA block. This solution would not be, therefore, very different from what was used in previous MCAs following a perceptual approach [21, 25, 65, 66].

The main issue with the self-motion perception model used in Figure 8.5 is that its outputs are largely influenced by one input. As seen when describing Figure 8.1, the perceived linear self-motion ($\tilde{v}$) is affected mostly by the specific force acting at the subject's head (f) while the perceived angular self-motion ($\tilde{\omega}$) is affected by the angular motion acting at the subject's head (ω). Only the perceived acceleration due to gravity ($\tilde{g}$) depends both on the linear and angular motion acting at the subjects' head, meaning that this is the only output in this model where the same result can be achieved from different inputs. To have the same with the other outputs, we need to include the contribution of the visual cues to self-motion perception.

8.2   Including knowledge on visual-vestibular interactions

The second part of this thesis focused on the scaling between visual and inertial cues. As seen in vehicle simulation studies [74–77], one-to-one scaling (i.e., when the inertial and visual cues have the same amplitude) does not always give the best perceived match. In Chapters 5 and 6 we found that subjects tended to decrease the motion gain (i.e., the ratio between inertial and visual cues) when both the frequency and the amplitude of the motion profiles increased. Additionally, this inertial overestimation seemed to be related to the visual cues shown in the simulator (Chapter 7). When there were more size and depth cues (e.g., objects of known size, relative size between objects, perspective) or when the horizontal field-of-view (FoV) was wider, the preferred motion gain was closer to one. This section tries to include these results in the self-motion perception model.

Figure 8.6 shows the self-motion perception model when visual cues are included. In the model of Bos et al. [63], both angular and linear visual flows (FLW blocks in Figure 8.6) have low-pass filter characteristics [42, 110]. The angular motion FLW block is a low-pass filter with a time constant in the same order of magnitude as the semicircular-canals (SCC) high-pass filter ($\approx 5s$), such that the sum of both filters is complementary [141]. The reader should know, however, that other SCC models could be used [48, 104]. Additionally, Bos et al. [63] defined the FLW used for linear motion as a first order low-pass filter with a time constant of approximately 2 seconds. In the following, we propose two different approaches to explain the results observed in the second part of this thesis.
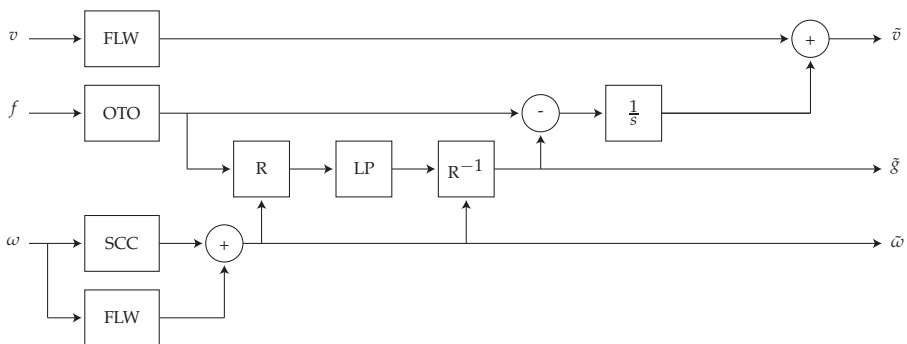

Figure 8.6: *Self-motion perception model with visual-vestibular information [51, 63].*

8.2.1 Visual path approach

The first approach is based on the results in Chapter 7, where the preferred motion gain was affected by the visual cues displayed in the simulator. In this experiment, subjects had to change the visual amplitude until it matched the inertial amplitude generated by the motion platform. Results showed that for surge and sway, subjects chose visual amplitudes higher than the inertial amplitude. This means that in a simulator environment, a visual amplitude is underestimated relative to an inertial amplitude and therefore, subjects had to increase it. To explain these results, we will change the visual path of the self-motion perception shown in Figure 8.6 since this is the path that is probably being affected by this visual underestimation. Figure 8.7 shows a possible implementation of this underestimation in the self-motion perception model, where G_{vis} is a matrix defined as:

Figure 8.7: *Self-motion perception model with visual-vestibular information in a simulator environment. This model includes a gain factor of visual linear velocity information (G_{vis}).*

$$G_{vis} = \begin{pmatrix} G_{vis}x & 0 & 0 \\ 0 & G_{vis}y & 0 \\ 0 & 0 & G_{vis}z \end{pmatrix}, \tag{8.1}$$

with $G_{vis}x$, $G_{vis}y$, and $G_{vis}z$ being the individual gains for visual underestimation for surge, sway, and heave motion, respectively. We did not include a similar gain matrix for angular motion since in Chapter 7, pitch and roll motions were not studied and there was no effect of the different visual cues in yaw motion since subjects chose approximately the same visual amplitude for visuals with different FoVs and scene content. However, we assume that other visual characteristics not addressed in Chapter 7 (e.g., stereopsis) might also affect the value of matrix G_{vis}.

   In a real-life situation, the gains $G_{vis}x$, $G_{vis}y$, and $G_{vis}z$ would be equal to one since the visual cues are matching one-to-one with the inertial cues. In a simulation environment, however, these gains should be lower than one to

explain the visual amplitude underestimation. Using the results of Chapter 7, $G_{vis}x$ and $G_{vis}y$ for the Desdemona simulator would be the inverse of the visual gains chosen by the subjects ($G_{vis}x \approx 0.23$ and $G_{vis}y \approx 0.39$). This model could then be used to create a perceptual MCA similar to what was done in Figure 8.5. The perceptual MCA with the visual channel included is shown in Figure 8.8.

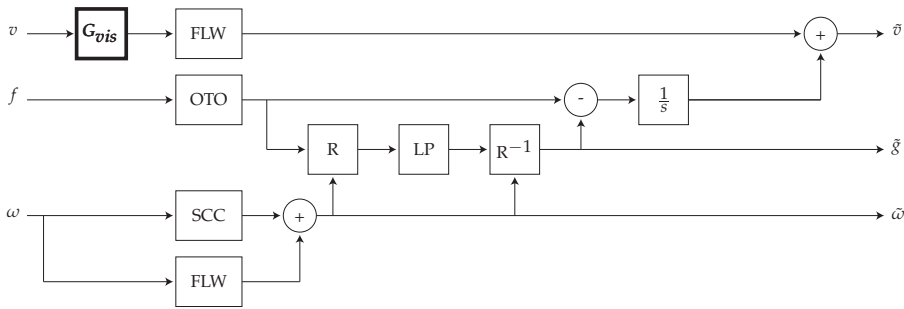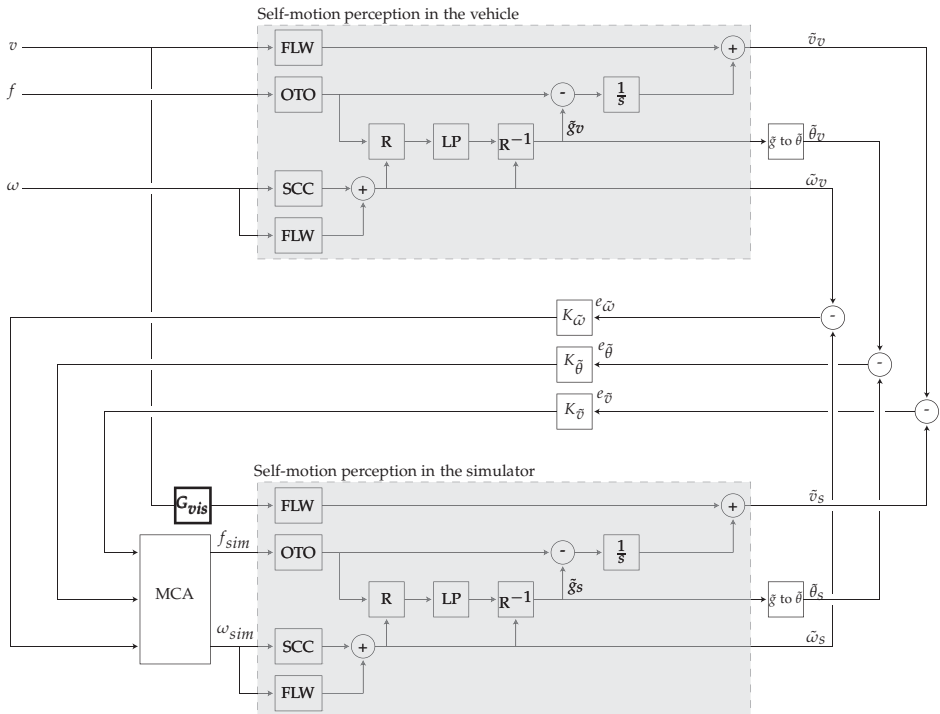**Figure 8.8:** *Perceptual motion cueing algorithm using a self-motion perception model with visual-vestibular information. This model includes a gain factor of visual linear velocity information (G_{vis}) at the simulator level.*

The first noticeable difference in this MCA is that the self-motion perception model that represents the human in the simulator is affected by the G_{vis} block, but not the self-motion perception model that represents the human in the real vehicle. This occurs because in the vehicle the human is either not affected by visual underestimation, or, if he is (for instance, when driving through fog [5]), there are no conflicts between the visual cues like with the simulator's displays [138]. Although visual flow in the simulator is underestimated, changing the visual amplitude (e.g., Chapter 7) is not an option because that would change the displacement of the simulated vehicle in the virtual world, leading to display visual information that does not correspond to the vehicle motion.

Therefore, instead of changing the visual amplitude, one compensates for the visual underestimation with the inertial motion generated by the MCA by trying to have the smallest $e_{\tilde{v}}$ (Figure 8.8) possible.

However, changes operated in the inertial motion affect mainly the high-frequency part of $\tilde{v}_s$ due to high-pass filtering operating at the inertial linear motion in the self-motion perception model. Therefore, the MCA will compensate the lack of visual information by creating inertial information at low frequencies. In a step acceleration, for example, the MCA would have to create an increasing acceleration to match $\tilde{v}_s$ with $\tilde{v}_v$ in order to affect the low-frequency part of $\tilde{v}_s$. This would increase the need of low-frequency inertial motion, which is something undesirable in a motion-base simulator. Additionally, the subject in the simulator is using the displayed visual information as reference for the perceived motion, which might be underestimated when compared to a real-life visual due to the simulator visual cues. Therefore, by focusing on the simulator visuals, the increase of inertial motion, needed to match the real vehicle motion, would be perceived as too strong, as shown in Chapters 5 and 6. This inertial overestimation cannot be modeled with the self-motion perception model of Figure 8.7, which made us look for a new approach.

8.2.2   Inertial path approach

The second approach is based on Chapters 5 and 6, where subjects changed the inertial amplitude until the best match with the visual amplitude displayed in the simulator was found. Results showed that the motion gain was generally smaller than one, which means that one-to-one motion would be overestimated. Figure 8.9 shows an approach to model this inertial motion overestimation in the self-motion perception model. Instead of affecting the visual channel and therefore, optic flow, like in Figure 8.7, we included a gain matrix (G_i) that directly affected linear motion perception. The gain matrix (G_i) included in Figure 8.9 is defined as:

$$G_i = \begin{pmatrix} G_i x & 0 & 0 \\ 0 & G_i y & 0 \\ 0 & 0 & G_i z \end{pmatrix}, \qquad (8.2)$$

where $G_i x$, $G_i y$, and $G_i z$ are the individual gains that, when larger than 1, create an overestimation of surge, sway, and heave linear motion, respectively. The value of these individual gains is affected by environmental cues. Therefore, in a simulator environment, $G_i x$, $G_i y$, and $G_i z$ should be larger than one due to, for example, the characteristics of the visual cues being displayed. G_i is not placed after the otolith model (OTO) because then it would affect not only perceived linear self-motion, but also perceived self-orientation, resulting in incorrect $\tilde{g}$

estimates, which is something we didn't find in Chapter 3. Additionally, the sinusoidal motion profiles used in Chapters 5 to 7 ranged between 1 rad/s to 5 rad/s, meaning that the results obtained there are mainly valid for specific forces perceived as translation because, as seen in Chapters 3 and 4, the time constant of the low-pass filter used to solve the tilt-translation ambiguity (LP in Figure 8.9) is in the order of 2 seconds.

Figure 8.9: *Self-motion perception model with visual-vestibular information in a simulator environment. This model includes a gain factor of inertial linear velocity information (G_i) that is affected by environmental cues.*

Chapter 7 showed that visual cues influence the perceived motion amplitude. However, this effect does not need to be modeled in the visual path as done in Figure 8.7. The visual path in the self-motion perception model is related to vection (i.e., perception of self-motion induced by a visual scene). However, we do not know if subjects perceived self-motion from the visuals used in Chapters 5, 6, and 7. Chapter 4 showed that cognitive effects might affect linear self-motion estimation. Therefore, although subjects might not have perceived self-motion from the visual cues (leaving the visual path with no signals), they might still be able to match the visual and inertial cues by cognitively estimating the visual amplitude [142] and then judging whether the inertial amplitude generated was too strong or too weak.

The model in Figure 8.9 also takes into account the frequency effect found in Chapters 5 and 6. The results from these chapters showed that when the frequency of the motion profile increased, subjects decreased the inertial amplitude. This means that high-frequency motion is overestimated in relation to low-frequency motion. If a sinusoid with the same amplitude but different frequency is applied to the self-motion perception model in Figure 8.9, the amplitude of $\tilde{v}$ will be higher for the higher frequency sinusoid. Therefore, if during the experiments subjects noticed that the visual amplitude was constant but that the higher frequency sinusoid felt much stronger, they would chose a smal-

ler inertial amplitude for the sinusoid with higher frequency. One could argue that the same effect occurs in real-life (Figure 8.6), however there, subjects are not expecting visual information decoupled from inertial information like in a simulator environment.

Figure 8.10 shows the perceptual MCA with the inertial overestimation gain matrix (G_i). This MCA has the same visual input for both the self-motion perception in the vehicle and in the simulator. The differences between the two visual qualities are modeled by the G_i blocks. The G_i matrix in the simulator contains gains larger than one to model the inertial motion overestimation occurring in a simulator environment. On the other hand, the G_i matrix in the vehicle contains gains equal to one.

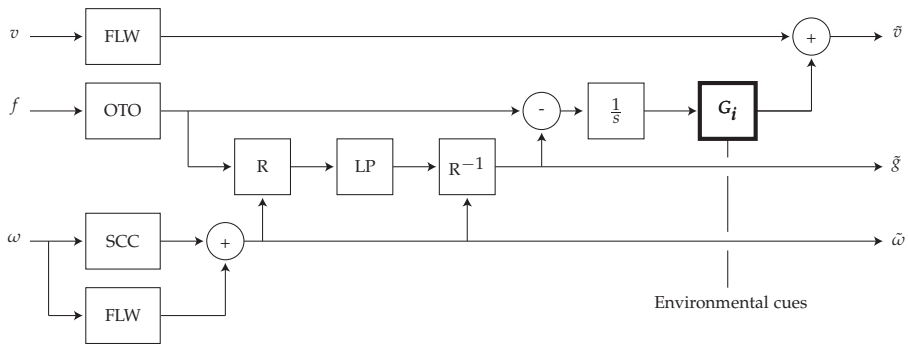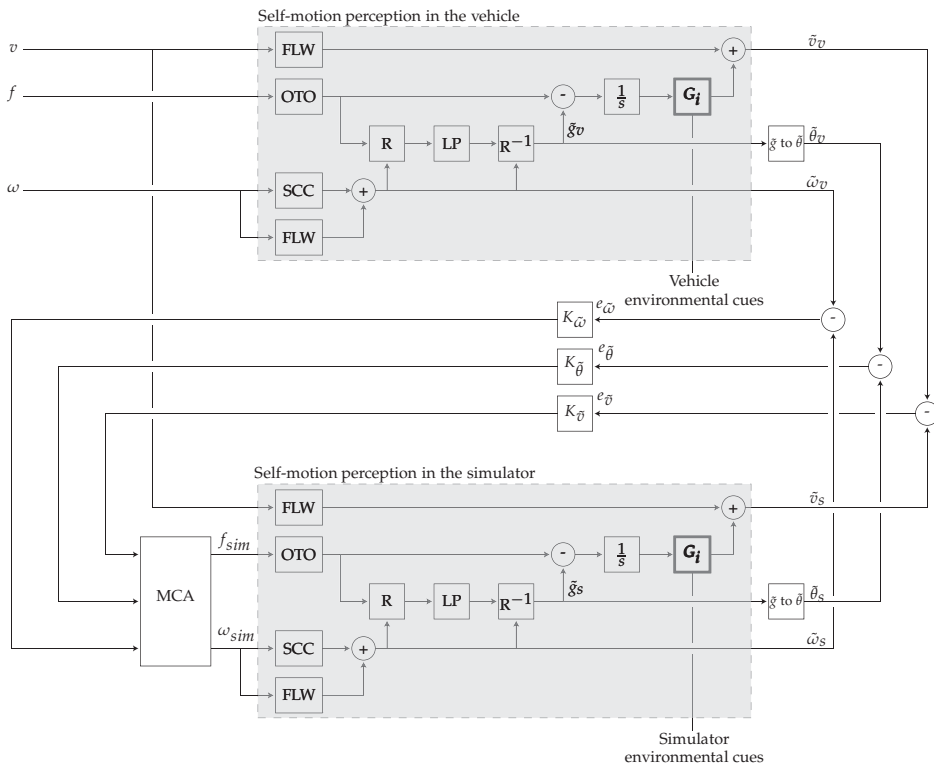**Figure 8.10:** *Perceptual motion cueing algorithm using a self-motion perception model with visual-vestibular information. This model includes a gain factor of inertial linear velocity information (G_i).*

Using the framework shown in Figure 8.10, the amplitude of the linear acceleration generated by the MCA block would be smaller than the one in the real vehicle by a factor determined by G_i matrix in the simulator. This means that to minimize the linear motion error ($e_{\bar{v}}$), the simulator would have to move less

than in the real situation. Additionally, in Chapters 5 and 6 we found that the simulator motion gain decreased with the increase of the stimulus amplitude. This result could be applied to the simulator G_i matrix by having gains that vary with the amplitude of the motion profile. However, such an algorithm needs to be tested experimentally because the amplitude distortion caused by a variable motion gain, similar to the trajectory distortion [27] found in adaptive MCAs [11, 143, 144], might be perceived by subjects.

The solution presented in Figure 8.10 shows a possible implementation of a perceptual MCA. However, for large motions the simulator will still violate its physical limits and therefore, the MCA block still needs high-pass filters to limit the motion platform physical movement. Additionally, a compromise between the gains $K_{\tilde{v}}$, $K_{\tilde{\theta}}$, and $K_{\tilde{\omega}}$ has to be made in order to have the smallest perceptual error possible. Therefore, although the framework shown in Figure 8.10 seems promising for motion cueing improvement, it is still not ideal and it still delivers similar perceptual results to a traditional MCA (Figure 8.3) where the inverse of the matrix G_i could be implemented in the aircraft linear motion Gain block. However, with the current framework the filter parameters of the MCA block can be optimized offline by minimizing the perceptual errors $e_{\tilde{v}}$, $e_{\tilde{\omega}}$, and $e_{\tilde{\theta}}$, creating then a MCA that delivers the smallest perceptual difference possible between the simulator and the real vehicle.

8.3   Improvements for perceptual MCAs

The previous sections showed that an effective perceptual MCA needs a self-motion perception model where an output can be affected by different inputs. If an output is only affected by one input, then similar perceptions in the vehicle and the simulator can only be achieved when the same input signal is used in both cases. In the previous self-motion perception model, tilt perception could be affected both by sustained linear acceleration and angular attitude. This explains why techniques like tilt-coordination show relatively good results in MCAs. However, the outputs $\tilde{v}$ and $\tilde{\omega}$ from the model in Figure 8.6 are mainly influenced by a single input. For example, even though $\tilde{v}$ is influenced both by v and f, the frequency segregation occurring in the self-motion perception model makes it that the low-frequency part of $\tilde{v}$ is mainly affected by v while the high-frequency part is mainly affected by f, with similar reasoning being used for $\tilde{\omega}$. Therefore, in this section we suggest, based on our results, new ways to affect the outputs of the self-motion perception model.

8.3.1 Improving a self-motion perception model

The self-motion perception model used in Figure 8.6 is not the full model proposed by Bos et al. [63]. Figure 8.11 shows again the visual-vestibular model [63] presented in Chapter 1. The main difference from this model to the one shown in Figure 8.6 is that it includes visual polarity and the contribution of the idiotropic vector.
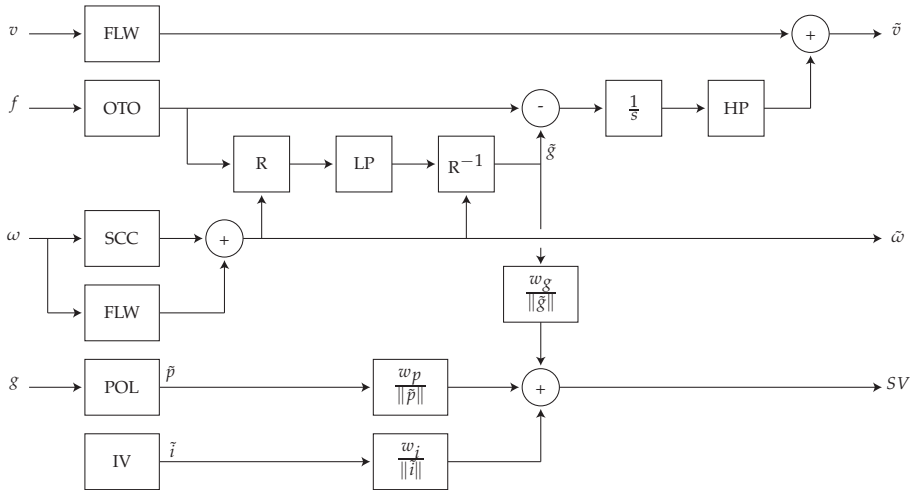
Figure 8.11: *Visual-vestibular model [63].*

In Chapter 2 we observed a phenomenon that is not described by the model in Figure 8.11. Here, subjects had to use a joystick to describe the perceived dynamic roll-tilt movement. In one experimental condition, subjects kept the joystick aligned with their sense of vertical, which we defined as the inside-out condition, whereas on another case, subjects rotated the joystick in the same angular direction of the perceived tilt, which we defined as the outside-in condition. The inside-out condition showed a decrease in the roll amplitude when compared to the actual tilt, typically explained in other studies by an effect of the idiotropic vector [63, 68, 91]. On the other hand, the outside-in condition showed no decrease in the roll amplitude, showing then a perceived tilt similar to the actual tilt. In Chapter 2 we concluded that humans have a perception of verticality and tilt. However, the model in Figure 8.11 only shows a subjective vertical output and not a subjective tilt output. Therefore, we propose to improve this self-motion perception model with the results of Chapter 2. The new model is shown in Figure 8.12, where the subjective vertical (SV) is affected by the idiotropic vector, but not the subjective tilt ($\tilde{\theta}$). In this model, we also included the linear motion results already discussed for Figure 8.1.
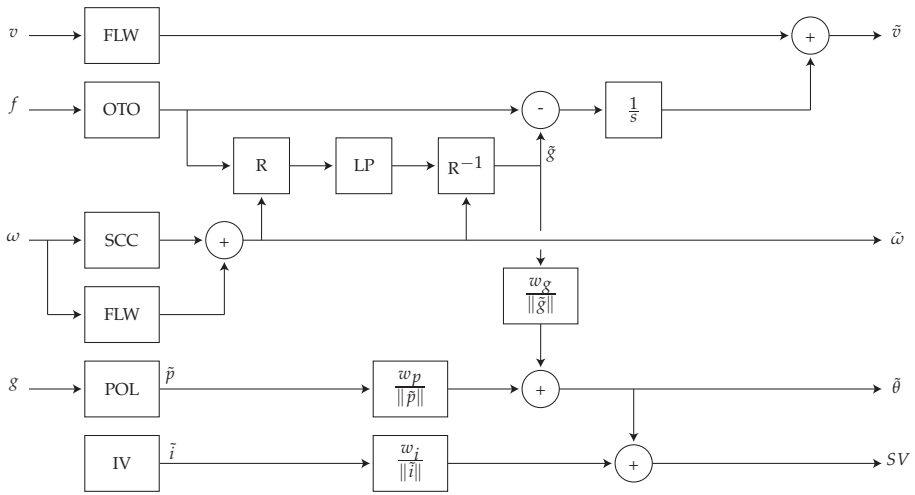
Figure 8.12: *Visual-vestibular model with perceived tilt output.*

Another feature that might be lacking in the visual-vestibular model is that angular self-motion perception and tilt perception are disconnected outputs. When there is a perceived dynamic tilt change, like with the somatogravic illusion of Chapter 3, there should be a perception of angular motion ($\tilde{\omega}$) since the perceived tilt angle is varying with a certain angular velocity. Additionally, perceived angular self-motion is not connected to tilt perception when the direction of the gravity vector is not affected (e.g., yaw movements when standing upright). However, in a recent study [145] subjects were asked to judge a stimulus based on their peak tilt roll-angle when lying on their back. According to the model, when subjects lie on their back their perceived tilt ($\tilde{\theta}$) is zero for roll movements because there is no change on the gravity vector direction, meaning that the subjects response in [145] should be always zero, which was not the case. Therefore, even though subjects might have performed the task based on their perception of angular velocity and not on their tilt percept, it is still possible that there is a connection between tilt perception and angular self-motion when there is no change on the direction of the gravity vector.

The visual-vestibular model should also include cognitive effects affecting the model's outputs. Wertheim et al. [111] showed that subjects perceived tilt in a linear sled when the experimental apparatus was unknown to them. The authors stated that these tilt percepts were cognitively suppressed when subjects knew a-priori that the system could not tilt. On another study, Pool et al. [146] compared pilot control behavior in real and simulated flight for a roll tracking task. In this study, the authors kept the differences between the two experimental setups to a minimum but, surprisingly, pilot tracking performance and

control activity in the real aircraft were still different from what was found in the simulator. The authors explained that these results might be caused by factors internal to the pilots like for example, being more careful in the aircraft than in the simulator. Schroeder and Grant [20] stated that comparison between a real vehicle and a simulator might not be possible due to the difference in mindsets between the two situations. Additionally, in Chapter 4 of this thesis we found that cognitive effects influenced the linear motion estimates of some subjects. Therefore, cognitive effects should be studied and included in the self-motion perception model. By improving self-motion perception models, one is directly improving perceptual MCAs.

8.3.2   From perception to perceptual MCAs

When creating a framework for perceptual MCAs, we showed that the effectiveness of these MCAs is influenced by using a HMPM for self-motion perception in the vehicle with different parameters from the HMPM for self-motion perception in the simulator. If the same parameters are used for the HMPM in the vehicle and in the simulator, we are assuming that the same perceptual output will be obtained from both situations when the same inputs are used in the different environments. However, this assumption seems to be incorrect even if the same visual and inertial motion are used, like shown by the influence of cognitive effects [146]. For example, in real-life humans do not question whether the inertial motion they are perceiving is coherent with the visual information they are seeing. However, because in the simulator they know that the two might be incoherent, they can question if these motion cues match. Therefore, because this uncertainty is present in the simulator but not in the vehicle, it needs to be included in the HMPM used for simulator perception to create an estimate that is closer to what is really perceived in the simulator. On the other hand, the same uncertainty does not exist in the real vehicle so it should not be included in the vehicle HMPM.

In Chapter 1 we showed that a perceptual approach to simulator fidelity was not yet feasible due to the lack of knowledge in how the CNS creates a percept of self-motion from different sensory inputs, particularly in a simulation environment. Although the self-motion perception models developed in this thesis cannot yet explain how the CNS generates a perception of self-motion, the foundation for achieving this goal is created and a possible framework to implement this knowledge in MCAs is proposed. Further research is needed to on the one hand, improve self-motion perception models, and on the other hand, describe the differences between self-motion perception in the real-world and in a simulation environment. By understanding the main perceptual differences between these two environments, we would be closer to develop a valid perceptual approach to improve simulator fidelity.

Chapter 9

Conclusions

One of the main difficulties in flight simulation is to generate inertial cues similar to the ones experienced in real-flight [1, 11]. This is especially true for specific forces which can quickly create large displacements of the motion platform [26, 27]. A solution to improve the flight experience in a simulator is the use of human self-motion perception models [21,25,65,66]. However, to use this knowledge we need first to understand how self-motion is perceived in a simulation environment. Therefore, in this thesis we conducted experimental work that aimed at improving current self-motion perception models. In this chapter, the main conclusions of the previous chapters will be summarized, then we draw the overall conclusions of this thesis and finally, we provide recommendations for future work.

9.1   Summary of the main results

This thesis was divided in two parts. In the first part we focused in the perception of self-motion due to specific force in the dark. In Chapter 2, subjects were exposed to dynamic roll-tilt to investigate if different joystick methods would lead to different self-tilt measurements. Although the first part of the thesis focused on perception of self-motion in the dark, in Chapter 2 both visual and inertial information were presented to the subjects so that all sensory information necessary to judge tilt was available. Subjects had to indicate their perceived tilt using different joystick methods. The results showed that for the same motion stimuli, the measured amplitude would be approximately the same as the actual tilt when subjects moved the joystick with the motion and would be smaller than the actual tilt when subjects moved the joystick against the motion (i.e., keeping the joystick vertical during the roll movement), resembling the studies

that measured the subjective vertical. We concluded that the former method measured perception of tilt whereas the latter method measured perception of vertical.

Chapter 3 investigated how humans perceive tilt when subjected to a sustained linear acceleration in the dark. Subjects were exposed to lateral centripetal accelerations and used a joystick to indicate their tilt percept. The results showed that this tilt illusion, since subjects are not actually tilting, had a time constant on the order of two seconds. Additionally, the simple Mayne equation fitted the experimental data accurately and therefore, we concluded that this equation can approximate the tilt percept that humans experience when subjected to a sustained acceleration in the dark.

After measuring tilt perception in Chapter 3, in Chapter 4 we studied how humans perceive linear displacement and velocity when subjected to a sinusoidal linear acceleration in the dark. The results showed that the perceived linear velocity had estimates, when transformed to position units, in the same order of magnitude of the perceived displacement estimates. We also showed that perceived displacement was accurately modeled by the Mayne equation when a leaky integrator is included, whereas perceived velocity is accurately modeled by the Mayne equation alone. We concluded the Mayne equation can be used to model the disambiguation of the tilt-translation perception, since the time constants found in this chapter were in the same order of magnitude as the ones found in Chapter 3.

In the second part of this thesis we studied visual-vestibular interactions, focusing mainly on investigating what was the preferred motion gain (i.e., the ratio between inertial and visual amplitudes) in a simulator environment. In Chapter 5 we asked subjects to indicate their preferred amplitude scaling between visual and inertial cues in a simulation environment for oscillatory lateral linear motion. Subjects changed the inertial motion amplitude until they obtained the best match between the visual and inertial cues. Results showed that the motion gain decreased with the increase of the amplitude and frequency of the visual cues. We also found that the preferred motion gain was not a single value but instead a range of values where subjects considered the inertial cues correctly matching the visual cues. This experiment showed that the inertial cues in a simulation environment were overestimated.

The range of preferred amplitudes we found in Chapter 5, which we defined as an optimal zone, seemed similar to the coherence zones described by Van der Steen [45] and Valente Pais et al [124]. The coherence zones are defined as a zone where the inertial and visual amplitudes are perceived as coherent, even though their values might be different. Therefore, in Chapter 6 we compared the coherence zone with the optimal zone in a simulator environment. Two simulators were used to measure these zones for linear motion in the sway axis.

The results showed that the optimal zone is contained within the coherence zone, with the main differences between the two zones being their upper limits. The optimal zone had the same trends found in Chapter 5, despite the fact that this experiment was conducted in different apparatuses. We concluded that the optimal zone is different from the coherence zone and that a certain visual-inertial combination of amplitudes might be perceived as coherent even though it is not the one preferred by subjects.

In Chapter 7 we investigated if the optimal zone measured in Chapters 5 and 6 was affected by different visual cues. To achieve this, subjects were exposed to visuals with different fields-of-view and size and depth cues. The motion profiles included linear motion in sway and surge and angular motion in yaw. Subjects had to vary the visual amplitude until it matched the perceived inertial amplitude. The results showed that a larger field-of-view (FoV) and a visual scene with more size and depth cues led to visual amplitudes closer to the inertial amplitudes of surge and sway motions. However, the different FoVs and visual scenes had no effect on the yaw visual amplitudes. We concluded that the difference between degrees-of-freedom was caused by the different optic flows generated by each degree-of-freedom and its relation to depth perception.

9.2   Implications of the main results

The results from the first part of this thesis showed that the Mayne equation can accurately describe how specific forces affect human self-motion perception in the dark, as hypothesized by Mayne [30] and shown theoretically plausible by Bos and Bles [51]. We confirmed experimentally that when humans experience a lateral specific force, the low-frequency component of this specific force is perceived as roll-tilt while the high-frequency component is perceived as lateral translation. In these situations, the Mayne equation was capable of estimating both the roll-tilt and lateral translation.

For translation, however, we needed to augment the Mayne equation with a leaky integrator if we intend to model perceived displacement. There were already earlier reports [62, 63, 114] suggesting that a leaky integrator might be needed. Additionally, we showed that the time constant of the Mayne equation is approximately the same both for the tilt and translation percept. This shows that the high-pass and low-pass mechanisms described by the Mayne equation are complementary and therefore, we concluded that this equation can accurately describe self-motion perception at the vestibular level.

There are still effects that are not explained by this model such as individual differences between subjects. Nevertheless, the self-motion perception models we want to use to improve motion-based simulation should be simple and able to describe, on average, how humans perceive self-motion, rendering the Mayne

equation a suitable candidate to describe how specific force affects self-motion perception when there is no visual information.

In a simulation environment, however, humans are seldom without visual cues. In fact, it is more common that a simulator has only visual cues than only inertial cues [6], since especially at low frequencies, visual cues dominate over inertial cues [39, 42, 45, 63]. In this thesis, the visual-vestibular interactions focused mainly on the scaling between visual and inertial cues in a simulation environment. In real life, the visual and inertial cues have the same amplitude, our central nervous system learned to combine these during our earlier years, possibly by means of an internal model [51], which might even explain why we perceive self-motion while dreaming [147]. Therefore, in real-life humans are not expecting to have the visual amplitude decoupled from the inertial amplitude. However, this assumption changes in a simulator environment, where humans know beforehand that these two sources of information might be decoupled [20]. In our studies we observed that in a simulation environment, subjects preferred an inertial amplitude smaller than the visual amplitude. This phenomenon was mainly attributed to the differences between the depth perception cues (e.g., objects of known size, optic flow) available in real-life visual cues and the ones available in a simulator environment. In yaw, depth perception does not play a significant role in self-motion perception [38] and consequently, subjects choose for this motion condition a visual amplitude that was approximately the same as the inertial amplitude.

This overestimation of the inertial specific forces might not be explained solely by differences in the visual cues. In Chapter 4, some displacement estimates were partially affected by cognitive effects. Here, subjects might have used the time that each experimental condition took to estimate their translation, possibly because they applied this strategy before. Therefore, previous experiences or additional information can affect self-motion perception. However, cognition is absent from current self-motion perception models. Cognitive factors might explain why different instructions (e.g., Chapter 6) might lead to two different perceptual zones or why inertial motion is perceived as "too strong" when subjects know that inertial and visual cues might be decoupled. For example, pilots might still feel that inertial motion is too strong in real life, but they do not follow this sensation since they know that vestibular and visual information are directly coupled. However, if we could replicate the experiments of Chapters 5 and 6 with real-life conditions, similar inertial overestimation might be obtained. Examples of cognition affecting self-motion perception can also be found in the literature [111, 142, 146] and the effect of previous experience was observed via personal communication in a previous driving study [148] where subjects with little or no experience in motion-based simulators already perceived self-motion in a no-motion condition, while subjects with simulator

experience perceived no self-motion during the no-motion condition. Therefore, cognitive effects can no longer be ignored and it is of the upmost importance to include them in current models to be able to correctly model self-motion in a simulation environment.

9.3   Recommendations

Although the results shown on this thesis revealed to be promising for motion-base simulation, new questions arose that need to be addressed before a perceptual approach can be effective in improving simulator fidelity. Based on these questions, the following recommendations for future research are stated.

9.3.1   Perceived magnitude of inertial motion

In Chapters 5 and 6 we observed that the motion gain decreased with the increase of the stimulus amplitude. This cannot be explained by the visual-vestibular model used in this thesis due to its linear properties. One could argue that this phenomenon only occurs for linear motion and is caused by the visual cues since in Chapter 7, the yaw motion condition showed visual gains (i.e., the inverse of motion gains) of approximately one. However, only one amplitude was used in Chapter 7. In a study that measured coherence zones, Valente Pais et al. [124] showed that, although the coherence zone included the one-to-one line for low amplitude yaw motion, when the amplitude increased the coherence zone dropped below the one-to-one line, revealing an non-linear relation for the coherence zone shape.

Additionally, we observed in Chapter 4 that the perceived gain between the two amplitudes used for the sinusoidal motion profiles was smaller than the actual physical gain. Therefore, the motion gain results observed in Chapters 5 and 6 might not only be caused by the visual cues but also because humans perceive the increase of inertial motion differently than the actual physical increase. For example, although an inertial stimulus doubles its amplitude, the perceived intensity increase might be smaller (or higher) than double. Stevens showed that for other sensor modalities, like brightness [112] or heaviness [113], the human's perceived intensity can be accurately modeled by a power law and Zaichik et al. [103] showed that the perception of acceleration values can be modeled by psychophysical laws, such as the Stevens or Weber-Fechner laws. Therefore, it should be investigated whether the motion gain dependency on the stimulus amplitude can be modeled by a power law, similar to what was proposed by Dos Santos Buinhas [149], and the visual-vestibular model should be updated accordingly.

9.3.2   Adaptive motion gain for motion cueing algorithms

In Chapter 8 we proposed to implement the motion gain dependency on stimulus amplitude and frequency on a motion cueing algorithm (MCA) since it would decrease the simulator's motion envelope. However, these results were obtained with passive profiles in which subjects focused on their perceived self-motion. Therefore, there is no evidence that applying an amplitude or frequency dependency algorithm on a MCA would be correctly perceived during in-the-loop tasks like flying or driving. For example, in an amplitude dependency algorithm, the shape of the motion profiles would be different because lower amplitudes would be less attenuated than higher amplitudes, meaning that the difference between 1 and 2 m/s^2 is higher than the difference between 2 and 3 m/s^2. Previous adaptive MCAs [11, 143, 144] suffered from trajectory distortion [27]. However, the adaptive parameters of these MCAs were not based on human self-motion perception. To investigate if a shape-change caused by adaptive motion gains is incorrectly perceived by subjects, an experiment could be performed where a MCA using this amplitude dependency algorithm would be compared to a classical MCA, similar to other to MCAs comparison experiments [116, 148, 150]. With this experiment we could, on the one hand, understand if this algorithm introduces unwanted perceptual distortions, and on the other hand, investigate if the perception of "too strong" inertial motion decreases when compared to a classical MCA.

9.3.3   Effect of reference motion on perception

We also found that the motion gains obtained for sway motion in Chapter 7 were smaller than the ones obtained in Chapter 5 for the same motion simulator. Although the visuals, frequency, and amplitude of the motion profiles were different between the two experiments, this does not justify the smaller motion gains in Chapter 7 because the frequency and amplitude were smaller and not bigger than those in Chapter 5, as expected from the trends that showed a decrease in motion gain with the increase of the amplitude and frequency of the motion stimulus. However, in Chapter 5 subjects judged the motion amplitude from the visual cues and then had to change the inertial cues until they obtained the best match between the visual and inertial information whereas in Chapter 7 subjects judged the motion amplitude from the inertial cues and changed the visual cues until the best match was obtained. Harris et al. [121] also found different results when using inertial cues as the reference motion compared to the situation where visual cues were used as reference. Because Chapters 5 and 7 were conducted in different conditions, we cannot say if this difference would also occur when the different tasks were conducted in the same experiment, with the same visual information and the same participants.

Therefore, it should be investigated if this task difference has an influence on the motion gains. If this is confirmed, it means that different processes occur at the central nervous system, depending whether visual or inertial cues are used as the reference motion stimulus.

9.3.4   Combination of visual and inertial cues

Additionally, investigation on visual and inertial cue combination needs to continue [57,59,142,151,152]. For linear motion, the visual-vestibular model shows that the contribution of the visual cues to self-motion perception originates from the optic flow perceived as vection, normally modeled as a low-pass filter [63] with a time constant based on the latency of vection onset (i.e., the time it takes to perceive self-motion from visual cues). In a simulation environment, however, subjects might use more than vection to infer linear self-motion. In the experiments conducted in the second part of this thesis, subjects were able to choose inertial cues that matched the visual cues, even if we do not know if they experienced vection. Therefore, in a simulation environment, self-motion perception is influenced by vection, like shown in the visual-vestibular model, but it might also be influenced by visual motion expectation, which is not present in the model. Possibly, this effect is influenced by a cognitive effect related with experiences subjects had with similar motion profiles in real-life. Therefore, future research should investigate the effect of this visual motion in a simulation environment and include it in a self-motion perception model.

9.3.5   From passive to active tasks

The experimental work conducted in this thesis showed that there are self-motion characteristics particular to a simulation environment, like the over-estimation of inertial cues, which improved the basic perceptual knowledge we had before this scientific work. However, the ultimate goal is to use this knowledge to improve in-the-loop simulations where subjects are, for example, driving, flying, or sailing. When performing these tasks, the mindset is different since subjects are no longer solely focusing on the motion cues being generated, but they are also focusing on their control performance. Due to the different mindsets, it is unknown if the results obtained here can be directly applied during in-the-loop simulations. Therefore, future experimental work should also focus on conducting in-the-loop experiments where perceptual knowledge is directly validated by measuring self-motion perception while subjects are conducting an active task, similar to the work of Valente Pais et al. [153] and Beckers et al. [154]. By conducting such experiments, we will be closer to create MCAs that, although do not use the same motion cues as the real vehicle, the motion perceived in the simulator will be similar to the one perceived in the real vehicle.

Perceptual tilt algorithm

A.1   Introduction

Motion simulators present pilots and drivers with maneuvers similar to the ones found in a real vehicle. These maneuvers are presented visually, via the simulator projection system, and inertially, via the simulator motion base. A challenge often encountered in motion simulation is the cueing of inertial linear motion. Long term accelerations (e.g., a car accelerating in a straight road) will create linear displacements that are normally higher than the simulator physical limits. Therefore, a Motion Cueing Algorithm (MCA) is used to transform the vehicle accelerations into accelerations that are well within the simulator physical limits [11]. Although MCAs are also used to transform angular motion, this study is focused solely on linear motion.

A MCA that is often used in flight simulation is the Classical Washout Filter (CWF) [13]. In this algorithm, the linear inertial motion is split in two parts: high-frequency and low-frequency motion. The high-frequency motion is obtained by high-pass filtering the vehicle motion. This filtered motion is then sent to the simulator linear motion. The parameters of the high-pass filter are tuned in such a way that the motion is below the simulator limits. The low-frequency motion is low-pass filtered. However, this low-pass filtered motion will create linear displacements outside the simulator limits. Therefore, researchers use the simulator rotational motion to tilt the simulator in the attempt of matching the direction of the gravity vector with the direction of the low-frequency acceleration vector. To prevent perception of rotational movement caused by this tilt, a rate limiter is used to limit the simulator tilt rates. The rate limiter is normally set to 3 deg/s [15]. This technique to simulate sustained acceleration by tilting the simulator is called tilt-coordination. The CWF is not the only MCA used in motion simulators. For example, the Coordinated Adaptive Algorithm [11] has a structure similar to the CWF but the algorithm parameters adapt during the simulation. There are also MCAs specific to certain maneuvers like the Lane Change Algorithm which is used to simulate lane changes in driving simulation [155]. However, most MCAs minimize the error between the vehicle and the simulator motion. So far, only the Optimal Control (OC) algorithm [25, 65, 66] tries to minimize the error between the perceived motion in the aircraft and the perceived motion in the simulator.

To minimize the perceived error, the parameters in the OC algorithm were optimized based on the output of the vestibular system. The vestibular system is sensible to linear motion, via the otolith, and angular motion, via the semicircular-canals. However, the vestibular system alone cannot explain some of the motion illusions experienced by humans. To understand these illusions, we need to understand how the Central Nervous System interprets the output of the vestibular, somatosensory, and visual systems. Several self-motion perception models [30, 50, 51, 55] have been proposed to explain how the CNS

might operate. So far, these self-motion perception models have not been used to optimize MCAs.

The aim of this study is to design and test a MCA that uses a self-motion perception model to improve the simulation of sustained linear accelerations. We used the Mayne equation [30, 51] as the self-motion perception model. This choice was made based on this model's ability to predict the most common motion illusions and on its mathematical simplicity. The new MCA was compared experimentally against a CWF and a MCA that only cued road rumble. The experiment consisted of accelerating a car up to 80 km/hr and then stop at a specific end line. Although we found no significant preference between the perceptual MCA and the CWF, subjects preferred these MCAs to the road rumble MCA. Our results also showed that performance with the road rumble MCA was worse than with the other MCAs.

A.2   Perceptual tilt

Humans perceive self-motion by combining information from the visual, vestibular and somatosensory system [51]. The visual system is sensitive to frame and optic flow information whereas the somatosensory system is sensitive to acceleration (via skin pressure sensors) [51]. Although the visual and somatosensory systems are very important for human self-motion, this study focuses solely on the vestibular system. The vestibular system is sensitive to self-motion by means of the otoliths and the semicircular-canals. The semicircular canals are sensitive to angular acceleration and its output is proportional to angular velocity. The otoliths are sensitive to specific force and its output is proportional to specific force. As shown in Equation (A.1), specific force is the vectorial sum between acceleration due to motion and gravity.

$$\vec{f} = \vec{a} + \vec{g} \tag{A.1}$$

The fact that the output of the otolith organ is specific force means that this organ cannot discriminate between the two sources of acceleration. However, such discrimination is essential for postural and body control [51]. Anecdotally, one could say that without such discrimination, humans would perceive upward movement when lying on their back. Therefore, the Central Nervous System (CNS) seems able to discriminate both components. However, this discrimination is not performed in an optimal way as evidenced by the motion illusions described in the literature [51].

In 1974, Mayne [30] proposed a 2-dimensional mathematical model to explain how the CSN discriminates between acceleration due to self-motion and gravity. This model was later extended by Bos and Bles [51] to a 3-dimensional

coupled equation, as shown by Equation (A.2).

$$\frac{d\tilde{g}}{dt} = \frac{1}{\tau}(f_{oto} - \tilde{g}) - \omega_{scc} \times \tilde{g} \tag{A.2}$$

In Equation (A.2), f_{oto} is the specific force signal given by the otolith afferents, ω_{scc} is the angular velocity signal given by the semicircular-canal afferents, τ is the time constant of the low-pass filter operating on the otolith afferents, and $\tilde{g}$ is the estimation of the acceleration due to gravity as taken by the CNS. From Equation (A.2), we obtain a estimation of acceleration due to gravity ($\tilde{g}$) and acceleration due to motion ($\tilde{a} = f_{oto} - \tilde{g}$). With this model, Bos and Bles [51] explained several motion illusions, in particular the somatogravic illusion.

When humans are subject to a sustained acceleration in the dark, they will perceive tilt after some seconds. This tilt perception is illusory, humans are not actually tilting but moving linearly, and the illusion is explained by the CNS interpreting acceleration due to self-motion as gravity. Equation (A.2) can explain how the somatogravic illusion works. When humans are subject to a sustained acceleration, the output of the semicircular canals is zero and the estimation of gravity and acceleration are respectively given by Equations (A.3) and (A.4).

$$\tilde{g}(s) = \frac{1}{\tau s + 1} f_{oto} \tag{A.3}$$

$$\tilde{a}(s) = \frac{\tau s}{\tau s + 1} f_{oto} \tag{A.4}$$

In this case, the estimated perception of gravity is the low frequency content of the specific force being signaled by the otolith afferents. Therefore, our tilt percept is related to the angle between the human spinal axis and the estimated gravity vector. Figure A.1 shows an example of the tilt percept predicted by the model when subjects experience a 2 m/s^2 step in the surge direction. In this example, the otolith dynamics were simplified to a unit gain as done in other studies [50] and the τ of Equation (A.3) was equal to 2 seconds [51]. The model shows that after some seconds, humans will interpret the specific force as gravity, which leads to a perceived tilt of approximately 11.5 degrees even though that they are not physically tilting. Based on this knowledge we developed the Motion Cueing Algorithm presented in the following section.

A.2.1   Motion Cueing Algorithm design

Past studies have shown that when humans are subject to a linear acceleration in the dark, there are two possible percepts: a percept of linear motion and a percept of tilt [51]. Equation (A.3) showed that the tilt percept can be modeled
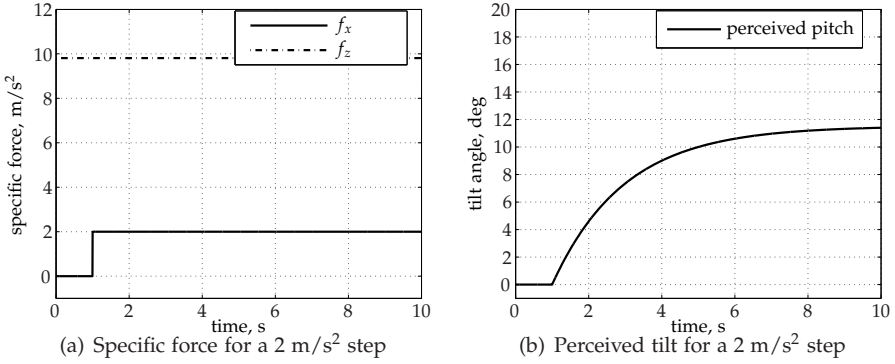
Figure A.1: *Tilt perception for a 2 m/s² step in surge.*

by a low pass filter acting on the specific force. As a first approach, we could think of feeding the tilt signal from Equation (A.3) directly into the simulator, similar to what is done in the Classical Washout Filter (CWF). Figure A.2 shows a typical configuration of a CWF when simulating specific force. The lower channel is constituted by a low-pass filter on the specific force followed by a rate limiter.
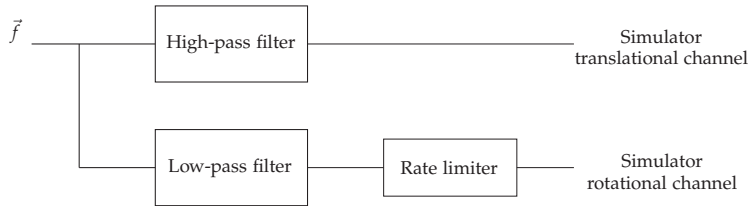
Figure A.2: *Structure of a Classical Washout Filter for simulating specific force.*

If the low-pass filter of the CWF is configured to be equal to Equation (A.3) and the rate limiter is left out, then we are feeding to the simulator rotational channel the tilt that the subject is perceiving in the real situation. However, the tilt perceived by the subject in the simulator is different from the tilt fed to the simulator. This happens because inside the simulator, self-motion perception is based on Equation (A.2) where the output of the semicircular canals is no longer zero due to the actual tilt of the simulator. This situation is shown in Figure A.3, where $H(s)$ is a first-order low pass filter, the "$\tilde{g}_r$ to $\tilde{\theta}_r$" block converts from perceived gravity to perceived tilt, $\tilde{\theta}_r$ is the perceived tilt in the real situation, HMP is the Human Motion Perception model of the subject inside the simulator, and $\tilde{\theta}_s$ is the perceived tilt inside the simulator.
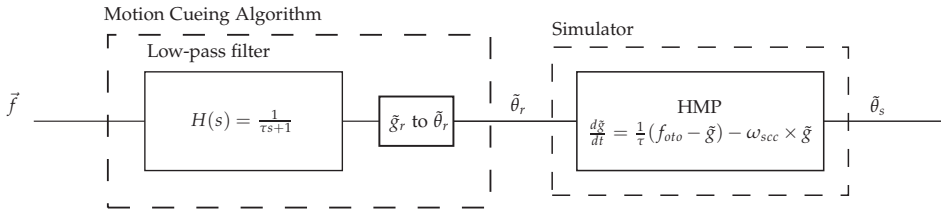
Figure A.3: *Tilt perception for a CWF without a rate limiter.*

From Figure A.3 we predict that the perceived tilt in the real situation is different from the perceived tilt in the simulator. Figure A.4 shows the perceived tilt for a step input of 2 m/s². The perceived tilt in the real world was obtained by transforming the output of Equation (A.3) into a perceived angle by using the "$\tilde{g}_r$ to $\tilde{\theta}_r$" block in Figure A.3. For this calculation, we considered that the otolith dynamics were approximately a gain of one [50], which leads to $f_{oto} \approx f$. The perceived tilt in the simulator was obtained from the output of the human perception model in the simulator (see $\tilde{\theta}_s$ in Figure A.3). The output of the perceived angular velocity of the semicircular canals (ω_{scc}), which is needed for the motion perception model in the simulator, was obtained using Equation (A.5) [63], where ω is the angular rate acting on the subject.
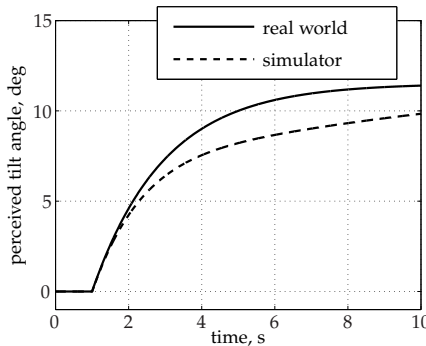
Figure A.4: *Comparison between the perceived tilt in the real world and the one in the simulator for the CWF.*

$$\omega_{scc}(s) = \frac{5.7s}{5.7s + 1}\omega \qquad (A.5)$$

As shown in Figure A.4, the perceived tilt in the simulator is different from the perceived tilt in the real world. However, the perceived tilt in the simulator should be as close as possible to the perceived tilt in the real world. To achieve this, we fed to the simulator the error between the perceived tilt in the simulator

and the one of the real situation. Figure A.5 shows the structure of this Motion Cueing Algorithm (MCA), where e is the error between $\tilde{\theta}_r$ and $\tilde{\theta}_s$, and c is the command being sent to the simulator rotational channel. The gain K is used to control the error value. A higher K will create a smaller error between the simulator and real perception. However, if the K is too high, the system will become unstable. In the remaining of the appendix we will refer to this algorithm as the Perceptual Tilt Algorithm (PTA).
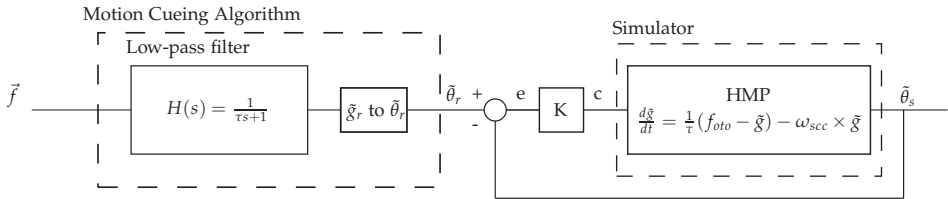
Figure A.5: *Schematic of the Perceptual Tilt Algorithm.*

Figure A.6 shows the perceived tilt using the PTA and the target tilt for the 2 m/s^2 longitudinal acceleration step used before. With the PTA, the tilt perceived in the simulator is closer to the target tilt. Figure A.7(a) compares the perceived tilt when using a CWF with a rate limiter, a CWF without a rate limiter and the PTA. Here, we observe the negative effect of the rate limiter on the perceived tilt. The rate limiter of the CWF was limited to 3 deg/s [15]. We also observe that theoretically, the perceived tilt of the PTA is closer to the real perceived tilt than the perceived tilt of both CWFs. The comparison between the angular rates commanded to the simulator pitch is shown in Figure A.7(b). We can observe that the PTA is slower than the CWF but much smoother. Theoretically, the PTA seems to induce a tilt percept closer to reality, however, this motion perception model does not feature all characteristics that humans use when perceiving self-motion. For instance, the visual system was not included in this model, which might mitigate the tilt percept. Therefore, we conducted an exploratory experiment to observe if the PTA could be used as an alternative to classical tilt-coordination.

A.3   Method

A.3.1   Subjects

Eighteen subjects participated in this experiment (14 male and 4 female). The subjects had an average age of 30 years with a standard deviation of 8 years and had an average driving experience of 9 years with a standard deviation of 7 years. All experimental conditions were approved by the local ethics committee.
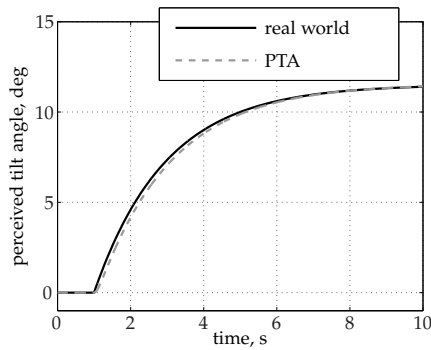
Figure A.6: *Comparison between the perceived tilt in the real world and the one in the simulator for the PTA.*
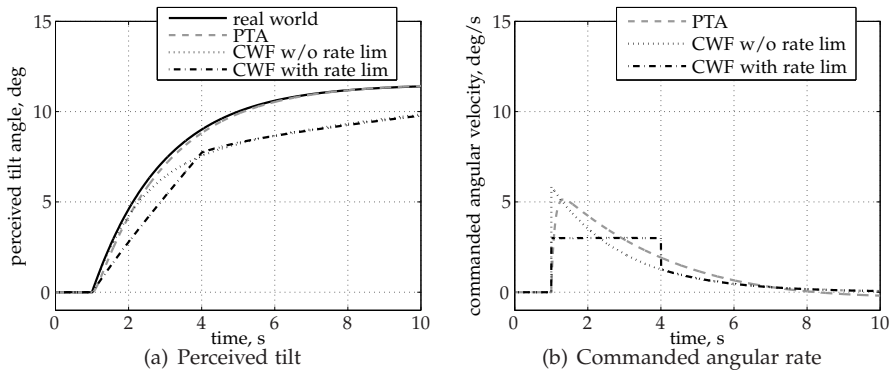
Figure A.7: *Perceived tilt and simulator angular rates for different MCAs.*

Subjects' rights were based on the Declaration of Helsinki on ethical principles for medical research involving human subjects.

A.3.2 Apparatus

The experiment was conducted at the Desdemona research simulator (shown in Figure A.8) located at the TNO institute in Soesterberg, the Netherlands. This simulator features a centrifuge based design with six degrees-of-freedom (DoF) [29]. In this study, the 8-meter horizontal actuator of the simulator was used to simulate the high-frequency longitudinal cues of the accelerating/braking maneuver. The yaw actuator was aligned with the roll actuator (see Figure A.8) so that the roll actuator produced cabin-pitch cues.

For this experiment, the Desdemona cabin contained a car mockup. This
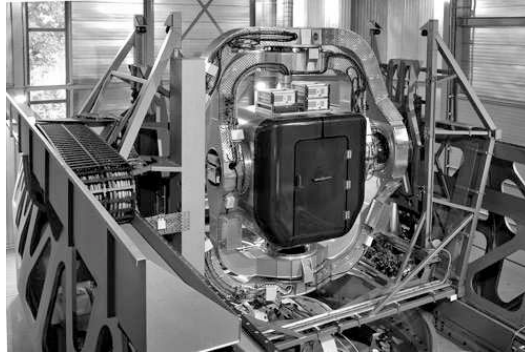
Figure A.8: *Desdemona research simulator.*

mockup included a force feedback steering wheel (40 cm) and two pedals (gas and brake) with force feedback. The electric control loading system for the wheel was configured to simulate inertia, damping, and hysteresis with values of 0.1 kg·m^2, 0.025 Nm·s/deg, and 1.5 Nm, respectively. The steering wheel torque was calculated by the car model [156]. Carsim 7.01b [156] was used to simulate car dynamics. The vehicle dynamics were similar to a Volkswagen Passat wagon. The car model had automatic transmission.

A.3.3 Motion Cueing Algorithm

Three different MCAs were used in this experiment: Road Rumble Algorithm (RRA), Classical Washout Filter (CWF), Perceptual Tilt Algorithm (PTA). The RRA is a MCA with no inertial motion except to simulate road rumble. For that, the vertical actuator of the simulator moved based on a velocity dependent sum of sines. Further details on the road rumble algorithm can be found in Valente Pais et al. [116].

The CWF was based on the block diagram showed in Figure A.2. To make the motions comparable with the ones of the PTA, the CWF had a first-order low-pass filter with a time constant of two seconds. The rate limiter was set to three deg/s.

The PTA was based on the block diagram showed in Figure A.5. The parameters used in this experiment were equal to those shown in Section A.2.1. Both the PTA and the CWF had an high-pass filter to cue high-frequency accelerations (see Figure A.2). The parameters used in this filter were equal for both the PTA and CWF.

A.3.4   Experimental design

In this study there were three experimental conditions, one for each MCA. The conditions were compared with each other in all possible orders, which means that there were six comparisons per subject. In each comparison the subject drives the maneuver twice, in a total of twelve maneuvers per subject. The six possible comparisons were randomized using a latin squares table.

A.3.5   Procedure

Subjects started the experiment by reading the briefing form and signing an informed consent. Before starting with the experimental measurements, subjects were seated in the simulator with the door open and drove the maneuver. Subjects had to drive in a 600 meters straight road (see Figure A.9). There were three phases in the driving maneuver: acceleration phase, constant velocity phase, and braking phase. During the acceleration phase subjects had to naturally accelerate the car (i.e., as they would do it with their own car) until they reached a speed of approximately 80 km/hr. When the car was at 80 km/hr, subjects had to keep this velocity until they saw two cones in the road marking a end line. At this phase, subjects would start a braking maneuver by pressing the brake pedal. Their objective would be to stop the car as close as possible to the end line in a natural way (e.g., like stopping the car at a traffic light). When the driving task was understood, subjects were secured in the simulator and the measurement phase started. During the experimental measurements, subjects wore a headset which allowed them to communicate with the experimenter. Live radio was also played via this headset to conceal simulator noise and give a more realistic driving sensation. Subjects drove the maneuver twelve times. After each maneuver, subjects had to answer two questions and report their motion sickness status. After driving two maneuvers, subjects had to choose which maneuver of the pair "felt more like accelerating and braking on a real car?". Subjects did this for the six pairs in the experiment. The experiment took approximately 45 minutes, including briefing, training, measurement, and de-briefing.

A.3.6   Data analysis

The measurements we used in this study were divided in subjective and objective measurements. For the subjective measurements we used a questionnaire and a paired comparison to understand which of the three MCAs subjects preferred. For the objective measurements we used typical performance measurements used during a braking maneuver [157].
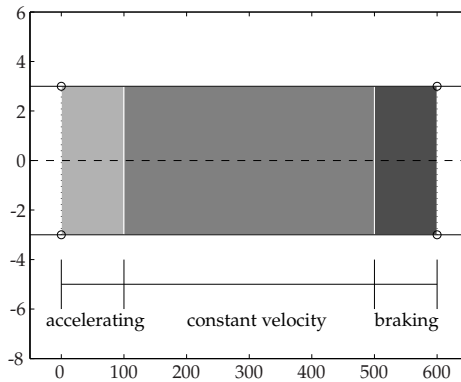
Figure A.9: *Driving maneuver.*

Subjective measures

Paired comparison A paired comparison was used to study which MCA subjects preferred. This technique had been already used on other driving studies [150,158]. In this experiment the maneuvers were driven in pairs. After each pair, subjects had to choose which maneuver they preferred by answering to the following question:

- **Overall**, which of the two motion conditions felt more like **accelerating and braking** in a real car?

After each comparison, the preferred experimental condition would get a score of one. The total score is then the number of times that an experimental condition was preferred over the other conditions.

Questionnaire Subjects had to rate two statements after each driving maneuver. The statements were the following:

- It felt like a real car **when accelerating**.
- It felt like a real car **when braking**.

A 7-point Likert-type scale [159] was used to rate the two statements. This scale ranged from "Strongly Disagree", which had a score of one, to "Strongly Agree", which had a score of seven.

The MIsery SCore After each maneuver, subjects told the experimenter their current motion sickness condition based in the MIsery SCore (MISC) table located in the cabin interior. The MISC scale is shown in Table A.1. This measurement was used to control the motion sickness level of the subjects during the

experiment. The experiment would stop when subjects reported a MISC higher than six. The MISC scores are not reported in this study since the average scores were below one.

Table A.1: *The MIsery SCore (MISC) rating scale used to measure motion sickness*

Symptom		MISC
No problems		0
Slight discomfort but no specific symptons		1
Dizziness, warm, headache, stomach awareness, sweating, etc.	Vague	2
	Some	3
	Medium	4
	Severe	5
Nausea	Some	6
	Medium	7
	Severe	8
	Retching	9
Vomiting		10

Objective measures

We analyzed three objective measures in this study: distance to target, approach speed, and mean deceleration. The distance to target measured the distance between where the car stopped and the end line. The approach speed measured the car speed when subjects started the braking maneuver.

A repeated measures ANOVA was used to analyze the objective measures and the questionnaire ratings. A Greenhouse-Geisser (G-G) correction was applied whenever the sphericity assumption was violated. All statistical tests were performed with SPSS 19.

A.4   Results

A.4.1   Subjective measures

Paired Comparison

Subjective preference was measured using a paired comparison. Figure A.10 shows the total scores obtained for each Motion Cueing Algorithm (MCA). The scores were 52, 47, and 9 respectively for the Perceptual Tilt (PTA), Classical Washout (CWF), and Road Rumble (RRA) algorithms. A chi-square test showed that there was a significant main effect of the MCA on the subjective preference, $\chi^2(2) = 30.7, p = 0.000$. A post-hoc test using a Bonferroni correction was

performed to compare preference between the MCAs. The PTA and the CWF were preferred to the RRA ($\chi^2(2) = 30.3$, $p = 0.000$ and $\chi^2(2) = 25.8$, $p = 0.000$, respectively). There was not a significant preference between the PTA and the CWF.
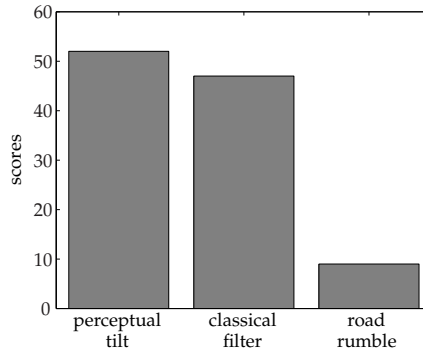
Figure A.10: *Total scores from the paired comparison.*

Questionnaire

Subjects rated the perception of accelerating and braking using a questionnaire. Figure A.11 shows the mean ratings of the accelerating and braking sections for the three MCAs. A repeated measures ANOVA was conducted to test the effect of the MCAs and the maneuver section on the subjective ratings as shown in Table A.2.

Table A.2: *Repeated measures ANOVA results for the questionnaire. ($* = 0.01 < p < 0.05$, $** = p \leq 0.01$)*

Independent Variables	Correction	F-ratio	p	sig.
Motion Cueing Algorithm	-	$F(2,108) = 140.6$	0.000	**
Maneuver section	-	$F(1,54) = 13.3$	0.001	**

The statistical analysis showed a significant main effect of the MCA on the subjective rating. A post-hoc test using a Bonferroni correction showed that the RRA had a significantly lower ratings than the CWF ($p = 0.000$) and the PTA ($p = 0.000$). There were no significant differences between the PTA and the CWF. Figure A.11 and Table A.2 also show that the braking section was rated significantly lower than the acceleration section.
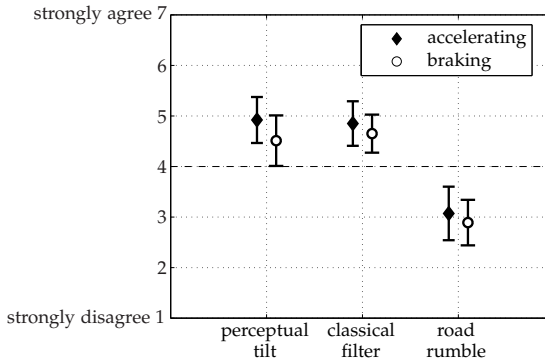
Figure A.11: *Mean questionnaires ratings and their 95% confidence intervals.*

A.4.2   Objective measures

The objective measures in this study focused solely on the braking section. Figure A.12 shows the mean values of the distance to target, approach speed, and mean deceleration. A repeated measures ANOVA was performed in these three measures to study the effect of the MCA. Table A.3 shows the result of this statistical analysis.

Table A.3: *Repeated measures ANOVA results. The independent variable is the motion cueing algorithm. ($* = 0.01 < p < 0.05$, $** = p \leq 0.01$)*

Dependent measures	Correction	F-ratio	p	sig.
Distance to target	G-G	F(1.7,87.0) = 47.9	0.000	**
Approach speed	-	F(2,102) = 7.4	0.001	**
Mean deceleration	-	F(2,102) = 8.1	0.001	**

The statistical analysis showed a significant main effect of the MCA on the objective measures. Post-hoc tests using a Bonferroni correction were performed for these three measures. In all the three measures there were no statistical differences between the PTA and the CWF. We found that the distance to target, mean deceleration and approach speed for the RRA were significantly lower than the ones found for the PTA and the CWF.

(a) Distance to target

(b) Approach speed

(c) Mean deceleration
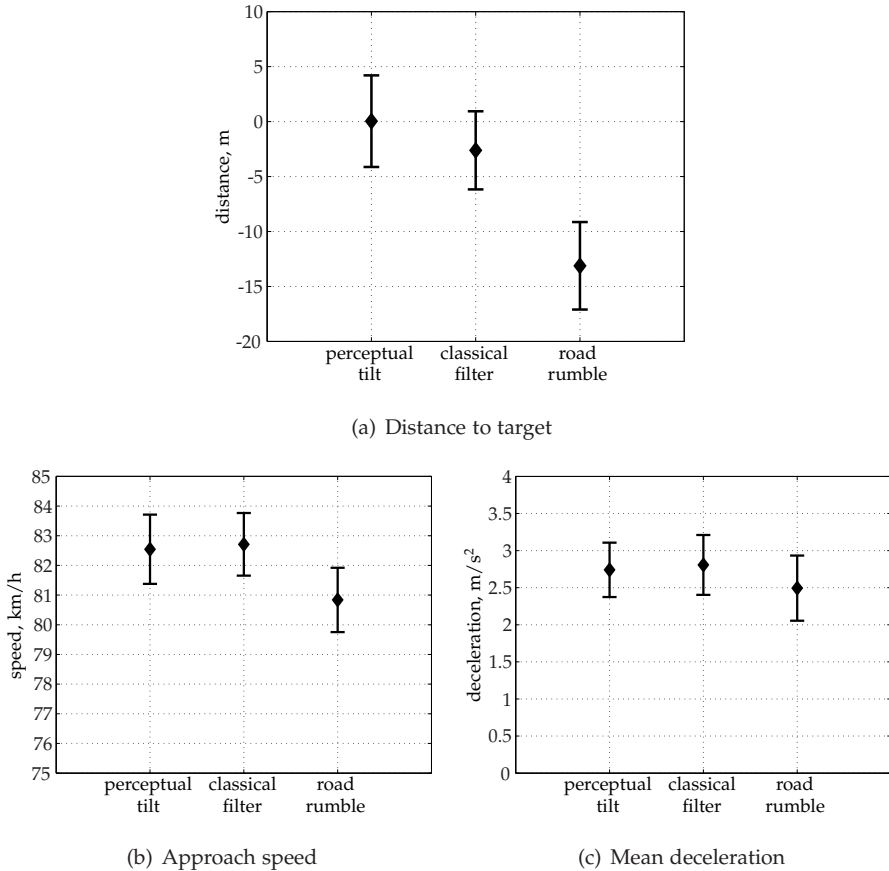
Figure A.12: *Objective measures of the braking maneuver. The error bars indicate the 95% confidence intervals.*

A.5 Discussion

In this study we developed a new Motion Cueing Algorithm (MCA), referred to as Perceptual Tilt Algorithm (PTA), to simulate sustained linear acceleration. An experiment was designed to compare the PTA with a Classical Washout Filter (CWF) and a Road Rumble Algorithm (RRA) that only cued road vibration. Subjective and objective measures were used to compare the MCAs. In this discussion, we focused in the comparison between the PTA and CWF and also on the comparison between motion and no motion MCAs.

A.5.1 Perceptual Tilt Algorithm versus Classical Washout Filter

Subjectively, we found no preference between the PTA or the CWF. Both the paired comparison and the questionnaires revealed no significant differences between these two MCAs. The same trend was found for the objective measures. We found no change in driving behavior between the PTA and the CWF. Regarding task performance, subjects were able to stop at the end line with similar accuracy. Therefore, all results in this study point to no significant differences between these two MCAs.

Although these results might be disappointing at first, the PTA can still be largely improved. We made assumptions during the PTA development that still need to be verified. One assumption was that humans perceive angular velocity during the somatogravic illusion. If humans perceive a change in tilt, then it is reasonable to assume that they also perceive the angular velocity that created that change. However, according to the Mayne equation (Equation (A.2)) the perception of tilt ($\tilde{g}$) does not affect the perception of angular velocity ($\tilde{\omega} \approx \omega_{scc}$). Therefore, the PTA matches the perceived tilt in the simulator with the one in the real world but it does not match the perceived angular velocity. Another assumption was that the somatogravic illusion can be inverted. The somatogravic illusion states that humans perceive tilt when subject to sustained linear acceleration. However, the PTA assumes that humans will perceive acceleration when the illusory tilt of the somatogravic illusion is generated by the simulator. Therefore, a perception experiment is needed to observe whether the somatogravic illusion can be inverted.

The PTA was our first attempt to include self-motion perception knowledge in a MCA. The results did not show a clear advantage or disadvantage of the PTA. However, the perception model we used to derive the PTA was simple and lacked features known in more complex models. The PTA only minimized the perception of tilt leaving out the perception of translation and of angular velocity. We believe that the subjective preference for MCAs using perception knowledge might increase with the introduction of other perception elements like visual perception (e.g., frame and flow information), perception thresholds, internal model, translation perception, among others.

A.5.2 Motion versus No Motion

In this experiment, there were two MCAs with considerable inertial motion (CWF and PTA) and one MCA with considerably low inertial motion. Both the PTA and the CWF were preferred to the RRA. The paired comparison showed a clear preference for the MCAs with strong inertial motion. The same was found for the questionnaires, where the PTA and CWF were rated significantly

higher than the RRA. Although this result seems obvious, there are other studies where conditions without inertial motion are rated equally or better than conditions with inertial motion. For example, Valente Pais et al. [116] used a road rumble algorithm, similar to the one used in this study, that was rated higher than a classical washout filter. However, the authors reported that the classical washout filter had false cues that might have led to these low preferences. Nevertheless, there are other studies that showed a subjective preference for MCAs with inertial motion [76,77,148].

Besides subjective preference, we also found differences in driving behavior. Subjects stopped significantly closer to the end line during the PTA and CWF conditions. In these conditions, the car stopped close to the end line (at approximately 1 meter from the end line) whereas in the RRA, the car was approximately at 13 meters from the end line. Analysis of the approach speed showed that this variable was significantly lower during the RRA. If not noticed, this could have caused the larger distance to the stop line. However, the mean deceleration for the RRA was significantly lower than for the other MCAs, which could have compensated for the lower speed. Nevertheless, it seems that the velocity dependent road rumble cued in the RRA was not enough for subjects to properly conduct the task. Task performance measured by the distance to target variable showed that the extra inertial information delivered by the PTA and CWF had a positive influence in driving behavior, allowing subjects to stop closer to the end line. The positive influence of inertial cues was also found for other driving maneuvers [160,161].

A.6   Conclusion

In this study we compared a new motion cueing algorithm based on a self-motion perception model with a classical washout filter and an algorithm only cueing road rumble. Results showed that both the new cueing algorithm and the classical washout were preferred to the road rumble algorithm. However, there was not a significant preference between the classical washout and the new cueing algorithm. Results also showed significantly different driving behavior during the road rumble algorithm which led to worse braking performance. With this study we could not draw conclusions regarding the improvements that self-motion perception models might introduce in motion cueing algorithms. However, we concluded that inertial feedback has a positive influence in driving behavior for a braking maneuver. This result shows that lacking inertial feedback in driving simulation might lead to unrealistic driving behavior and poor task performance.

Bibliography

[1] Baarspul, M., "A review of flight simulation techniques," *Progress in Aerospace Sciences*, Vol. 27, No. 1, 1990, pp. 1–120.

[2] Burton, R. R. and Whinnery, J. E., "Operational G-induced loss of consciousness: someting old; something new," *Aviation, Space, and Environmental Medicine*, Vol. 56, No. 8, 1985, pp. 812–817.

[3] Crosbie, R. J. and Kiefer, D. A., "Controlling the human centrifuge as a force and motion platform for the dynamic flight simulator," *AIAA Flight Simulation Technologies Conference*, No. 85-1742, St. Louis, MO, July 1985.

[4] Spenny, C. H., Liebst, B. S., Chelette, T. L., Folescu, C., and Sigda, J., "Development of a sustainable-g dynamic flight simulator," *AIAA Modeling and Simulation Technologies Conference and Exhibit*, No. 00-4075, Denver, CO, August 2000.

[5] Snowden, R. J., Stimpson, N., and Ruddle, R. A., "Speed perception fogs up as visibility drops," *Nature*, Vol. 392, 1998, pp. 450.

[6] Kemeny, A. and Panerai, F., "Evaluating perception in driving simulation experiments," *TRENDS in Cognitive Sciences*, Vol. 7, 2003, pp. 31–37.

[7] Greenberg, J., Artz, B., and Cathey, L., "The Effect of Lateral Motion Cues During Simulated Driving," *DSC 2003 North America*, Dearborn, MI, October 2003.

[8] Wertheim, A. H., Bos, J. E., and Bles, W., "Contributions of roll and pitch to sea sickness," *Brain Research Bulletin*, Vol. 47, No. 5, 1998, pp. 517–524.

[9] Bos, J. E., MacKinnon, S. N., and Patterson, A., "Motion sickness symptoms in a ship motion simulator: effects of inside, outside, and no view," *Aviation, Space, and Environmental Medicine*, Vol. 76, No. 12, 2005, pp. 1111–1118.

[10] Ten Hove, D. and Roza, M., "Research into the Effects of Motion Simulation on Tugboat Captain and Performance in Bridge Simulators," *HPAS2010: Human Performance at Sea*, Glasgow, Scotland, UK, June 2010.

[11] Nahon, M. A. and Reid, L. D., "Simulator Motion-Drive Algorithms: A Designer's Perspective," *Journal of Guidance, Control and Dynamics*, Vol. 13, No. 2, March-April 1990, pp. 356–362.

[12] Conrad, B. and Schmidt, S. F., "Motion drive signals for piloted flight simulators," Tech. Rep. CR-1601, NASA, 1970.

[13] Reid, L. D. and Nahon, M. A., "Flight simulation motion-base drive algorithms: part 1 - developing and testing the equations," Tech. Rep. 296, Institute for Aerospace Studies, University of Toronto, December 1985.

[14] Grant, P. R. and Reid, L. D., "Motion Washout Filter Tuning: Rules and Requirements," *Journal of Aircraft*, Vol. 34, No. 2, March-April 1997, pp. 145–151.

[15] Groen, E. L. and Bles, W., "How to Use Body Tilt for the Simulation of Linear Self Motion," *Journal of Vestibular Research*, Vol. 14, No. 5, 2004, pp. 375–385.

[16] Zaal, P. M. T., *Pilot Control Behavior Discrepancies Between Real and Simulated Flight Caused by Limited Motion Stimuli*, Ph.D. thesis, Delft University of Technology, 2011.

[17] Pool, D. M., *Objective Evaluation of Flight Simulator Motion Cueing Fidelity Through a Cybernetic Approach*, Ph.D. thesis, Delft University of Technology, 2012.

[18] Sinacori, J. B., "The determination of Some Requirements for a Helicopter Flight Research Simulation Facility," Tech. Rep. CR-152066, NASA, September 1977.

[19] Schroeder, J. A., "Helicopter Flight Simulation Motion Platform Requirements," Tech. Rep. TP-1999-208766, NASA, July 1999.

[20] Schroeder, J. A. and Grant, P. R., "Pilot Behavioral Observations in Motion Flight Simulation," *AIAA Modeling and Simulation Technologies Conference and Exhibit*, No. AIAA 2010-8353, Toronto, Ontario Canada, August 2010.

[21] Ariel, D. and Sivan, R., "False Cue Reduction in Moving Flight Simulators," *IEEE Transactions on Systems, Man, and Cybernetics*, Vol. SMC-14, No. 4, 1984, pp. 665–671.

[22] Idan, M. and Nahon, M. A., "Off-Line Comparison and Robust Flight Simulator Motion Control," *Journal of Guidance, Control and Dynamics*, Vol. 22, No. 5, September-October 1999, pp. 702–709.

[23] White, A. D. and Rodchenko, V. V., "Motion Fidelity Criteria Based on Human Perception and Performance," *AIAA Modeling and Simulation Technologies Conference and Exhibit*, No. 99-4430, AIAA, Portland, OR, August 1999, pp. 485–493.

[24] Groen, E. L. and Bos, J., "Identification of "Bad Simulator Motion"," *DSC 2008 Europe*, Monaco, January-February 2008.

[25] Telban, R. J., Cardullo, F. M., and Houck, J. A., "Developments in human centered cueing algorithms for control of flight simulator motion systems," *AIAA Modeling and Simulation Technologies Conference and Exhibit*, No. 99-4328, Portland, OR, August 1999.

[26] Advani, S. K., *The Kinematic Design of Flight Simulator Motion-Bases*, Ph.D. thesis, Delft University of Technology, 1998.

[27] Advani, S. K., Nahon, M. A., Haeck, N., and Albronda, J., "Optimization of Six-Degrees-of-Freedom Motion Systems for Flight Simulators," *Journal of Aircraft*, Vol. 36, No. 5, 1999, pp. 819–826.

[28] Wentink, M., Bles, W., Hosman, R. J. A. W., and Mayrhofer, M., "Design & evaluation of spherical washout algorithm for Desdemona simulator," *AIAA Modeling and Simulation Technologies Conference and Exhibit*, No. AIAA 2005-6501, San Francisco, CA, August 2005.

[29] Roza, M., Wentink, M., and Feenstra, P., "Performance Testing of the Desdemona Motion System," *AIAA Modeling and Simulation Technologies Conference and Exhibit*, No. AIAA 2007-6472, Hilton Head, SC, August 2007.

[30] Mayne, R., "A Systems Concept of the Vestibular Organs," *Handbook of Sensory Physiology, vol VI. Vestibular System Part 2: Psychophysics Applied Aspects and General Interpretations*, edited by H. H. Kornhuber, Springer-Verlag Berlin Heidelberg New York, 1974, pp. 493–580.

[31] Guedry, F. E., "Psychophysics of Vestibular Sensation," *Handbook of Sensory Physiology, vol VI. Vestibular System Part 2: Psychophysics Applied Aspects and General Interpretations*, edited by H. H. Kornhuber, Springer-Verlag Berlin Heidelberg New York, 1974, pp. 3–154.

[32] Guedry, F. E. and Harris, C. S., "Labyrinthine Function Related to Experiments on the Parallel Swing," Tech. Rep. NSAM-874, Naval School of Aviation Medicine, Pensacola, FL, 1963.

[33] Clark, B. and Graybiel, A., "Perception of the Visual Horizontal in Normal and Labyrinthine Defective Observers During Prolonged Rotation," *The American Journal of Psychology*, Vol. 79, No. 4, 1966, pp. 608–612.

[34] Bles, W. and De Graaf, B., "Ocular Rotation and Perception of the Horizontal under Static Tilt Conditions in Patients without Labyrinthine Function," *Acta Otolaryngologica*, Vol. 111, No. 3, 1991, pp. 456–462.

[35] Mittelstaedt, H., "Somatic versus Vestibular Gravity Reception in Man," *Annals of the New York Academy of Sciences*, Vol. 656, 1992, pp. 124–139.

[36] Gibson, J. J., *The perception of the visual world*, Houghton Mifflin, 1950.

[37] Monen, J. and Brenner, E., "Detecting changes in one's own velocity from the optic flow," *Perception*, Vol. 23, 1994, pp. 681 – 690.

[38] Cornilleau-Pérès, V. and Gielen, C. C. A. M., "Interactions between self-motion and depth perception in the processing of optic flow," *TRENDS in Neurosciences*, Vol. 19, No. 5, 1996, pp. 196–202.

[39] Lappe, M., Bremmer, F., and Van der Berg, A. V., "Perception of self-motion from visual flow," *TRENDS in Cognitive Sciences*, Vol. 3, No. 9, 1999, pp. 329–336.

[40] Warren, W. H., *The Visual Neurosciences, v. II.*, chap. Optic flow, MIT Press, Cambridge, MA, 2004, pp. 1247–1259.

[41] Fischer, M. H. and Kornmüller, A. E., "Optokinetisch ausgelöste Bewegungswahrnehmungen und optkinetischer Nystagmus," *Journal für Psychologie und Neurologie*, Vol. 41, 1930, pp. 273–308.

[42] Dichgans, J. and Brandt, T., *Visual-vestibular interaction: effects on self-motion perception and in postural control*, Vol. 8, Handbook of Sensory Physiology, Springer-Verlag, Heidelberg, 1978, pp. 755–804.

[43] Howard, I. P. and Heckmann, T., "Circular vection as a function of the relative sizes, distances, and postions of two competing visual displays," *Perception*, Vol. 18, No. 5, 1989, pp. 657–665.

[44] Howard, I. P. and Howard, A., "Vection: the contributions of absolute and relative visual motion," *Perception*, Vol. 23, No. 7, 1994, pp. 745–751.

[45] Van der Steen, H., *Self-Motion Perception*, Ph.D. thesis, Delft University of Technology, 1998.

[46] Gibson, J. J. and Mowrer, O. H., "Determinants of the perceived vertical and horizontal," *Psychological Review*, Vol. 45, No. 4, 1938, pp. 300–323.

[47] Howard, I. P. and Childerson, L., "The contribution of motion, the visual frame, and visual polarity to sensations of body tilt," *Perception*, Vol. 23, No. 7, 1994, pp. 753–762.

[48] Hosman, R. J. A. W., *Pilot's perception and control of aircraft motions*, Ph.D. thesis, Faculty of Aerospace Engineering, Delft University of Technology, 1996.

[49] Holly, J. E., "Vestibular Coriolis Effect Differences Modeled with Three-Dimensional Linear-Angular Interactions," *Journal of Vestibular Research*, Vol. 14, No. 6, 2004, pp. 443–460.

[50] Merfeld, D. M., Young, L. R., Oman, C. M., and Shelhamer, M. J., "A Multidimensional Model of the Effect of Gravity on the Spatial Orientation of the Monkey," *Journal of Vestibular Research*, Vol. 3, 1993, pp. 141–161.

[51] Bos, J. E. and Bles, W., "Theoretical considerations on canal-otolith interaction and an observer model," *Biol. Cybern.*, Vol. 86, 2002, pp. 191–207.

[52] Fernandez, C. and Goldberg, J. M., "Physiology of Peripheral Neurons Innervating Otolith Organs of the Squirrel Monkey. III. Response Dynamics," *Journal of Neurophysiology*, Vol. 39, No. 5, 1976, pp. 996–1008.

[53] Wentink, M., Bos, J., Groen, E. L., and Hosman, R. J. A. W., "Development of the Motion Perception Toolbox," *AIAA Modeling and Simulation Technologies Conference and Exhibit*, No. AIAA 2006-6631, Keystone, Colorado, August 2006.

[54] Einstein, A., "Über das Relativitätsprinzip und die aus demselben gezogene Folgerungen," *Jahrbuch der Radioaktivitaet und Elektronik*, Vol. 4, 1908, pp. 411–462.

[55] Holly, J. E., Vrublevskis, A., and Carlson, L. E., "Whole-motion Model of Perception During Forward- and Backward-facing Centrifuge Runs," *Journal of Vestibular Research*, Vol. 18, No. 4, 2008, pp. 171–186.

[56] Ernst, M. O. and Banks, M. S., "Humans integrate visual and haptic information in a statistically optimal fashion," *Nature*, Vol. 415, 2002, pp. 429–433.

[57] Ernst, M. O. and Bülthoff, H. H., "Merging the senses into a robust percept," *TRENDS in Cognitive Sciences*, Vol. 8, No. 4, 2004, pp. 162–169.

[58] Laurens, J. and Droulez, J., "Bayesian processing of vestibular information," *Biol. Cybern.*, Vol. 96, No. 4, 2007, pp. 389–404.

[59] MacNeilage, P. R., Banks, M. S., Berger, D. R., and Bülthoff, H. H., "A Bayesian model of the disambiguation of gravitoinertial force by visual cues," *Exp Brain Res*, Vol. 179, No. 2, 2007, pp. 263–290.

[60] Clemens, I. A. H., De Vrijer, M., Selen, L. P. J., Van Gisbergen, J. A. M., and Medendorp, W. P., "Multisensory Processing in Spatial Orientation: An Inverse Probabilistic Approach," *Journal of Neuroscience*, Vol. 31, No. 14, 2011, pp. 5365–5377.

[61] Seidman, S. H., Telford, L., and Paige, G. D., "Tilt perception during dynamic linear acceleration," *Exp Brain Res*, Vol. 119, No. 3, 1998, pp. 307–314.

[62] Merfeld, D. M., Park, S., Gianna-Poulin, C., Black, F. O., and Wood, S., "Vestibular Perception and Action Employ Qualitatively Different Mechanisms. I. Frequency Response of VOR and Perceptual Responses During Translation and Tilt," *Journal of Neurophysiology*, Vol. 94, No. 1, 2005, pp. 186–198.

[63] Bos, J. E., Bles, W., and Groen, E. L., "A theory on visually induced motion sickness," *Displays*, Vol. 29, 2008, pp. 47–57.

[64] Oman, C. M., "A heuristic mathematical model for the dynamics of sensory conflict and motion sickness," *Acta Otolaryngol Suppl*, Vol. 392, 1982, pp. 1–44.

[65] Telban, R. J. and Cardullo, F. M., "A nonlinear, human-centered approach to motion cueing with a neurocomputing solver," *AIAA Modeling and Simulation Technologies Conference and Exhibit*, No. AIAA 2002-4692, Monterey, California, 2002.

[66] Telban, R. J. and Cardullo, F. M., "Motion Cueing Algorithm Development: Human-Centered Linear and Nonlinear Algorithms." Tech. Rep. CR-2005-213747, NASA, Langley Research Center, 2005.

[67] Glasauer, S., "Interaction of Semicircular Canals and Otoliths in the Processing Structure of the Subjective Zenith," *Annals of the New York Academy of Sciences*, Vol. 656, 1992, pp. 847–849.

[68] Mittelstaedt, H., "A New Solution to the Problem of the Subjective Vertical," *Naturwissenschaften*, Vol. 70, 1983, pp. 272–281.

[69] Groen, E. L., Jenkin, H. L., and Howard, I. P., "Perception of self-tilt in a true and illusory vertical plane," *Perception*, Vol. 31, 2002, pp. 1477–1490.

[70] Glasauer, S., *Das Zusammenspiel von Otolithen und Bogengängen im Wirkungsgefüge der Subjektiven Vertikale*, Ph.D. thesis, Technical University Munich, 1991.

[71] Clément, G., Moore, S. T., Raphan, T., and Cohen, B., "Perception of Tilt (Somatogravic Illusion) in Response to Sustained Linear Acceleration during Space Flight," *Exp Brain Res*, Vol. 138, No. 4, 2001, pp. 410–418.

[72] Merfeld, D. M., Zupan, L. H., and Gifford, C. A., "Neural Processing of Gravito-Inertial Cues in Humans. II. Influence of the Semicircular Canals During Eccentric Rotation," *Journal of Neurophysiology*, Vol. 85, 2001, pp. 1648–1660.

[73] Vingerhoets, R. A. A., Medendorp, W. P., and Van Gisbergen, J. A. M., "Time Course and Magnitude of Illusory Translation Perception During Off-Vertical Axis Rotation," *Journal of Neurophysiology*, Vol. 95, No. 3, 2006, pp. 1571–1587.

[74] Groen, E. L., Valenti Clari, M. S. V., and Hosman, R. J. A. W., "Evaluation of perceived motion during a simulated takeoff run," *Journal of Aircraft*, Vol. 38, No. 4, 2001, pp. 600 – 606.

[75] Groen, E. L., Smaili, M. H., and Hosman, R. J. A. W., "Perception Model Analysis of Flight Simulator Motion for a Decrab Maneuver," *Journal of Aircraft*, Vol. 44, No. 2, 2007, pp. 427 – 435.

[76] Feenstra, P., Wentink, M., Correia Grácio, B. J., and Bles, W., "Effect of Simulator Motion Space on Realism in the Desdemona Simulator," *DSC 2009 Europe*, Monaco, 2009.

[77] Pretto, P., Nusseck, H. G., Teufel, H. J., and Bülthoff, H. H., "Effect of lateral motion on driver's performance in the MPI motion simulator," *DSC 2009 Europe*, Monaco, 2009.

[78] Grant, P. R. and Haycock, B., "Effect of Jerk and Acceleration on the Perception of Motion Strength," *Journal of Aircraft*, Vol. 45, No. 4, 2008, pp. 1190 – 1197.

[79] Graybiel, A., "Oculogravic Illusion," *AMA Arch Ophthalmol.*, Vol. 48, No. 5, 1952, pp. 605–615.

[80] Glasauer, S., "Linear Acceleration Perception: Frequency Dependence of the Hilltop Illusion," *Acta Otolaryngol Suppl*, Vol. 520, 1995, pp. 37–40.

[81] Jaggi-Schwarz, K. and Hess, B. J. M., "Influence of dynamic tilts on the perception of earth-vertical," *Exp Brain Res*, Vol. 149, No. 3, 2003, pp. 340–350.

[82] Wright, W. G. and Glasauer, S., "Subjective somatosensory vertical during dynamic tilt is dependent on task, inertial condition, and multisensory concordance," *Exp Brain Res*, Vol. 172, No. 3, 2006, pp. 310–321.

[83] Groen, E. L., Howard, I. P., and Cheung, B. S. K., "Influence of Body Roll on Visually Induced Sensations of Self-Tilt and Rotation," *Perception*, Vol. 28, 1999, pp. 287–297.

[84] Tribukait, A. and Eiken, O., "Roll-Tilt Perception During Gondola Centrifugation: Influence of Steady-State Acceleration (G) Level," *Aviation, Space, and Environmental Medicine*, Vol. 77, No. 7, 2006, pp. 695–703.

[85] Van Beuzekom, A. D., Medendorp, W. P., and Van Gisbergen, J. A. M., "The Subjective Vertical and the Sense of Self Orientation During Active Body Tilt," *Vision Research*, Vol. 41, 2001, pp. 3229–3242.

[86] Mars, F., Vercher, J.-L., and Konstantin, P., "Dissociation Between Subjective Vertical and Subjective Body Orientation Elicited by Galvanic Vestibular Stimulation," *Brain Research Bulletin*, Vol. 65, No. 1, 2005, pp. 77–86.

[87] Van Erp, J. B. F., Groen, E. L., Bos, J. E., and Van Veen, H. A. H. C., "A Tactile Cockpit Instrument Supports the Control of Self-Motion During Spatial Disorientation," *Human Factors*, Vol. 48, No. 2, 2006, pp. 219–228.

[88] Previc, F. H. and Ercoline, W. R., "The "Outside-In" Attitude Display Concept Revisited," *International Journal of Aviation Psychology*, Vol. 9, No. 4, 1999, pp. 377–401.

[89] Benson, A. J., Spencer, M. B., and Stott, J. R. R., "Thresholds for the Detection of the Direction of Whole-Body, Linear Movement in the Horizontal Plane," *Aviation, Space, and Environmental Medicine*, Vol. 57, No. 11, 1986, pp. 1088–1096.

[90] Field, A., *Discovering Statistics Using SPSS*, Sage Publications Ltd, 2nd ed., 2005.

[91] Aubert, H., "Eine scheinbare bedeutende Drehung von Objecten bei Neigung des Kopfes nach rechts oder links," *Virchows Archiv*, Vol. 20, No. 3, 1861, pp. 381–393.

[92] Merfeld, D. M., Park, S., Gianna-Poulin, C., Black, F. O., and Wood, S., "Vestibular Perception and Action Employ Qualitatively Different Mechanisms. II. VOR and Perceptual Responses During Combined Tilt&Translation," *Journal of Neurophysiology*, Vol. 94, No. 1, 2005, pp. 199–205.

[93] Cohen, M. M., Crosbie, R. J., and Blackburn, L. H., "Disorienting Effects of Aircraft Catapult Launchings," *Aviation, Space, and Environmental Medicine*, Vol. 44, No. 1, 1973, pp. 37–39.

[94] Cohen, M. M., "Disorienting Effects of Aircraft Catapult Launchings II. Visual and Postural Contributions," *Aviation, Space, and Environmental Medicine*, Vol. 47, No. 1, 1976, pp. 39–41.

[95] Cohen, M. M., "Disorienting Effects of Aircraft Catapult Launchings III. Cockpit Displays and Piloting Performance," *Aviation, Space, and Environmental Medicine*, Vol. 48, No. 9, 1977, pp. 797–804.

[96] Curthoys, I. S., "The Delay of the Oculogravic Illusion," *Brain Research Bulletin*, Vol. 40, No. 5-6, 1996, pp. 410–412.

[97] Clément, G., Maciel, F., and Dequine, O., "Perception of Tilt and Ocular Torsion of Normal Human Subjects During Eccentric Rotation," *Otol Neurotol.*, Vol. 23, No. 6, 2002, pp. 958–966.

[98] De Graaf, B., Bos, J. E., Tielemans, W., Rameckers, F., Rupert, A. H., and Guedry, F. E., "Otolith Contribution to Ocular Torsion and Spatial Orientation During Acceleration," Technical Memorandum 96-3, Naval Aerospace Medical Research Laboratory, Pensacola, Fa, 1996.

[99] Bles, W. and Groen, E. L., "The DESDEMONA Motion Facility: Applications for Space Research," *Microgravity Science and Technology*, Vol. 21, 2009, pp. 281–286.

[100] Graybiel, A. and Brown, R. H., "The Delay in Visual Reorientation Following Exposure to a Change in Direction of Resultant Force on a Human Centrifuge," *Journal of General Psychology*, Vol. 45, No. 2, 1951, pp. 143–150.

[101] Young, L. R. and Meiry, J. L., "A Revised Dynamic Otolith Model," *Aerospace Medicine*, Vol. 39, No. 6, 1968, pp. 606–608.

[102] Park, S., Gianna-Poulin, C., Black, F. O., Wood, S., and Merfeld, D. M., "Roll Rotation Cues Influence Roll Tilt Perception Assayed Using a Somatosensory Technique," *Journal of Neurophysiology*, Vol. 96, No. 1, 2006, pp. 486–491.

[103] Zaichik, L. E., Rodchenko, V., Rufov, I. V., Yashin, Y. P., and White, A. D., "Acceleration Perception," *AIAA Modeling and Simulation Technologies Conference and Exhibit*, No. AIAA-99-434, Portland, OR, August 1999, pp. 512–520.

[104] Heerspink, H. M., Berkouwer, W. R., Stroosma, O., Van Paassen, M. M., Mulder, M., and Mulder, J. A., "Evaluation of Vestibular Thresholds for Motion Detection in the SIMONA Research Simulator," *AIAA Modeling and Simulation Technologies Conference and Exhibit*, No. AIAA 2005-6502, San Francisco, CA, August 2005.

[105] Soyka, F., Robuffo Giordano, P., Beykirch, K. A., and Bülthoff, H. H., "Predicting Direction Detection Thresholds for Arbitrary Translational Acceleration Profiles in the Horizontal Plane," *Exp Brain Res*, Vol. 209, No. 1, 2011, pp. 97–107.

[106] Van Egmond, A. A. J., Groen, J. J., and Jongkees, L. B. W., "The mechanics of the semicircular canal," *The Journal of Physiology*, Vol. 110, No. 1-2, 1949, pp. 1–17.

[107] Correia Grácio, B. J., De Winkel, K. N., Groen, E. L., Wentink, M., and Bos, J. E., "The time constant of the somatogravic illusion," *Exp Brain Res*, Vol. 224, No. 3, 2013, pp. 313–321.

[108] Wright, W. G., DiZio, P., and Lackner, J. R., "Vertical linear self-motion perception during visual and inertial motion: More than weighted summation of sensory inputs," *Journal of Vestibular Research*, Vol. 15, No. 4, 2005, pp. 185–195.

[109] Vingerhoets, R. A. A., Van Gisbergen, J. A. M., and Medendorp, W. P., "Verticality perception during off-vertial axis rotation," *Journal of Neurophysiology*, Vol. 97, No. 5, 2007, pp. 3256–3268.

[110] Berthoz, A., Pavard, B., and Young, L. R., "Perception of Linear Horizontal Self-Motion Induced by Peripheral Vision (Linearvection) Basic Characteristics and Visual-Vestibular Interactions," *Exp Brain Res*, Vol. 23, No. 5, 1975, pp. 471–489.

[111] Wertheim, A. H., Mesland, B. S., and Bles, W., "Cognitive suppression of tilt sensations during linear horizontal self-motion in the dark," *Perception*, Vol. 30, No. 6, 2001, pp. 733–741.

[112] Stevens, S. S., "Duration, luminance, and the brightness exponent," *Attention, Perception & Psychophysics*, Vol. 1, No. 2, 1966, pp. 96–100.

[113] Stevens, S. S. and Davis, H., *Hearing: Its psychology and physiology*, New York: Wiley, 1938.

[114] Merfeld, D. M. and Zupan, L. H., "Neural Processing of Gravitoinertial Cues in Humans. III. Modeling Tilt and Translation Responses," *Journal of Neurophysiology*, Vol. 87, No. 2, 2002, pp. 819–833.

[115] Wentink, M., Valente Pais, A. R., Mayrhofer, M., Feenstra, P., and Bles, W., "First Curve Driving Experiments in the Desdemona Simulator," *DSC 2008 Europe*, Monaco, January-February 2008.

[116] Valente Pais, A. R., Wentink, M., Van Paassen, M. M., and Mulder, M., "Comparison of Three Motion Cueing Algorithms for Curve Driving in an Urban Environment," *PRESENCE: Teleoperators and Virtual Environments*, Vol. 18, 2009, pp. 200–221.

[117] Naseri, A., Grant, P. R., and Dufort, P., "Modeling the Perception of Acceleration and Jerk using Signal Detection Theory," *AIAA Modeling and Simulation Technologies Conference and Exhibit*, No. AIAA 2008-6846, Honolulu, Hawaii, August 2008.

[118] Soyka, F., Teufel, H. J., Beykirch, K. A., Robuffo Giordano, P., Butler, J. S., Nieuwenhiuzen, F. M., and Bülthoff, H. H., "Does jerk have to be considered in linear motion simulation?" *AIAA Modeling and Simulation Technologies Conference and Exhibit*, No. AIAA 2009-6245, Chicago, IL, August 2009.

[119] Valente Pais, A. R., Van Paassen, M. M., Mulder, M., and Wentink, M., "Perception Coherence Zones in Flight Simulation," *AIAA Modeling and Simulation Technologies Conference and Exhibit*, No. AIAA 2009-6242, Chicago, IL, August 2009.

[120] Van der Steen, H., "An Earth-Stationary Perceived Visual Scene During Roll and Yaw Motions in a Flight Simulator," *Journal of Vestibular Research*, Vol. 8, No. 6, 1998, pp. 411–425.

[121] Harris, L. R., Jenkin, M., and Zikovitz, D. C., "Visual and Non-visual Cues in the Perception of Linear Self Motion," *Exp Brain Res*, Vol. 135, No. 1, 2000, pp. 12–21.

[122] Grant, P. R. and Lee, P. T. S., "Motion-Visual Phase-Error Detection in a Flight Simulator," *Journal of Aircraft*, Vol. 44, No. 3, 2007, pp. 927–935.

[123] Valente Pais, A. R., Van Paassen, M. M., Mulder, M., and Wentink, M., "Perception of Combined Visual and Inertial Low-Frequency Yaw Motion," *AIAA Modeling and Simulation Technologies Conference and Exhibit*, No. AIAA 2010-8093, Toronto, Ontario Canada, August 2010.

[124] Valente Pais, A. R., Van Paassen, M. M., Mulder, M., and Wentink, M., "Perception Coherence Zones in Flight Simulation," *Journal of Aircraft*, Vol. 47, No. 6, 2010, pp. 2039–2048.

[125] Correia Grácio, B. J., Van Paassen, M. M., Mulder, M., and Wentink, M., "Tuning of the Lateral Specific Force Gain Based on Human Motion Perception in the Desdemona Simulator," *AIAA Modeling and Simulation Technologies Conference and Exhibit*, No. AIAA 2010-8094, Toronto, Ontario Canada, August 2010.

[126] Jonik, P. M., Valente Pais, A. R., Van Paassen, M. M., and Mulder, M., "Phase Coherence Zones in Flight Simulation," *AIAA Modeling and Simulation Technologies Conference and Exhibit*, No. AIAA 2011-6555, Portland, OR, August 2011.

[127] Lean, D. and Gerlach, O. H., "AGARD Advisory Report No 144: Dynamics Characteristics of Flight Simulator Motion Systems," Tech. Rep. AGARD-AR-144, North Atlantic Treaty Organization, Advisory Group for Aerospace Research and Development, 1979.

[128] Nieuwenhuizen, F. M., Van Paassen, M. M., Mulder, M., Beykirch, K. A., and Bülthoff, H. H., "Towards Simulating a Mid-size Stewart Platform on a Large Hexapod Simulator," *AIAA Modeling and Simulation Technologies Conference and Exhibit*, No. AIAA 2009-5917, Chicago, IL, August 2009.

[129] Correia Grácio, B. J., Valente Pais, A. R., Van Paassen, M. M., Mulder, M., Kelly, L. C., and Houck, J. A., "Optimal and coherence zone comparison within and between flight simulators," *Journal of Aircraft*, Vol. 50, No. 2, 2013, pp. 493–507.

[130] Brandt, T., Dichgans, J., and Koenig, E., "Differential Effects of Central Versus Peripheral Vision on Egocentric and Exocentric Motion Perception," *Exp Brain Res*, Vol. 16, No. 5, 1973, pp. 476–491.

[131] Andre, A. D. and Johnson, W. W., "Stereo Effectiveness Evaluation for Precision Hover Tasks in a Helmet-Mounted Display Simulator," *Systems, Man and Cybernetics*, Chicago, IL, October 1992.

[132] Duh, H. B. L., Lin, J. J. W., Kenyon, R. V., Parker, D. E., and Furness, T. A., "Effects of Field of View on Balance in an Immersive Environment," *Virtual Reality*, edited by IEEE, Yokohama, Japan, March 2001, pp. 235–240.

[133] Chung, W. W. Y., Sweet, B. T., and Kaiser, M. K. an Lewis, E., "Visual Cueing Effects Investigation for a Hover Task," *AIAA Modeling and Simulation Technologies Conference and Exhibit*, No. AIAA 2003-5524, Austin, TX, August 2003.

[134] Berger, D. R., Terzibas, C., Beykirch, K. A., and Bülthoff, H. H., "The Role of Visual Cues and Whole-Body Rotations in Helicopter Hovering Control," *AIAA Modeling and Simulation Technologies Conference and Exhibit*, No. AIAA 2007-6798, Hilton Head, SC, August 2007.

[135] Pretto, P., Ogier, M., Bülthoff, H. H., and Bresciani, J. P., "Influence of the size of the field of view on motion perception," *Computer & Graphics*, Vol. 33, No. 2, 2009, pp. 139–146.

[136] Arthur, K. W., *Effects of Field of View on Task Performance with Head-Mounted Displays*, Ph.D. thesis, University of North Carolina at Chapel Hill, 1999.

[137] Alfano, P. L. and Michel, G. F., "Restricting the Field of View: Perceptual and Performance Effects," *Perceptual and Motor Skills*, Vol. 70, No. 1, 1990, pp. 35–45.

[138] Sweet, B. T. and Kaiser, M. K., "Depth perception, cueing, and control," *AIAA Modeling and Simulation Technologies Conference and Exhibit*, No. AIAA 2011-6424, Portland, OR, August 2011.

[139] Bos, J. E. and Bles, W., "Modelling motion sickness and subjective vertical mismatch detailed for vertical motions," *Brain Research Bulletin*, Vol. 47, No. 5, 1998, pp. 537–542.

[140] Correia Grácio, B. J., Wentink, M., Bos, J. E., Van Paassen, M. M., and Mulder, M., "An Application of the Canal-Otolith Interaction Model for Tilt-Coordination During a Braking Maneuver," *AIAA Modeling and Simulation Technologies Conference and Exhibit*, No. AIAA 2012-4493, Minneapolis, Minnesota, August 2012.

[141] Robinson, D. A., "Linear Addition of Optokinetic and Vestibular Signals in the Vestibular Nucleus," *Exp Brain Res*, Vol. 30, No. 2-3, 1977, pp. 447–450.

[142] Jürgens, R. and Becker, W., "Perception of angular displacement without landmarks: evidence for Bayesian fusion of vestibular, optokinetic, podokinesthetic, and cognitive information," *Exp Brain Res*, Vol. 174, No. 3, 2006, pp. 528–543.

[143] Parrish, R. V., Dieudonne, J. E., Bowles, R. L., and Martin, D. J., "Coordinated adaptive washout for motion simulators." *Visual and Motion Simulation Conference*, No. 73-930, AIAA, Palo Alto, California, September 1973.

[144] Nahon, M. A., Reid, L. D., and Kirdeikis, J., "Adaptive Simulator Motion Software with Supervisory Control," *Journal of Guidance, Control and Dynamics*, Vol. 15, No. 2, 1992, pp. 376–383.

[145] De Winkel, K. N., *Multisensory Perception of Spatial Orientation and Self-Motion*, Ph.D. thesis, Utrecht University, 2013.

[146] Pool, D. M., Zaal, P. M. T., Damveld, H. J., Van Paassen, M. M., and Mulder, M., "Evaluating Simulator Motion Fidelity using In-Flight and Simulator Measurements of Roll Tracking Behavior," *AIAA Modeling and Simulation Technologies Conference and Exhibit*, Minneapolis, Minnesota, August 2012.

[147] Shepard, R. N., "Ecological Constraints on Internal Representation: Resonant Kinematics of Perceiving, Imagining, Thinking, and Dreaming," *Psychological Review*, Vol. 91, No. 4, 1984, pp. 417–447.

[148] Correia Grácio, B. J., Wentink, M., Valente Pais, A. R., Van Paassen, M. M., and Mulder, M., "Driver Behavior Comparison Between Static and Dynamic Simulation for Advanced Driving Maneuvers," *PRESENCE: Teleoperators and Virtual Environments*, Vol. 20, No. 2, 2011, pp. 143–161.

[149] Dos Santos Buinhas, L., Correia Grácio, B. J., Valente Pais, A. R., Van Paassen, M. M., and Mulder, M., "Modeling Coherence Zones in Flight Simulation During Yaw Motion," *AIAA Modeling and Simulation Technologies Conference and Exhibit*, No. AIAA 2013-5223, Boston, MA, August 2013.

[150] Grant, P. R., Blommer, M., Cathey, L., Artz, B., and Greenberg, J., "Analyzing Classes of Motion Drive Algorithms Based on Paired Comparison Techniques," *DSC 2003 North America*, Dearborn, MI, October 2003.

[151] De Winkel, K. N., Weesie, J., Werkhoven, P. J., and Groen, E. L., "Integration of visual and inertial cues in perceived heading of self-motion," *Journal of Vision*, Vol. 10, No. 12, 2010, pp. 1–10.

[152] Dokka, K., MacNeilage, P. R., DeAngelis, G. C., and Angelaki, D. E., "Estimating distance during self-motion: A role for visual-vestibular interactions," *Journal of Vision*, Vol. 11, No. 13, 2011, pp. 1–16.

[153] Valente Pais, A. R., Van Paassen, M. M., Mulder, M., and Wentink, M., "Effect of Performing a Boundary-Avoidance Tracking Task on the Perception of Coherence Between Visual and Inertial Cues," *AIAA Modeling and Simulation Technologies Conference and Exhibit*, No. AIAA 2011-6324, Portland, OR, August 2011.

[154] Beckers, N. W. M., Pool, D. M., Valente Pais, A. R., Van Paassen, M. M., and Mulder, M., "Perception and Behavioral Phase Coherence Zones in Passive and Active Control Tasks in Yaw," *AIAA Modeling and Simulation Technologies Conference and Exhibit*, No. AIAA 2012-4794, Minneapolis, Minnesota, August 2012.

[155] Chapron, T. and Colinot, J.-P., "The New PSA Peugeot-Citroën Advanced Driving Simulator Overall Design and Motion Cue Algorithm," *DSC 2007 North America*, Iowa City, September 2007.

[156] "http://www.carsim.com/," July 2012.

[157] De Groot, S., De Winter, J. C. F., Wieringa, P. A., and Mulder, M., "An Analysis of Braking Measures," *DSC 2009 Europe*, Monaco, February 2009.

[158] Grant, P. R., Artz, B., Blommer, M., Cathey, L., and Greenberg, J., "A Paired Comparison Study of Simulator Motion," *DSC 2002 Europe*, Paris, France, September 2002.

[159] Likert, R., "A technique for the measurement of attitudes," *Archives of Psychology*, Vol. 22, No. 140, 1932, pp. 1–55.

[160] Reymond, G., Kemeny, A., Droulez, J., and Berthoz, A., "Role of Lateral Acceleration in Curve Driving: Driver Model and Experiments on a Real Vehicle and a Driving Simulator," *Human Factors*, Vol. 43, No. 3, 2001, pp. 483 – 495.

[161] Brünger-Koch, M., Briest, S., and Vollrath, M., "Do you feel the difference? - A motion assessment study," *DSC - Asia/Pacific*, Tsubaka, Japan, May-June 2006.

Samenvatting

De invloed van specifieke krachten op de waarneming van zelfbeweging in simulatoromgevingen

Bruno Jorge Correia Grácio

Het gebruik van bewegingsplatformen stelt de mens in staat specifieke manuevres in een veilige en gecontroleerde omgeving na te bootsen. Hierbij wordt de illusie van het besturen van een voertuig gewekt door het genereren van specifieke visuele en fysieke stimuli. Hoewel de amplitude van visuele beweging die wordt waargenomen in een voertuig één-op-één kan worden nagebootst in een simulator, vereist het nabootsen van de lineaire- en hoekversnellingen die in een voertuig worden ervaren doorgaans een grotere fysieke verplaatsing dan die waar de simulator toe in staat is. In simulatoren worden fysieke bewegingen daarom met behulp van zgn. Motion Cueing Algoritmes (MCA's) getransformeerd in stimuli die binnen de fysieke grenzen van de simulator liggen.

Aanvankelijk waren MCA's gericht op het minimaliseren van het verschil tussen de stimuli die ontstaan door bewegingen in het daadwerkelijke voertuig en de bewegingen op een bewegingsplatform. Deze methode is in principe geschikt voor het nabootsen van voertuigbewegingen, maar wanneer deze bewegingen toenemen in duur en amplitude worden mensen zich meer bewust van de beperkingen van de simulator. Dit heeft zijn weerslag op de ervaren immersie en op de effectiviteit van trainingen. Een mogelijke oplossing is om, in plaats van de exacte bewegingen die het voertuig maakt, de door de mens waargenomen bewegingen in de simulator na te bootsen. In deze benadering

wordt het verschil tussen de waargenomen bewegingen in het voertuig en die in de simulator geminimaliseerd.

De menselijke waarneming van zelfbeweging komt tot stand in het centrale zenuwstelsel (CNS), door het samenvoegen van informatie uit verschillende sensorische modaliteiten. Een accurate waarneming van zelfbeweging is essentieel voor voortbeweging en ruimtelijke oriëntatie. Wanneer mensen echter worden bewogen in simulatoromgevingen (bijvoorbeeld voor vliegen of autorijden), zijn zij ontvankelijk voor bewegingsillusies. Zo kan specifieke kracht (dat is, de resultante kracht op een ruimtelijk lichaam per eenheid van massa in m/s^2) resulteren in een waarneming van translatie (lineaire beweging), een waarneming van kanteling, of in een combinatie van beide soorten beweging. Voor het ontwikkelen van MCA's die inspelen op de karakteristieken van menselijke waarneming is een grondige kennis van de menselijke waarneming van zelfbeweging in simulatoren daarom onontbeerlijk.

Hierbij is met name specifieke kracht interessant, vanwege de ambiguïteit tussen kanteling en translatie, en vanwege het feit dat een plotselinge verandering van de specifieke kracht ervoor kan zorgen dat een simulator tegen zijn fysieke grenzen aanloopt.

Het hoofddoel van het onderzoek dat in deze dissertatie wordt beschreven is een beter begrip te ontwikkelen van hoe menselijke waarneming van zelfbeweging in simulatoromgevingen wordt beïnvloed door specifieke kracht.

Het onderzoek is verdeeld in twee delen: een deel met een focus op het vestibulair systeem (het evenwichtsorgaan, bestaande uit de otolieten en de halfcirkelvormige kanalen) en een deel met een focus op visueel-vestibulaire interacties.

In het eerste deel, bestaande uit de hoofdstukken twee tot en met vier, wordt beschreven hoe specifieke kracht in afwezigheid van visuele stimuli enerzijds kan leiden tot waarneming van kanteling en anderzijds tot waarneming van translatie. In het tweede deel, bestaande uit de hoofdstukken vijf tot en met zeven, wordt onderzoek naar schaling tussen visuele en fysieke stimuli in een simulatoromgeving beschreven.

In hoofdstuk twee worden mogelijke artefacten in de waarneming van kanteling beschreven. Proefpersonen werden sinusoïdaal rond hun naso-occipitale as gekanteld, waarbij ze de door hen ervaren kanteling aangaven met een joystick. De instructie daarbij was ofwel de joystick in de richting tegengesteld aan de eigen kanteling te bewegen, de 'inside-out'-conditie (IO), of de joystick mee te bewegen in de richting van de kanteling, de 'outside-in'-conditie (OI). Voorts werd onderzocht of er verschil bestaat tussen het boven, rond, en onder het draaipunt vasthouden van de joystick. De resultaten toonden een significant verschil in gemeten kanteling tussen de IO en OI condities, maar geen effect van de wijze waarop de joystick werd vastgehouden. Op basis van de

resultaten werd geconcludeerd dat de aangegeven kanteling in de IO conditie correspondeert met de subjectieve verticaal en dat de aangegeven kanteling in de OI conditie overeenkomt met de waargenomen kanteling.

In hoofdstuk drie wordt onderzoek beschreven naar illusoire kanteling, bekend als de 'somatogravische illusie'. Deze illusie ontstaat wanneer mensen in een verder donkere omgeving worden blootgesteld aan een continue lineaire versnelling. Waargenomen kanteling werd gemeten met een joystick, met de in hoofdstuk twee beschreven OI-conditie. De bewegingsprofielen werden gegenereerd met een techniek waarbij proefpersonen werden gecentrifugeerd met een variabele radius. Hierbij ontstaat een laterale centripetale versnelling die als kanteling om de naso-occipitale as wordt ervaren. De resultaten lieten zien dat de tijdsconstante van de somatogravische illusie in de orde van twee seconden was. Daarnaast werd aangetoond dat de illusie kan worden beschreven met een in 1974 door Mayne ontwikkeld model van waarneming van zelfbeweging, bekend als de 'vergelijking van Mayne'.

Naar aanleiding van het in hoofdstukken twee en drie beschreven onderzoek, wordt in hoofdstuk vier onderzoek beschreven naar waargenomen translatie wanneer mensen in het donker blootgesteld worden aan veranderingen in de specifieke kracht. Proefpersonen werden op lateraalsinusoidale wijze bewogen, waarbij de bewegingen verschilden in frequentie en amplitude. Proefpersonen werden gevraagd de waargenomen zijdelingse verplaatsing en pieksnelheid te rapporteren. Uit de resultaten bleek dat de gerapporteerde verplaatsing in dezelfde orde van grootte was als de gerapporteerde pieksnelheid, wanneer deze werd geconverteerd naar verplaatsing. Voor de meeste proefpersonen kon de waargenomen snelheid adequaat worden gemodelleerd met de vergelijking van Mayne. Voor het modelleren van waargenomen verplaatsing was een extra "leaky integrator" (een zogenaamde benaderde integratie) nodig. De resultaten van een klein aantal proefpersonen leken te worden beïnvloed door cognitieve processen die niet in huidige modellen van waarneming van zelfbeweging worden vertegenwoordigd.

Uit de resultaten van hoofdstukken drie en vier blijkt dat de vergelijking van Mayne een accurate beschrijving van de ambiguïteit tussen kanteling en translatie in afwezigheid van visuele informatie geeft. De gemeten tijdsconstante van het model was in dezelfde orde van grootte voor beide onderzoeken. De vergelijking van Mayne kan echter alleen worden toegepast in situaties met verminderde visuele informatie, zoals 's nachts, of door wolken vliegen. Daarom is het vervolg van het onderzoek in deze dissertatie gericht op visueel-vestibulaire interacties.

In hoofdstuk vijf is onderzocht welke schaling tussen visuele en fysieke beweging de voorkeur van proefpersonen geniet. Proefpersonen werden sinusoïdaal bewogen, waarbij visuele en fysieke bewegingen met gelijke frequentie en

fase, maar met verschillende amplitude werden aangeboden. De taak van de proefpersonen was de amplitude van de fysieke beweging aan te passen tot een optimale schaling was bereikt. Het bleek dat de gain van de bewegingen, gedefinieerd als de verhouding tussen de fysieke en visuele amplitude, afnam voor grotere visuele amplitudes en bewegingsfrequenties. Over het geheel genomen waren de gains kleiner dan één, wat betekent dat de geprefereerde fysieke amplitude kleiner is dan visuele amplitude. Ook vonden we dat niet één waarde voor de gain de voorkeur heeft, maar dat de geprefereerde gain afhankelijk is van de beginwaarde van de amplitude van de fysieke beweging. Dit onderzoek bevestigt eerdere bevindingen dat fysieke beweging in een simulator wordt overschat.

Het bereik van de fysieke waarden dat in hoofdstuk vijf werd gevonden -hier gedefinieerd als 'optimale zone' (OZ) - leek op de in de literatuur beschreven 'coherentiezone' (CZ). De CZ wordt gedefinieerd als het bereik van de ver houdingen tussen visuele en fysieke beweging die als coherent wordt ervaren, ongeacht verschillen in amplitude of fase. Om deze gelijkenis te duiden werd in hoofdstuk zes een vergelijking gemaakt tussen de OZ en CZ. Proefpersonen werden sinusoïdaal-lateraal bewogen. Voor het bepalen van de OZ werd proefpersonen gevraagd de amplitude van de fysieke beweging aan te passen tot een optimale match werd bereikt; voor het bepalen van de CZ werd proefpersonen gevraagd de boven- en ondergrens van fysieke beweging op te zoeken die nog als coherent met de visuele beweging werd ervaren. De resultaten lieten zien dat de OZ en CZ van elkaar verschillen, waarbij de eerstgenoemde binnen de laatstgenoemde viel. De gains van de OZ lieten dezelfde trends met betrekking tot amplitude en frequentie zien als die gevonden in hoofdstuk vijf, namelijk dat de gain afnam met toenemende frequentie en amplitude en dat de geprefereerde gain kleiner dan 1 is - ondanks het feit dat de onderzoeken in verschillende simulatoren werden uitgevoerd.

De waarneming in zowel hoofdstuk vijf als zes, dat de geprefereerde gain kleiner dan 1 is, is mogelijk te verklaren aan de hand van de visuele stimuli die getoond werden in de simulatoren. Daarom is in hoofdstuk zeven onderzocht of de schaling tussen visuele en fysieke stimuli afhankelijk is van de grootte van het blikveld (de "Field-of-View"), en de inhoud van de virtuele wereld, waarbij cues met betrekking tot grootte en diepte werden gevarieerd. In dit onderzoek werd proefpersonen gevraagd de amplitude van visuele stimuli aan te passen tot een optimale overeenstemming met de fysieke beweging was bereikt. De taak werd uitgevoerd voor sinusoïdale schrik- (longitudinale), verzet (laterale), en gier- (rotatie om de verticale as) bewegingen (in het Engels *surge*, *sway*, en *yaw*, respectievelijk). De resultaten toonden aan dat de gain van de visuele stimulus, gedefinieerd als de verhouding tussen de visuele en fysieke beweging, dichter bij één lag wanneer de blikveldgrootte toenam en ook wanneer meer

grootte-diepte-cues beschikbaar waren in de virtuele wereld. Op basis hiervan werd geconcludeerd dat perceptie van diepte een groot effect heeft op de gain van de visuele stimulus.

Voor de rotatiebeweging, waar de snelheid van optische stroming (optic flow) onafhankelijk is van de afstand van objecten tot de waarnemer, was de gain van de visuele beweging gelijk aan één en onafhankelijk van de inhoud van de virtuele wereld. Voor de longitudinale en laterale translatiebewegingen, waar de snelheid van optische stroming wél afhankelijk is van de afstand van objecten tot de waarnemer, waren de gains veel hoger dan één, en afhankelijk van de inhoud van de virtuele wereld. De visuele gains lijken hiermee een goede maat om te evalueren hoe grootte en diepte worden geïnterpreteerd in simulatoromgevingen.

In hoofdstuk acht worden de implicaties van de resultaten van de voorgaande hoofdstukken voor het ontwerp van MCA's geëvalueerd. Enerzijds werdt een model van de waarneming van zelfbeweging uit de literatuur uitgebreid om de bevindingen van het onderzoek uit de eerdere hoofdstukken van deze dissertatie te accommoderen, anderzijds wordt in dit hoofdstuk een theoretisch kader voorgesteld voor het ontwikkelen van 'perceptuele' MCA's. Hoewel het in dit hoofdstuk beschreven perceptuele model nog geen substituut vormt voor klassieke MCA's, biedt de voorgestelde aanpak voordelen voor simulatie van specifieke maneeuvres en kunnen nieuwe bevindingen op het gebied van de waarneming van zelfbeweging vrij eenvoudig in deze aanpak worden geïntegreerd.

Samenvattend laat het werk in deze dissertatie zien dat waarneming van zelfbeweging die wordt geïnduceerd door veranderingen in de specifieke kracht in afwezigheid van visuele stimulatie, adequaat kan worden beschreven met de vergelijking van Mayne. De verwachting is dat toekomstig onderzoek zal bevestigen dat interacties tussen de otolieten en halfcirkelvormige kanalen met deze vergelijking kunnen worden beschreven. Ook hebben we laten zien dat waarneming van zelfbeweging in simulatoromgevingen voornamelijk van waarneming in natuurlijke omgevingen verschilt door een gebrek aan effectieve visuele grootte- en dieptecues en ook door de cognitieve effecten van eerdere ervaringen en verwachtingen van de proefpersoon. De rol van cognitie in de waarneming van zelfbeweging is dan ook een uitgangspunt voor vervolgonderzoek.

Dat vervolgonderzoek zou gericht kunnen worden op het verwerken van cognitieve effecten in modellen van waarneming van zelfbeweging. Evenzeer dient onderzocht te worden hoe visuele en fysieke informatie in het centraal zenuwstelsel wordt gecombineerd om de verschillende methoden die in recent onderzoek worden gebruikt voor het modelleren van waarneming van zelfbeweging met elkaar te kunnen verenigen. Tot slot dient te worden genoemd dat de hier gepresenteerde experimenten van passieve aard waren, in de zin

dat proefpersonen zich concentreerden op hun waarnemingen, terwijl MCA's voornamelijk ontwikkeld worden voor simulaties waarin proefpersonen actieve stuurtaken uitvoeren. In de toekomst dient daarom de toepasbaarheid van de huidige bevindingen op menselijk gedrag in actieve taken te worden onderzocht, om zo te komen tot meer immersieve en efficiënte voertuigsimulatie.

Acknowledgements

It is Sunday morning and I sit at my breakfast table, looking at my empty coffee cup while translating these last four years into words, probably the only words you will read from this book. It has been a great ride, and like all great rides, it comes to an end. All PhD experiences are different, and I was most fortunate to share mine with great people.

I would like to start by thanking Mark Wentink, that together with Wim Bles, wrote the proposal for this thesis and fought to have it accepted. Although this thesis followed a different road than initially planned, Mark continued to support me during these years and pushing me, until the end, to achieve the best results possible. I learned a lot with our discussions, which made me a more critical person and a better engineer. Mark, thank you for your guidance and friendship.

Since this work is the result of a cooperation between TU Delft and TNO, I had the luck to have two great promoters, Max Mulder, from TU Delft, and Jelte Bos, from TNO. I thank Max for giving me the opportunity to work as a PhD student at the Control and Simulation Division. Max trusted me and accepted this project with open arms, even though at the beginning its scientific goal was not completely clear. Max also gave me valuable feedback that helped us to publish high-quality papers at notorious scientific journals.

Jelte Bos was the main responsible to guide me in the right scientific direction. Jelte entered this project some months after its beginning and took me under his wing. His office door was always open and I used it quite often. We discussed new experiments, data analysis, and how to improve our story. Most importantly, Jelte taught me to be responsible and accountable for my actions. He gave me autonomy to run full experiments from his own projects, giving me guidance when needed, but letting me decide the best course of actions to

follow. Jelte, I thank you for all you taught me and for the trust you have put on my work. It was a pleasure working with you.

I also want to thank my co-promotor, René van Paassen. If at TNO, Jelte's door was always open, at TU Delft, I found that René's door had the same characteristics. When I had difficult questions, I would go to René and the answers would become evident. René always had good comments to improve the quality of my work and helped me solving problems I had with hardware/software during my experiments. To prove that he goes the extra mile, once he even drove all the way to Soesterberg to help out preparing an experiment.

Although during these four years I was mostly at TNO in Soesterberg, I also spent some of my time at the Control and Simulation Division in Delft. I want to thank all my colleagues that, even though I was not there often, treated me as part of the team. I really enjoyed the coffee breaks and all the fun we had at the AIAA conferences, even though that my "baby face" made us get carded at some pubs in the US.

I am thankful to my "partner in crime" at TU Delft, Rita Valente Pais. She coached me a lot at the beginning of this project, explaining me how things worked. It was really a pleasure to work with Rita and I think we achieved many cool things in our experiments. I am also grateful to Luísa dos Santos Buinhas, a great student that I had the opportunity to co-supervise with Rita.

From TU Delft, I also want to thank the friends I made via the PhD Startup event. It was really important to know that we were not alone in this adventure. Thank you for all the nice dinners, parties, and events we had.

I would like to thank Lon C. Kelly and Jacob A. Houck for the opportunity to conduct an experiment at the NASA Langley Research Center. Their help and dedication to conduct this experiment contributed to a publication in the Journal of Aircraft, described in this book in Chapter 6.

I want to thank to all the people at TNO in Soesterberg, where I spent most of these last four years. I learned a lot from you all and I had a lot of fun in all the social events, like the football and volleyball tournaments. I would like to thank Bart Kappé, who was a really nice roommate in my first years at TNO, Wim Bles for all the nice discussions we had, Philippus Feenstra with whom I cooperated in several experiments, Sam Besselink for the football discussions, Ingmar Stel for always making time for me, and Rob van de Pijpekamp for building the joystick we used in Chapters 2 and 3. I would like to thank Eric Groen, Wietse Ledegang, Mark Houben, Jelte Bos, Pierre Valk, and Ksander de Winkel from the E&O group with whom I did experiments, attended workshops and conferences, participated in projects, and had delicious dinners.

I also want to thank all the past and present people from the Desdemona BV, who helped me a lot when conducting my experiments. Mark Wentink, Bernd de Graaf, Suzanne Nooij, Paul Bakker, Frank Geurtsen, and Fred, thank you all

for making my work much easier.

Life at TNO would be much harder without my PhD buddies. Our special days were something awesome. Thank you for all the market days, junky Fridays, donderdag pizzadag, the games we played together, the borrels we tried to introduce, among other things. Ksander, Iris, Roald, Tom, Vanessa, Dylan, Janne, and Puck, thank you for making it fun and epic. A special thanks goes to Ksander, my TNO "bro". Ksander, we walked this road almost simultaneously, facing similar problems and accomplishments. It was a lot of fun and I think we did really good work together by complementing each other skills. Working with you was "most def" one of the best times of my PhD.

O apoio da família e amigos foi essencial para suportar os altos e baixos envolvidos num projecto desta envergadura. Queria agradecer aos meus companheiros de longa data que me fazem sentir sempre em casa quando vou a Portugal. Boavida, Paulo, Escórcio, Fred, Júlio, Nuno, Posturas, Tatiana, Henrique, e Serra, as jantaradas, festas, e passagens de ano são sempre memoráveis e ajudaram a manter a sanidade nestes últimos anos. Por falar em sanidade, queria também agradecer à Ana, que esteve a morar connosco durante 2 semanas e agora é da família, e ao André por a ter enviado para cá. Um obrigado à minha família de Beja por me receberem sempre bem, e pelas visitas que nos têm feito.

Um beijinho especial vai para os meus pais, a minha irmã, os meus avós e o meu tio. Vocês sempre acreditaram em mim e isso sempre me deu forças para continuar e conseguir chegar onde por vezes pensei não ser possível. Ao meu pai, à minha mãe e irmã, obrigado por nos visitarem sempre que podem, é sempre bom ter-vos cá e custa sempre quando se vão embora. Obrigado por todo o apoio e ajuda que nos têm dado.

O meu ultimo agradecimento vai para a Maria por toda a paciência que teve para aturar o meu mau feitio durante estes últimos 4 anos. Ela foi a pessoa mais importante nesta aventura que aqui acaba, sem ela nunca teria conseguido chegar onde cheguei hoje. Obrigado por todo o apoio nos bons e maus momentos. Esta já está... venha a próxima?

Curriculum Vitae

Bruno Jorge Correia Grácio was born on October 13, 1984 in Rio de Mouro, Portugal. From 1999 to 2002 he attended the Escola Secundária da Amadora, in Amadora, Portugal.

In 2002 he enrolled as an aerospace engineering student at the Instituto Superior Técnico, Universidade Técnica de Lisboa, in Lisbon, Portugal. He graduated in Aerospace Engineering in 2007, after spending his final year in the Netherlands, at the Faculty of Aerospace Engineering of the Delft University of Technology, under the European student exchange program ERASMUS. In 2007, he enrolled as a master student at the Control and Simulation Division of the Faculty of Aerospace Engineering at Delft University of Technology. For his master studies, he performed an internship at TNO Defence, Security and Safety in Soesterberg, the Netherlands, where he developed a Classical Washout Filter for the new Desdemona research simulator. Also at TNO, he did his M.Sc. thesis where he investigated the effect of motion feedback in driver behavior for advanced driving maneuvers. In 2009 he obtained his M.Sc. degree (*cum laude*).

In 2009 he worked as a research engineer in the Perception and Simulation department at TNO Defence, Security and Safety, where he designed human motion perception experiments. In the same year he started his Ph.D. research at the Control and Simulation Division of the Faculty of Aerospace Engineering at Delft University of Technology. His research focused on human self-motion perception induced by specific forces in a simulation environment.

Publications

Correia Grácio, B. J., Bos, J. E., Van Paassen, M. M., and Mulder, M., "Perceived Displacement and Velocity During Lateral Linear Motion in the Dark," *Exp Brain Res (to be submitted)*, 2013.

Correia Grácio, B. J., Bos, J. E., Van Paassen, M. M., and Mulder, M., "Effect of Visual Characteristics and Degrees-of-Freedom on the Perceptual Scaling Between Visual and Inertial Cues," *Exp Brain Res (submitted)*, 2013.

Dos Santos Buinhas, L., **Correia Grácio, B. J.**, Valente Pais, A. R., Van Paassen, M. M., and Mulder, M., "Modeling Coherence Zones in Flight Simulation During Yaw Motion," *AIAA Modeling and Simulation Technologies Conference and Exhibit*, No. AIAA 2013-5223, Boston, MA, August 2013.

Berthoz, A., Bles, W., Bülthoff, H. H., **Correia Grácio, B. J.**, Feenstra, P., Filliard, N., Hühne, R., Kemeny, A., Mayrhofer, M., Mulder, M., Nusseck, H. G., Pretto, P., Reymond, G., Schlüsselberger, R., Schwandtner, J., Teufel, H., Vailleau, B., Van Paassen, M. M., Vidal, M., and Wentink, M., "Motion Scaling for High-Performance Driving Simulators," *IEEE Transactions on Human-Machine Systems*, Vol. 43, No. 3, 2013, pp. 265–276.

Correia Grácio, B. J., Valente Pais, A. R., Van Paassen, M. M., Mulder, M., Kelly, L. C., and Houck, J. A., "Optimal and Coherence Zone Comparison Within and Between Flight Simulators," *Journal of Aircraft*, Vol. 50, No. 2, 2013, pp. 493–507.

Correia Grácio, B. J., De Winkel, K. N., Groen, E. L., Wentink, M., and Bos, J. E., "The time constant of the somatogravic illusion," *Exp Brain Res*, Vol. 224, No. 3, 2013, pp. 313–321.

Correia Grácio, B. J. and Bos, J. E., "Measuring dynamics of the subjective vertical and tilt using a joystick," *Journal of Vestibular Research*, Vol. 22, No. 4, 2012, pp. 181–189.

Correia Grácio, B. J., Bos, J. E., Wentink, M., Van Paassen, M. M., and Mulder, M., "Perceived Mismatch Between Visual and Inertial Cues in a Simulation Environment," *AIAA Modeling and Simulation Technologies Conference and Exhibit*, No. AIAA 2012-5011, Minneapolis, Minnesota, August 2012.

Correia Grácio, B. J., Wentink, M., Bos, J. E., Van Paassen, M. M., and Mulder, M., "An Application of the Canal-Otolith Interaction Model for Tilt Coordination During a Braking Maneuver," *AIAA Modeling and Simulation Technologies Conference and Exhibit*, No. AIAA 2012-4493, Minneapolis, Minnesota, August 2012.

Correia Grácio, B. J., Valente Pais, A. R., Van Paassen, M. M., Mulder, M., Kelly, L. C., and Houck, J. A., "Relationship Between Optimal Gain and Coherence Zone in Flight Simulation," *AIAA Modeling and Simulation Technologies Conference and Exhibit*, No. AIAA 2011-6556, Portland, OR, August 2011.

Correia Grácio, B. J., Wentink, M., Valente Pais, A. R., Van Paassen, M. M., and Mulder, M., "Driver Behavior Comparison Between Static and Dynamic Simulation for Advanced Driving Maneuvers," *PRESENCE: Teleoperators and Virtual Environments*, Vol. 20, No. 2, 2011, pp. 143–161.

Correia Grácio, B. J., van Paassen, M. M., Mulder, M., and Wentink, M., "Tuning of the Lateral Specific Force Gain Based on Human Motion Perception in the Desdemona Simulator," *AIAA Modeling and Simulation Technologies Conference and Exhibit*, No. AIAA 2010-8094, Toronto, Ontario Canada, August 2010.

De Winkel, K. N., **Correia Grácio, B. J.**, Groen, E. L., and Werkhoven, P. J., "Visual-Inertial Coherence Zone in the Perception of Heading," *AIAA Modeling and Simulation Technologies Conference and Exhibit*, No. AIAA 2010-7916, Toronto, Ontario Canada, August 2010.

Feenstra, P., Horst, A. R. A., **Correia Grácio, B. J.**, and Wentink, M., "The Effect of Simulator Motion Cuing on Steering Control Performance," *TRB: Journal of the Transportation Research Board*, Vol. 2185, 2010, pp. 48–54.

Feenstra, P., Horst, A. R. A., **Correia Grácio, B. J.**, and Wentink, M., "The Effect of Simulator Motion Cueing on Steering Control Performance - a Driving Simulator Study," *TRB 89th Annual Meeting*, No. 10-1281, Transportation Research Board, Washington, January 2010.

Correia Grácio, B. J., Wentink, M., Groen, E. L., and Bles, W., "Subjective Estimates of G-load in Centrifuge-Based Simulation and Applications for G-cueing in Desdemona," *AIAA Modeling and Simulation Technologies Conference and Exhibit*, No. AIAA 2009-5919, Chicago, IL, August 2009.

Wentink, M., **Correia Grácio, B. J.**, and Bles, W., "Frequency Dependence of Allowable Differences in Visual and Vestibular Motion Cues in a Simulator," *AIAA Modeling and Simulation Technologies Conference and Exhibit*, No. AIAA 2009-6248, Chicago, IL, August 2009.

Correia Grácio, B. J., Wentink, M., Feenstra, P., Mulder, M., Van Paassen, M. M., and Bles, W., "Motion Feedback in Advanced Driving Manoeuvres," *DSC 2009 Europe*, Monaco, 2009.

Feenstra, P., Wentink, M., **Correia Grácio, B. J.**, and Bles, W., "Effect of Simulator Motion Space on Realism in the Desdemona Simulator," *DSC 2009 Europe*, Monaco, 2009.

Wentink, M., **Correia Grácio, B. J.**, Groen, E. L., Feenstra, P., and Bles, W., "New technologies & applications in the desdemona simulator," *Expanding Horizons: Technology Advances in Flight Simulation*, Royal Aeronautical Society, 2008.